Universitat Autònoma de Barcelona

MOLECULAR MECHANISMS INVOLVED IN PLATINUM-INDUCED PERIPHERAL NEUROPATHY. An exploratory study

Aina Calls Cobos

Universitat Autònoma de Barcelona

MOLECULAR MECHANISMS INVOLVED IN PLATINUM-INDUCED PERIPHERAL NEUROPATHY.

An exploratory study

ACADEMIC DISSERTATION

To obtain the degree of PhD in Neuroscience by the

Universitat Autònoma de Barcelona

June 2021

PhD Candidate

Aina Calls Cobos

Thesis Supervisors

Dr. Jordi Bruna Escuer

Dr. Esther Udina Bonet

Academic Tutor

Dr. Xavier Navarro Acebes

Group of Neuroplasticity and Regeneration,

Departament de Biologia Cel·lular, Fisiologia i Immunologia,

Institut de Neurociències

This study was funded by:

- The *Instituto Carlos III* through the PI15/01303 grant “Estudio Exploratorio sobre la etiopatogenia, biomarcadores de riesgo y mecanismos implicados en la generación de la neuropatía inducida por platinos” to Jordi Bruna Escuer.
- The *Departament de Salut* from *La Generalitat de Catalunya* (CERCA Program) through the grant SLT008/18/00028 to Jordi Bruna Escuer.
- The *Secretaria d’universitats i recerca* from *La Generalitat de Catalunya* by means of a predoctoral FI-DGR grant to Aina Calls Cobos, co-funded by the European Social Found.
- The EMBO by means of a short-term fellowship to Aina Calls Cobos to perform an international internship in the Cellular Senescence and Age-related pathologies Group (STF8725).

"Normality is a paved road: It’s comfortable to walk,
but no flowers grow on it”
-Vincent Van Gogh-

INDEX

I. ABSTRACT

Platinum-Induced Peripheral Neuropathy (PIPN) is a frequent serious dose-limiting adverse event of the platinum-based cytostatic agent cisplatin, oxaliplatin and carboplatin, which are given as a first line treatment against high prevalent cancers. Due to its severity, PIPN often causes cancer treatment reduction or even cessation, thus decreasing the survival probabilities of oncologic patients. It has been extensively reported that PIPN severity correlates with the amount of platinum drugs cumulated in sensory neurons of the dorsal root ganglia (DRG). Several pathophysiological mechanisms have been described for PIPN development, including DNA damage, mytotoxicity and channels dysfunction in DRG sensory neurons, among others. Despite the efforts of clinicians and researchers during the last decades, no successful translation from pre-clinical settings to the clinics has been achieved.

The aim of this study was to determine the exact molecular mechanisms involved in the development of PIPN following a non-hypothesis driven methodology to find new therapeutical targets. By single-cell RNA sequencing (scRNA-seq), we studied the transcriptomic profile of DRG sensory neurons from 2 well characterized neurophysiological mice models of PIPN: one induced by cisplatin administration, and the second by oxaliplatin.

We demonstrated that cisplatin treatment induced DNA damage and the up-regulation of the *Cdkn1a* gene and its protein product p21 in the DRG neuronal population. While apoptosis activation pathways were not observed in DRG sensory neurons of cisplatin-treated mice, these neurons did express several senescence hallmarks, including senescence-associated β-galactosidase (SA-βGAL), phosphor(p)-H2AX and nuclear Nfkb-p65 proteins. The senescent phenotype seen in sensory neurons persisted up to 6 weeks after cisplatin treatment discontinuation.

Regarding oxaliplatin study, results of scRNA-seq showed an up-regulation of *Lxn* and *Klk5* genes, and a down-regulation of *Kyat3* gene in oxaliplatin treated animals, which have been involved in the modulation of inflammatory responses, the immune system and pain behaviors. Although the protein products of *Lxn* and *Klk5* genes did not appear up regulated in the DRG of oxaliplatin-treated mice, we did see an increase in the pro-inflammatory cytokine profile in both the DRG and the sciatic nerves of oxaliplatin-treated mice, altogether with infiltrated cells. Based on that, we checked for factors involved of the so-called Immunogenic Cell Death (ICD) response, which is activated in tumor cells after oxaliplatin treatment. However, we did not find any evidence of ICD activation in DRG of oxaliplatin treated mice. On the other hand, and in contrast to cisplatin, the rapid repair of DNA damage after oxaliplatin treatment cessation could explain the lack of establishment of a full and durable senescence phenotype in the DRG.

In vivo data showed that senescence pathways could play a key role in platinum neurotoxicity. Thus, we finally set up an *in vitro* model of cisplatin-induced neuronal senescence in which to start the screening of potential neuroprotective targets in a cost- and time-effective way.

II. ABBREVIATIONS

Ape-1: Apyrimidinic endonuclease/redox effector factor
ATP: Adenosine Triphosphate
BBB: Blood Brain Barrier
BDB: Blood DRG Barrier
BER: Base Excision Repair
BNB: Blood Nerve Barrier
Ca^{2+}: Calcium
Ca_v: Voltage-gated calcium channels
CDDP: Cisplatin-treated
CGRP: Calcitonin Gene Related Peptide
CIPN: Chemotherapy-Induced peripheral Neuropathy
Cl^-: Chloride
CMAP: Compound Muscle Action Potential
CNAP: Compound Nerve Action Potential
CNS: Central Nervous System
CTR: Copper Transporter
DACH: Diaminocyclohexane
DDR: DNA Damage Response
DEG: Differentially Expressed Genes
DNA: Deoxyribonucleic Acid
DPBS: Dulbecco's Phosphate Buffered Saline
DRG: Dorsal Root Ganglia
ECAR: Extracellular Acidification Rate
FDA: Food and Drug Administration
FDR: False Discovery Rate
GAPDH: Glyceraldehyde 3-Phosphate Dehydrogenase
GFAP: Glial Fibrillary Acidic Protein
GO: Gene Ontology
hiFBS: heat inactivated Fetal Bovine Serum
ICD: Immunogenic Cell Death
IENF: Intraepidermal Nerve Fibers
IENFD: Intraepidermal Nerve Fibers Density
IF: Immunofluorescence
i.p.: intraperitoneally
i.v.: intravenously
K^+: Potassium
K_v: Voltage-gated Potassium channels
KAT3: Kynurenine Aminotrasnferease 3
KLK5: Kallikrein 5
LTMR: Low-Threshold Mechano Receptors
mPTP: mitochondrial Permeable Transition Pore
mtDNA: mitochondrial DNA
Na^+: Sodium
Na_v: Voltage-gated sodium channels
NCS: Nerve Conduction Studies
nDNA: nuclear DNA
NDS: Normal Donkey Serum
NEF: Neurofilament
NER: Nucleotide Excision Repair
NGF: Nerve Growth Factor
NP: Non-Peptidergic
NSCLC: Non-small Cell Lung Cancer
NT: Non-treated
OCR: Oxygen Consumption Rate
OCT1: Organic Cation Transporter 1
OCT2: Organic Cation Transporter 2
OXA: Oxaliplatin-treated
PAR: Proteinase Activated Receptors
PB: Phosphate Buffer
PBS: Phosphate Buffer Saline
PDL: Poly-D-Lysine
PEP: Peptidergic
PFA: Paraformaldehide
PGP9.5: Protein Gene Product 9.5
PI: Propidium Iodide
PIPN: Platinum-Induced Peripheral Neuropathy
PN: Peripheral Neuropathy
PNS: Peripheral Nervous System
Pt: Platinum
QST: Quantitative Sensory Testing
RNA-seq: RNA-sequencing
Pol k: Polymerase Kappa
ROS: Reactive Oxygen Species
SA-βGAL: Senescence-Associated β-Galactosidase
SASP: Senescence-Associated Secretory Phenotype

s.c.: subcutaneously
scRNA-seq: single cell RNA-sequencing
SGC: Satellite Glial Cell
SNAP: Sensory Nerve Action Potential
TCD: Total Cumulated Dose
TEM: Transmission Electron Microscopy
TH: Tyrosine Hydroxylase
Trk: Tyrosine Receptor Kinase
TRP: Transient Receptor Potential
t-SNE: t-distributed Stochastic Neighbor Embedding
Tx: Tumor inoculation
WB: Western Blot

III. INTRODUCTION

Cancer is among the leading causes of death worldwide. In 2018, there were 18.1 million new cases and 9.5 million cancer-related deaths in the word (source: National Cancer Institute; International Agency for Research on Cancer, WHO). As consequence, plenty of therapies have been developed with the aim to treat it, including surgical debulking strategies, cytostatic agents, ionizing radiation, and more recently immunotherapy. Most of these treatments are designed to kill cells with high rates of proliferation. One of the cornerstones of chemotherapy, which is systemically administered, is that not only acts on tumor cells but also on many others proliferative cells residing in healthy tissues of the organism (i.e., mucous membranes of the mouth, throat, stomach, and intestines; bone marrow or hair follicles). As a result, oncologic patients treated with chemotherapy can suffer from different side-effects like gastrointestinal alterations, immunodepression, hematologic cytopenia or loos of hair. Fortunately, diverse therapeutic strategies as antiemetic drugs or haemopoietic colony stimulating factors can minimize the impact of these adverse events. Conversely, there are some non-proliferative cells of the organism that are susceptible to the toxic effect of anti-neoplastic drugs. Neurons residing in the Peripheral Nervous System (PNS) are one of the main post-mitotic cell populations affected by some cytostatic drugs widely used for high prevalent cancers. Nowadays, this neurotoxicity, known as Chemotherapy-Induced Peripheral Neuropathy (CIPN), is the main dose-limiting side effect of these cancer treatments. Its chronic nature once appears and the impact on patients' quality of life results on dose reductions or even the treatment withdrawal, with the consequent negative impact on patient overall survival probabilities.

This dissertation is mainly focused on the peripheral neuropathy induced by a specific type of cytostatic drugs, the platinum-based agents. Although the general mechanisms related with their neurotoxicity have been further investigated in literature, no effective treatment exists for Platinum-Induced Peripheral Neuropathy (PIPN). In this thesis, non-hypothesis driven molecular pathways related with the development of PIPN have been studied to find new therapeutic targets to prevent this relevant treatment adverse event. Results from this thesis will also help to build a global and comprehensive etiopathogenesis of PIPN.

1. The Peripheral nervous system

The PNS is one of the two main divisions that conforms the nervous system, being the other one the Central Nervous System (CNS). PNS is composed by all the neuronal tissue outside the CNS, including the peripheral nerves and the neuronal somas located in peripheral ganglia (dorsal root ganglia (DRG) and autonomic ganglia). The peripheral nerves generally contain sensory axons coming from DRG primary sensory neurons, motor axons coming from lower motoneurons of the spinal cord, and autonomic axons coming from autonomic ganglia. The main function of the PNS

is to connect the CNS with the muscles, organs, and skin, serving as a relay between the brain and spinal cord and the rest of the body. For doing that, the PNS is divided in two components. The sensory or afferent component transmits all the information from receptors in peripheral tissues and organs (skin, skeletal muscle, organs) to the CNS. The motor or efferent component of the PNS carries motor commands from the CNS to effector organs (Figure 1).

Unlike the CNS, the PNS is not protected by the blood-brain-barrier (BBB) but by the Blood-nerve-barrier (BNB) or the Blood-DRG-barrier (BDB) (Reinhold et al., 2020). Both BNB and BDB are more permissive barriers that allow the crossing of several substances from the blood stream to the nervous tissue (Allen and Kiernan, 1994). Therefore, the PNS is more exposed and susceptible to toxic damage than the CNS.

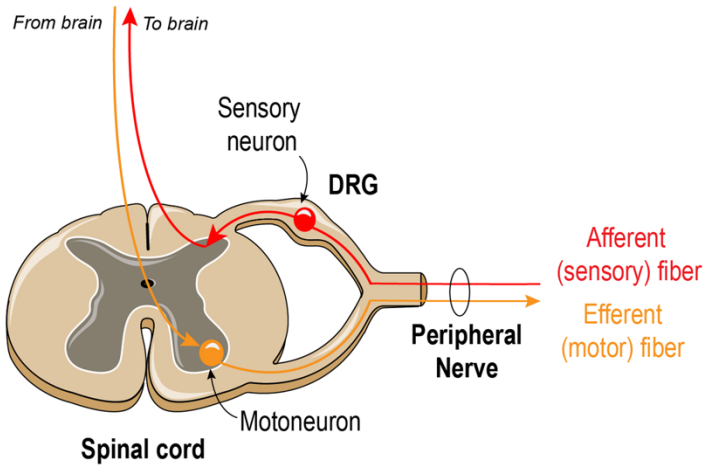

Figure 1. PNS: from structure to function. Sensory neurons of the DRG act as peripheral receptors that convey all the information from periphery to the CNS. Motoneurons located in the spinal cord integrate all the motor commands and control contraction of the peripheral executor organs, the skeletal muscles. Peripheral nerves are composed by afferent (sensory) and efferent(motor) fibers.

1.1 Dorsal Root Ganglia

DRGs harbour the cell bodies of primary sensory neurons, which are in charge to convey somatosensory information from the periphery into CNS. DRGs are located near the entrance of dorsal root into the spinal cord, in the intervertebral foramina along the spin. DRG neurons are pseudounipolar, with spherical cell bodies projecting a single axon that bifurcates into two branches. The peripheral branch leaves the ganglion through the spinal nerve and innervates the skin, organs, and muscles, while the central branch forms the dorsal root of the spinal nerve, which makes a synapse in the dorsal horn of the spinal cord or ascends itself towards the brain stem and shape the sensory ascending spinal cord pathways (Figure 1) (Watson, 2012). The ability to

perceive and discriminate diverse sensory modalities, including touch, temperature, pain, itch, and proprioception, sustained by the existence of functionally specialized receptors and sensory neurons tuned to respond to specific stimuli.

1.1.1 Sensory neuron populations of the DRG

The DRG neuronal population is highly heterogeneous not only in their physiology properties but also in terms of anatomy (related with the size of the soma), neurochemical phenotype and neurotrophic dependence. Based on these features, sensory neurons have been classically classified in three major subpopulations (Priestley et al. 2002) (Figure 2a). The first major group is defined by the expression of the heavy chain neurofilament protein (NEF) and comprises about 40% of DRG neurons. This subpopulation is composed by large-size neurons that give rise to myelinated axons (Aα/β fibers) corresponding to proprioceptive neurons that innervate deep structures such as muscle spindle and Golgi tendon organ, sensing limb movement and position. This population expresses parvalbumin protein and the neurotrophic receptor Tyrosine receptor kinase (Trk) C. NEF neurons also comprise medium-size neurons corresponding to Low-threshold mechanoreceptors (LTMR) that project their axon to cutaneous sites, transducing touch, pressure and vibration sensation. These neurons have been classically identified by TrkB receptor.

The second major neuronal subpopulation in the DRG are the peptidergic nociceptors (PEP) which correspond to small-size neurons defined by the constitutive expression of neuropeptides. The best marker to identify them is calcitonin gene relate peptide (CGRP). TrkA receptor is mainly expressed in this population. This second group comprises approximately 40% of DRG neurons. They are polymodal pain sensing neurons that convey mechanical and thermal noxious stimuli from periphery to the spinal cord. These neurons project mainly unmyelinated axons (C fibres). A small percentage (10%) have small myelinated axons (Aδ fibres), and co-express neurofilament protein altogether with CGRP. DRG neurons that express substance P are mainly classified in this category.

Finally, there is the non-peptidergic neuronal subpopulation (NP, about 30% of cells) which can be identified by their binding of the ioslectin B4 (IB4) from *Griffona simplicifolia,* and by the expression of Fluoride-resistant acid phosphatidase (FRAP). These are small-size neurons that project C fibers and function as polymodal pain-sensing nociceptors, although they generally do not contain neuropeptides. NP neurons are characterized for Ret receptor expression.

On the recent years, and thanks to the advances in single-cell transcriptomics, an unbiased classification of DRG sensory neurons has emerged, which is exclusively based on the gene expression profile of each neuronal population. Many studies using this technology revealed the complexity and diversity of sensory neurons underlying somatic sensation and led to the discovery

of new subpopulations like the Tyrosine Hydroxylase (TH) expressing neurons, which correspond to C- LTMR. Moreover, these studies manifest that the three main populations defined above (NF, PEP and NP) can be subsequently divided in many other subgroups (Figure 2b) (Usoskin et al., 2015).

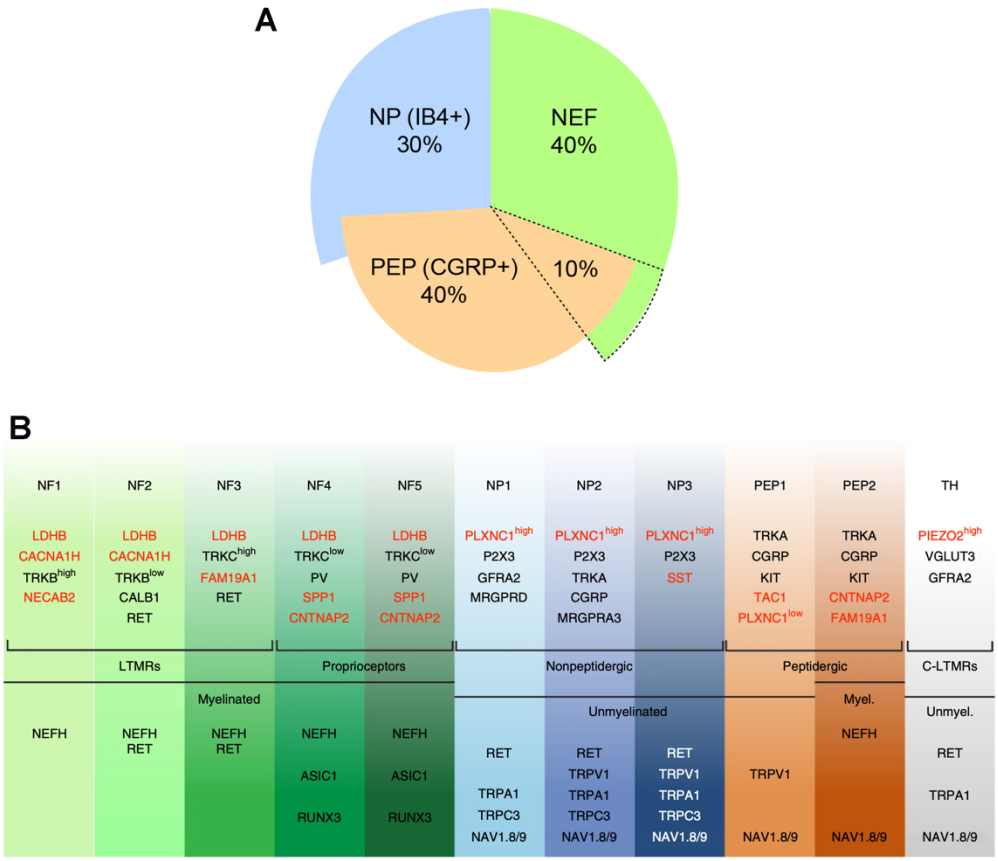

Figure 2. Classification of DRG sensory neurons. **A**: Classical subsets of sensory neurons, based on parameters like size, neurotrophic dependence, and chemical properties. **B:** Novel and unbiased classification of sensory neurons based on gene expression profile. NF= NEF neurons. *Table from Usoskin et al., 2015.*

Due to differences in neurotrophic dependence, physiological properties and biochemical profile, sensory neurons can respond distinctly to the same noxious stimuli (Jamieson et al., 2005; Hu et al., 2016), so care must be taken when analyzing the response of sensory neurons in front of different noxious stimuli, including platinum drugs.

1.1.2 Satellite Glial Cells

In addition of sensory neurons, DRGs also harbor Satellite Glial Cells (SGCs). These are unique cells that wrap around neuronal cell bodies specifically in peripheral ganglia like DRG (Figure 3). The number of SGCs enclosing a neuron is proportional to the size of the neuronal soma and is in

the range of 4-10 SGCs per neuron in mice. The SGCs surrounding a neuronal soma are connected by gap junctions, forming a distinct functional unit. In most cases, neurons are wrapped individually with several SGCs, but there is evidence that a small proportion of DRG neurons share a common glial envelope, forming a 'cluster' with one or two other neurons. In some cases, the neurons in a cluster are separated only by a thin layer of extracellular space, whereas in other cases they are separated by a thin glial sheet, which allows neuron–SGC–neuron chemical interaction. The gap between SGCs and neuronal surface is about 20nm, allowing a tight control of neuronal homeostasis. In fact, SGCs have been found to play a variety of roles, like those of astrocytes in the CNS. They supply nutrients to the surrounding neurons and have some structural functions (Hanani and Spray, 2020). Despite SGCs are the main population of the DRG in terms of percentage, little is known on the exact function of these cells and how they interfere with neuronal pathology. A reason that can explain this lack of knowledge about SGCs is that their intimate spatial relationship with neurons difficult their isolation and posterior analysis. Therefore, the function and biology of SGCs is not well characterized under normal nor pathophysiological conditions.

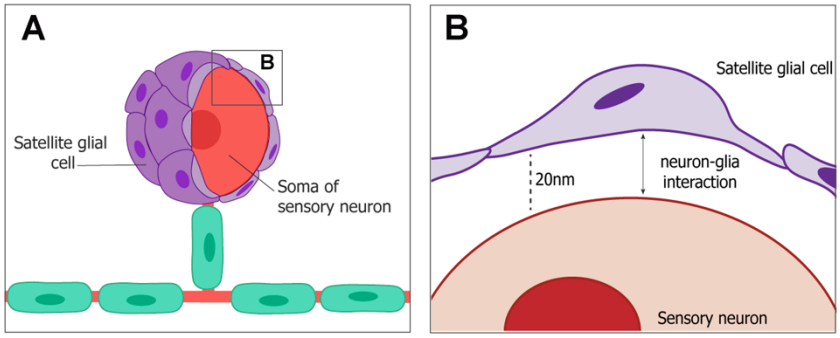

Figure 3. **Satellite glial cells of the DRG**. **A**: View of a single neuronal soma wrapped by SGCs**. B:** Schematic diagram showing the gap (20nm) between sensory neurons and SGCs. *Modified from Gonçalves et al., 2018.*

2. CIPN: An overview

CIPN is a board term used to designate the neurotoxic effects of different types of chemotherapies on the PNS. It is the main neurological complication seen in oncologic patients treated with neurotoxic cytostatics (Kannarkat et al., 2007), and affects around 50% of them (Wolf et al., 2008; Bhagra and Rao, 2007; Shah et al., 2018). However, the exact incidence of CIPN is quite variable because it depends on the type of drug and the treatment schedules used.

CIPN can emerge because of the neurotoxic action of cytostatic drugs in either the peripheral nerves or the neuronal somas of the PNS, preferentially the sensory neurons of the DRG (Velasco and

Bruna 2010; Park et al., 2013). In contrast, motoneurons are rarely affected by neurotoxic chemotherapies since their cell body is in the spinal cord and so protected by the BBB.

There are six major families of cytostatic drugs that can cause CIPN: vinca alkaloids (vincristine, vinblastine, vinorelbine, eribuline, vinflunine), proteasome inhibitors (bortezomib), thalidomide, platinum-based compounds (cisplatin, oxaliplatin and carboplatin) and microtubule-stabilizing agents, including taxanes (paclitaxel, docetaxel) and epothilones (Park et al., 2013). They differ in the specific cellular targets and mechanisms of action (Figure 4). Consequently, the clinical and electrophysiological alterations, risk factors and prognostic of CIPN will vary among neurotoxic cytostatic drugs (Table 1) (Verstappen et al., 2003; Park et al., 2013). Independently of the type of chemotherapy, large sensory neurons are most affected in CIPN, being rare the damage of smaller sensory fibers and specific of selected chemotherapies as bortezomib (Park et al., 2013). A recent study shows that BDB is considerably more permeable than the BNB, as the neuron-rich DRG areas show a higher capillary density and lower expression of key tight junction proteins, allowing increased contact between neurons and anticancer agents from the blood (Reinhold et al., 2020). It supports the predominance of sensory nerve damage over motor nerve damage in CIPN. In concordance with that, at the clinical level CIPN is defined as a predominantly sensory neuropathy that can be accompanied by motor and autonomic dysfunctions. Symptoms often manifest symmetrically in a “glove-and-stocking” manner with the first ones appearing on the distal parts of the body (fingers of hands and feet) and progressing to the proximal ones (Figure 4). The symptoms include altered touch sensation, and numbness, tingling, paresthesia, and dysesthesia. Pain sensation including spontaneous burning, shooting or electronic shock-like pain frequently occurs, as well as thermal allodynia or hyperalgesia. In the most severe cases, symptoms can progress to a loss of proprioception and ataxic gait. Autonomic symptoms, which are generally milder than the sensory ones, comprise orthostatic hypotension, constipation and male sexual impotence functions. Motor dysfunctions occur less frequently and often involve distal weakness. In rare occasions, CIPN can lead to paresis and severe disability. However, these cases are usually related with non-diagnosed underlying genetic degenerative neuropathies (Velasco and Bruna, 2010).

Toxicity mainly occurs in a dose-dependent manner after several cycles of treatment with the neurotoxic agent. In fact, the main risk factors to develop CIPN are the dosage and duration of treatment. Therefore, symptoms normally emerge weeks or months after starting the chemotherapy treatment. In some cases, patients experience a paradoxical worsening of symptoms after the cessation of the treatment in a phenomenon known as “coasting effect” (Park et al., 2013). In addition of dose-associated risk factors, some demographic and clinical factors (i.e., comorbidity, age or genetic factors) have been proposed to increase the risk of developing CIPN after the

treatment with neurotoxic neuropathies. Nevertheless, none has been properly validated and widely accepted (Velasco and Bruna, 2010).

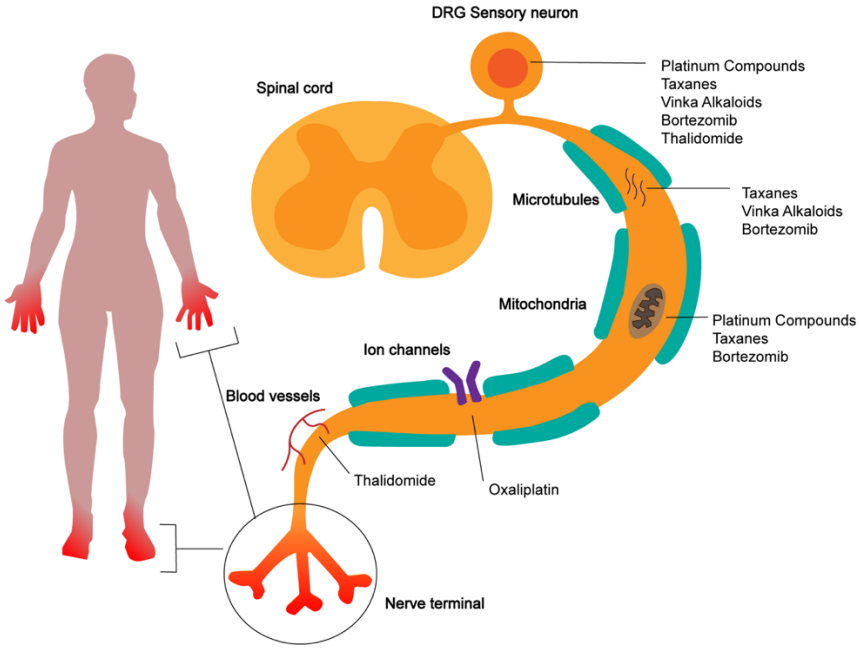

Figure 4. Representation of the typical "Glove-and-Stocking" distribution of CIPN symptoms. Putative targets of each neurotoxic chemotherapy in the PNS are depicted, including the DRG, the axon and axonal components (myelin, microtubules, mitochondria, ion channel and vascular network) and the distal nerve terminals. *Image modified from Park et al., 2013.*

Two main problems emerge when CIPN develops. On one hand, the symptoms can be disabling and interfere with functional ability and life quality of the patients. On the other hand, neuropathic symptoms can also interfere with the chemotherapy treatment, leading to a dose reduction or even early cessation of chemotherapy. Therefore, efficacy of treatment and survival of patients is dramatically decreased. Thanks to the advances in medicine, nowadays cancer is often successfully addressed by therapy (including chemotherapy), with cancer survivors increasing in number and living longer worldwide. Unfortunately, due to its high prevalence and long-lasting effects, CIPN constitutes a major issue for both cancer patients and cancer survivors. Consequently, CIPN impact implies a significant economic burden on health-care systems with a tremendous socio-sanitary cost (Pike et al., 2012).

Table 1. Overview of peripheral neurotoxic features associated with various chemotherapy drugs. NC: Nerve conduction; SNAP: Sensory nerve action potential; CMAP: Compound muscle action potential; SNAP: Sensory nerve conduction velocity; MNCV: Motor nerve conduction velocity. *Inspired by Argyriou et al., 2014*

Agent	Main target in the PNS	Mechanism of action	Type of Neuropathy	Alterations in NC	Clinical Picture
Cisplatin	DRG	Binding to the DNA; Neuronal death by apoptosis	Pure Sensory (Neuronopathy)	Decreased SNAP; mildly decreased SNCV	Paresthesia, numbness in a stocking-and-glove distribution
Carboplatin	DRG	Binding to the DNA; Neuronal death by apoptosis	Pure Sensory (Neuronopathy)	Decreased SNAP; mildly decreased SNCV	Same as cisplatin but less severe
Oxaliplatin	DRG; ion channels	Chronic: Binding to the DNA; Neuronal death by apoptosis Acute: ion channels dysregulation	Chronic: Pure Sensory (Neuronopathy) Acute: cold transient neuropathy	Chronic: Decreased SNAP; mildly decreased SNCV Acute: Hyperexcitability in motor nerves	Chronic: same as cisplatin with possible neuropathic pain Acute: cold hyperalgesia and neuromtonia-like symptoms
Paclitaxel	DRG; microtubules; nerve terminals	Alterations of axonal transport due to microtubule disruption	Sensory; occasionally sensorimotor	Decreased SNAP; sometimes reduced CMAP, MNCV and SNCV	Paresthesia, numbnes and/or neuropathic pain in a stocking-and-glove distribution; myalgia, myopathy
Docetaxel	DRG; microtubules; nerve terminals; mitochondria	Alterations of axonal transport due to microtubule disruption	Sensory; occasionally sensorimotor	Decreased SNAP and CMAP; moderately reduced MNCV	Same as paclitaxel
Epothilones	DRG; microtubules; nerve terminals	Alterations of axonal transport due to microtubule disruption	Sensory; occasionally sensorimotor	Decreased SNAP	Same as paclitaxel
Vincristina	DRG; microtubules; nerve terminals	Alterations of axonal transport due to microtubule disruption	Sensorimotor; Autonomic	Decreased SNAP and CMAP; mildly reduced MNCV and SNCV	Paresthesia, numbnes and/or neuropathic pain in a stocking-and-glove distribution; muscle cramps, mild distal weakness
Bortezomib	Microtubules; mitochondrial and endoplasmic reticulum	Reversible inhibition of proteosome? Unknown	Painful sensory	Low or absent SNAP; reduced CMAP in severe cases; mild slowing MNCV and SNCV	Neuropathic pain and paresthesia in distal extremitie of limbs
Thalidomide	Blood vessels; DRG	Reduction of blood suply to peripheral nerves? Unknown	Pure Sensory	Decreased SNAP	Same as Bortezomib

3. Platinum-based cytostatic drugs

There are three platinum-based drugs regularly prescribed in cancer treatment: cisplatin, carboplatin and oxaliplatin. Since the discovery of cisplatin as antineoplastic agent in the 1970s, the use of platinum-based agents has been increasing in the routine clinical practice due to its efficiency in the treatment of several malignances (see in next sections). In basis of the incidence of these malignancies, it is estimated that around 50-70% of all cancer patients are treated with these drugs (Dyson and Sava, 2006).

3.1 Chemical and pharmacokinetic properties

All three platinum drugs are synthetic inorganic and water-soluble heavy metal compounds. All platinum drugs contain two types of ligands attached to a central platinum cation. These are the ammine or ammine carrier ligand, and the labile chloride or carboxylate leaving group. However, the three platinum drugs differ in some chemical and pharmacokinetic properties.

Cisplatin, the first-generation platinum agent, has two ammine groups and two labile chloride groups oriented in a *cis* planar configuration around the central platinum ion (Figure 5). Carboplatin is a second-generation platinum drug that differs from cisplatin in the presence of a bis-carboxylate group instead of two chloride ligands as leaving group. Similarly, oxaliplatin, the third-generation platinum-agent, differs from cisplatin in the presence of a dicarboxylate (oxalate) leaving group. Moreover, oxaliplatin also replaces the two ammine ligands for a diaminocyclohexane (DACH) group.

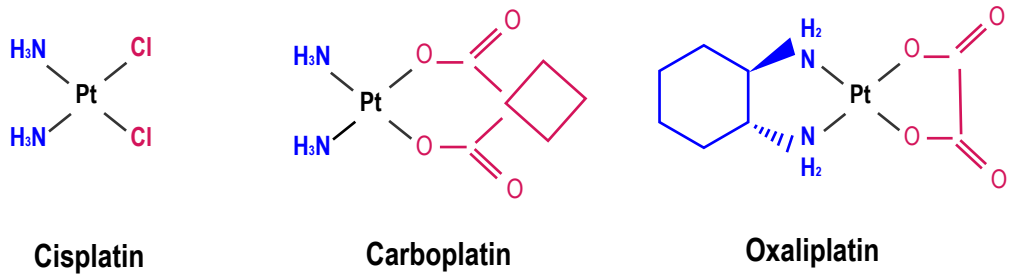

Figure 5. Chemical structure of the approved platinum drugs. Ammine or ammine carrier ligands appear in blue; the labile chloride (cisplatin) or carboxylate-based (carboplatin and oxaliplatin) leaving groups appear in magenta.

Cisplatin has a molecular weight of 300.046 g/mol and a distribution volume at a steady state of 11-12 L/m^2. Around 90% of cisplatin is bound to proteins after a few hours of administration. Following administration of 50-100 mg/m^2, cisplatin levels decay monoexponentially with a plasma half-life (t1/2) of 20–30 minutes. The complexes between plasma proteins and the platinum group

do not dissociate to a significant extent and are slowly eliminated with a minimum t1/2 of 5 days or more (Source: go.drugbank.cat). However, circulating platinum complexes have been identified for as long as 6 months and sometimes even decades after the last cisplatin infusion (Gietema et al., 2000).

Carboplatin has a molecular weight of 395.278 g/mol and a distribution volume of 16 L/m^2. It presents an initial plasma half-life (t1/2α) of 1–2 hours and a post distribution plasma half-life (t1/2β) of 2.6–5.9 hours (Source: go.drugbank.cat). In contrast to cisplatin, carboplatin does not bind to plasma proteins (Oguri et al., 1988).

Oxaliplatin has a molecular weight of 395.278 g/mol and a distribution volume at steady state of 11-12 L/m^2. Like cisplatin, oxaliplatin is irreversibly bound to plasma proteins but also to erythrocytes. After infusion, approximately 15% of the administrated platinum is present in the systemic circulation whereas the remaining 85% is distributed into tissues or eliminated by renal excretion. The decline of oxaliplatin levels is triphasic, with two distribution phases: t1/2α at 0.43 hours and t1/2β at 16.8 hours. It is followed by a long terminal elimination phase (t1/2γ) that lasts 391 hours after administration (Source: go.drugbank.cat). A unique feature of oxaliplatin is that once in the bloodstream, it is rapidly and non-enzymatically transformed into two metabolites: oxalate and the reactive platinum dichloro-DACH. This occurs via the replacement of the oxalate group with chloride (Cl^-)and water in the blood plasma (Ehrsson et al., 2002) (Figure 6).

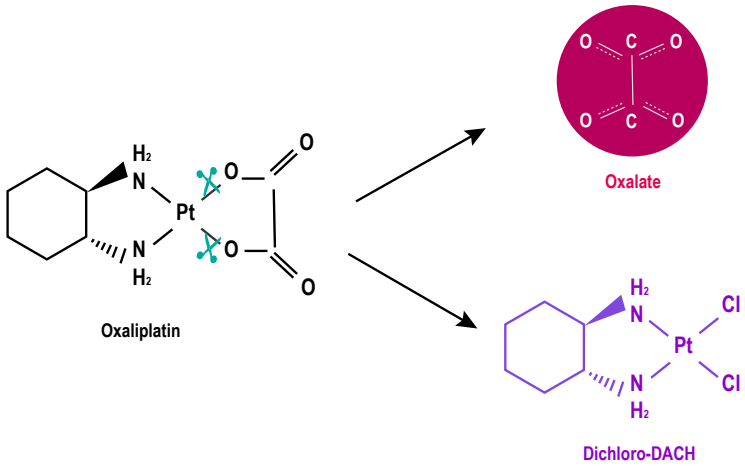

Figure 6. Biotransformation pathway of oxaliplatin. Oxaliplatin is rapidly hydrolyzed *in vivo* to oxalate and dichloro-DACH by displacement of the oxalate group by H_2O and Cl^- ions.

3.2 Clinical use

Platinum drugs have been the treatment of preference for several tumor malignances over the past decades, and nowadays remain as the first line treatment against high prevalent cancers, including

small and non-small cell lung cancer (NSCLC), prostate, testicular, head-and-neck, bladder, gynecologic, and colorectal cancers. In addition, they are highly used in the treatment of pediatric caners such as neuroblastoma, osteosarcoma, hepatoblastoma, retinoblastoma and brain tumors (Ghosh, 2019).

In 1978, the US Food and Drug Administration (FDA) approved for the first time the use of cisplatin for the treatment of several solid cancers. Nowadays, cisplatin is the first-line treatment against germ cell tumors. In addition, it is used as an adjunctive treatment in ovarian, cervical, medulloblastoma, bladder, head-and-neck, esophageal and lung cancers (Ghosh, 2019). First observations of cisplatin-induced peripheral neuropathy rapidly appeared in a young woman treated with cisplatin for osteosarcoma (Kedar et al., 1978).

Following the success of cisplatin as a chemotherapeutic agent, and with the aim of reducing its neurotoxic profile, new platinum-based agents were developed. Carboplatin was accepted for their usage in the clinical practice in 1989. Nowadays, it is the drug of choice for ovarian cancer and can be administered as adjuvant in other malignances like germ cell, bladder, endometrial and head-and-neck tumors. Carboplatin is considered to be less potent than cisplatin in terms of its antineoplastic action. In fact, depending on the type of cancer, carboplatin can only be 1/8 to 1/45 as effective (Lokich and Anderson, 1998). In contrast, carboplatin presents a lower excretion rate than cisplatin (Siddik et al., 1987)

Oxaliplatin is the most recent platinum drug approved as an antineoplastic agent. During the last years, it has been incorporated in combination with other agents (Leucovorin, 5-FU and/or Bevacizumab) as a first-line treatment against colorectal cancer (Grothey and Goldberg, 2004). Moreover, it has been approved for the treatment of other gastrointestinal malignances.

All three drugs are administered intravenously. However, recommended doses differ between them. Cisplatin is administered in 21-days cycles in a dosage range of 20-100mg/m^2 surface area depending on the primary tumor and the adjunctive therapy. Recommended doses for oxaliplatin depend on the duration of the treatment cycle. Most commonly, 85mg/m^2 are administered in 14-days cycles, whereas 110-130mg/m^2 is less common given in 21-days cycles. In the case of Carboplatin, dosage is calculated according to a target area under the curve (AUC) based on the glomerular infiltration rate instead of mg/m^2 of body surface. Target AUC is normally between 5 and 7mg/mL/min for previously untreated patients and between 4-5mg/mL/min for previously treated patients (Chu and DeVita, 2021).

In addition of the three approved platinum drugs, other second and third platinum analogues are being tested in clinical trials around world (picoplatin, zeniplatin, satraplatin, tetraplatin,

heptaplatin and LA-112). A liposomal formulation of cisplatin (lipoplatin) has demonstrated efficacy in phase II and III trials in NSCLC and it is being currently tested in other type of cancers (Xu et al., 2018). Other analogues as Nedaplatin and Lobaplatin are approved only in Japan and China, respectively.

3.3 Mechanisms of action in cancer treatment

The anti-tumor effectiveness of platinum drugs has been mainly attributed to their capacity of binding Doxyribonucleic Acid (DNA), thus interfering with DNA repair mechanisms, inhibiting DNA synthesis and mitosis, and inducing apoptotic cell death.

Platinum agents can get into the cells by two main mechanisms: passive diffusion through the plasma membrane, or active transport through the Copper Transporters (CTR) and the Organic Cation/Carnitine Transporters 1 and 2 (OCT1 and OCT2, respectively) (Sprowl et al., 2013) (Figure 7a).

All platins act as prodrugs, requiring replacement of their leaving ligands (chlorides or carboxylate-based ligands) with water to be activated. This process is known as aquation and takes place inside the cell, where the low Cl^- concentration results in the replacing of the leaving groups for water ligands (Figure 7a). Then, activated platinum agents are highly reactive and can bind to different intracellular biomolecules. One of the main targets of active platinum agents are the nucleophilic centers on nuclear DNA (nDNA). Specifically, platinum drugs crosslink with the N7 reactive center on purine bases. Predominantly, they bind to guanine (G), but also can bind to adenosine (A). In fact, the most common changes in the DNA template are the 1,2-intrastrand d(GpG) adducts and the 1,2-intrastrand d(ApG) adducts, which represent about the 85-90% of all adducts (Figure 7b). 1,3-intrastrand d(GpXpG) adducts and other adducts like inter-strand crosslinks and nonfunctional adducts have been reported to also contribute to platinum toxicity and represent the 2-6% of total adducts (Ghosh, 2019). Because of platinum-DNA (Pt-DNA) crosslinks, DNA transcription and replication are inhibited, resulting in apoptotic cell death of tumor cells.

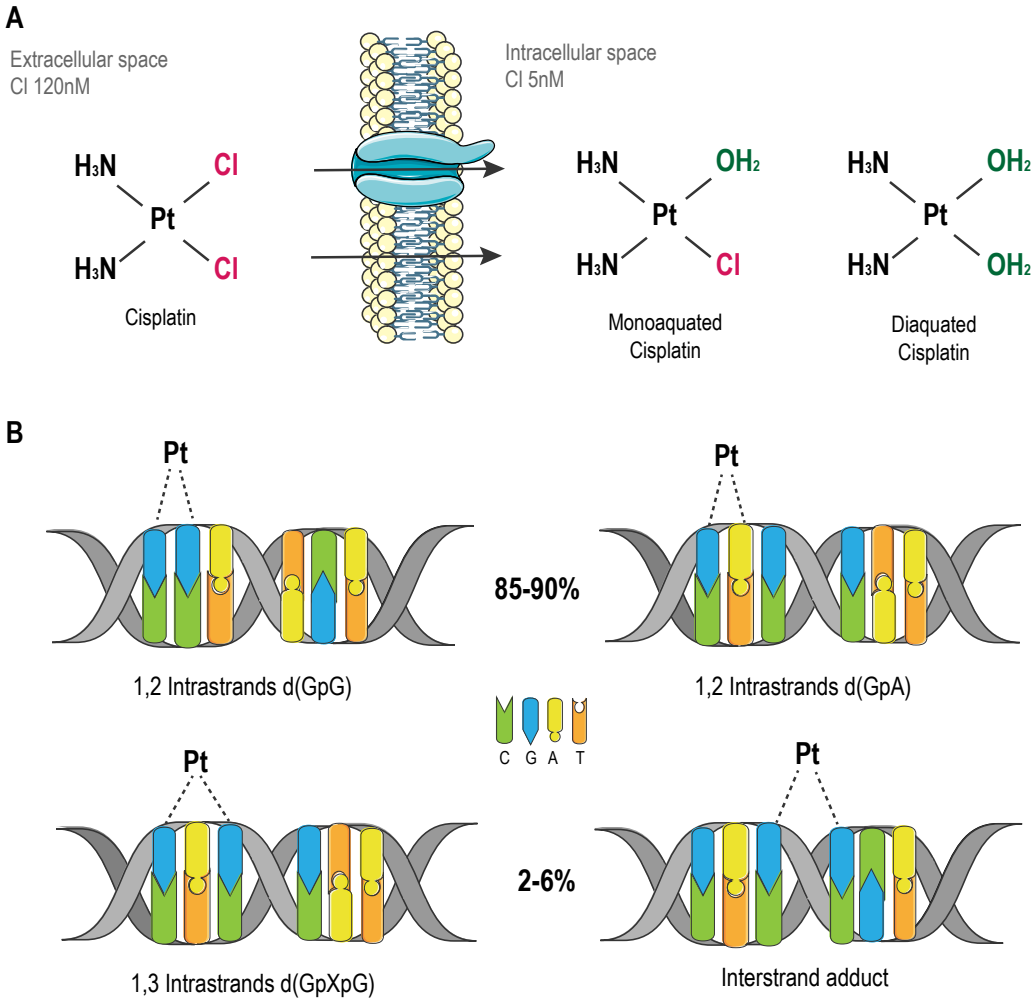

Figure 7. **Cellular uptake, aquation and DNA crosslink of platinum agents. A:** Schematic representation of cisplatin uptake by the cells, which can be done by passive diffusion or through transporters. Once inside the cell, the low concentrations of chloride (Cl^-) replace the leaving group by water in a process known as aquation. Similar processes take place with carboplatin and oxaliplatin. **B:** Examples of the most common Pt-DNA adducts formed in the DNA template.

Another mechanism related with platinum cytotoxicity is the induction of oxidative stress due to depletion of the cytoplasmatic antioxidant reserves. This phenomenon takes place when activated platinum agents bind to glutathione, methionine, metallothionein and other cysteine-rich proteins of the cytoplasm, which have an antioxidant potential. Therefore, there is an increase of reactive oxygen species (ROS), which induce the oxidation of several lipids, proteins and nucleotides of the cell (Ghosh 2019). The increase in ROS levels is also exacerbated by the damage of mitochondria due to the binding of platinum drugs to the mitochondrial DNA (mtDNA).

Despite their high efficiency in the treatment of cancer, the use of platinum drugs is limited due to their dose-limiting side effects, caused by the poor selectivity of platinum drugs for cancerous tissue over normal tissue. Their clinical use has revealed as many as 40 off-target side effects related to

these drugs. It includes nephrotoxicity, ototoxicity, hematological toxicity, cardiotoxicity, gastrointestinal toxicity, hepatotoxicity and neurotoxicity. On the following sections, we will talk about the neurotoxic effect of platinum drugs in the PNS.

4. Platinum-Induced Peripheral Neuropathy (PIPN)

Despite the extensive use of platinum drugs in the last 50 years, peripheral neuropathy remains one of the most relevant and not modifiable, dose-limiting, adverse events (Argyriou et al., 2012). The development of PIPN is a common event of all three platinum analogues. However, the general neurotoxic profile differs among them due to significant differences in their solubility, chemical reactivity, leaving groups and pharmacokinetics.

4.1 Incidence and risk factors

Equally to other neurotoxic cytostatic agents, the main risk factors for PIPN development are the total cumulated dose (TCD) and the dose-intensity that patients receive during the treatment. As commented before, TCD and dose-intensity will vary depending on the platinum analogue. In addition, the combination schedule with different neurotoxic chemotherapies is also a factor that increases the risk of developing PIPN (Chaudry et al., 1994, 2003; Viens et al., 2006).

Regarding cisplatin, 60% of patients receiving conventional cumulated doses of 250-300mg/m^2 develop a peripheral neuropathy. At high cumulated doses of 500-600mg/m^2, PIPN is present in almost all the patients, and it is severely disabling in at least 10% of them. The recovery is usually incomplete, and neuropathy can persist for 15 years in the 30% of patients. From those, 10% will still have neuropathic symptoms 30 years after the treatment cessation (Argyriou et al., 2012).

Carboplatin is associated with a lower risk of peripheral neuropathy probably because its development was based on its structure-activity relationship. Replacement of the chloride ligands of cisplatin by bis-carboxylate ligand of carboplatin results in a significantly reduced rate of aquation, and so, reduced level of toxicity compared with cisplatin. In fact, at conventional doses (≤6 AUC), only 6-10% of patients treated with carboplatin develop symptoms of neuropathy, which are less severe than the ones seen in cisplatin-treated patients with conventional doses. However, at high doses (>6 AUC), carboplatin causes higher rates of neuropathy with features of cisplatin neurotoxicity (Argyriou et al., 2012).

In the case of oxaliplatin, PIPN occurs in up to 80% of patients receiving conventional doses. Severe neuropathy manifests in 10% of patients with cumulated doses around 510-765mg/m^2, and in a 50%

of patients at doses up to 1000mg/m^2. Oxaliplatin-induced neuropathy persists in the 35% of patients during 5-6 years after treatment completion. As an exceptional feature of oxaliplatin, it also causes an acute transitory neurotoxic syndrome that manifests within or some hours after the treatment infusion. This acute syndrome is experienced by almost all patients receiving oxaliplatin at any moment along the treatment (See details in the next section) (Argyriou et al., 2012).

In addition of treatment-related risk factors (TCD, dose-intensity and combination schedules, other individual factors have been related with a higher probability of developing PIPN. Possible predisposing conditions include age, gender, renal dysfunction, diabetes, or pre-exiting neuropathies. However, there are conflicting results in regards with the potential higher risk of developing PIPN under these situations (Velasco and Bruna, 2010).

During the last years, few studies have attempt to determine gene polymorphisms that could be useful to identify patients at high-risk of developing PIPN. The first studies on that field were focused on polymorphisms of genes involved in the biotransformation of platinum drugs and mechanisms of DNA repair. More recently, interest has grown around genes encoding for proteins related with PIPN pathophysiology such as ion channels activity, neuronal development and function, apoptosis and oxidative stress (see in next sections). Despite different studies have been conducted on that field, none of them have yet yielded any validated marker for genetic susceptibility to PIPN (For an extended review on this topic see Argyriou et al., 2017).

4.2 Clinical, electrophysiological, and morphological features

As commented in the section above, the incidence and severity of PIPN differ between platinum compounds. However, once the neurotoxicity is stablished, the clinical picture is common for the three drugs, with only few distinct patterns between them.

The chronical exposure to platinum drugs causes a progressive pure sensory neuropathy in which the damage of large myelinated sensory fibers is predominant. The first symptoms and signs that appear include a decreased vibratory sensitivity in the toes and loss of ankle jerks, associated with numbness and paresthesia in finger and toes that manifest in a typical sock-and-glove distribution. Prolonged treatment aggravates the signs and symptoms and extends them to more proximal limb areas, with a loss of deep tendon reflexes. Pain and thermal sensation, joint position and light touch perception are less severely affected. In some cases, Lhermitte's sign can also be observed. In the worst cases, the loss of proprioception may result in ataxic gait. According to the clinical picture, nerve conduction studies (NCS) consistently demonstrated that PIPN is a sensory neuronopathy. Patients experience a reduction of sensory nerve action potential (SNAP) with normal or slightly decreased sensory nerve conduction velocities (SNCV). No changes in motor nerve conduction

velocities (MNCV) or compound muscle action potential (CMAP) are reported (Krarup-Hansen et al., 2007; Roelofs et al., 1984). Despite PIPN mainly develops during or at the end of the treatment, signs and symptoms can worsen or even appear 2-6 months after treatment cessation, in the so-called coasting effect phenomenon (Brouwers et al., 2009). Unfortunately, in most of the cases complete recovery of the symptoms is never achieved (Briani et al., 2014; Velasco and Bruna, 2014).

In addition, oxaliplatin-induced acute syndrome is characterized for being transient and not cumulated dose dependent. It is characterized by a cold-induced disturbing paresthesias and dysesthesias in the distal extremities and perioral region, as most prominent and frequent symptom. Less common but well described manifestations are jaw stiffness, cramps, shortness of breath, and difficulty in swallowing. These symptoms start during or within hours after oxaliplatin infusion and resolve within a week (Velasco and Bruna, 2014). Electrophysiological findings related to acute oxaliplatin neuropathy show the presence of repetitive CMAPs after one single stimulus and high frequency discharges of motor units, typical of excessive nerve excitability (Lehky et al., 2004; Wilson et al., 2002; Hill et al., 2010). These abnormalities are solved within 3 weeks after oxaliplatin administration (Lehky et al., 2004). Quantitative sensory testing (QST) shows that perception thresholds to vibration and thermal stimuli are usually impaired after oxaliplatin infusion. Moreover, a reduction in refractoriness parameters and superexcitability has been demonstrated in axonal excitability studies (Park et al., 2011). Acute peripheral neuropathy to oxaliplatin, documented by either clinical symptoms or QST, is associated with the development of chronic peripheral neuropathy (Park et al., 2009, Velasco et al., 2015).

Clinical and electrophysiological evaluations suggest peripheral nerve degeneration after platinum treatment. However, a morphological corroboration of this data is difficult due to limited accessibility of peripheral nerves or DRGs samples from patients. In fact, only post-mortem DRGs samples are available. In contrast, biopsies of the sural nerve have been performed in some studies. Electron microscopy of peripheral nerves from cisplatin-treated patients revealed axonal degeneration of large-myelinated fibers as well as secondary myelin breakdown (Thompson et al., 1984). However, patient tissue samples are under confounding factors like other chemotheray treatments or the heterogeneity in the time between treatment and sample collection, among others. Morphological data of intra-epidermal nerve fibers (IENF) is easier to acquire as skin biopsies are simple to perform and less aggressive for patients. Some studies report morphological alterations of IENF such as axonal swellings (axonal enlargements) and fragmentation (Velasco et al., 2017). However, conflicting results have been published regarding the degeneration of IENF after platinum treatment (Kroigard et al., 2014; Koskinen et al., 2011; Burakgazi et al., 2011).

5. Pathophysiological mechanisms of PIPN

The main target of platinum drugs in the PNS are the neuronal somas located in the DRG. In fact, many studies demonstrated that the severity of PIPN correlates with the amount of platinum drugs cumulated in the DRG (Gregg et al., 1992). The functional nature of these neurons altogether with the fact that they are the main target of platinum drugs justify the pure sensory profile of PIPN.

As happens in tumor cells, platinum agents can get into neurons by passive diffusion through the plasma membrane or by active transport through the CTR1, OCT1 and OCT2 (Jong et al., 2011; Liu et al., 2013). Once inside the neuron, platinum agents are activated by aquation.

Many studies point out apoptosis of DRG sensory neurons as the main cellular mechanisms involved in PIPN development. DNA damage, mitochondrial dysfunction and oxidative stress seem to play a key role in the activation of pro-apoptotic pathways after platinum exposure in neurons. Moreover, alterations in ion channel's function, calcium homeostasis and inflammatory processes have been linked to the development of PIPN, mainly to the oxaliplatin-induced acute syndrome. The main pathophysiological mechanisms described up to now for PIPN development are summarized in Figure 8.

5.1 Nuclear DNA damage as a trigger of apoptosis

Although DRG sensory neurons are post-mitotic and non-dividing cells, several studies show that the number of Pt-DNA adducts formed in their nDNA correlates with the neuronal apoptotic phenomena in dissociated cultures of the DRG (Ta et al., 2006). Moreover, there is a correlation between the amount of Pt-DNA adducts levels in DRG neurons and the severity of neuropathy measured by NCS in *in vivo* models of PIPN (Dzagnidze et al., 2007). *In vitro* studies show that at the same equimolar concentration, cisplatin present a higher neurotoxic profile than oxaliplatin (Ta et al., 2006). This could be explained by the fact that cisplatin forms about three times more Pt-DNA adducts than oxaliplatin. This further confirms the idea that the severity of the neuropathy induced by platinum drugs depends on the levels of Pt-DNA adducts. On the other hand, the number of Pt-DNA adducts also correlates with a decrease in the global neuronal transcription and body size, resulting in neuronal atrophy (Yan et al., 2015).

Activation of pro-apoptotic pathways could be caused by the lack of repair of the structural DNA damage. The Nucleotide Excision repair (NER) system represents the main recognition mechanism and possible fixing system of Pt-DNA adducts (Acklin and Xia, 2021). Although NER recognizes all types of intra-strands cross-links, the 1,2 intra-strand crosslinks induced by platinum drugs are less efficiently repaired by NER, suggesting that these DNA lesions are more cytotoxic. Moreover,

several DNA repair mechanisms including NER are down-regulated in terminally differentiated neuronal cells (Nouspikel and Hanawalt, 2002). Thus, DRG neurons may not be able to efficiently remove Pt-DNA adducts due to an inefficient NER pathway. On the other hand, remaining Pt-DNA adducts hinder a correct transcription by the ribosomal RNA polymerase (Ang et al., 2010), causing an incomplete protein synthesis and the consequent cell atrophy. As neurons have a high metabolic activity, the lack of dense ribosomal RNA synthesis could be lethal for them. Similarly, NER is also involved in the repair mechanisms of nucleosome DNA damage. It has been reported that NER is completely inhibited by Pt-DNA adducts in nucleosomes, so damage cannot be fixed, and transcription of cisplatin-damaged nucleosomes is completely blocked at Pt sites (Todd and Lippard, 2010). As nucleosome is crucial for modulating many cellular processes like recombination, replication, transcription and DNA repair, its alteration has strong detrimental consequences for the cells and could be involved in platinum neurotoxicity.

So NER pathway plays a crucial role in modulating platinum neurotoxicity. In fact, studies on the kinetics of cisplatin-DNA adducts formation in mice either proficient or deficient for NER machinery show how essential is the role of NER systems in the survival of DRG neurons after the exposure to platinum drugs (Dzagnidze et al., 2007). Thus, an increasing expression of genes encoding proteins involved in the NER repair systems could help in eliminating Pt-DNA adducts in sensory neurons and thus avoid the activation of pro-apoptotic pathways.

A recent study has shown that the treatment with cisplatin up-regulates the levels of DNA polymerase kappa (Pol k) in DRG cultures (Zhuo et al., 2018). DNA pol k is involved in bypass synthesis of diverse DNA lesions and is considered a vital player in cellular survival under injurious conditions. When depleting the levels of Pol k by small inhibitory RNA (siRNA), the cisplatin-induced DNA repair synthesis was decreased. Moreover, Pol k down-regulation exacerbated the suppression in global transcription induced by cisplatin in DRG neurons. These findings provide evidence for critical role of Pol k in neuronal DNA damage response after cisplatin treatment (Zhuo et al., 2018).

In addition to nDNA damage caused by the direct binding of platinum drugs to purine bases of the DNA, neurons can also experience a DNA oxidative injury due to the increased levels of oxidative stress in the cell (further explained in the following section). The main mechanism used to repair DNA oxidative injuries is the base excision repair (BER) pathway, in which the apyrimidinic endonuclease/redox effector factor (Ape-1) plays a key role. This is a multifunctional protein with both redox and endonuclease activity that seems to be crucial in platinum neurotoxicity. In fact, the treatment of DRG cultures with cisplatin causes a neuronal death associated with an increased levels of ROS and Ape-1 protein. When up-regulating Ape-1 expression, neuronal survival improved significantly (Jiang et al., 2008). On the other hand, Ape-1 has also been involved in NER

machinery and so in the repair of Pt-DNA adducts. In fact, when silencing this protein, the repair of Pt-DNA adducts is inhibited and the number of apoptotic phenomena dramatically increase in neuronal cultures treated with cisplatin (Kim et al., 2015). Similar results were seen in cultures treated with a mutant form of Ape-1 that lack the endonuclease activity, but not when lacking the redox one (Kim et al., 2015). These results suggest that the endonuclease activity of Ape-1 is important for the regulation of DNA repair pathways of Pt-DNA adducts and oxidative injury induced by platinum drugs.

Gill and Windebank hypothesized that the cytotoxic action of cisplatin in DRG neurons could be promoted by the attempt to re-entry into the cell cycle after DNA damage (Gill and Windebank, 1998). However, as the DNA of those neurons present multiple lesions, they are unable to complete DNA replication and rapidly die by apoptosis. This idea was later confirmed with the findings reported by Alaedini and colleagues (2008), in which they found an increased expression of genes related with cell cycle regulation and apoptosis like *Ccnd1* (Cyclin D1), *Cdkn1a* (p21), and *Hrk* (BID3). However, apoptosis activation has not been further reported in other *in vivo* models of PIPN.

5.2 Mitochondrial damage and oxidative stress as triggers of apoptosis

Mitochondria are small organelles involved in many important cellular processes including energy production, storage of intracellular calcium and calcium signaling, apoptosis, regulation of membrane potential and cell metabolism. The main function of mitochondria is to produce adenosine triphosphate (ATP) via aerobic respiration. In healthy tissues, mitochondria produce small amounts of ROS such as peroxide, superoxide, hydroxyl radicals and singlet oxygen as a by-product of oxygen metabolism. These radicals carry out important functions in cell signaling (Starobova and Vetter, 2017).

Platinum agents and other cytostatic drugs cause mitochondrial damage (mytotoxicity) in non-neuronal and neuronal cells. Several studies using both *in vitro* and *in vivo* models show functional and morphological changes in neuronal mitochondria after platinum exposure. In general terms, mitochondria appear swollen and vacuolated, and with altered ATP production (Podratz et al., 2011). But, why are mitochondria damaged by platinum drugs?

As happens with nDNA, platinum drugs can directly bind to the mtDNA forming Pt-mtDNA adducts randomly around the mitochondrial genome. mtDNA is a circular DNA that encodes for 13 proteins. These proteins are involved in mitochondrial electron transport chain subunits synthesis and so in cellular energy production. mtDNA also encodes the 22 transfer RNA (tRNA) and 2 ribosomal RNA (rRNA), which are essential to produce these proteins. Similar to nDNA,

mtDNA platination causes the disruption of mtDNA replication and transcription, leading to altered protein synthesis and functional errors of the respiratory chain. Because NER and BER pathway do not work at the mitochondrial level, mtDNA lesions are not removed and chronically remain in the DNA template. The result of this chronic mtDNA damage is and energy deficit of the cell due to the constant alteration in ATP production. In the PNS, mitochondria are crucial for axonal transport, a process highly energy dependent (Canta et al., 2015). Energy failure due to mytotoxicity has been linked to degeneration of peripheral nerve fibers in different neurodegenerative diseases as well as after chemotherapy treatment (Pathak et al, 2013; Bennet et al., 2014). In fact, a recent study suggests that mtDNA damage by platinum drugs is sufficient to induce axon degeneration independently of nDNA damage and p53 activation in primary sympathetic neuronal cultures (Geden et al., 2021).

Myotoxicity induced by platinum drugs is also associated with an increased production of ROS in the DRG (Leo et al., 2020; Khasabova et al., 2019). In addition, and as commented above, activated platinum drugs bind to glutathione, methionine, metallothionein and other cysteine-rich proteins, leading to a depletion of cytoplasmatic antioxidant defenses. In tumor cells, all these phenomena contribute to the onset of oxidative stress, which has been linked to the opening of mitochondrial permeability transition pores (mPTP) and the consequent cell death through release of cytochrome C (Bernardi et al., 2006; Cullen et al., 2007). Similarly, the increased levels of ROS in neurons after cisplatin and oxaliplatin treatment have been associated to an activation of apoptotic mitochondrial (intrinsic) pathway through release of cytochrome C, Bax translocation and activation of Caspase-3 (Gill and Windebank, 1998; McDonald and Windebank, 2002; Donzelli et al., 2004; Massicot et al., 2013; Waseem and Parvez, 2016). Other pro-apoptotic phenomena associated to oxidative stress in neurons after platinum exposure are translocation of Smac/Diablo and HtrA2/Omi factors to the mitochondria and activation of PARP1 protein (Calls et al., 2020).

On the other hand, oxidative stress also leads to damage of intracellular biomolecules such as proteins, lipids, and nucleotides. Oxidation of intracellular molecules has been related with demyelination, inactivation of antioxidant enzymes, and damage to microtubules (Areti et al., 2014). Intracellular oxidative stress has been also related to peripheral nociceptor sensitization by elevating the levels of proinflammatory cytokines after some cytostatic agents' exposure (Cook et al., 2018; Malcangio, 2019). All these metabolic, bioenergetic and functional deficits in neurons contribute to peripheral nerve degeneration, inflammatory processes, and the development of neuropathic pain (Xiao et al., 2012; Fukuda et al., 2017; Areti et al, 2014).

5.3 Calcium homeostasis dysregulation

Calcium (Ca^{2+}) has a key role in regulating many cellular physiological processes. Its free intracellular concentration, which is usually maintained at nanomolar levels, is tightly regulated by various transport and sequestration mechanisms, including extracellular influx and release from internal stores, as well as efflux via plasma membrane pumps and uptake into the endoplasmic reticulum and mitochondria. Changes in intracellular Ca^{2+} concentration influence membrane excitability, neurotransmitter releases and gene expression on neuronal and glial cells (Starobova and Vetter, 2017; Carozzi et al., 2015). Alterations in Ca^{2+} homeostasis and signaling have been suggested to contribute to the development of oxaliplatin and cisplatin neurotoxicity.

Oxalate is a Ca^{2+} chelator that has been proposed to contribute to the development of oxaliplatin-induced cold syndrome and pain. Chelation of extracellular Ca^{2+} by oxalate treatment leads to an increase in Na^{+} conductance and decrease of threshold potential and membrane resistant in mice (Deuis et al., 2013), which has been linked to pain development. In contrast, increased levels of extracellular Ca^{2+} concentrations increase the probability of Na^{+} channel closure and result in decreased excitability of peripheral neurons (Armstrong and Cota, 1999). Indeed, local injection of oxalate into the footpad of mice induces spontaneous nocifensive behaviors (Sakurai et al., 2009; Deuis et al.,2013). However, the dose needed to observe those effect is much higher than the dose of oxaliplatin required to induce neuropathic pain (Deuis et al., 2013). In addition, the phenotype of pain behaviors indued by oxalate differs from oxaliplatin-induced neuropathy, which is characterized by cold allodynia and a lack of spontaneous nocifensive behavior (Deuis et al., 2013). These data suggest that oxalate may be not the unique responsible for pain development in oxaliplatin-induced neuropathy.

Although effects on intracellular calcium levels have been reported in sensory neurons, the contribution of Ca^{2+} to cisplatin-induced neuropathy is poorly understood. In sensory neurons, cisplatin increased the expression of N-type voltage-gated Ca^{2+} (Ca_v) channels, although it differentially affects the functions of specific Ca_v channel subtypes (Tomaszewski and Büsselberg, 2007; Leo et al., 2017). Erol et al., reported that high levels of cisplatin increased the levels of intracellular Ca^{2+} ions through the release from internal stores, whereas low concentrations of cisplatin induce the accumulation of Ca^{2+} into the cells by activating L-type Ca_v (Erol et al., 2016). Similar, a recent study reported that acute oxaliplatin treatment increased the spike's amplitude, expression, and current densities of L- and T-type Ca_v channels in rat small DRG neurons (Schmitt et al., 2018). However, the contribution of these effects to the clinical presentation of cisplatin- and oxaliplatin-induced neuropathy remains unclear.

Finally, the increase of oxidative stress and the impairment of mitochondrial buffering capacity via opening of the mPTP have been associated to increased levels of basal intracellular Ca^{2+} in small DRG neurons after paclitaxel (Siau and Bennet, 2006). These results could be translated to platinum drugs neurotoxicity, as they also cause mitotoxicity and opening of mPTP.

5.4 Ion channels dysregulation

The hypothesis that ion channel dysregulation is an inductor of platinum neurotoxicity is mainly limited to the acute syndrome generated by oxaliplatin infusion.

Changes in sensory nerve excitability in patients treated with oxaliplatin, including a significant increase in the duration of the relative refractory period, have been attributed to effects on voltage-gated Na^+ (Na_v) channels expressed at the nodes of Ranvier (Krishnan et al., 2005). Altered Na_v channel function was observed in rodent peripheral axons as well as DRG neurons, where oxaliplatin caused an increase in Na^+ current, inhibition of maximal amplitude, and the emergence of enhanced resurgent and persistent current amplitudes (Adelsberger et al., 2000; Webster et al., 2005; Sittl et al., 2012). The chelator activity of oxalate against Ca^{2+} and Magnesium (Mg^{2+}) ions can alter the kinetics of Na_v channels inducing prolonged open state and thus neuronal hyperexcitability (Grolleau et al, 2001). The $Na_v1.6$ isoform seems to be involved in the development of oxaliplatin-induced cold allodynia. Cooling-induced bursts of action potential firing were abolished in neurons from mice lacking functional $Na_v1.6$ (Sittl et al., 2012). Moreover, acute oxaliplatin-induced pain behaviors were abolished by treatment with a selective $Na_v1.6$ inhibitors (Egashira et al., 2010; Kawashiri et al., 2012; Deuis et al., 2013, 2014). Similar, cisplatin-induced mechanical allodynia was also ameliorated with that inhibitor, although cisplatin does not directly affect gating properties of $Na_v1.6$ (Deuis et al., 2014).

In addition to Na_v channels, there is also growing evidence supporting a possible role of potassium (K^+) channels in acute oxaliplatin neurotoxicity. However, it stills remain controversy. There are four major types of K^+ channels expressed in the PNS: voltage-gated K^+ (K_v) channels, Ca^{2+}-activated K^+ channels (K_{ca}), two-pore K^+ channels (K_{2p}) and inwardly rectifying K^+ channels (K_{ir}). Effect of neuronal K^+ channels further exacerbate altered neuronal excitability in PIPN. Specifically, decreased expression of several K_v channels was found after oxaliplatin treatment in rodent DRG neurons (Descoeur et al., 2011). The decreased level of a specific type of these channels ($K_v2.2$) was related with pain behaviors and neuronal hyperexcitability in the cortex (Thibault et al., 2012). In addition, a repetitive firing following a single stimulus and a dose-dependent increase of the duration of the repolarization phase after hyperpolarization were observed by treatment with oxaliplatin in the isolated sciatic nerve of adult rat (Kagiava et al., 2008). All these phenomena are consistent with an inhibition of K_v channels.

In addition of acute effects on sensory neuron excitability, it has also been reported that exposure to either oxaliplatin and cisplatin increase expression and enhance activity of several thermo- and mechano-sensitive Transient receptor potential (TRP) channels, including TRPV1, TRPA1 and TRPM8 (Gauchan et al., 2009; Ta et al., 2010; Descoeur et al., 2011; Nassini et al., 2011; Yamamoto et al., 2015; Mizoguchi et al., 2016). These ion channels are activated by stimuli of different nature (physical, mechanical, thermal or chemical) and are involved in the transduction of noxious stimuli (Marmiroli et al., 2015). However, the contribution of these channels to PIPN is not clear, with studies attributing functional effect to all, some or none of these transducer ion channels.

5.5 Contribution of non-neuronal cells and inflammation

Although sensory neurons have been the focus of almost all studies related to PIPN pathogenesis, it is important not to forget the potential role of other non-neuronal cells in the pathogenesis of PIPN.

It is well known that chemotherapy activates the innate and adaptative immune systems, which can lead to neuroinflammation and thus contribute to the development of peripheral neuropathy (Starobova and Vetter, 2017). It has been reported that oxaliplatin-induced mechanical hyperalgesia and IENF loss was prevented by treating animals with minocycline, an antibiotic that inhibits macrophages and microglia (Boyette-Davis and Dougherty, 2011; Di Cesare Mannelli et al., 2014). Oxaliplatin also leads to an increase in the levels of some proinflammatory cytokines in the periphery (Stojanovska et al., 2019) and the nervous system (Xu et al., 2018), which can lead to sensitization of nociceptors (Loprinzi et al., 2007, 2011; Callizot et al., 2008; Wang et al., 2012; Zhang et al., 2012, 2016; Makker et al., 2017). In addition, this agent also increased the levels of circulating and peripheral CD4+ and CD8+ lymphocytes in mice and down-regulates regulatory T cells (Makker et al., 2017; Stojanovska et al., 2018, 2019).

On the other hand, chemotherapy seems to also have an effect on peripheral glial cells, including Schwann cells and SGCs. As commented above, SGCs are unique cells that wrap around neuronal cell bodies in the DRGs. They supply nutrients to the surrounding neurons and also have some structural functions. Additionally, they express a variety of receptors that allow for interactions with neuroactive chemicals. Many of these receptors and other ion channels have recently been implicated in pathological conditions including chronic pain (Hananai and Spray, 2020). There is much more to be learned about these cells, and research surrounding additional properties and roles of the SGCs is ongoing. Regarding PIPN, it has been reported that oxaliplatin increased glial fibrillary acidic protein (GFAP) expression in SGCs. Gap junction-mediated coupling between SGCs surrounding neighboring neurons was increased by up to five-fold after oxaliplatin treatment

(Warwik and Hanani, 2013). This is consistent with works on other pain models showing that augmented SGCs coupling contributes to chronic pain. In fact, administration of the gap junction blocker carbenoxolone to chemotherapy-treated mice produced an analgesic-like effect (Ledda et al., 2009; Huang et al., 2010). In agreement with this finding, studies demonstrated that the number and activation of SGCs significantly increased after oxaliplatin treatment in rat DRG, when thermal allodynia and mechanical hyperalgesia were significantly induced (Di Cesare Mannelli et al., 2013, 2014). Corsetti and colleagues studied the morphological changes in SGC after cisplatin treatment in a rat model of PIPN. They showed that SGCs sheath around neurons was increased. Moreover, SGCs had increased number of dense bodies and increased volume of mitochondria. Comparative analysis from SGCs and neurons showed that morphological changes occurred primary in the SGC, supporting the idea that SGC could be the initial target of cisplatin treatment (Corsetti et al., 2000). A recent study showed that cisplatin-induced activation and functional modulation of SGCs lead to cytokine-mediated modulation of sensory neurons excitability in culture (Leo et al., 2021).

Schwann cells are in charge of myelinating the peripheral axons and play a crucial role in the outgrowth and guidance of regrowing peripheral axons after neve injury. Therefore, impairment of Schwann cells and consequent disruption of intercellular interactions between myelin-forming mature Schwann cells and axons by anti-cancer agents may be important for the pathogenesis of peripheral neuropathy. Both cisplatin and oxaliplatin induced Schwann cells toxicity accompanied with mitochondrial dysfunction at concentrations lower than those required to induce neurotoxicity *in vitro* (Imai et al., 2017). In addition, after cisplatin treatment there was a decrease in myelin-forming Schwann cells in a Schwann cell/DRG neuron co-culture, without causing any evident damage to neurons (Imai et al., 2017). However, NCS in animal models neither in patients show features compatible with peripheral demyelination issues.

Glial cells from the CNS can also contribute to PIPN establishment. Studies on microglia and astrocytes show increased levels and reactivity of both cell types in spinal cord and some brain regions related with pain after oxaliplatin treatment. This glial reactivity has been linked with the induction of mechanical and thermal hyperalgesia in both mouse and rat models of PIPN (Lee and Kim., 2020).

Finally, it is well known that tumor progression induces systemic changes in different tissues like liver, bone, adipose tissue and skeletal muscle, giving place to a general metabolic wasting syndrome known as cachexia (Biswas and Acharyya, 2020). On the other hand, it has been reported that tumor malignances also modulate the immune system of oncologic patients (Allen et al., 2020). However, the role of the systemic effects of tumor malignances in the development of PIPN has been scarcely explored. Only one study reported that the development of thermal and mechanical

allodynia did not differ between rats treated with cisplatin alone and rats receiving cisplatin with previous tumor inoculation (Lin et al., 2015).

5.6 Other pathways

Phosphoinositide 3 kinase (PI3K) is a key anti-apoptotic effector that promotes cell survival by phosphorylation and activation of the protein Akt. It has been observed in primary and organotypic DRG neuron cultures that cisplatin induced a transient decrease of pAKT levels, which could impair neuronal survival (Maggioni et al., 2010).

Previous studies demonstrated that the interaction of cisplatin with cytoskeletal microtubule proteins (MTP) can also contribute to neuron viability impairment (Boekelheide et al., 1992; Tulub and Stefanov, 2001). The cisplatin-MTP interactions might negatively affect the morphological integrity of axons and axonal transport. Both fast anterograde and retrograde axonal transport of organelles and macromolecules are required for delivery of membrane components and trophic factors necessary for cell maintenance. A failure in these deliveries could contribute to the development of peripheral neuropathy (McLean, 1984, 1997).

Finally, López-González et al. (2018) investigated the mechanisms of oxaliplatin toxicity on axons through the evaluation of molecules involved in axon guidance. They showed that overexpression of a particular miRNA molecule (miR-204) in sensory neurons was responsible for the reduction in the neurites' length after oxaliplatin treatment. This up-regulation was correlated with the down-regulation of the semaphorin membrane receptor PLXNA2, a miR204 target, but not with any change in apoptosis rate. PLXNA2 mediates axon repulsion, dendritic arborization, axonal projection and neurite outgrowth and is important for peripheral nerve sprouting and correct positioning (Ebert et al., 2014; Kunath et al., 2017). In addition, López-González et al. (2018) demonstrated that other miRNAs, such miR-30-5p, miR-15-5p and miR-101-3p, were also overexpressed in response to oxaliplatin treatment and are predicted to target several axon guidance molecules.

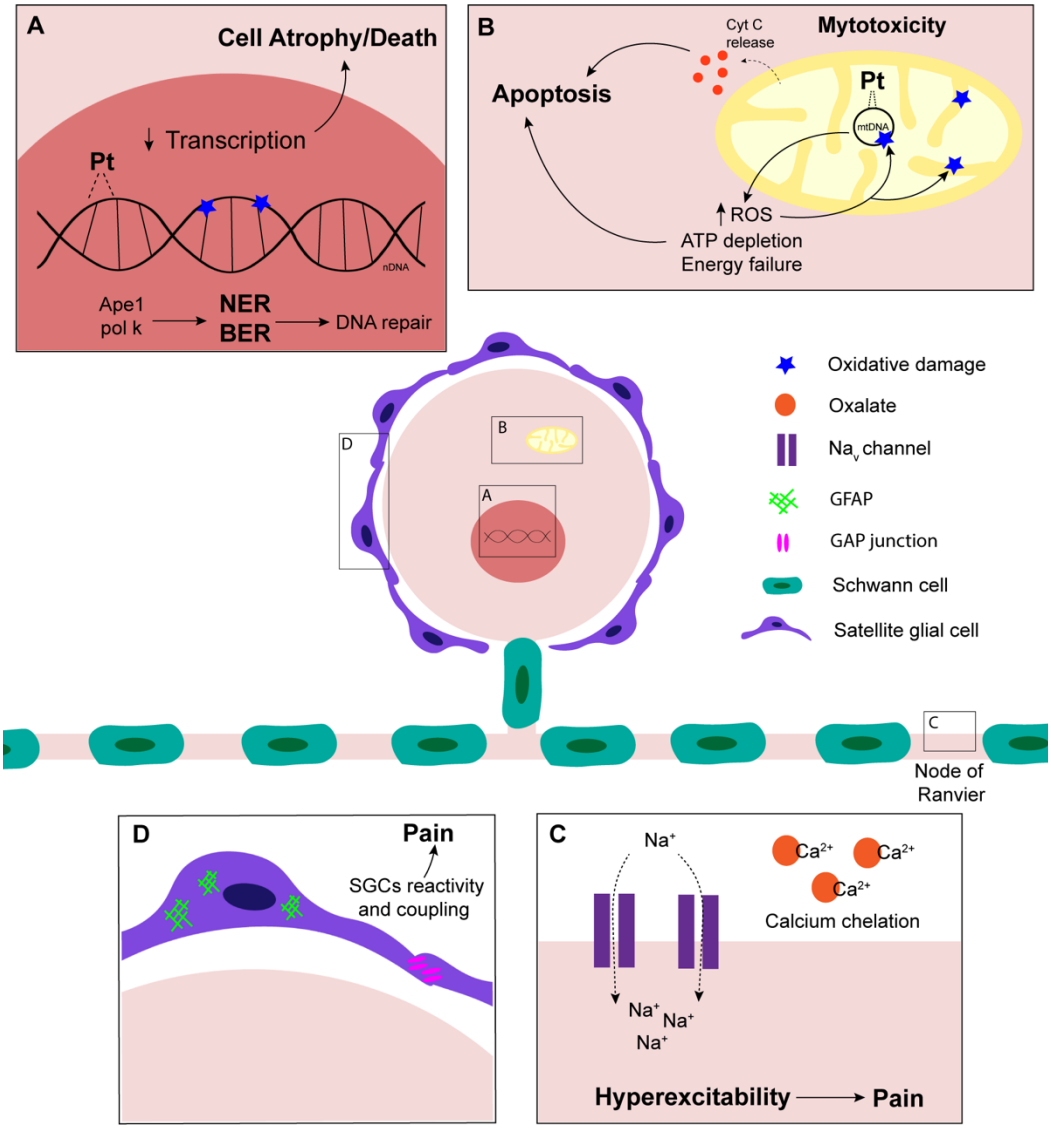

Figure 8. Summary of the main mechanisms involved in PIPN pathophysiology. A-B: After cellular uptake and aquation, activated platinum (Pt) can react with different macromolecules of the cell, including nDNA (A) and mtDNA (B). Due to inefficiently NER and BER pathways, nDNA and mtDNA damage remains and activates pro-apoptotic intrinsic pathways leading to neuronal death. Increased levels of oxidative stress due to mitotoxicity and depletion of antioxidant reserves enhance apoptosis activation. **C:** Increased activity of Na_v channels results in hyperexcitability of the neurons, which is involved in nociceptive behaviors. Chelation of extracellular Ca^{2+} ions by oxalate seems contribute to the hyperexcitability phenomena. **D:** Satellite glial cell (SGC) reactivity and coupling could play a key role in the development of pain after platinum infusion.

6. Translation of the preclinical data

As discussed above, the development of PIPN emerge as multifactorial and involves several heterogeneous mechanisms. However, it is still unclear which effect(s) initiate the pathological

cascade leading to neuronal dysfunction. Thanks to the cumulated knowledge on PIPN pathogenesis, mostly based on *in vivo* and *in vitro* models, several neuroprotectant molecules have been tested for the prevention and treatment of PIPN. Although many of these molecules have been effective in preclinical settings, none have been successfully translated into the clinics. This lack of transnationality may reflect the limitations on the current knowledge on PIPN etiopathogenesis, ranging from the reliability of the preclinical models, that not always are able to closely mimic the clinic scenario, to the consistency and relevance of the pathophysiological pathways explored.

6.1 Limitations of PIPN experimental models

There are two main models used for the study of PIPN: *in vitro* and *in vivo* models (for an extended review on this topic see Calls et al., 2020). On the next sections, their advantages and limitations are going to be exposed (Table 2).

6.1.1 In vitro models

Most of the studies focused on a better understanding and modeling of PIPN are based on *in vitro* models of platinum neurotoxicity. Considering that the main target of platinum compounds are the sensory neurons of the DRG, most of the studies use primary cell cultures derived from mouse or rat DRGs. However, neuronal cell lines like PC12, the human neuroblastoma cell line SH-SY5Y or immortalized DRG neurons are also used (Lehmann et al., 2020). There are several *in vitro* models reported for the study of platinum neurotoxicity, and each of them uses different cell types, doses ranges and outcome measures (Calls et al., 2020).

Although *in vitro* models are cost- and time-effective and allow controlling the physico-chemical environment surrounding the neurons (i.e pH, temperature or supply of nutrients), the translation of the results into the clinic is rarely successful due to many limiting factors. On one hand, cellular cultures do not allow the study of complex interactions among different types of cells residing in the tissue of interest. For example, DRG dissociated primary cultures are often treated with nerve growth factor (NGF), which promotes the survival and growth of a specific subtype of sensory neurons: the small, unmyelinated or thin myelinated ones. Thus, the larger neurons are loss and not included in the results. Taking into account that platinum drugs mainly affect the large and myelinated sensory nerve fibers, NGF+ selection may be artificing the results. Similarly, in some cases cultures are treated with anti-mitotic drugs (i.e Floxuridine or arabinosie) to avoid the proliferation of non-neuronal cells residing in the DRG (SGC, Schwann Cells, fibroblasts, macrophages and others) and thus obtaining a pure neuronal culture. In all that cases, the complex interaction between different cell populations that take place *in vivo* is completely missed. Moreover, antimitotic agents can be toxic for the neuronal population, and thus artefact the

experimental outcomes. In that scenario, mixed cultures could seem less artificial and resemble more to the physiological situation. Nevertheless, the presence of non-neuronal cells to the cultures can be a limiting factor when analyzing the activation of specific signaling cascades in the neurons. In that cases, single-cell strategies or immunofluorescence analysis using specific neuronal/glial markers should be conducted (Lehmann et al., 2020).

On the other hand*, in vitro* models do not mimic the drug pharmacokinetics of PNS exposure to the platinum agents in terms of entry, distribution and elimination of compounds to the cells, which are protected by the *BNB* or *BDB.*

Another limitation of *in vitro* studies is that most of them are based on rodent models. Although it has been reported that rat and human DRG proteomes share >75% of similarities (Schwaid et al., 2018), rodent-based *in vitro* models are considered artificial. Moreover, the mouse/rat strain used in the studies can interfere with the results due to differences in neurotoxic susceptibility. For example, neurons obtained from C57BL/6J and Balb/CJ mice are more vulnerable to cisplatin neurotoxicity than the ones obtained from other strains (Podratz et al., 2016). The age of the animal when dissecting the DRGs is also a crucial aspect to considerate when working *in vitro*. Postnatal neurons rapidly downregulate TrkA receptor (Bennet et al., 1996; Molliver and Snider, 1997), which is essential for NGF signaling, and may respond differentially to molecules of the environment (Filbin, 1995; Mukhopadhyay et al., 1994). Moreover, postnatal neurons change the expression of signaling pathways and transcription factors in culture (Isensee et al., 2017). In that way, adult-derived DRG cultures are more appropriated than the embryonic- or postnatally derived ones for modeling PIPN as it primarily affects adults whose sensory neurons are fully mature (Lehmann et al., 2020). However, many studies used embryonic cells for that purpose.

To bypass the species handicap, some people have set up human cell-based *in vitro* models as they are considered less artificial. Humanized *in vitro* models are based in the induction of pluripotent embryonic stem cells into neurons by using specific cell culture conditions (Chambers et al., 2011). Neurons derived from these methods are heterogenous with regard to expression of specific markers for neuronal subpopulations, and so comparable to the situation *in vivo* (Alshawaf et al., 2018). Recent studies demonstrate that human induced pluripotent stem cells (hiPSC) offer an opportunity to generate sensory neurons (Wainger et al., 2015; Hoelting et al., 2016; Wheeler et al., 2015; Wing et al., 2017). However, the process to convert these cells into neurons is tedious and time intensive with low efficiency in terms of reprogramming and genetic instability. Moreover, they are not originally neurons, and small variations in the differentiation protocols may result in significant changes (Lehmann et al., 2020).

Another problem of *in vitro* models is the outcome analyzed as a measure for platinum neurotoxicity or for the potential neuroprotective action of new therapies. In many cases, the measured outcome is quite different from the one used in patients settings, so its relevance to human disease is uncertain. For example, as apoptosis has been reported as the main mechanisms underlying PIPN, the neuronal viability after platinum exposure is one of the most used outcomes when testing neuroprotective molecules. Different probes can be used for that purpose, including propidium iodide (PI), that only penetrate in permeabilized (death) cells; fluorescein diacetate that label alive cells; or TUNEL (terminal deoxynucleotidyl transferase dUTP nick end labeling). Metabolic-based assays are also used for neuronal survival assessments. It includes MTT, which is a direct measure of mitochondrial function, and quantification of ATP levels, which decrease along with cell death. An important limitation of cell viability assays is that other mechanisms rather than neuronal cell death may contribute to platinum neurotoxicity *in vivo*, and functional and metabolic impairment can occur even at sublethal doses. Moreover, other process rather than cell death can also affect mitochondrial function or ATP levels. However, most of the viability assays are easily adaptable for high throughput screening and may be used in an initial screen for potential neuroprotective compounds (Lehmann et al., 2020). Another important outcome for the *in vitro* study of platinum neurotoxicity are electrophysiological recordings. The patch clamp technique allows the study of channels and receptors function of neurons *in vitro*. Thanks to these techniques, it was known that oxaliplatin alters currents of Ca_v channels (Leo et al., 2017; Schmitt et al., 2018). An alternative to the classical patch clamp technique is the use of multi-well multielectrode arrays to record spontaneous activity in whole DRG cell cultures (Newberry et al., 2016). Finally, axon integrity and neurite length have also been used to assess platinum neurotoxicity, although DRG neurons do not develop any arborization *in vivo* (Lehmann et al., 2020).

It is obvious that *in vitro* models have been essential to determine some of the main molecular mechanisms involved in platinum neurotoxicity. However, results obtained from *in vitro* studies need to be validated in animal models as they can better reproduce the clinical features of PIPN and so give us a better understanding of the exact pathophysiological mechanisms. In fact, animal models maintain signaling pathways and complex cellular interactions that can be essential for the progression of PIPN. Moreover, *in vivo* models are better than the *in vitro* ones for a long-term drug exposition studies due to the limited viability of cells in culture.

6.1.2 In vivo models

For PIPN study, rodent models are the most extensively used as their genome is similar to the human one with an average homology of 85% for the protein-coding regions (source: National Human Genome Research Institute). Moreover, a good genetic/molecular toolbox is available, and the animal's small size facilitates large scale/high throughput studies making it a cost-efficient

model. Nevertheless, other species like Drosophila melanogaster, guinea pig or Non-human primates have been used in few studies (Working et al., 1998; Szilvássy et al., 2006; Shidahara et al., 2016; Podratz et al., 2017; Groen et al., 2018).

There are several rodent animal models of PIPN reported in the bibliography, which have been developed using different strains of either mouse or rat, and different dose schedules of platinum drugs, mainly oxaliplatin and cisplatin. Due to this high heterogeneity in animal models development, results regarding electrophysiological, functional and morphological features are rarely reproducible between them and not always comparable with the symptoms seen in patients (Calls et al., 2020). In addition, differences in platinum susceptibility among mouse strains can also contribute to this heterogeneity (Marmiroli et al., 2017). Similar, Seto et al., demonstrated that the time of the day in which cisplatin was administered influenced the severity of the neuropathy in mice (Seto et al., 2016). Thus, it is crucial to specify the dosing time as it can be a confusing factor when analyzing the results.

In most of the studies, the TCD, calculated by suing the FDA system to equalize humans and animal doses (Reagan-Shaw et al., 2008; Nair and Jacob, 2016), is far from those employed in patients in the regular schedule of cancer treatment. On the other hand, the route for drug administration differs between patients and animals in many cases, thus compromising the pharmacokinetic variables potentially involved in the PIPN genesis. Platinum drugs are administered by intraperitoneal route in most of the animal models, and few administered oxaliplatin intravenously, in contrast with the endovenous administration in patients treated with platinum drugs (Calls et al., 2020).

The methods used to evaluate the development and severity of PIPN are another limiting factor of *in vivo* models. Clinical examination and anamnesis are the best practices to diagnose and grade the severity of PIPN in patients, in addition to the complementary information provided by NCS. However, the first one cannot be applied to animals for obvious reasons. Thus, NCS are one of the most used outcomes when assessing PIPN in *in vivo* models. In fact, NCS are often used to determine the starting point and severity of the neuropathy. Nevertheless, many studies only report nerve conduction velocities, which are minimally affected or preserved in patients, and only few report SNAPs. In some models, motor conductions also appear decreased, which is a feature not recorded in patients. To complement NCS data, behavioral tests are also conducted. Von Frey, Plantar, Tail immersion and Cold Plate tests are frequently used to assess the development of mechano- and thermal- hyperalgesia after platinum treatment. Similar to NCS, there is a lot of controversy regarding the results of these behavioral tests among models (Calls et al., 2020).

Another frequently used outcome in animal models of PIPN is the morphological evaluation of both DRGs and peripheral nerves. Some morphological alterations have been seen in DRGs of rats and

mice treated with oxaliplatin or cisplatin, including a decrease in the somatic and nuclear size of sensory neurons, which also present multiple and segregated nucleoli. Axonal degeneration, loss of myelinated fibers, decreased fiber caliber, increased G-ratio or loss of IENF have been reported in some animal models. However, results are often contradictory between studies, doses and schedules of treatment (Calls et al., 2020). Moreover, it is not clear that patients also suffer peripheral nerve or IENF degeneration. Molecular techniques such as western blot, qPCR or RNA sequencing of peripheral nerves and DRGs have been key for determining the main molecular mechanisms related with platinum neurotoxicity in animal model. However, as happens with *in vitro* models, in all the studies reported until the date the whole DRG is analyzed without previous isolation of sensory neurons. Thus, results can be masked by other cell types present in the DRG and peripheral nerves. This problem is only bypassed by immunofluorescence staining, so collabeling the molecules of interest with neuronal specific markers, or alternatively, by the previous isolation of cells before any downstream analysis.

Table 2. Advantages and limitations of experimental models of PIPN. Inspired by *Lehmann et al., 2020*

	In vitro	In vivo
Advantages	Cost and time effective	Less artificial
	Easly adaptable for high throuhput screening	Allow the interaction of different functional systems/organs/cell types
	Allow controling the physico-chemical environment surrounding the neurons	Allow to identify potential interactions among neuroprotectant drugs and the efficiency of the antitumor treatment
		More suitable for pharmacokinetic and pharmacodinamic studies
Limitations	Dosn't allow the study of different cell types interactions	Time and cost consuming
	Artificial	Microenvironment less well controled
	Analyzed outcomes not always relevant for human disease	Analyzed outcomes not always relevant for human disease
	Don't reflect potential metabolism of compounds to active metabolites in non-neuronal tissues	Cumulated doses and administration routes are not equivalent to the patient's ones

6.2 Current clinical trial strategies for PIPN neuroprotection and treatment

Neuroprotection could be defined as a group of strategies focused on protecting the PNS from the toxic effects of anticancer drugs. In contrast, treatment of the neuropathy includes those strategies that intent to regenerate the PNS after the damage has already occurred.

Treatment of stablished PIPN aims to relieve the so called “positive symptoms” like neuropathic pain or tingling. The type of drugs typically recommended for those symptoms are topic analgesics, antidepressant and anticonvulsants including duloxetine, gabapentin, pregabalin or amitriptyline. Despite the widespread use of these drugs, duloxetine is the only drug found to be associated with a significant reduction in neuropathic pain induced by PIPN in a randomized phase III intervention (Smith et al., 2013). For that reason, the American Society of Cancer and American Society of Clinical Oncology does not endorse the prescription of other pharmacological therapy or nutraceutical agents besides duloxetine. When duloxetine treatment fails or is not indicated, other conventional anticonvulsants or tricyclic antidepressant drugs may be useful for symptomatic control in patients with CIPN. However, evidence of their effectivity, specifically in CIPN, is still limited. As such, the treatment approach is analogous to usage of these drugs in other forms of neuropathic pain (Jordan et al., 2019). For the negative symptoms related with PIPN (i.e. mechanical and vibration hypoesthesia), no drug has yet been stablished.

Nowadays, the most effective strategy to prevent the development of severe PIPN is the dose reduction of chemotherapy or even the complete cessation of treatment. Observations of reversibility of oxaliplatin-induced neurotoxicity led de Gramont and colleagues develop the Stop and Go (OPTIMOX) approach with the goal of increasing the cumulative oxaliplatin dose that can be given. Briefly, the therapy was disrupted before severe neurotoxicity developed and the drug was later reintroduced. Although this strategy showed lower rates of grade 3 neurotoxicity without compromising response rates, results were no significant (de Gramont et al., 2000). For that reason, it is not a routine practice in clinic.

Some clinical trials show that moderate-intensity exercise may have beneficial effects in both the neuroprotection and treatment against CIPN from several chemotherapeutic agents including platinum drugs. Patients undergoing exercise experience a reduction in temperature sensitivity and sensory neuropathic symptoms (Kleckner et al., 2018). However, higher quality research is warranted as exercise interventions, dosages, and settings have been too heterogeneous to identify the most beneficial intervention for CIPN-related outcomes (Kanzawa-Lee et al., 2020; Tanay et al., 2021).

Regarding pharmacological prevention of PIPN, none of the neuroprotective agents tested in human prevented or limited neurotoxicity by platinum compounds (Albers et al., 2014). Most of the strategies tested were focused on targeting mechanisms related with PIPN development such as oxidative stress, mitochondrial impairment, calcium homeostasis dysregulation and ion channels (more specifically TRP and Na^+ channels) (Quintao et al., 2019). Most of these agents correspond to dietary antioxidant and nutraceuticals due to their wide range of safety and tolerability. They include acetyl-L-carnitine, acetylcysteine, α-lipoic acid, Glutathione, omega-3 fatty acids,

Glutamine, Vitamin E or Vitamin B (Areti et al., 2014). Other strategies that showed no significant outcomes included Ca^{2+}/Mg^{2+}infusion before and after oxaliplatin treatment, carbamazepine, diethyldithiocarbamate or minocycline (Hershman et al., 2014; Hou et al., 2018; Jordan et al., 2019). However, results must be interpreted with caution as clinical trials in this area are often underpowered and heterogeneous.

Novel pathways are currently being tested in preclinical settings to prevent the development of PIPN. One pathway focuses on cellular transport of platinum drugs and aims to perform genetic or pharmacological knockout of transporters localized to the DRG in mice. Novel studies show that knockout or pharmacological modulation of the organic cation transporter novel type 2 (OCTN2) protects from oxaliplatin-induced neuropathy (Sprowl et al., 2016). In that sense, there is an ongoing phase Ib trial and double-blinded, placebo-controlled, randomized phase II study with the aim to determine the safety and pharmacology of dasatinib, an OCTN2 inhibitor (NCT04164069). The findings obtained from this study will provide future directions on the potential of inhibition of uptake transporters as a prevention strategy to reduce the onset, incidence, and severity of various forms of CIPN.

A second molecule of interest is Ape-1 due to its role in eliminating Pt-DNA adducts. The pharmacological induction of Ape-1 by the small-molecule APX3330 showed an increase in BER activity, while simultaneously showing anticancer effects (Kelley et al., 2016). APX3330 is entering on human clinical trials as an antineoplastic agent as well for prevention of PIPN (NCT03375086).

Carvedilol, an antihypertensive and cardioprotectant drug, also shows promising activity in preclinical settings. In rodent models, administration of carvedilol reduced the levels of ROS and increased the expression of mitochondria superoxide dismutase (SOD) in sciatic nerve and DRG. Moreover, this drug has the potential to prevent alterations in mitochondrial membrane potential in sciatic nerves and thus the loss of IENF (Areti et al., 2017). There are ongoing studies evaluating carvedilol for a variety of clinical conditions but none for the prevention of CIPN. As there are current cancer trials evaluating the cardioprotective properties of carvedilol, prevention of CIPN might be considered as an exploratory endpoint (Hu et al., 2019).

The drug Calmangafodipir mimics the mitochondrial enzyme manganese superoxide dismutase and reduces ROS levels and subsequent nerve damage (Karlsson et al., 2015). This drug was associated with reduction in CIPN symptoms during and after oxaliplatin treatment in a phase II double-blinded randomized study (Glimelius et al., 2018). Two international trials (POLAR A and POLAR M) were started with the goal to determine the efficacy of this drug for the prevention of oxaliplatin-induced neuropathy in colorectal patients. These phase III, multicenter, placebo-controlled trials

evaluate stage II and III patients (POLAR A, NCT04034355) and metastatic patients (POLAR M, NCT03654729).

MR309, a selective sigma-1 receptor (S1R) antagonist, has been tested in a proof-of-concept, explorative, phase II, randomized, double- blind, placebo-controlled clinical trial (Bruna et al., 2018). S1R antagonism or inactivation has demonstrated analgesic activity in several models of neuropathic pain in animals, including CIPN (Romero et al., 2012; Nieto et al., 2012, 2014). The results of the clinical trial showed that MR309 significantly reduced cold hypersensitivity and allodynia as well as the hyperexcitability motor symptoms and signs in active patients. This demonstrates its usefulness in decreasing acute oxaliplatin syndrome, considered one of the first steps to developing chronic peripheral neuropathy. Secondly, MR309 significantly reduced the proportion of patients who developed severe chronic peripheral neuropathy compared with the placebo group. Interestingly, premature withdrawal due to cancer progression was less frequent in the MR309 group. In conjunction with the good tolerability adverse events reported, MR309 showed a safety profile for being used in oncological patients. However, MR309 usefulness on the neuroprotective effect against chronic peripheral neuropathy induced by oxaliplatin remains to be clarified. In fact, no differences were observed in NCS and neurological assessment scales between active and placebo groups. However, the implicit limitations in the nature of the exploratory design of the trial cannot be overlooked (Bruna et al., 2018).

Moreover, recent pre-clinical studies have shown the efficacy of activators of the peroxisome proliferator-activated receptor gamma (PPARγ) on neuropathic pain models (Okine et al., 2019). Compounds that activate PPARγ are known as glitazones and can be employed to treat type 2 diabetes and metabolic syndrome. Moreover, they have been considered potential therapeutic drugs to treat a large number of neurological conditions such as neurodegenerative diseases, traumatic injury demyelinating diseases, chronic pain and also neuropathic pain induced by PIPN (Quintao et al., 2019).

Finally, it is important to take in consideration that any putative treatment for PIPN must not interfere with the anti-tumor effects of the causative chemotherapeutic agent. This is not easy due to similarities in the toxic mechanisms of platinum drugs in both tumor and neuronal cells.

IV. HYPOTHESIS & OBJECTIVES

Hypothesis

A constellation of heterogeneous mechanistic pathways related with PIPN have been studied and described in the past 50 years. Most of the times, no comparable results have been obtained between studies. It is partially caused by differences in models and outcomes used. In general, these studies were hypothesis-driven from the known actions of platinum drugs in neoplastic cells. However, the harsh reality shows a lack of relevant advances in PIPN prevention and treatment in basis of these results. We hypothesize that a throughout mechanistic study, without driven-hypothesis and using well characterized animal models resembling PIPN in patients, can arise significant mechanistic pathways related with PIPN and will help to identify relevant therapeutic targets.

Objectives

The general objective of the present thesis is to determine specific molecular pathways related with the development of PIPN that could lead to therapeutic actions against this adverse event. The specifics objectives were:

1. **To develop and characterize mouse models of peripheral neuropathy induced by the main neurotoxic platinum drugs, oxaliplatin and cisplatin.**
2. **To study the influence of a tumor environment in the development of PIPN.**
3. **To study the changes in the gene expression profile of DRG sensory neurons after platinum (cisplatin or oxaliplatin) treatment.**
   - 3.1 To isolate mice DRG cell populations by single-cell sorting.
   - 3.2 To compare the transcriptomic profile of DRG sensory neurons between control and platinum-treated mice by single-cell RNA-sequencing (scRNA-seq).
   - 3.3 To corroborate the results of the scRNA-seq at the protein levels
4. **To characterize an *in vitro* model of platinum neurotoxicity to test new therapeutical targets based on the *in vivo* data.**
   - 4.1 To set up an *in vitro* model that mimics the cisplatin-induced neuronal toxicity observed *in vivo*.
   - 4.2 To characterize the pathological profile of cultured neurons by RNA-sequencing (RNA-seq).

V. MATERIALS & METHODS

1. *In vivo*-based studies

All the procedures of this thesis involving mice were approved by the Ethics Committee of the Universitat Autònoma de Barcelona (CEEA) and the *Direcció General de Polítiques Ambientals I Medi Natural, Departament de Territori I Sostenibilitat* from *Generalitat de Catalunya*. All the experiments complied with the European Council Directive (2010/63/EU) and the Spanish National law (Real Decreto 53/2013).

1.1 Experimental design

To explore the molecular mechanisms involved in the development of PIPN, we followed the experimental design scheduled in Figure 9. Briefly, we developed two animal models of PIPN by injecting cisplatin or oxaliplatin to female adult mice. Once the animals developed the neuropathy, control and platinum-treated mice were scarified and their DRGs were freshly harvested and enzymatically dissociated. By single-cell sorting, individual cells of the DRGs were isolated in 96-well plates. Each sorted cell was sequenced by scRNA-seq, and its identity (neuron, SGC, endothelial cell, etc.) was defined by checking the expression of well stablished cell population markers. Finally, we compared the gene expression profile of DRG sensory neurons of control and platinum-treated mice. This way, we obtained the so called differentially expressed genes (DEGs), which are potential molecular targets for the treatment of PIPN. After identifying the DEGs, we corroborated the data by measuring protein levels of the genes of interest by western blot and immunofluorescence staining.

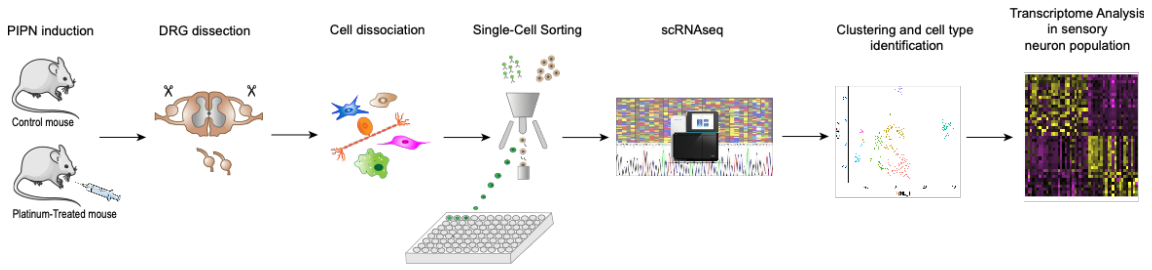

Figure 9. Schematic representation of the experimental design followed for the *in vivo* studies. Individual DRG cells of control and platinum-treated mice were isolated in 96-well plates by single-cell sorting. Each sorted cell was then sequenced by scRNA-seq and differences in the transcriptomic profile between control and platinum-treated cell populations were analyzed.

1.2 Animal models of PIPN

1.2.1 Animals

10-weeks-old female BALB/cAnNCrl (BALB/c) mice (19–22g on arrival at the housing room, Janvier) were used for the studies. Animals were housed in a limited access animal facility with ad libitum access to water and food. Artificial lighting provided a 24-hour cycle of 12 hours light/12 hours dark (light 8 a.m.–8 p.m.).

1.2.2 Platinum-based drugs

Cisplatin (Selleckchem, Cat# S1166) was dissolved in a sterile saline solution at a concentration of 0.5mg/ml and stored at -80ºC until its use. Oxaliplatin (Selleckchem, Cat #S1224) was prepared freshly the day of its use by dissolving it in 5% glucose solution to a concentration of 1mg/ml.

1.2.3 Induction of peripheral neuropathy by cisplatin treatment

To develop the cisplatin-induced peripheral neuropathy, mice were intraperitonially (i.p.) injected with cisplatin once a week for a total of 10 weeks. During the first 2 weeks of study (0-1 weeks), animals received a cisplatin dose of 7mg/kg. After that, mice were i.p. administered with 3.5mg/kg cisplatin for 8 additionally weeks (2-9 weeks). The TCD of cisplatin at the end of the study was 42mg/kg. As control group, mice received an i.p. injection of saline solution once a week for 10 weeks (Table 3). Immediately after each administration, mice received a subcutaneous (s.c.) injection of 1ml saline to prevent cisplatin-induced nephrotoxicity. Cisplatin was always administered around 3-4pm.

1.2.4 Induction of peripheral neuropathy by oxaliplatin treatment.

To induce oxaliplatin-induced peripheral neuropathy, mice were intravenously (i.v.) injected with 5mg/kg oxaliplatin twice a week for 8 weeks. TCD at the end of the study was 80mg/kg. In animals that experience a weight loss higher than 10%, the oxaliplatin dose was reduced to a half (2.5mg/kg) and maintained until the lost weight was recovered. In the control group, mice received an i.v. injection of 5% glucose solution twice a week for 8 weeks (Table 4). Immediately after each administration, mice received a s.c. injection of 1ml saline to prevent oxaliplatin-induced nephrotoxicity. Oxaliplatin was always administered around 3-5pm.

1.2.5 Tumor inoculation

To evaluate the effect of a neoplastic environment in the development of PIPN, a group of mice was inoculated with Colon 26 (C-26) cell line as previously reported (Acharyya et al., 2004). C-26

cells (Cell line Services, CLS Cat #440156) are a colorectal adenocarcinoma cell line derived from BALB/c mice. C-26 cells were maintained in RPMI 1640 medium (CLS, Cat#820700) containing 10% heat-inactivated Fetal Bovine Serum (hiFBS, Sigma, Cat #F7524). The day of tumor inoculation, C-26 cells were trypsinized, pelleted in complete medium, and subsequently resuspended in Dulbecco's Phosphate Buffered Saline (DPBS, Sigma, Cat #D8537) at a concentration of $5x10^4$ cells/ml. 200µl of cell suspension were injected s.c. into the left flank of mice one week before chemotherapy treatment started (Figure 10). Tumor size and body weight were monitored every week starting one week after tumor cell inoculum.

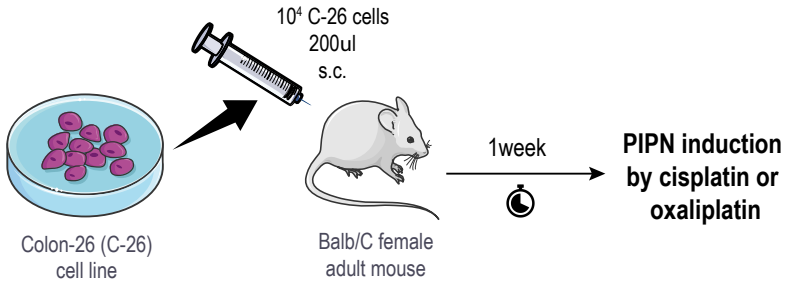

Figure 10. Schematic representation of the tumor inoculation. 10^4 Colon-26 (C-26) cells were injected subcutaneously (s.c.) into the mice one week before starting cisplatin or oxaliplatin treatment.

Tables 3 and 4 show a summary of all the experimental groups used in this thesis.

Table 3. Experimental groups used in the cisplatin study. CDDP: Cisplatin; Tx: Tumor; TCD: Total Cumulated Dose; i.p.: intraperitoneally; s.c.: subcutaneously; 1xw: once a week

	Group			
	Control	**CDDP**	**Tx**	**CDDP+Tx**
Chemotherapy treatment	Saline i.p. 1xw for 10w	0-1w: 7mg/kg Cisplatin i.p. 1xw 2-9w: 3.5mg/kg Cisplatin i.p. 1xw (TCD: 42mg/kg)	Saline i.p. 1xw for 10w	0-1w: 7mg/kg Cisplatin i.p. 1xw 2-9w: 3.5mg/kg Cisplatin i.p. 1xw (TCD: 42mg/kg)
Tumor inoculation	X	X	10^4 C-26 cells s.c.	10^4 C-26 cells s.c.

Table 4. Experimental groups used in the oxaliplatin study. OXA: Oxaliplatin;Tx: Tumor; TCD: Total Cumultated Dose; i.v.: intravenously; s.c.: subcutaneously; 2xw: twice a week

	Group			
	Control	**OXA**	**Tx**	**OXA+Tx**
Chemotherapy treatment	Glucose 5% i.v. 2xw for 8w	5mg/kg Oxaliplatin i.v. 2xw for 8w (TCD: 80mg/kg)	Glucose 5% i.v. 2xw for 8w	5mg/kg Oxaliplatin i.v. 2xw for 8w (TCD: 80mg/kg)
Tumor inoculation	X	X	10^4 C-26 cells s.c.	10^4 C-26 cells s.c.

1.3 General toxicity

The physical condition, behavior and reaction to touch of mice were evaluated once a week. Body weight was recorded for the assessment of the general toxicity and for dose adjustment. The last evaluation of the general toxicity was performed at the end of the experiment.

1.4 Nerve conduction studies (NCS)

To determine when the neuropathy started and how it progressed along time, we assessed the sensory and motor nerve conductions by using electrophysiological tests. The sciatic nerve was stimulated percutaneously through a pair of needle electrodes placed at the sciatic notch or at the ankle. The compound muscle action potential (CMAP) was recorded by electrodes placed at the plantar muscle. The sensory compound nerve action potentials (SNAPs) were recorded from the fourth toe near the digital nerve. The caudal nerve action potentials (CNAP) were also recorded by placing a couple of recording needle electrodes at the base of the tail and a couple of stimulating needle electrodes at 3.5cm or at 5cm distally to the recording points, elucidating the proximal and distal orthodromic sensory conductions respectively. Electrophysiological tests were performed before starting the treatment (baseline) and every two weeks during all experimental time.

1.5 Behavioral tests

To assess mechanical and thermal hyperalgesia in the animal models of PIPN, we conducted several behavioral tests, including Von Frey test, Plantar test, and Cold Plate test.

1.5.1 Von Frey test

Mechanical allodynia was tested by using electronic Von Frey test at baseline and either every three (cisplatin) or two (oxaliplatin) weeks during all the induction and coasting-effect times. Mice underwent training sessions three days prior to the first day of testing. On testing days, mice were placed in individual clear plastic cages on a wire mesh screen with a flat-surfaced plastic platform with holes through which von Frey hairs were inserted and applied to the plantar surface of the paw. Before every session, mice were acclimatized for 15 minutes to the experimenter, the room in which the behavioral experiments took place and the transparent chamber used for von Frey testing. The combined mean percent withdrawal of three applications to the left foot was calculated for each animal, and group means were calculated.

1.5.2 Plantar test

Plantar test was used to assess heat evoked hyperalgesia in the oxaliplatin animal model as previously reported (Cheah et al., 2017). Tests were performed at baseline and then every two weeks after starting the oxaliplatin administration and during all the induction and coasting-efect times. All the animals that had to be tested underwent training sessions three days prior to the first day of testing. In the training sessions, animals were used to the behavioral room and the investigator for 15 minutes. After that time, mice were individually placed into the transparent chambers situated in a farmed glass panel. To perform the test, the infrared emitter/detector was placed underneath the center of the mice paw and time (seconds) until paw withdrawal was measured. Three applications to the left foot were assessed for each animal, and group means were calculated. We set the Infrared intensity (IR) at 50 units.

1.5.3 Cold plate test.

Cold hyperalgesia was assessed in the oxaliplatin animal model with a Cold plate test (Biolabs) based on previous studies (Iftinca et al., 2020; Wang et al., 2021). Test was conducted every 2 weeks during all the induction and coasting-effect time. Animals underwent training sessions three days prior to the first day of testing. In the training sessions, animals got used for 15 minutes to the behavioral room, the investigator and the testing apparatus, a metal plate surrounded by a transparent metiplax cylinder. On testing days, the metal plate was cooled at -4ºC and cold hyperalgesia was assessed by measuring the withdrawal threshold time (seconds). Withdrawal was assessed as the first hind paw lift. Lifting for normal locomotion was excluded. Four tests were assessed for each mice and group means were calculated. 10 minutes interval between each measurement was established. To prevent tissue damage, a cut-off time of 60 seconds was adopted.

1.6 scRNA-seq analysis

At the end of the neuropathy induction time (10w for cisplatin study and 8 weeks for oxaliplatin study), 3-5 control and 3-5 treated mice of each group were scarified, intracardially perfused with DPBS w/o Ca^{2+} and Mg^{2+}(Sigma, Cat #D8537) and the transcriptomic profile of their DRG cell populations analyzed by scRNA-seq. For those studies, cisplatin- and oxaliplatin-treated mice were not selected in a randomized way but taking into account the data of the NCS. Thus, only those mice who have a decrease in their SNAP or CNAP >15% were selected.

The gene expression study of the cisplatin model was performed in collaboration with the Centro Nacional de Análisis genética (CNAG) from the Scientific Parc of Barcelona. For that study, the bioinformatic analysis of the data was conducted by Dr. Abel Torres-Espín from University of San Francisco. In the case of the oxaliplatin model, the transcriptomic study was performed in

collaboration with the Genomic Core facility from the Universitat Pompeu Fabra. The bioinformatic analysis was conducted by Marc Tormo Puiggros, the bioinformatician form the same facility. Thus, although the general concept of methodology was the same for both studies, some differences appear in regards with the library preparation and the bioinformatic analysis of the data.

1.6.1 Single-cell sorting of DRG cells

In each mouse, all DRGs were removed and cleaned from blood, connective tissue and root debris. Then, DRGs were enzymatically dissociated in $Ca2^{+}$ and Mg^{2+} free Hank's medium (Sigma, Cat #14170-088) with 10x trypsin (Sigma, #T-4674), 1µg/ml collagenase A (Sigma, Cat #C2674) and 1µg/ml DNAse (Roche, Cat #11284932001) for 30 minutes at 37ºC and with constant agitation. DMEM medium (Sigma, Cat #41966052) supplemented with 10% hiFBS (Sigma, #F7524) was added to stop the enzymatic reaction, and DRGs were exposed to mechanical dissociation with a glass pipette. After complete dissociation, cells were filtered in a 70µm cell strainer and centrifuged at 500rcg for 5 minutes to remove enzymes. Cells were incubated 1 hour at 4ºC and with constant agitation with primary antibodies rabbit anti-TrkA (1:200, Abcam, Cat #Ab76291), goat anti-TrkB (1:200, R&D systems, Cat #AF1494) and goat anti-TrkC (1:200, R&D Systems. #Cat AF1404), diluted in 200 µl incubation medium (Neurobasal-A (NB-A, Gibco, Cat #10088022) supplemented with 6mg/ml glucose, 2mM Glutamine (Sigma, Cat #G7513) and 5% hiFBS). After incubation time, collector tubes were complete filled with washing medium (Gey's Balanced medium (Sigma, Cat #G9779) supplemented with 6mg/ml glucose and 5% hiFBS) and centrifuged 3 times at 500rcg for 5 minutes at 4ºC. Samples were then incubated for 45 minutes at room temperature in dark conditions and with constant agitation with secondary antibodies Alexa 488-conjugated anti-goat (1:200, Invitrogen, Cat #A11039) and Alexa 488-conjugated anti-rabbit (1:200, Invitrogen, Cat #A21206) diluted in 200µl incubation medium. After incubation time, collector tubes were filled up with washing medium and centrifuged at 500rcg for 5 minutes at 4ºC. This step was repeated a total of three times to remove secondary antibody excess. At the same day, single-cell sorting of DRG cells was carried out using a FacsAria Fusion sorter (Beckton Dickinson), equipped with the ACDU (Automatic Cell Deposition Unit) option. Just before the sorting, cells were labeled with Propidium Iodide (PI, excitation at 561 nm – emission at 610/20nm) to exclude permeabilized cells. Alexa488 was excited with a blue (488nm) laser, and fluorescence collected at 530/30 nm. An unstained control was used to place the gate for the positive events. PI-/TRK+ single-cells were sorted into 96-well plates containing RNase Inhibitor solution (Life technologies). After sorting, plates were centrifuged for 1 minute at 4ºC and stored at -80ºC until their analysis by scRNA-seq (Figure 11).

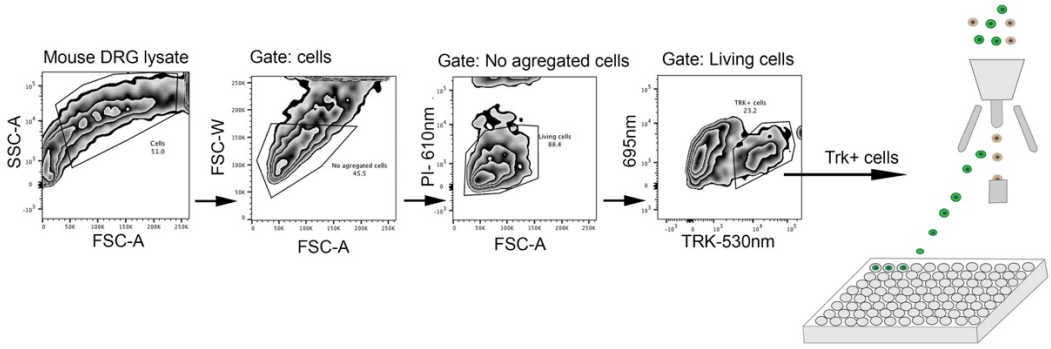

Figure 11. Single cell sorting strategy used to isolate DRG cells. Only cells that were negative for PI and positive for TRK labeling were selected and sorted into the 96-well plates. All other events were discarded.

1.6.2 RNA-isolation and library construction.

- **Cisplatin study**. Full-length scRNA-seq libraries were prepared using the Smart-seq2 protocol (Picelli et al. 2014) with minor modifications. Reverse transcription was performed using SuperScrpit II (Invitrogen) in the presence of oligo-dT30VN, template-switching oligonucleotides and betaine. The cDNA was amplified using the KAPA Hifi Hotstart ReadyMix (Kappa Biosystems), ISPCR primer and 25 cycles of amplification. Following purification with Agencourt Ampure XP beads (Beckmann Coulter), product size distribution and quantity were assessed on a Bioanalyzer using a High Sensitvity DNA Kit (Agilent Technologies). Two hundred picogram of the amplified cDNA was fragmented using Nextera® XT (Illumina) and amplified with indexed Nextera® PCR primers. Products were purified twice with Agencourt Ampure XP beads and quantified again using a Bioanalyzer High Sensitivity DNA Kit. Sequencing of Nextera® libraries was carried out on a HSeq2500 (Illumina) to obtain approximately 500,000 paired-end 75 bp reads per cell.

- **Oxaliplatin study**. scRNA-seq libraries were prepared using the NEBNext® Single Cell/Low Input cDNA Synthesis & Amplification Module (New England Biolabs) following the manufacturer's protocol, cDNA was amplified with 20 PCR cycles and validated in a Bioanalyzer High Sensitvity DNA Kit (Agilent Technologies, Cat #5067-4626), and between 2-5ng of cDNA was then used to prepare the libraries which were also validated using a Bioanalyzer High Sensitvity DNA Kit. Equimolar proportions of each library were mixed and the subsequent pool was quantified by qPCR and sequenced in a NextSeq High Output 2x75 run (Illumina).

1.6.3. Cell type clustering and transcriptome analysis

- **Cisplatin study.** After loading the count data into R as a Seurat object, the percentage of mitochondrial (%mit) counts in respect of all the counts per cell was calculated as a quality control measure. Cells with less than 100 total counts and with a %mit > 15% were discarded. Subsequently, count data was normalized using the "LogTransformation" method in the package. The 15000 most variable transcripts were kept for downstream analysis. For dimensionality reduction, principal component analysis (PCA) was performed after scaling and centering the data, and a permutation test (JackStraw() function in the package) was conducted to determine the number of principal components (PCs) to keep (the final number of PCs was 20). For cluster analysis, a shared nearest neighbor graph was constructed and the number of communities (clusters) identified by optimizing modularity (FindClusters() function with resolution = 0.6). A total of 7 clusters were obtained. We determined cluster identity (cell type) by computing the conserved transcripts (expressed in 95% of the cells of a given cluster, FindConservedMarkers() function) across cells from control and cisplatin animals and using the http://mousebrain.org/ atlas as reference (Linnarsson lab Mouse Brain Atlas, RRID:SCR_016999, Zeisel et al., 2018) for specific profile cell markers. For visualization purposes, a t-Distributed Stochastic Neighbor Embedding (tSNE) was conducted over the 20 PCs. The subsequent analysis was performed in the neuronal subset. DEGs between cells coming from control and cisplatin-treated animals were determined using the "MAST" method from the MAST R package (Finak et al., 2015) called through the FindMarkers() function in Seurat. Gene Ontology (GO) enrichment analysis was conducted using the limma package (Ritchie et al., 2015) on up-regulated (cisplatin vs. control) DEGs with p value ≤ 0.01.

- **Oxaliplatin study**. Reads were mapped using STAR software against the mouse reference GRCm38 and the Gencode annotation vM23. Thereafter, counts were obtained with HTSeq software and those results were assessed using MultiQC software. The total counts and percentage of mitochondrial (%mit) counts in respect of all the count per cells were calculated as a quality control measure. Cells that have more than 3 MADs (median absolute deviation) in some of these parameters were removed from the analysis as considered low-quality cells. After that, normalization by deconvolution was applied: Pool-based size factors (pool counts from many cells to increase the size of the counts for accurate size factor estimation) are "deconvolved" into cell-based factors for normalization of each cell's expression profile. For dimensionality reduction, PCA was performed after scaling and centering the data. After clustering the obtained PCs, data was subset to 8 PCs to reduce dimensionality. For cluster analysis, a shared nearest neighbor graph was

constructed and corrected by possible batch effects by plate. A total of 8 corrected clusters were obtained. The determination of cluster identity (cell type) was performed by SingleR comparing expression to published datasets (http://mousebrain.org/ atlas as reference - Linnarsson lab Mouse Brain Atlas, RRID:SCR_016999, Zeisel et al., 2018). For visualization purposes, a tSNE was conducted over the 8 identified clusters. The subsequent analysis was performed in the neuronal subset. DEGs between cells coming from control and oxaliplatin-treated animals were determined using "SCDE" method. Gene Ontology (GO) enrichment analysis was conducted on up-regulated or down-regulated (cisplatin vs. control) DEGs with p value ≤ 0.01.

1.7 Molecular methods

Different molecular techniques were performed to corroborate the data obtained in the scRNA-seq. For that, mice were deeply anaesthetized and intracardially perfused with saline (NaCl, 0.9%) solution at two main different time points: just at the end of the neuropathy induction time (10 weeks for cisplatin and 8 weeks for oxaliplatin) and at the end of the coasting-effect evaluation time (16 weeks for cisplatin and 10 weeks for oxaliplatin).

1.7.1 Western Blot analysis

All DRGs from lumbar to cervical segments were dissected from cold saline (NaCl 0.9%) perfused mice and immediately snap freeze in liquid nitrogen. DRGs were then homogenized in modified RIPA lysis buffer (50 mM Tris–HCl pH 7.5, 1% Triton X-100, 0.5% sodium dodecyl sulfate (SDS), 100 mM NaCl, 1 mM EDTA) adding 10 µl/ml of Protease Inhibitor cocktail (Sigma, Cat #P8340) and PhosSTOP phosphatase inhibitor cocktail (Roche, Cat #4906845001). Protein was quantified by BCA protein assay (Thermo Scientific, Cat #BCA1-1KIT) following the manufactured protocol. 15-30µg of protein of each sample were loaded into SDS-polyacrylamide gels. The transfer was made 1.5 hours at room temperature with a constant voltage of 90V. Membranes were then blocked with 5% Non-Fat Dried Milk (NFDM) or 5% Bovine Serum Albumin (BSA) in 0.1% Tween-20 in Tri-Buffered Saline (TBS) for 1 hour, and then incubated overnight at 4ºC and in constant agitation with primary antibodies (Table 5). Incubation with Horseradish peroxidase (HRP)-coupled secondary antibodies was performed for 90 minutes at room temperature and with constant agitation. Membranes were visualized using enhanced chemiluminescence method with the clarity western ECL substrate (Bio Rad, Cat #1705061). Images were collected using a chemidoc apparatus. Western blots were then analyzed using the Lane and band plugin form the Image Lab software (Bio Rad). Data were normalized first by the loading control (Glyceraldehyde 3-phosphate dehydrogenase (GAPDH) or Actin) and afterwards by the mean of the control samples. 3-6 samples were analyzed per each treatment condition and timepoint of study.

Table 5. List of primary antibodies used for Western Blot. NFDM: Non-fat Dried Milk. BSA: Bovine Serum Albumin

Antibody	Dilution	Blocking	Description	Reference number
p21	1:1000	5% NFDM	Rabbit monoclonal	Abcam #ab188224
p-H2AX	1:1000	5% BSA	Rabbit monoclonal	Cell Signaling #9718
Nfkb-p65	1:1000	5% NFDM	Rabbit monoclonal	Cell Signaling #8242
Latexin	1:2000	5% NFDM	Sheep polyclonal	R&D Systems #AF3620
KAT3	1:500	5% NFDM	Rabbit polyclonal	Sigma #HPA027168
KLK5	1:1000	5% NFDM	Rabbit polyclonal	Abcam #ab7283
Hsp70	1:10000	5% NFDM	Rabbit polyclonal	Abcam #ab79852
Calreticulin	1:1000	5% NFDM	Chicken polyclonal	TermoFischer #PA1-902A
Hsp90	1:50000	5% NFDM	Rabbit polyclonal	Abcam #ab13495
eIF2α	1:1000	5% NFDM	Rabbit polyclonal	Cell Signaling #5324
p-eIF2α	1:1000	5% BSA	Rabbit polyclonal	Cell Signaling #9721
Bcl-2	1:1000	5% NFDM	Rabbit polyclonal	Abcam #ab59348
Caspase-3	1:1000	5% NFDM	Rabbit polyclonal	Cell Signaling #9662
Cleaved Caspase-3	1:500	5% NFDM	Rabbit polyclonal	Cell Signaling #9661
GAPDH	1:1000	5% NFDM	Mouse polyclonal	Millipore #MAB374
Actin	1:1000	5% NFDM	Mouse polyclonal	Sigma #A5316

1.7.2 Multiplex analysis for cytokine profile

Sciatic nerves and DRGs were rapidly harvested from mice perfused intracardially with cold saline, snap frozen in liquid nitrogen and kept at -80ºC. The two sciatic nerves for each mouse were pooled for protein tissue extraction. Similar, all the DRGs from lumbar to cervical segments were pooled for protein tissue extraction. For tissue processing, sciatic nerves were manually homogenized in 300µl HEPES buffer (HEPES 6.25mM, IGEPAL 2%, PMSF 1mM, EGTA 1mM (pH=8), EDTA 16.9mM (pH=8), $MgCl_2$ 5mM) adding 10 µl/ml of protease inhibitory cocktail (Sigma, Cat #P8340) and PhosSTOP phosphatase inhibitor cocktail (Roche, Cat #4906845001). After homogenization, a pulse with an ultrasonic homogenizer for 5 seconds at 40kHz was applied to samples. DRGs where manually homogenized in 60µl HEPES buffer followed by a pulse with an ultrasonic homogenizer for 5 seconds at 40kHz. After homogenization, samples were centrifuged 20 minutes at 4ºC at 12000rcg and supernatants were collected. Protein was quantified by BCA protein assay (Thermo Scientific, Cat #BCA1-1KIT) following the manufactured protocol. Protein concentration was set to 3.3µg/µl in DRG samples and 3µg/µl in sciatic nerve samples. The protein levels of Eotaxin (CCL11), GM-CSF, GROα (CXCL1), IFNγ, IL-1β, IL-10, IL12p70, IL-13, IL17A (CTLA-8), IL-18, IL-2, IL-22, IL-23, IL-27, IL-4, IL-5, IL-6, IL-9, IP-10 (CXCL10), MCP-1

(CCL2), MCP-3 (CCL7), MIP-1α (CCL3), MIP-1β (CCL4), MIP-2α (CXCL2), RANTES (CCL5) and TNFα were then determined and analyzed using a custom-designed Milliplex Cytokine/Chemokine Magnetic Bead Panel on a MAGPIX system (EMD Millipore, Cat #EPXR260-26088-901) in accordance with the manufacturer's protocol. Standard curves were generated using the specific standards supplied by the manufacturer. Data were normalized by the total protein concentration and afterwards by the mean of the control samples. 3-6 samples were analyzed per each treatment condition, tissue and timepoint of study. Some cytokines were not detected due to their low levels in sample.

1.8 Histology and Imaging

Histological studies were performed to further describe the animal model and to corroborate the data obtained in the scRNA-seq. For that, mice were deeply anaesthetized and intracardially perfused with cold saline at the same timepoints than molecular studies: at the end of the neuropathy induction time (10 weeks for cisplatin and 8 weeks for oxaliplatin) and at the end of the coasting-effect evaluation time (16 weeks for cisplatin and 10 weeks for oxaliplatin).

1.8.1 Myelinated axons density

A segment of the sciatic nerve at mid-thigh and the distal part of the tibial nerve were removed and fixed in 3% Glutaraldehyde-3% Paraformaldehyde (PFA) in Phosphate Buffer (PB) 0.1M. The samples were then post-fixed with 2% osmium tetroxide (Sigma, Cat #75633) for 2 hours, dehydrated in graded concentrations of ethanol and embedded in eponate resin. Semithin sections 0.5µm thick were stained with toluidine blue. To estimate the number of myelinated fibers in the sciatic and tibial nerves, axon density and whole area of the nerve was calculated. In a light microscope (Olympus BX40) attached to a digital camera (Olympus DP73) at least the 30% of the nerve cross-section area was systematically photographed in images taken at 100x magnification. Myelinated axons were manually counted, and total area of the field used was measured. The whole area of sciatic and tibial nerves was measured in 40x final magnification images using Image J software (NIH, Bathesda, MA). Finally, the total number of myelinated axons per nerve was estimated.

1.8.2 Intraepidermal nerve fiber density (IENFD)

Distal plantar pads from mice were removed and fixed in 4% paraformaldehyde (PFA) in Phosphate Buffered Saline (PBS) during 1h at 4ºC. Samples were subsequently washed in PB with sucrose at 4ºC. Cryotome sections of a thickness of 60µm were washed free-floating once in PBS, and then three times in 0.3% PBS-X-triton for 10 minutes each. After it, samples were blocked for 1 hour at

room temperature with 1.5% Normal Donkey Serum (NDS, Millipore) in 0.3% PBS-X-triton. Samples were incubated with primary antibodies to label the Protein Gene Product 9.5 (PGP9.5) and the CGRP (Table 6). Primary antibodies were diluted in blocking solution overnight at 4ºC. After incubation time, samples were washed with 0.3% PBS-X-triton for three times, 10 minute each. Secondary antibody was then diluted in blocking solution and samples were incubated overnight at 4ºC. For staining nuclei, DAPI 0.1mg/ml in PBS was added to the samples for 2 minutes. Finally, samples were dehydrated with 50, 70, 96 and 100% alcohols for ten minutes each, mounted in gelatin coated slides and viewed in an epifluorescence microscope (Olympus BX51) using appropriate filter. Five sections from each sample were used to quantify the mean number and density of nerve fibers present in the epidermis of the paw pads.

1.8.3 Transmission electron microscopy

Right L4 DRG were removed from mice and post fixed in a solution of 3% Glutaraldehyde-3% PFA in PB 0.1M. Following fixation, DRGs were washed with PB followed by centrifugation at 1.278rcg for 10 minutes. The supernatant was discarded, and the samples resuspended in 1% paraformaldehyde diluted in PB. The samples were centrifuged at 7.676rcg for 5 minutes and rinsed three times with PB. Then, DRGs were postfixed for 2 hours with 1% osmium tetroxide (TAAB Lab.) containing 0.8% potassium hexocyanoferrate prepared in PB, followed by four washes with deionized water and sequential dehydration in acetone. All procedures were performed at 4ºC. Samples were embedded in Eponate 12^{TM} resin (Ted Pella Inc.) and polymerized at 60ºC for 48 hours. Semithin sections (1µm thick) were obtained with a Leica ultracut UCT microtome (Leica Microsystems GmbH), stained with 1% (w/v) toluidine blue solution and examined with a light microscope to identify DRG areas containing neurons. Ultrathin sections (70nm thick) were then cut with a diamond knife (45º, Diatome), placed on non-coated 200 mesh copper grids and contrasted with conventional uranyl acetate solution for 30 minutes and Reynolds lead citrate for 5 minutes. Sections were observed with a Joel 1400 transmission electron microscope (Joel Ltd) equipped with a Gatan Ultrascan ES1000 CCD Camera.

1.8.4 Senescence-Associated β-galactosidase activity assay in DRG slices.

Senescence-Associated β-galactosidase (SA-βGAL) activity was determined in DRG slices following the protocol instructions of the Senescence-detection Kit (Abcam, Cat #ab65351). Briefly, left L4 DRG were dissected from DPBS perfused mice and immediately snap freeze in liquid nitrogen. Then, DRGs were embedded in OCT (Tissue Tek) and cryostat sections of 15µm thick were obtained and mounted in gelatin-coated slides. Immediately, samples were fixed in the fixative solution for 10 minutes and then washed twice with PBS. Sections were then incubated with the staining solution at 37ºC overnight. After the incubation time, slides were washed three

times with PBS. Images were taken in a light phase microscope (Nikon ECLIPSE Ni) attached to a digital camera (DS-Ri2) at 40x magnification chosen by systematic random sampling of squares. The intensity of the β-galactosidase reaction (seen as a blue precipitate) was quantified in a total of 50 neurons for each animal using Image J software.

1.8.5 Morphometric analysis of the DRG.

L5 DRG were fixed in 4% PFA in PBS during 1.5 hours at 4ºC. Following fixation, DRG were dehydrated and then embedded in paraffin. Microtome sections of 5µm thick were deparaffined with xylene (Panreac), dehydrated with series of graded ethanol and stained with a standard hematoxylin-eosin (HE) protocol. Briefly, slices were immersed in Hematoxylin Harris (Sigma) for 10 minutes and washed in water followed by 1% HCl in 70% ethanol solution for 5 seconds. Then, sections were rewashed with water and stained with fresh Eosin for 2 minutes. Finally, samples were rehydrated with series of graded ethanol and mounted with DPX (Sigma, Cat #44581). Images were taken with a light microscope (Nikon ECLIPSE Ni) attached to a digital camera (DS-Ri2) at 1000x final chosen by systematic random sampling of squares. The area of the soma, nucleus and nucleoli of 250-280 neurons for each animal were measured with the plugin ObjectJ (University of Amsterdam) from the Image J software.

1.8.6 Immunofluorescence of DRG slices

- **Cisplatin study**: DRG microtome sections of 5µm thickness were deparaffinized with Xylene (Panreac), dehydrated and washed. Antigen retrieval was performed by incubating samples with pre-boiled citrate buffer (10mM sodic citrate and 1mM EDTA in dilated water) for 30 minutes. Samples were then permeabilized and endogenous peroxidases were blocked for 40 minutes in a solution composed by 70% Methanol and 2% H_2O_2 in water. After that, endogenous biotins were blocked by the Endogenous Biotin-blocking kit following the manufactured protocol (Invitrogen, Cat #E-21390). Then samples were incubated with blocking solution (0.3% Triton-100X in PBS with 10% NDS) for 1 hour at room temperature. After blocking, slices were incubated overnight at 4ºC with primary antibodies against p21, p-H2AX, Nfkb-p65 and β-III-tubulin (Table 6). After washes, samples were incubated for 2 hours at room temperature with secondary antibodies (Table 6). Some antibodies were amplified by Tyramide Signal Amplification (TSA) method (Table 8) with the TSA Biotin Systems (Perkin Elmer, NEL700A001KT) following the manufactured protocol. For staining nuclei, DAPI 0.1µg/ml was added to slices for 2 minutes at room temperature. Finally, samples were mounted with Fluoromount-G media (Southern Biotech, Cat #01-0035). Images were taken with an epifluorescence microscope (Nikon ECLIPSE Ni) attached to a digital camera (DS-Ri2) at 100x magnification. The

same threshold of detection and binarization was applied to all the images. The number of positive neuronal nuclei for p21, p-H2AX and Nfkb-p65 were quantified. Percentage of positive nuclei was calculated in respect to the total number of neurons. Among 50-70 neurons were quantify for each animal. All the editing and analysis of images were performed using the Image J software.

- **Oxaliplatin study:** DRG cryosections of 20μm thick were washed twice with PBS. Then, antigen retrieval was performed by incubating samples with pre-boiled citrate buffer for 30 minutes. Samples were then permeabilized with 0.1% Tween-20 in PBS for 10 minutes and endogenous peroxidases were blocked for 40 minutes in a solution composed by 70% Methanol and 2% H_2O_2 in water. After that, endogenous biotins were also blocked by the Endogenous Biotin-blocking kit following the manufactured protocol (Invitrogen, Cat #E-21390). Then, samples were incubated with blocking solution (0.3% Triton-100X in PBS with 10% NDS) for 1 hour at room temperature. After blocking, slices were incubated over night at 4ºC with primary antibodies against latexin, kallikrein-5 (KLK5), calreticulin and β-III-tubulin (Table 6). After incubation time, samples were washed with 0.1% Tween-20 in PBS for 10 minutes. Slices were then incubated with secondary antibodies O.N at 4ºC (Table 6). Some antibodies were amplified by Biotin-Streptavidin or TSA method (Table 8) with the TSA Biotin Systems (Perkin Elmer, NEL700A001KT) following the manufactured protocol. Finally, samples were mounted with DAPI Fluoromount-G media (Southern Biotech, Cat #0100-20). Using appropriate filters, images were taken with a confocal microscope (LSM 700 Axio Observer, Carl Zeiss) at 20x magnification chosen by systematic random sampling of squares. The same threshold of detection and binarization was applied to all the images. The number of positive neuronal nuclei for KLK5 or latexin proteins was quantified. Percentage of positive nuclei was calculated in respect to the total number of neurons. For calreticulin analysis, the percentage of neurons with surface expression of calreticulin was calculated. Among 150-250 neurons were quantified for each animal. All the editing and analysis of images were performed using the Image J software.

Table 6. List of antibodies used for tissue immunofluorescence. [a]Used for DRG immunostaining. [b]Used for IENFD studies; [c]For TSA/Biotin amplifyed antibodies. [d]For TSA amplifyed antibodies only.

	Antibody	Dilution	Amplification method	Description	Reference number
Primary antibodies	p21[a]	1:200	TSA	Rabbit monoclonal	Abcam #ab188224
	p-H2AX[a]	1:200	TSA	Rabbit monoclonal	Cell Signaling #9718
	Nfkb-p65[a]	1:200	TSA	Rabbit monoclonal	Cell Signaling #8242
	Latexin[a]	1:200	TSA	Sheep polyclonal	R&D Systems #AF3620
	KLK5[a]	1:200	TSA	Rabbit polyclonal	Abcam #ab7283
	Calreticulin[a]	1:200	Biotin	Chicken polyclonal	Thermo Fisher #PA1-902A
	β-III-tubulin[a]	1:500	None	Mouse polylonal	Biolegend #MMS-435P
	CGRP[b]	1:500	None	Goat polylonal	Abcam #ab36001
	PGP9.5[b]	1:500	None	Rabbit polyclonal	Cederlane #CL7756AP
Secondary antibodies	Anti-rabbit Cy3	1:500	N/A	N/A	Millipore #AP187C
	Anti-goat Cy3	1:500	N/A	N/A	Millipore #AP180C
	Anti-mouse A488	1:200	N/A	N/A	Invitrogen #A21202
	Anti-rabbit Biotinylated IgG[c]	1:200	N/A	N/A	Vector #BA-1100
	Anti-sheep Biotinylated IgG[c]	1:200	N/A	N/A	Vector #BA-6000
	Anti-chicken Biotinylated IgG[c]	1:200	N/A	N/A	Vector #BA-9010
	Streptavidin HRP conjugated[d]	1:100	N/A	N/A	Perkin Elmer #NEL750001EA
	Streptavidin A594 conjugated[c]	1:200	N/A	N/A	Invitrogen #S32356

2. *In vitro*-based studies

Some of the work regarding *in vitro* studies was conducted in the Cellular Senescence and Age-Related pathologies Group (Demaria's Lab) from the European Research Institute for the Biology of Ageing (ERIBA) situated in Groningen (The Netherlands), in the context of an international internship during the PhD.

2.1 DRG primary neuronal cultures

10-weeks old C57BL/C male mice were sacrificed and all their DRGs were dissected and placed in cold Gey's salt solution (Sigma, Cat #G9779) supplemented with 6mg/ml glucose in ice. DRGs were cleaned from debris and blood and then enzymatically dissociated in Ca^{2+} and Mg^{2+} free Hank's medium (Sigma, Cat #14170-088) with 10% trypsin (Sigma, #T-4674), 10% Collagenase A (Sigma, Cat #C2674) and 10% DNAse (Roche, Cat #11284932001), for 20 minutes at 37ºC, followed by mechanical dissociation. After dissociation, enzymes were inhibited with 10% hiFBS in DMEM medium (Sigma, Cat #41966052) and cells were then centrifuged at 900 rpm for 7 minutes. Supernatant was withdrew and 1ml of culture medium was added, which consisted of NB-A (Gibco, Cat #10088022) supplemented with 2% B27 (Gibco, Cat #17504044), 6mg/ml glucose, 1mM Glutamax (Gibco, Cat #35050-038) and 1X penicillin/streptomycin (Sigma, Cat #P0781). Neurons were then platted at a density of $40x10^3$ neurons/ml and incubated at 37ºC and 5% CO_2. Plates had been previously coated with 100µg/ml Poly-D-lysine (PDL, Sigma, Cat #P6407) for 2 hours at 37ºC, washed, dried and further coated with 1µl/ml laminin for a minimum of 2 hours (Sigma, Cat #L-2020). Medium was changed after 2 hours of culture to eliminate debris and non-attached death cells. After 24h in culture, neurons were treated with cisplatin at different concentrations (0.25, 1 or 4µg/ml) (Figure 12). After 24 hours of treatment, the medium was completely changed for fresh culture medium. Different assays at different time-points (1, 3 and 7 days after starting cisplatin treatment) were conducted to choose the best dose for senescence induction.

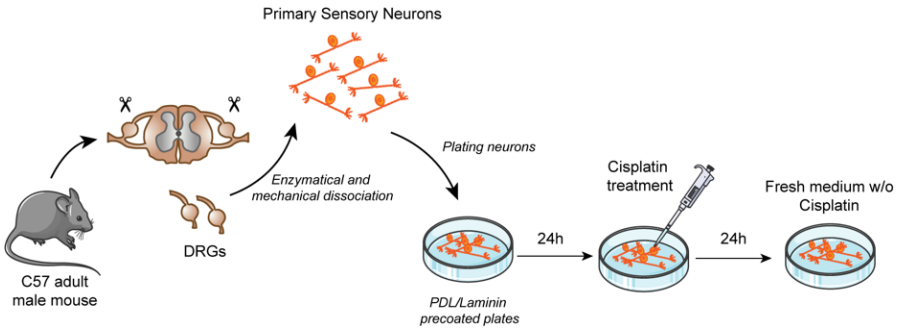

Figure 12. Schematic diagram of the primary DRG sensory neurons culture. One day after plating the cells, cisplatin was added to the medium for 24 hours. After that, (continued on next page, legend follows)

medium was removed and medium free of drug was added. Cultures were followed at 1, 3 and 7 days after initial of cisplatin administration. w/o, without.

2.2 Neuronal survival quantification

Cell viability was determined using a method similar to the one described by Ta et al. (2006). Briefly, the number of viable neurons was quantified in the same field (previously labeled) at baseline and then at 1, 3 and 7 days after starting cisplatin treatment under a phase-contrast microscope. Viable neurons were identified by a bright outline that is absent in dead cells. Around 45-70 neurons were quantified at baseline. Results from at least three independent experiments are reported.

2.3 Immunofluorescence of DRG neuronal cultures

At 1, 3 or 7 days after starting cisplatin treatment, cultures were fixed with 4% PFA in PBS for 20 minutes at room temperature. After washing with PBS, cultures were incubated in blocking solution (PBS Tween 0.1% supplemented with 1.5% NDS) for 1 hour at room temperature. Primary antibodies rabbit p-H2AX (1:200, Cell Signaling, Cat #9718) and mouse β-III-tubulin (1:500, Biolegend, Cat #MMS435P) were incubated overnight at 4ºC. Dilutions were made in blocking solution. Biotinylated antibody anti-rabbit IgG (1:200, Vector, Cat #BA-1100) was incubated for 90 minutes at room temperature in blocking solution. After that, cultures were incubated with secondary antibodies streptavidin-A488 conjugated (1:200, Life Technologies, Cat #S11223) and anti-mouse A594 (1:200, Life Technologies, Cat #A21203) in blocking solution overnight at 4ºC. Coverslips were dehydrated with series of graded ethanol, mounted with DPX (Sigma, Cat #44581) and analyzed under a fluorescence microscope (Nikon ECLIPSE Ni) attached to a digital camera (DS-Ri2). Images were taken at 100x final magnification, and the fluorescence intensity of neuronal nuclei analyzed with Image J. At least 15 fields and a total of 40-100 neurons were quantified per each condition and time point. A total of three independent replicates were conducted and their mean was calculated.

2.4 SA β-GAL assay of neuronal cultures

Neurons were stained as described previously (Hernandez-Segura et al., 2018). In short, at 3 and 7 days after starting cisplatin treatment (1μg/ml), cells were fixed by incubation in 2% formaldehyde + 0.2% glutaraldehyde in PBS for 3 minutes. Then, cells were washed and incubated for 14-16 hours at 37 degrees in de dark, in freshly prepared staining solution containing 40mM citric acid/sodium phosphate buffer (pH 6.0), 5mM potassium ferrocyanide, 5mM potassium ferricyanide, 150mM Magnesium Chloride, 2mM Sodium Chloride and 20mg/ml X-gal (Cayman

Chemical, Cat# 16495) in water. After staining, cells were washed with PBS and representative images were acquired at 100x final magnification using a microscope (Nikon ECLIPSE Ni) attached to a digital camera (DS-Ri2). SA-βGAL+ neurons were counted using the ImageJ software. The percentage of SA-βGAL+ neurons was quantified in respect with the total of neurons.

2.5 Multiplex analysis for cytokine profile in culture medium

At 1, 3 and 7 days after initial of cisplatin treatment (1µg/ml), culture supernatans were collected and protein concentrated to a final volume of 50µl with centrifugal filter units (Merck, Cat #MRCPRT010). The protein levels of Eotaxin (CCL11), GM-CSF, GROα (CXCL1), IFNγ, IL-1β, IL-10, IL12p70, IL-13, IL17A (CTLA-8), IL-18, IL-2, IL-22, IL-23, IL-27, IL-4, IL-5, IL-6, IL-9, IP-10 (CXCL10), MCP-1 (CCL2), MCP-3 (CCL7), MIP-1α (CCL3), MIP-1β (CCL4), MIP-2α (CXCL2), RANTES (CCL5) and TNFα were then determined and analyzed using a custom-designed Milliplex Cytokine/Chemokine Magnetic Bead Panel on a MAGPIX system (EMD Millipore, Cat #EPXR260-26088-901) in accordance with the manufacturer's protocol. Standard curves were generated using the specific standards supplied by the manufacturer. Data were normalized by the mean of the control samples for each specific time point. 4 independent cultures were analyzed per each treatment condition and timepoint of study. Some cytokines were not detected in the assay due to their low levels in samples.

2.6 Metabolism studies

For the metabolic studies, DRGs from 10-weeks old C57BL/C6 male mice were dissected and dissociated as described above. After obtaining the cell suspension, 15.000 neurons were plated into PDL/laminin coated (described above) XFp 8-well plates (Agilent, Cat #103025-100) in NB-A medium (described above). After 24h in culture, cisplatin was added at a concentration of 1µg/ml for 24 hours. On days 3 and 7 after cisplatin treatment, metabolic potential of the cells was evaluated using the Seahorse Xp analyzer (Agilent) and the Energy phenotype kit (Agilent, Cat# 103325-100) according to manufactured instructions and as previously described (Ulisse et al., 2020, Styr et al., 2019). Briefly, on the day of experiment cells were washed one time and incubated for 1 hour in Assay Medium (Bicarbonate free unbuffered DMEM medium (Agilent, Cat#103680-100) supplemented with 2mM sodium pyruvate (Gibco, Cat #11360070), 2mM Glutamine (Sigma, Cat #G7513), 10mM Glucose and 2% B27 (Gibco, Cat #17504044). Incubation with Assay medium was performed in a non-CO_2 incubator at 37ºC. Respiration was measured three times under basal conditions and then five times in response to the simultaneously exposition to 1µM Oligomycin and 3µM carbonyl cyanide-p-trifluoromethoxyphenylhydrazone (FCCP). Both OCR (Oxygen Consumption Rate) and ECAR (Extracellular acidification rate) were acquired. Metabolic potential

was calculated as the percentage of stressed OCR over baseline OCR, or stressed ECAR over baseline ECAR. Metabolic potential is defined as the cells' ability to meet an energy demand via respiration (OCR) and glycolysis (ECAR). Two independent cultures with 2 well each for each condition were used at 3 days. One independent culture with 2 wells for each condition were used at 7 days.

2.7 Real Time PCR (RT-qPCR)

Total RNA from cultures was isolated using the Isolate II RNA Micro Kit (Bioline, Cat# BIO-52075) and quantified using a NanoDrop. 50-100ng of RNA was reverse transcribed into cDNA using a kit (Applied Biosystems, Cat# 4368813). RT-qPCR reactions were performed using the Universal Probe Library system (Roche) and a SensiFast Probe kit (Bioline, Cat# BIO-84020). The geometric mean of the expression levels of Actin and GAPDH were used to normalize the expression of Cp values. List of primers and probes is provided in Table 7.

Table 7. List of primers and probes related to RT-qPCR. *From Cellular Senescence and Age-related Pathologies Group (Demaria Lab).*

Gene	Specie	Direction	Sequence	UPL Probe
Actin	Mouse	Forward	ctaaggccaaccgtgaaaag	#64
		Reverse	accagaggcatacagggaca	
GAPDH	Mouse	Forward	aagagggatgctgcccttac	#30
		Reverse	ccattttgtctacgggacga	
Cdkn1a (p21)	Mouse	Forward	aacatctcagggccgaaa	#16
		Reverse	tgcgcttggagtgatagaaa	
Cdkn2a (p16)	Mouse	Forward	aatctccgcgaggaaagc	#91
		Reverse	gtctgcagcggactccat	
Lamin B1	Mouse	Forward	gggaagtttattcgcttaaga	#15
		Reverse	atctcccagcctcccatt	
IL6	Mouse	Forward	ctaaggccaaccgtgaaaag	#6
		Reverse	accagaggcatacagggaca	
IL1α	Mouse	Forward	ttggttaaatgacctgcaaca	#52
		Reverse	gagcgctcacgaacagttg	
Mmp1-α	Mouse	Forward	tagcccttcctttgctgttgc	#26
		Reverse	gcccaagttgtagtagttttcca	
Cxcl1	Mouse	Forward	gactccagccacactccaac	#83
		Reverse	tgacagcgcagctcattg	
Gdnf	Mouse	Forward	tccaactgggggtctacg	#70
		Reverse	gacatcccataacttcatcttagagtc	

2.8 RNA-seq of DRG cultures

RNA-seq was conducted in DRG cultures 7 days after cisplatin exposure. 2 experimental conditions were analyzed: Non-treated (NT) and cisplatin-treated (CDDP) cultures.

2.8.1 RNA isolation

DRG cultures (3 biological replicates per condition) were prepared for RNA extraction via Isolate II RNA Micro Kit (Bioline, BIO-52075). The extracted RNA was quantitated using a NanoDrop and RNA quality was measured via 2100 Bioanalyzer Instrument (Agilent) with the High Sensitivity RNA (HS RNA) ScreenTape system (Agilent) (RIN of 8,5 or greater). Then, Poly(A) messenger RNA (mRNA) was purified from total RNA by the NEXTflex Poly(A) Beads' kit (BioSicetific, Cat# 512979) following the manufactured protocol. 240-800ng of total RNA input were used for the isolation.

2.8.2 RNA-seq library preparation

RNA-seq library preparation was carried out using a NETFLEX Rapid Directional RNA-Seq kit (BioScientific, Cat# NOVA-5130-01D) according to the manufacturer's protocol. Briefly, purified poly(A) mRNA was reverse transcribed into cDNA. Then, cDNA was fragmented, blunt-ended, and indexed (barcoded) adaptors were ligated to the ends of the fragments, which were then amplified using 15 cycles of PCR. The final library size distribution was validated via 2100 Bioanalyzer Instrument (Agilent) with the High Sensitivity D5000 (HSD5000) ScreenTape assay (Screen Tape HSD5000). Qubit dsDNA HS assay kit (Thermo Fisher Cat# Q3285) was used to corroborate the cDNA concentration obtained by the Bioanalyzer. Indexed libraries were then normalized and pooled to 3.5nM in EBT (Elution Buffer with 0.02% Tween). Sequencing of libraries was carried out on a NextSeq (Illumina).

2.8.3 Data analysis

Processing, quality control and sequence alignment of data to reference genome (mm10) was performed in the cloud through Galaxy. The files were formatted using *Groomer* and their quality assessed using *fastQC*. Alignment with the mouse reference genome (mm10) was performed using *Bowtie2* with an overall >80% of alignment for all of the 6 samples. The number of counts per transcript was extracted using *featureCounts* with the default settings. The sequence depth was evaluated for each sample and the count matrix was normalized using the *median ratio* method. A PCA was conducted across samples for all genes that have above 0 counts. We considered the variable "culture" as a factor for the modeling as an intend to control the technical variability. DEG was performed using *DESeq()* from the *{DESeq2}* package, which fits a negative binomial model

of the raw counts, and accounting for sequencing depth and dispersion on the model. Genes were considered worth keeping by an adjusted p-value <0.1 and a |log2 Fold Change| > 1. A heatmap with hierarchical clustering is performed over the top 30 genes, sorted by p-val-adj (ascending sort). Enrichment pathway analysis of the DEGs was performed for GO (biological process only).

3. Statistical analysis

The results of body weight loss and NCS are expressed as the percentage with respect to baseline values for each mouse. Statistical analysis of body weight, NCS, and behavioral testes was performed by using Repeated Measures (RM) 2-Way ANOVA test. For other comparisons in collected independent variables, a one-way ANOVA or 2-way ANOVA test were used. Bonferroni test was used as the post hoc test for multiple comparisons when needed.

Graph Pad Prism 8 software was used for data analysis and to graphically represent the data, which is expressed as Group Mean±SD. Differences among groups or timepoints were considered significant when $p<0.05$.

VI. RESULTS

1. Animal models of peripheral neuropathy induced by cisplatin and oxaliplatin

This section is based on the first objective of the thesis: "To develop and characterize mouse models of peripheral neuropathy induce by the main neurotoxic platinum drugs oxaliplatin and cisplatin". It will be divided in two main parts. The first one will describe the animal model induced by cisplatin treatment, and the second one the mouse model induced by oxaliplatin.

1.1 Characterization of a mouse model of cisplatin-induced peripheral neuropathy

1.1.1 General toxicity

Animals treated with cisplatin experienced a progressive decrease in their body weight during all the PIPN-induction time (Figure 13a-b). Some of the animals lost more than 30% of their body weight and had to be sacrificed before completing the treatment. The percentage of death after treatment was 26%. After treatment cessation, animals that were not euthanized recovered their body weights reaching basal values (Figure 13b). During coasting-effect time, no animal died.

1.1.2 NCS and behavioral tests

Mice treated with cisplatin experienced a significant progressive decrease in their SNAPs recorded in the digital nerves (Figure 13c). Similarly, the mixed sensory-motor CNAP recorded in the proximal and distal caudal nerves also suffered a significant and progressive decrease over time in cisplatin-treated mice (Figure 13d-e). The decrease in SNAPs and CNAPs started around 10 weeks of study and gradually worsened over time, with a maximum negative peak at 16 weeks of follow-up. It indicates that animals experienced the coasting-effect phenomenon. In contrast to sensory conductions, the amplitude of CMAP recorded in the plantar muscle was maintained in the cisplatin-treated group at similar levels than the control one (Figure 13f). Not all the animals developed a peripheral neuropathy (PN), defined as a decrease in the SNAP and/or CNAP. At 10 weeks, the 43% of all cisplatin-treated animals experience a reduction >15% in SNAP and caudal CNAP; the 33% only in one of the parameters and the rest (24%) shown values close to normal. In contrast, at 16 weeks, all animals that were follow-up experienced a reduction >15% in SNAP and caudal CNAP (Figure 13h).

In the Von Frey test, cisplatin-treated animals had significantly reduced withdrawal thresholds to mechanical stimulation applied to the plantar paw, indicative of hyperalgesia. This increased response to mechanical stimuli reached a peak at 9 weeks and tended to recover to basal values during the coasting effect follow-up period (Figure 13g).

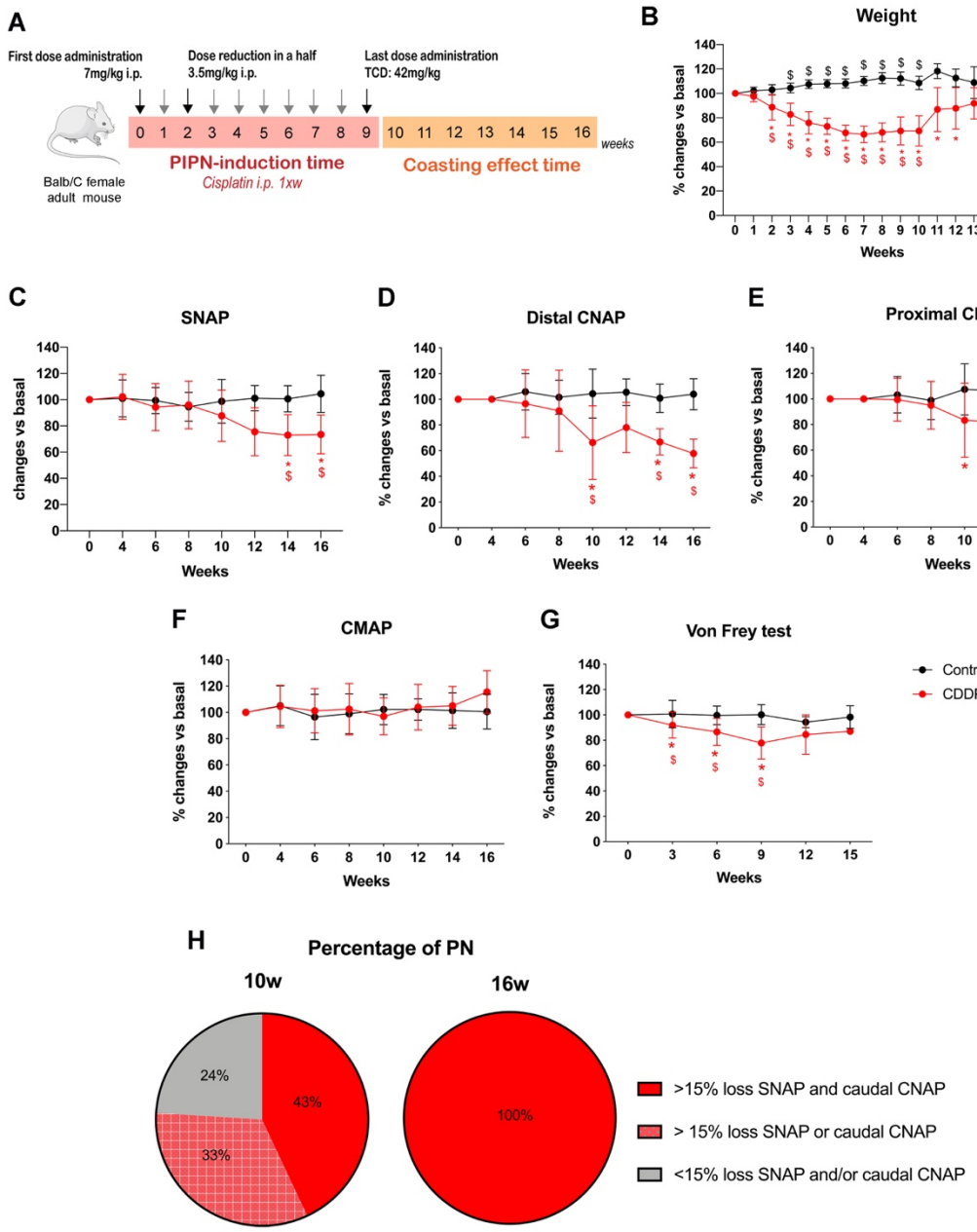

Figure 13. Functional and behavioral characterization of the cisplatin-induced peripheral neuropathy mouse model. A: Scheme of the development of the experimental model. Cisplatin was administered i.p. once a week (1xw) for 10 weeks (PIPN-induction time). After this time, animals were further evaluated to assess the coasting effect (coasting-effect time). **B**: Body weight loss of control and cisplatin-treated (CDDP) mice along time. **C-G**: Functional tests. SNAP (C) and proximal and distal caudal CNAP (D and E) decreased along time in the CDDP group whereas CMAP was not affected (F). Mice treated with cisplatin developed mechanical allodynia along time, but withdrawal threshold to noxious stimuli normalized during the coasting effect time (**G**). **H**: Percentage of animals that developed a peripheral neuropathy (PN) at 10 (left) and 16 (right) weeks of follow-up. n=20-25 mice per group. RM ANOVA with Bonferroni post-hoc test for multiple comparisons. *p<0.05 vs Control; $p<0.05 vs Basal. Data from body weight, NCS and Von Frey test are represented as percentage vs basal values (Group Mean± SD).

All the functional and behavioral findings are in accordance with those reported in patients with cisplatin-induced neuropathy (Staff et al., 2019).

1.1.3 Morphological features

At the morphological level, the number of myelinated axons quantified in semithin cross-sections of the sciatic and tibial nerves did not differ between control and cisplatin-treated mice at the different time points evaluated (Figure 14).

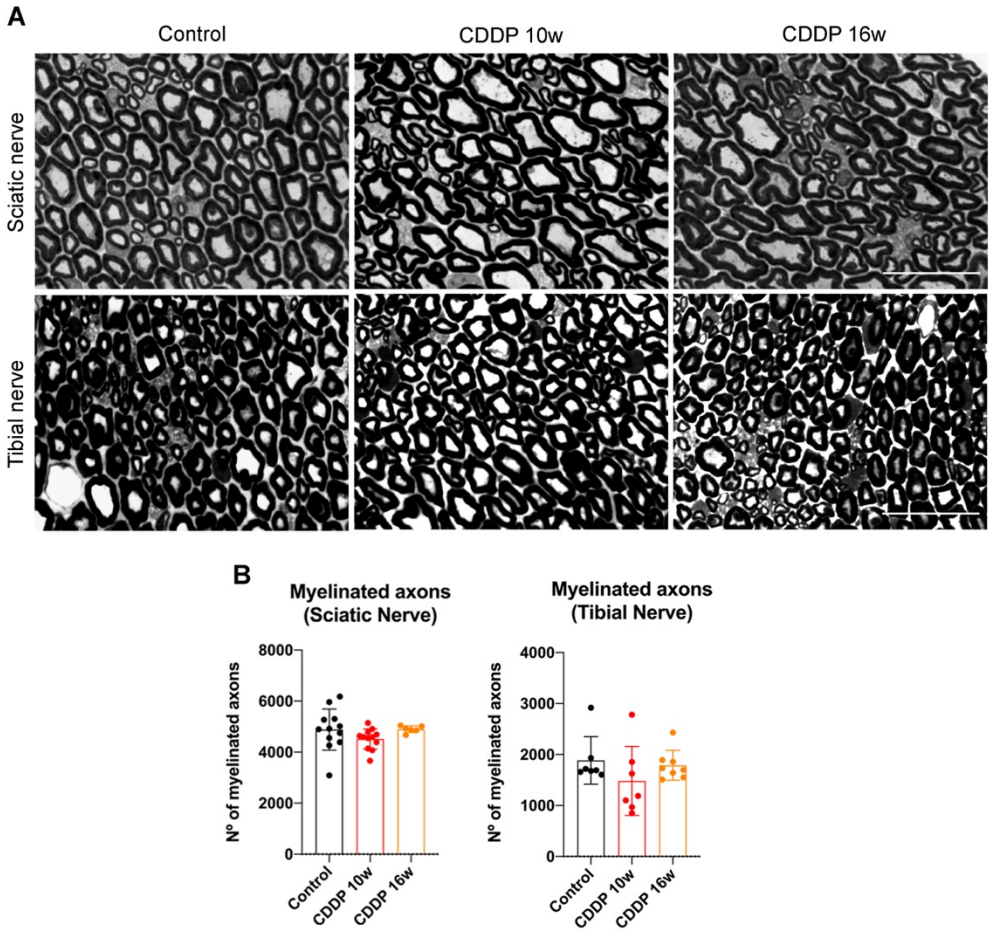

Figure 14. Myelinated axons in sciatic and tibial nerves A: representative images of the corresponding nerves (tibial or sciatic) and experimental conditions (control or cisplatin-treated (CDDP)). Scale bar: 50µm. **B:** Quantification of the number of myelinated axons in the sciatic and the tibial nerves. n= 6-12 mice per group. One Way ANOVA with Bonferroni post-hoc test. Data is represented as Group Mean± SD.

The IENF density (IENFD) in the hind paw pad did not show differences between control and cisplatin-treated mice when labeling fibers with the pan-neuronal marker PGP9.5 (Figure 15). However, we did see a decrease in the number of CGPR+ fibers in animals treated with cisplatin at

10 weeks (just after treatment cessation) but not at 16 weeks (at the end of the coasting effect time) (Figure 15).

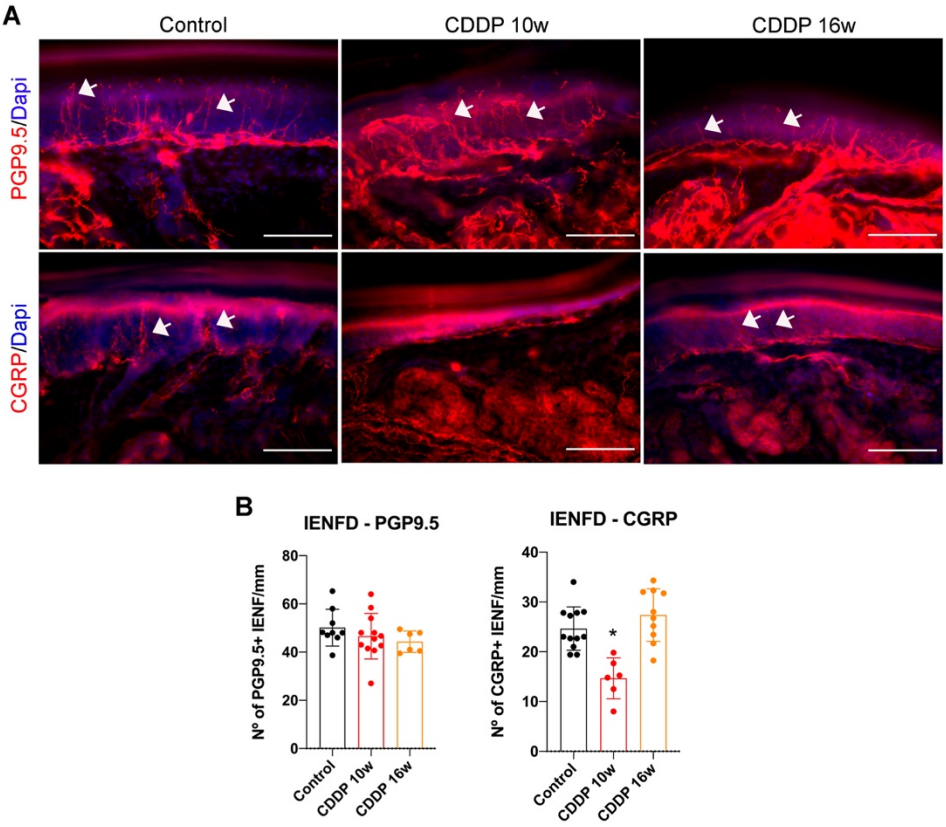

Figure 15. IENFD in mice hind paw pad. **A:** Representative images of the epidermis immunolabeled against PGP9.5 or CGRP (red) in the hind pad paw from control and cisplatin treated (CDDP) mice at 10 weeks and 16 weeks. Dapi (blue) was applied to constrain nuclei. White arrows indicate PGP+ (above) or CGRP+ (below) IENF. Scale bar: 100µm. **B:** Quantification of the number of PGP+ or CGRP+ IENF in the hind pad paw of control and CDDP mice. n= 6-12 mice per group. One Way ANOVA with Bonferroni post-hoc test. *p<0.05 vs Control. Data is represented as Group Mean± SD.

Finally, no significant differences were seen in the somas and nuclei size after cisplatin treatment at any of the time point evaluated (Figure 16).

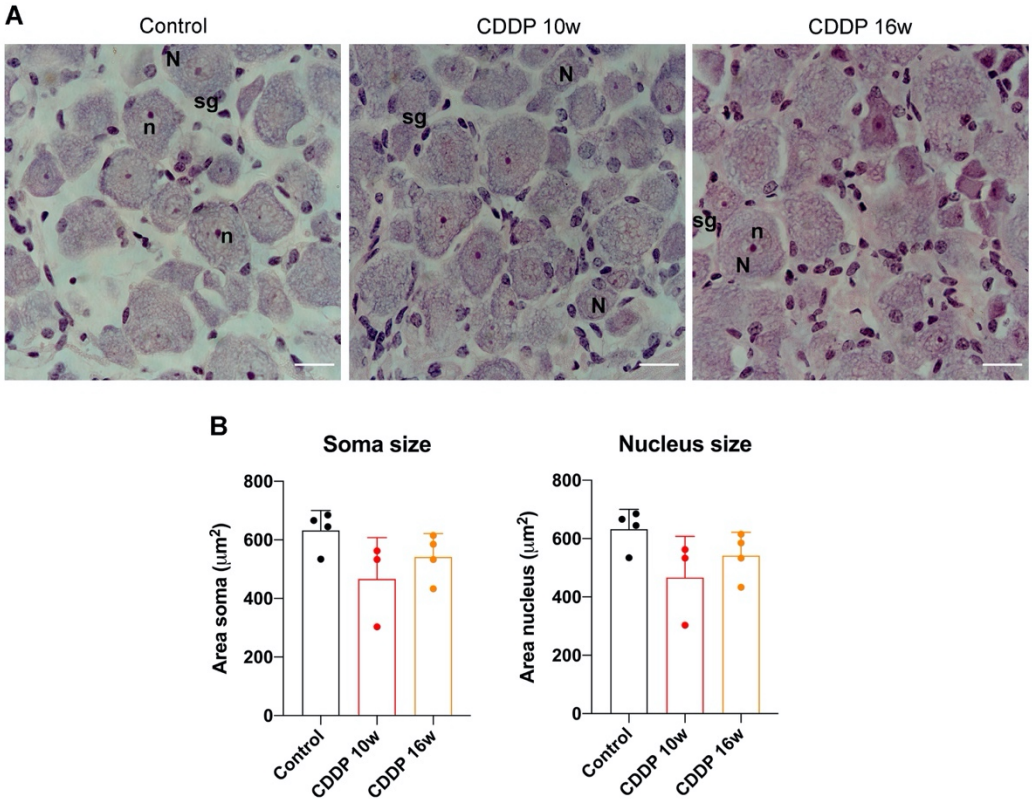

Figure 16. DRG morphometry studies. A: representative images of the paraffin embedded DRG slices stained with Hematoxylin-Eosin from control and cisplatin-treated (CDDP) mice at 10 and 16 weeks. Scale bar: 20µm. sg: Satellite glial cell; N: Neuron; n: nucleus. **B:** bar graphs representing the quantification of the DRG neuronal somas and nuclei's size. n=3-4 mice per group. One Way ANOVA with Bonferroni post-hoc test. *p<0.05. Data is represented as Group Mean± SD.

1.2 Characterization of a mouse model of oxaliplatin-induced peripheral neuropathy

1.2.1 General toxicity

Animals treated with oxaliplatin experienced a progressive decrease in their body weight during all the PIPN-induction time (Figure 17a-b). Some of the animals did not respond to the reduction of half the dose. When losing more than 30% of their body weight, mice were sacrificed before completing the treatment. The percentage of death due to oxaliplatin treatment was around 40%. After treatment cessation, animals that were not euthanized rapidly recovered their body weights reaching basal values on week later (Figure 17b).

1.2.2 NCS and behavioral tests

Mice treated with oxaliplatin experienced a significant progressive decrease in their SNAPs recorded at the digital nerves, reaching the significance at 8 weeks of treatment. In contrast with

the cisplatin model, SNAP was not worsened during the coasting-effect time (10 weeks) but seemed to stabilize (Figure 17c). The mixed sensory-motor CNAP recorded in the distal and proximal caudal nerves also experienced a significant progressive decrease over time in the oxaliplatin-treated mice. Again, amplitudes recorded in the caudal nerves no further decrease during the coasting-effect time in animals treated with oxaliplatin (Figure 17d-e). Amplitude of CMAP recorded in the plantar muscle was maintained in the oxaliplatin-treated group at similar levels than the control one (Figure 17f). All these data suggest that in contrast to the cisplatin animal model, mice treated with oxaliplatin did not experience a clear coasting effect. On the other hand, not all the animals treated with oxaliplatin developed a PN (>15% in the SNAP and/or CNAP). At 8 weeks, the 29% of all oxaliplatin-treated animals experience a reduction >15% in SNAP and caudal CNAP; the 43% in only one of the parameters and the 28% in none of them. At 10 weeks, only the 22% of the animals monitored during the coasting effect time experienced a reduction >15% in SNAP and caudal CNAP; the 56% in one of the parameters and 22% did not develop PN (Figure 17g). Although the percentage of mice developing a neuropathy was significant, the severity of that PN was milder than the one developed by cisplatin treatment.

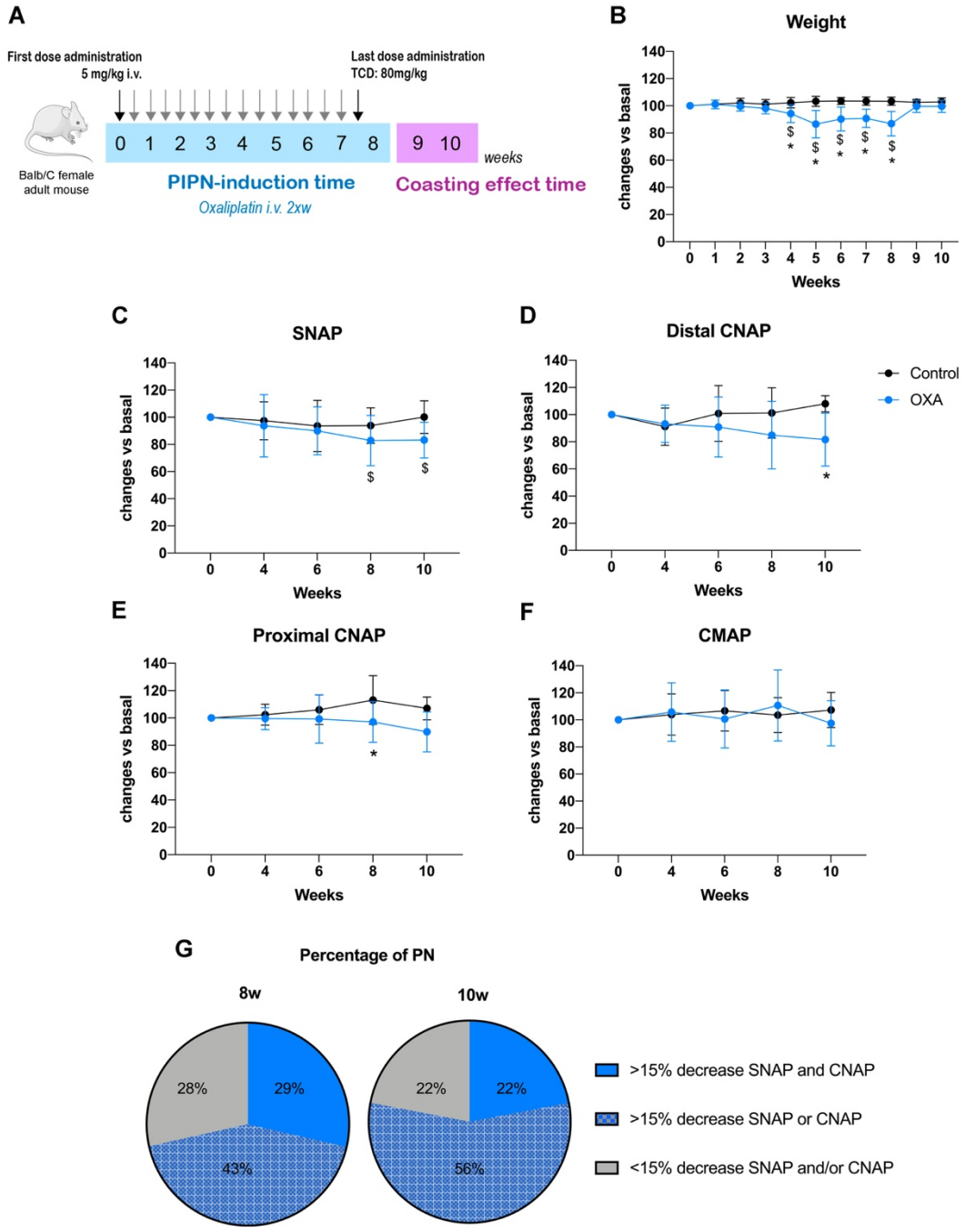

Figure 17. General toxicity and NCS in the mouse model of oxaliplatin-induced peripheral neuropathy. **A:** Scheme of the development of the experimental model. Oxaliplatin was administered i.v. twice a week (2xw) for 8 weeks (PIPN-induction time). After this time, animals were further evaluated to assess the coasting effect for 2 additional weeks (coasting-effect time). **B**: Body weight loss along time in control and oxaliplatin-treated (OXA) mice. **C-F**: NCS: SNAP (C), distal caudal CNAP (D), proximal caudal CNAP (E) and CMAP (F) recordings. **G**: Percentage of animals that developed a peripheral neuropathy (PN) at 8 (left) and 10 (right) weeks of follow-up. n=15-35 mice per group. RM ANOVA with Bonferroni post-hoc test for multiple comparisons. *p<0.05 vs Control; $p<0.05 vs Basal. NCS and body weight are represented as percentage vs basal values (Group Mean± SD).

In the Von Frey test, oxaliplatin-treated animals had significantly reduced withdrawal thresholds to mechanical stimulation applied to the plantar paw, indicative of mechanical allodynia. This increased response to mechanical stimuli was significative at 6 weeks after starting the treatment with oxaliplatin and maintained until the last evaluation (10 weeks) (Figure 18a). In the Cold plate test, oxaliplatin treatment induced a decrease in the time of first paw flick at 2 and 4 weeks of treatment. However, at weeks 6, 8 and 10, some animals treated with oxaliplatin have a slightly increased withdrawal time to the cold stimuli (Figure 18b). This phenomenon overlaps with the onset of divergence in SNAP recordings (Figure 17c). Plantar test did not show differences among control and oxaliplatin-treated mice at any time point evaluated (Figure 18c).

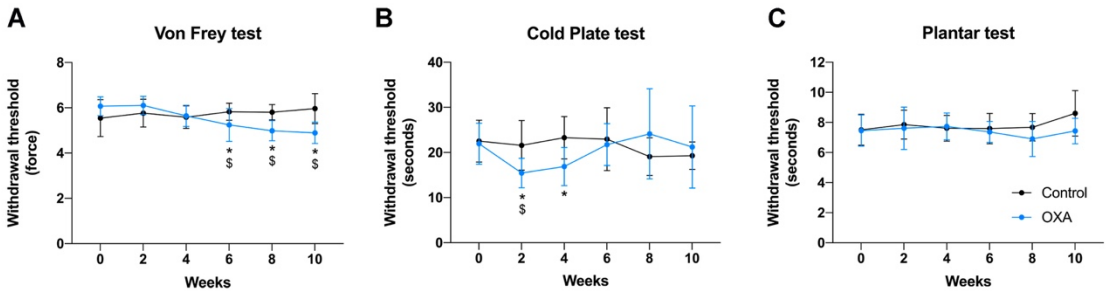

Figure 18. Behavioral characterization of the oxaliplatin-induced peripheral neuropathy. A: Von Frey test of control and oxaliplatin-treated (OXA) mice. Withdrawal threshold (force) to mechanical stimuli is represented. **B:** Cold plate test of control and OXA mice. Time (seconds) of first hind paw lift to -4ºC noxious stimuli is represented. **C:** Plantar test of control and OXA mice. Time (seconds) of paw lift to heat stimuli (IR: 50) is represented. RM ANOVA with Bonferroni post-hoc test for multiple comparisons. *p<0.05 vs Control; $p<0.05 vs Basal. Data is represented as Group Mean± SD.

1.2.3 Morphological features

At the morphological level, the number of myelinated axons quantified in semithin cross-sections of the sciatic and tibial nerves did not differ between control and oxaliplatin-treated mice at the different time points evaluated (Figure 19a-b). Infiltrated cells were seen in tibial and sciatic nerves of both control and oxaliplatin-treated mice (Figure 19c). However, the number of these cells in cross-sections of the sciatic nerve was significative higher in the oxaliplatin-treated animals at 8 weeks compared with control animals (Figure 19d).

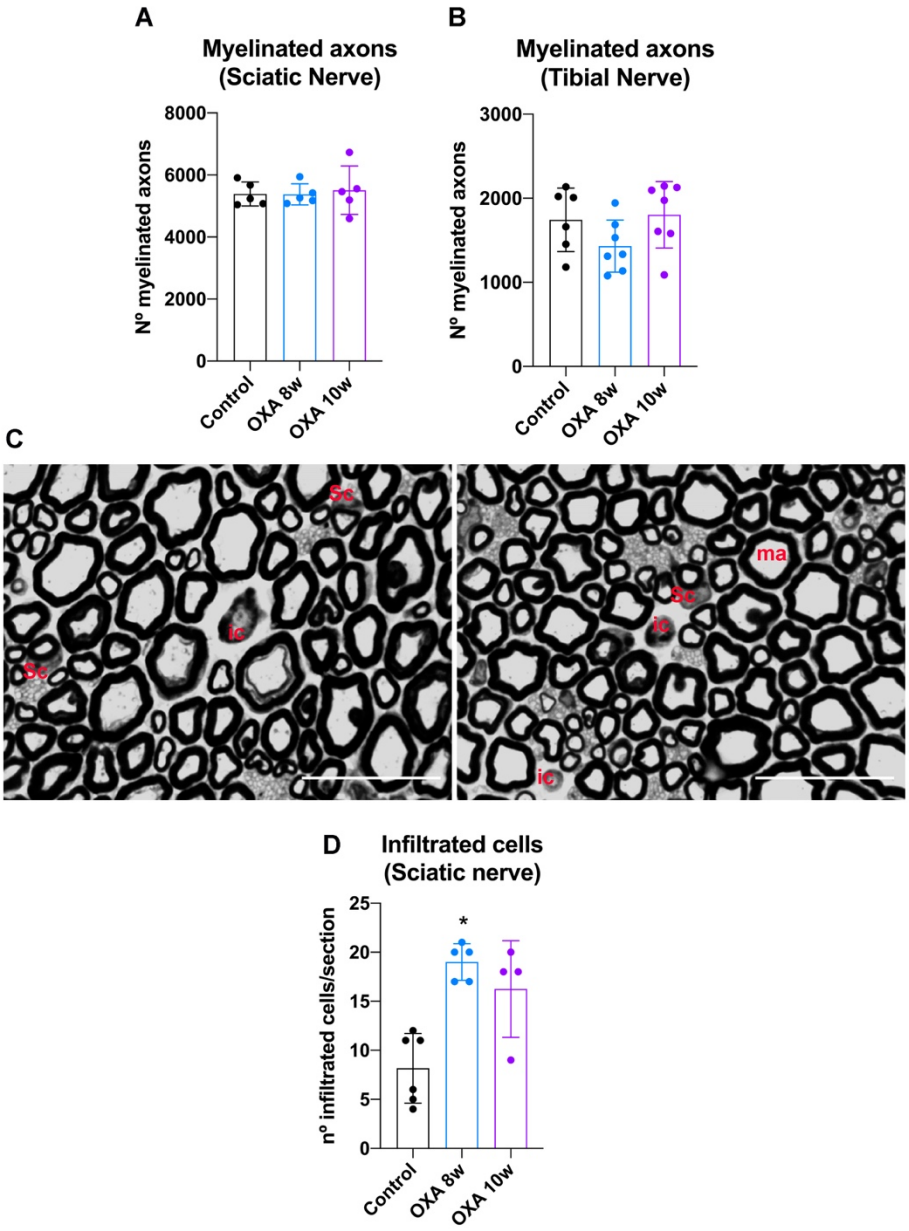

Figure 19. Number of myelinated axons in the sciatic and tibial nerves. A-B: Quantification of the number of myelinated axons in the sciatic (A) and the tibial (B) nerves of control and oxaliplatin-treated (OXA) mice at 8 and 10 weeks. n= 4-5 mice per group in sciatic nerve; n=7 mice per group in tibial nerve. **C**: Representative images of sciatic nerve cross-sections of OXA mice. Scale bar: 20µm. ic: infiltrated cell; ma: myelinated axon; Sc: Schwann cell. **D:** Quantification of the number of infiltrated cells in the sciatic nerve of control and OXA mice at 8 and 10 weeks. n= 4-6 mice per group. One Way ANOVA with Bonferroni post-hoc test for multiple comparisons. *p<0.05 vs Control. Data is represented as Group Mean± SD.

The IENFD in the hind paw pad was not different between control and oxaliplatin-treated mice when labeling fibers against PGP9.5 or CGRP markers (Figure 20).

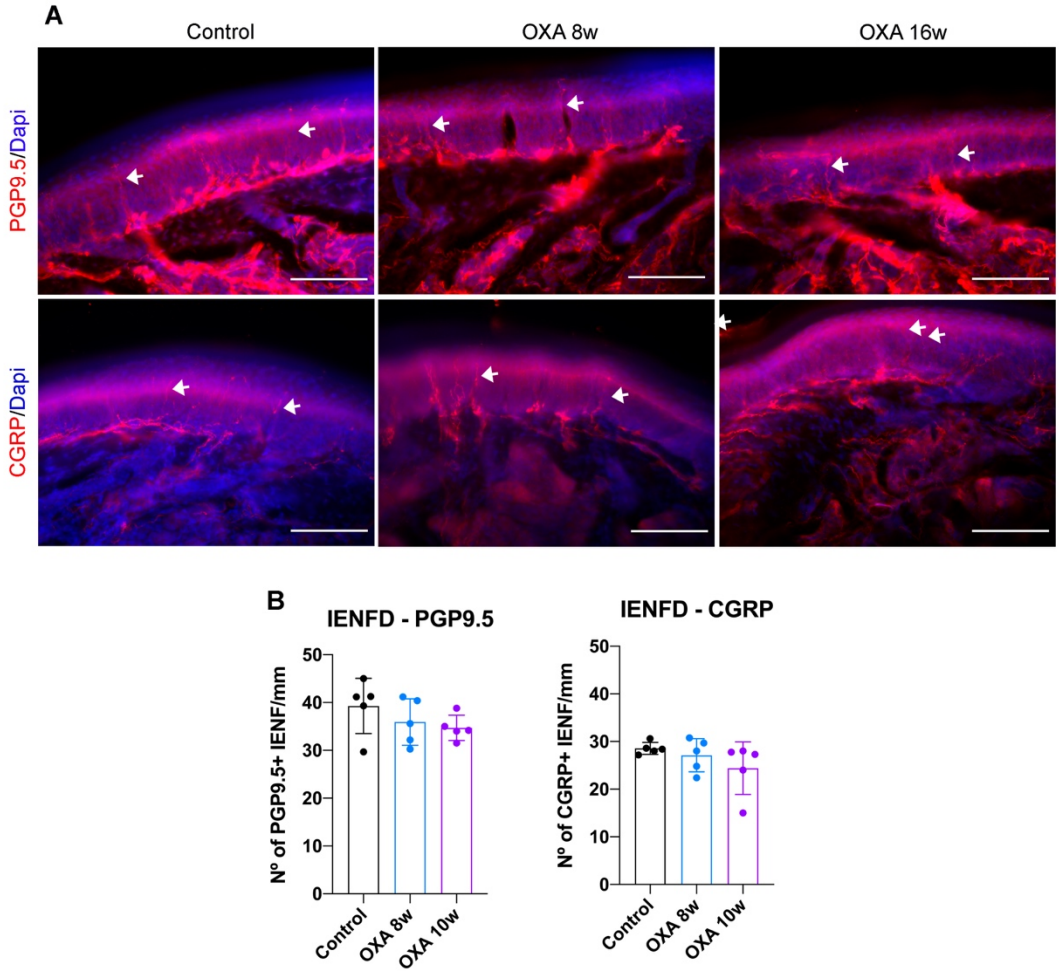

Figure 20. IENFD in mice hind paw pad. **A:** Representative images of the epidermis immunolabeled against PGP9.5 or CGRP (red) in the pad paw from control and oxaliplatin-treated (OXA) mice at 8 and 10 weeks. Dapi (blue) was applied to constrain nuclei. White arrows indicate PGP+ (above) or CGRP+ (below) IENF. Scale bar: 100µm. **B:** Quantification of the number of PGP+ or CGRP+ IENF. n= 5 mice per group. One Way ANOVA with Bonferroni post-hoc test for multiple comparisons. Data is represented as Group Mean± SD.

2. Effects of the tumor environment in the development of PIPN

This section will focus on the second objective of the thesis "To study the influence of a tumor environment in the development of PIPN". To achieve this objective, we injected Colon-26 (C-26) cells s.c. to mice one week before starting the chemotherapy treatment with cisplatin or oxaliplatin.

It is important to highlight that those mice inoculated with C-26 cells not treated with oxaliplatin or cisplatin (Tx mice) had to be sacrificed at four weeks of study due to the high size tumor reached, which was completely disabling for the mice. This tumor started developing around 2 weeks after inoculation and was growing at very high rates until animals were euthanized. Although these animals were a good positive control regarding inoculation of the tumor, they were not included in any of the follow-up studies (NCS, Von Frey test or histological studies).

Regarding the influence of the tumor environment in the development of PIPN by cisplatin, no differences were found in terms of body weight, nerve conductions, mechanical allodynia, or morphological parameters between CDDP and CDDP+Tx experimental groups (Figure 21). Animals that had been inoculated with C-26 cells and that received cisplatin treatment (CDDP+Tx mice) did not experience tumor growth until week 10 of study, so after cessation of cisplatin treatment. To avoid the development of a disabling tumor, these animals were sacrificed at 10 weeks and evaluation during the coasting effect period was not possible. Thus, we only report functional and morphological data up to 10 weeks of study. The suppression on tumor growing all together with the body weight loss of mice treated with cisplatin suggest that this cytostatic drug was acting systemically in mice.

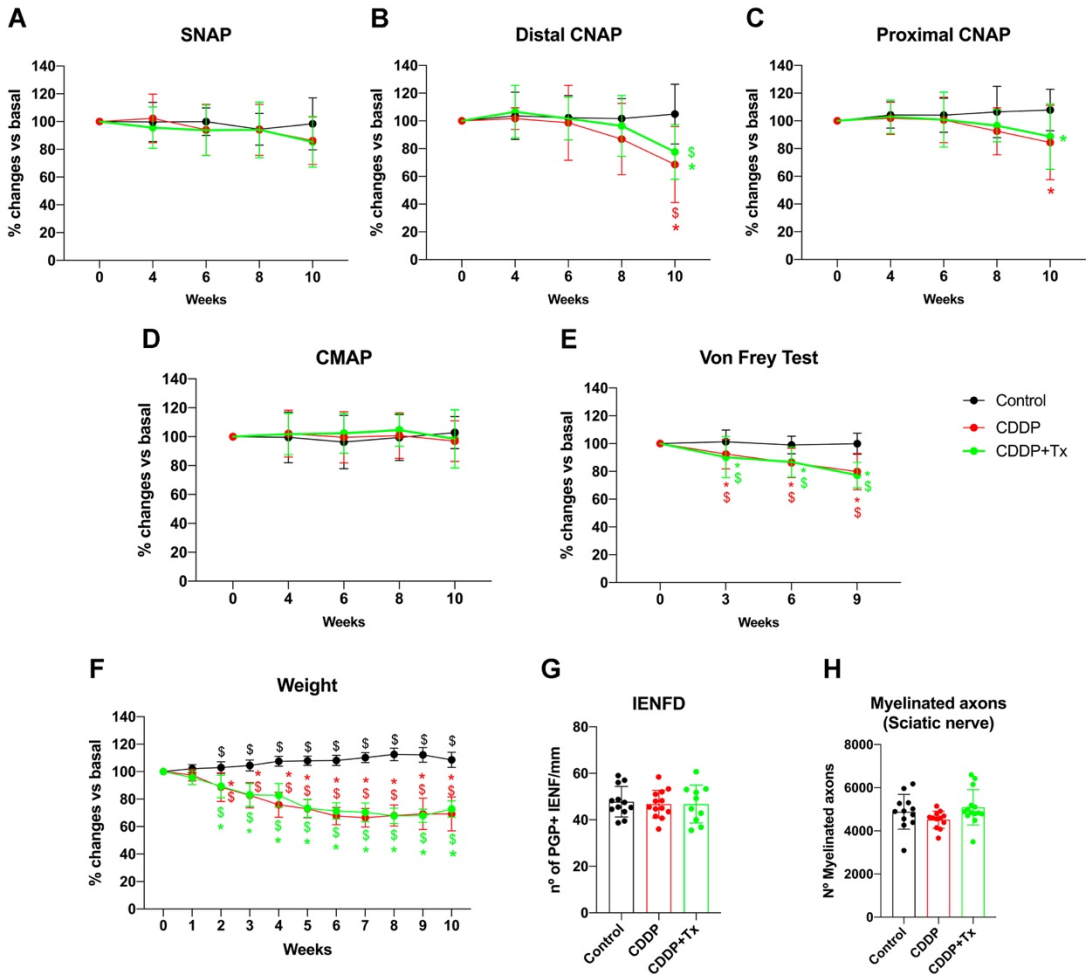

Figure 21. Effects of tumor environment on the development of cisplatin-induced peripheral neuropathy. A-E: Functional tests. SNAP (A), proximal (B) and distal (C) caudal CNAP and CMAP (D). No differences between CDDP and CDDP+Tx groups were seen. Mechanical allodynia was seen in both groups treated with cisplatin along time (E). **F**: Body weight loss did not differ between CDDP and CDDP+Tx animals. n=20-25 mice per group. RM ANOVA with Bonferroni post-hoc test for multiple comparisons. *p<0.05 vs Control; $p<0.05 vs Basal. Data is represented as percentage of change vs basal values (Group Mean± SD). **G-H**: Histological studies. No differences in the number of myelinated axons in the sciatic nerve (G) nor the number of PGP+ IENF (H) were seen between experimental groups. n=12-14 mice per group. One Way ANOVA with Bonferroni post-hoc test for multiple comparisons. Data is represented as Group Mean± SD.

In contrast to cisplatin, oxaliplatin treatment did not avoid the growth of the inoculated tumor. It seems paradoxical as C-26 cell line comes from murine colon adenocarcinoma, and oxaliplatin is the preferential treatment for these types of tumor malignances. In fact, around 4 weeks after C-26 cells injection, tumor start growing in a fast way in animals treated with oxaliplatin. Around 5-6 weeks animals had to be sacrificed and oxaliplatin treatment could not be complete. Therefore, functional evaluation was performed up to 6 weeks after starting the treatment. No differences in

nerve conductions and Von Frey test were seen among OXA and OXA+Tx experimental groups during all the follow-up (Figure 22). Regarding body weight, OXA+Tx animals start losing weight before OXA animals (Figure 22f). We did not assess morphological features in the OXA+Tx group as animals did not get the complete treatment and did not survive to the stablished time point for morphological evaluation (8 weeks).

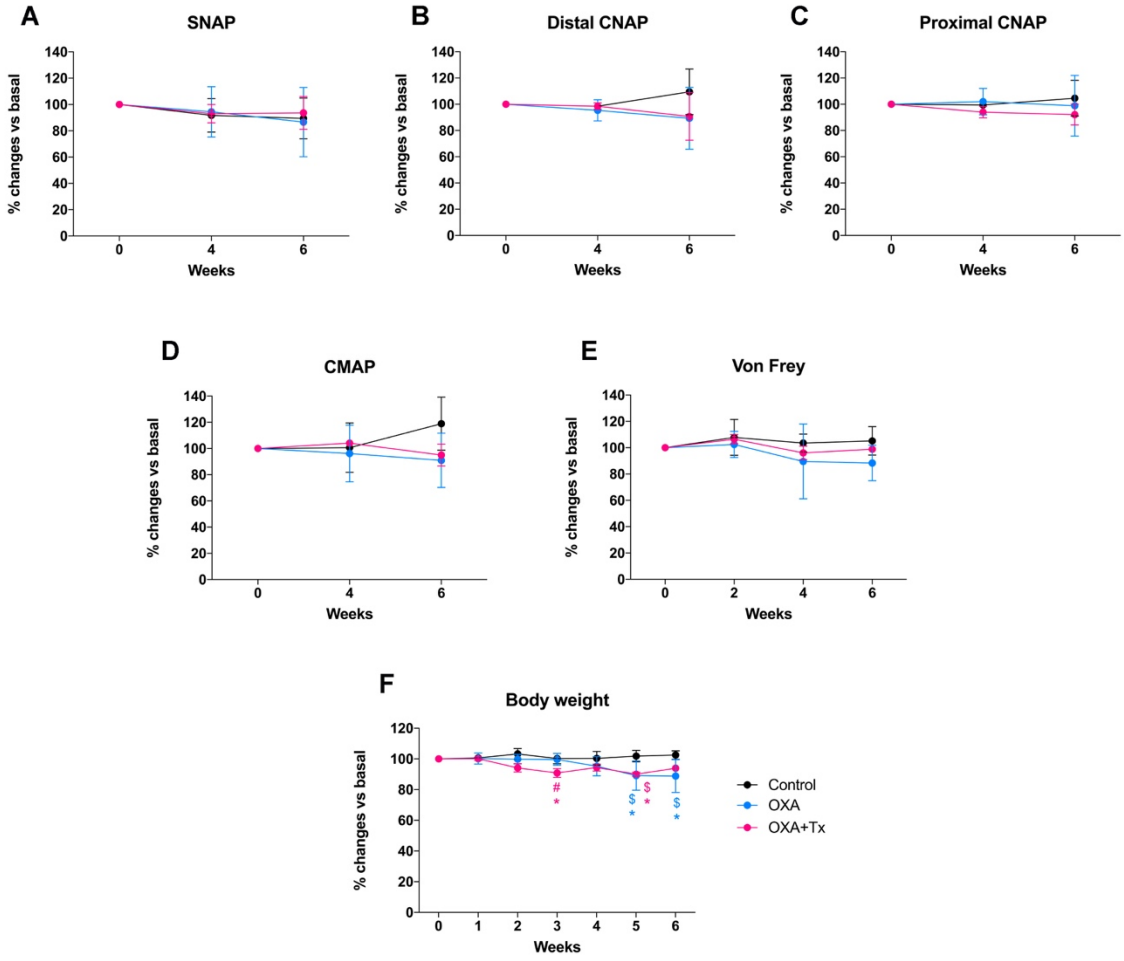

Figure 22. Effects of tumor environment on the development of oxaliplatin-induced peripheral neuropathy. **A-D**: NCS showed no differences between OXA and OXA+Tx mice. **E:** No differences in the Von Frey test were seen between OXA and OXA+Tx mice. **F**: OXA+Tx mice started losing weight before OXA mice. n=5 Control, 15 OXA and 15 OXA+Tx mice per group. RM ANOVA with Bonferroni post-hoc test for multiple comparisons. *p<0.05 vs Control; $p<0.05 vs Basal; #p<0.05 vs OXA. Data is represented as percentage of change vs basal values (Group Mean± SD).

3. Study of the changes in the gene expression profile of DRG sensory neurons after platinum treatment

This section will focus on objective 3 "To study the changes in the gene expression profile of DRG sensory neurons after platinum (cisplatin or oxaliplatin) treatment". It will be subdivided in two main sections, each one focused on a specific cytostatic drug (cisplatin or oxaliplatin).

For both studies, to evaluate the intrinsic response of sensory neurons and SGCs to cisplatin or oxaliplatin exposure, we performed scRNA-seq of DRG cells previously isolated by single-cell sorting from control and platinum-treated mice. We did not include the CDDP+Tx or OXA+Tx groups in the analysis to (1) simplify posterior comparisons and (2) because the tumor environment did not seem to affect the development of PIPN in terms of functional and morphological features.

3.1. Molecular mechanisms involved in the cisplatin-induced peripheral neuropathy

For the cisplatin study, the gene expression analysis was performed at 10 weeks of study, so one week after cisplatin treatment cessation. We chose this timepoint as decrease in SNAPs and/or CNAPs was firstly detected. Thus, transcriptomic data at this time point would give us information about the initial mechanisms in being activated/inactivated due to cisplatin treatment and so involved in PIPN development. Results described in this section have been published in Neuro-Oncology journal.

3.1.1 Isolation and identification of DRG cell populations by scRNA-seq

After isolating DRG cells by single-cell sorting, only the ones meeting the quality control parameters were used for the transcriptomic analysis. It corresponded to a total of 182 cells coming from control mice and 179 cells coming from cisplatin-treated mice. The first step was to identify each isolated cell as a specific cell type (sensory neurons, SGCs, or other less common cell types residing in the DRG). For doing that, we performed the Principal Component Analysis (PCA) of expression magnitudes across all cells and genes sequenced, which revealed 7 distinct cellular clusters. These clusters are represented in a t-distributed stochastic neighbor embedding (t-SNE) plot to simplify their visualization (Figure 23a). In order to identify cluster-specific marker genes, the difference in expression of each gene between one cluster and the average in the resting clusters was calculated. Once we obtained the specific-cluster marker genes (Figure 23b), the identification of each cell cluster was determined by comparing these genes with the mouse nervous system scRNA-seq database published by Linnarsson Lab (Zeisel et al., 2018). The different cell clusters were compatible with SGCs, glial-like cells, neurons, endothelial/pericytes, perivascular macrophages, and vascular smooth muscle cells. Overlaying cells in the t-SNA plot with classical

markers for neurons (*Tubb3, Eno2*) (Usoskin et al., 2015) and satellite glial cells (*Cdh19, Fabp7*) (Avraham et al., 2020; George et al., 2018) corroborate the identity of these two main cell populations of the DRG (Figure 23c). The identity of one of the clusters was unclear, presenting mixed markers for different cell types, and therefore was noted as undefined. It is important to highlight that cisplatin treatment did not alter the expression of cellular hallmarks for each specific population (Figure 23b).

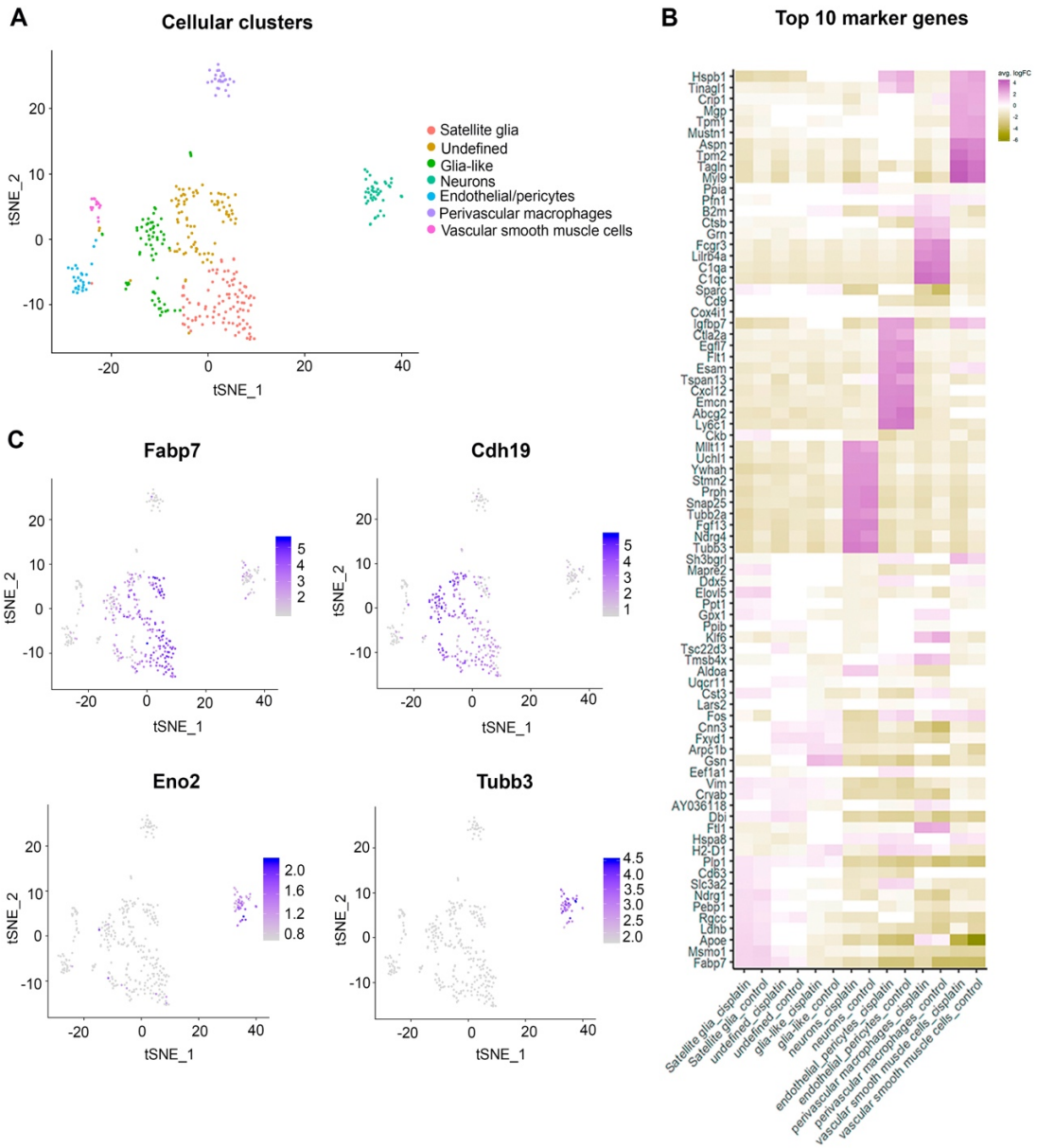

Figure 23. Specific DRG cell populations were obtained by scRNA-seq with previous cell isolation by single-cell sorting. A: t-SNA plot representing the data of the PCA analysis of mRNA transcriptome in the individual sorted DRG cells (each point refers to an individual cell). Cells were tagged for a specific cell type according to their different expression patterns of marker genes. **B:** Heat map showing the Top 10 genes defining each cellular cluster. Unique cell clusters were not altered by cisplatin treatment. Color key represents normalized gene expression with the highest expression (continued on next page, legend follows)

marked pink and the lowest marked green. **C:** Relative expression levels of DRG SGCs (C*dh19* and *Fabp7*) and sensory neurons (*Tubb3* and *Eno2*) markers are mapped to each cell in the t-SNA plot. Color key represents normalized gene expression with the highest expression marked purple and the lowest marked gray.

3.1.2 Transcriptomic changes in the sensory neuron population and SGCs after cisplatin treatment

Once the populations of interest were identified, the mRNA transcriptome profiles of 15 control and 43 cisplatin-treated sensory neurons were compared. A total of 122 DEGs ($p<0.05$) were detected between both experimental conditions (Figure 24a; Supplementary Table 1). Gene Ontology (GO) analysis of DEG with $p<0.01$ revealed that most of the biological processes up-regulated in the CDDP group were related with DNA integrity checkpoints as well as DNA damage response (DDR) (Supplementary Table 3). To reduce the risk of false significant results after multiple comparisons, p-values were corrected and adjusted using the False Discovery Rate (FDR) method, thus obtaining the adjusted p-value (p-val-adj). In our experiment, among all the 122 DEGs, only 5 genes (*Cdkn1a, Rbm3, Rcor3, Igsf3* and *Brix1*) had a p-val-adj<0.05, so they were considered as a reliable DEGs between control and cisplatin-treated mice (Figure 24a). When focusing on the SGCs population, we saw a total of 176 DEG with $p<0.05$. From those genes, only 2 were significantly differentially expressed after correcting p-value for multiple comparisons. Again, *Cdkn1a* gene was one of the significantly up-regulated DEGs in the cisplatin-treated mice (Figure 24b; Supplementary Table 2). The other up-regulated gene in SGC population was the *Socs3* (Figure 24b; Supplementary Table 2).

To corroborate these significant findings, we first performed a western blot analysis of whole DRG lysates from control and cisplatin-treated mice at 10 and 16 weeks to check the levels of p21 protein, which is the product of the *Cdkn1a* gene. We observed a progressive increase of p21 protein levels during the assessment, that become significant at 16 weeks (Figure 24c). In addition, we wanted to corroborate that sensory neurons were indeed overexpressing p21. Immunofluorescence analysis of DRG cross-sections revealed an increase of neuronal nuclei positive for p21 immunoreactivity in the cisplatin-treated group, which reached significance at 16 weeks (Figure 24d).

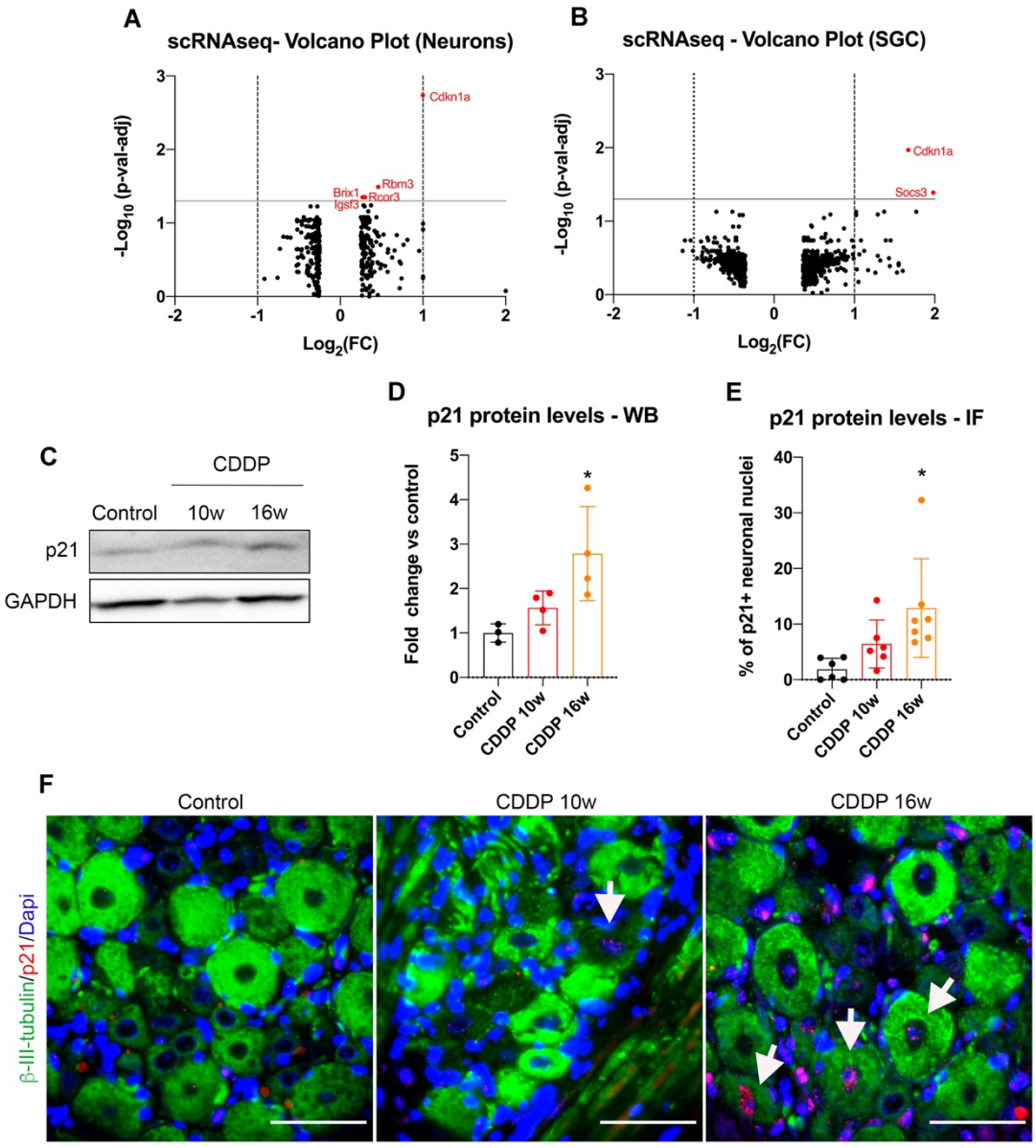

Figure 24. Transcriptomic changes in DRG sensory neurons and SGCs after cisplatin treatment. A-B: Volcano plots of DEGs with p<0.05 in sensory neurons (A) and SGCs (B) populations. The negative log of p-val-adj (base 10) is plotted on the Y-axis, and the log of the FC (base 2) is plotted on the X-axis. The red points on the graphs represent DEGs that are significantly differently expressed in cisplatin-treated (CDDP) mice compared to controls (p-val-adj<0.05). Vertical lines indicate Log_2(FC) of 1 or -1. Horizontal line indicates the point in which p-val-adj<0.05 (-log10(p-val-adj) =1.3). **C-D**: representative blot (C) and quantification (D) of p21 protein levels after western blot (WB) analysis of DRG from control and cisplatin-treated mice at 10 and 16 weeks. n= 3-4 mice per group. One Way ANOVA with Bonferroni post-hoc test for multiple comparisons. *p<0.05 vs Control. Data is represented as Group Mean± SD **E:** Quantification of the percentage of neuronal nuclei positive for p21 protein after immunofluorescence (IF) staining of the DRG. n=6-7 mice per group, One Way ANOVA with Bonferroni post-hoc test for multiple comparisons. *p<0.05 vs Control. Data is represented as Group Mean± SD. **F:** Representative images of p21 immunofluorescence (red) in the DRG of control and CDDP mice at 10 and 16 weeks (continued on next page, legend follows).

Neurons were stained with the pan-neuronal marker β-III-tubulin (green) and nuclei were counterstained with Dapi (blue). White arrowheads indicate neuronal nuclei positive for p21. Scale bar: 50μm.

3.1.3 Activation of a Senescence-like phenotype in sensory neurons after cisplatin treatment

According to our scRNA-seq results, p21 emerges as the most relevant downstream checkpoint of the cisplatin-induced DNA damage response in DRG sensory neurons. However, in non-quiescent cells, p21 can be involved in two different and opposite adaptative cellular responses to stressors: apoptosis and senescence (Manu et al., 2019). Up until now, apoptosis has been extensively described as the main molecular mechanism underlying cisplatin neurotoxicity (Alaedini et al., 2008; Gil and Windebank, 1998; McDonald et al., 2005). To study the activation of apoptosis in our animal model, we checked the levels of cleaved caspase-3, which is necessary for apoptosis execution (Mcllwain et al., 2013). Western blot analysis in the whole DRG showed that there was no active fragment of caspase-3 (15-17Kda) in any of the time points evaluated in mice treated with cisplatin (Figure 25a). Moreover, levels of Bcl-2 protein were not different among control and cisplatin groups (Figure 25b). Similarly, no nuclear apoptotic changes were observed in DRG sensory neurons of cisplatin-treated mice (Figure 25c). These data point out that the increased levels of p21 do not lead to apoptosis activation. Therefore, we wondered whether cisplatin could be inducing a senescence-like phenotype in DRG neurons in our animal model.

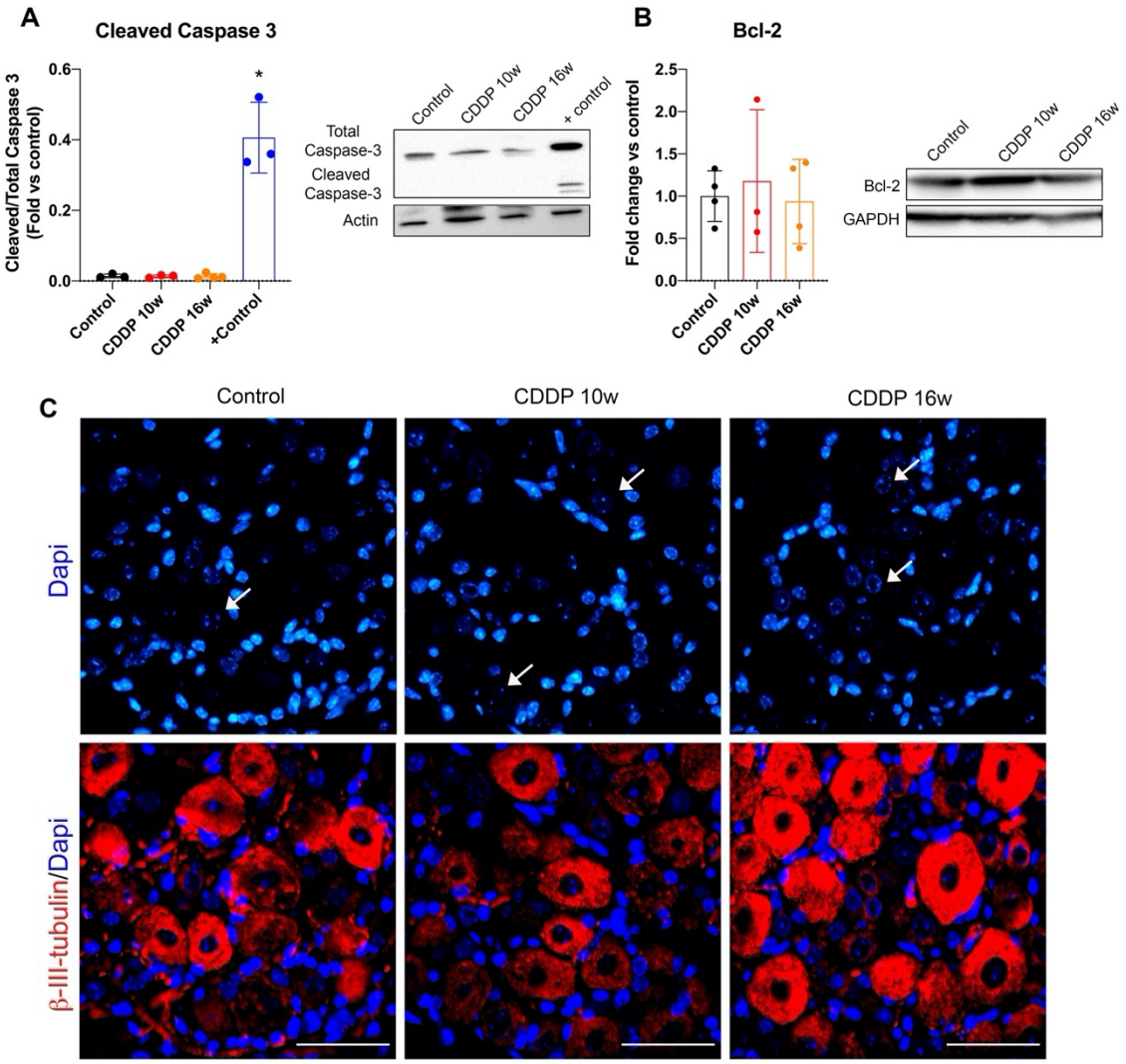

Figure 25. No evidence of apoptosis induction is seen in DRG after cisplatin treatment. A-B: Quantification of cleaved caspase 3 (A) and Bcl-2 (B) protein levels by western blot analysis of DRG from control and cisplatin-treated (CDDP) mice at 10 and 16 weeks. Representative cropped blots of the corresponding proteins are shown. +Control refers to SH-ST5Y cells treated with 1µM staurosporine for 6 hours (a gift from Dr. Yuste). n=3-4 mice per group. One Way ANOVA with Bonferroni post-hoc test for multiple comparisons. *p<0.05 vs Control. **C**: Images of neuronal nuclei from DRG slices stained with Dapi (blue) and β-III-tubulin (red). Neither sensory neurons nor other cell types present in the DRG of treated mice show morphological signs of apoptosis in their nuclei at 10 and 16 weeks follow up. White arrows indicate neuronal nuclei. Scale bar: 50µm.

Cellular senescence is a multifaceted process that arrests the proliferation of cells exposed to permanent DNA damage, thus protecting tissue integrity. The activation of p21/p53 signaling pathway is one of the key inductors of senescence pathways (Campisi and d'Adda di Fagagna, 2007). Senescent cells show a lack of uniform definition and phenotype, especially when talking about postmitotic cells. Thus, a combination of multiple biomarkers and morphological features

have been used to define this anti-apoptotic and non-proliferative cellular state (Hernandez-Segura et al., 2018). To corroborate the hypothesis of a cisplatin-induced senescence-like phenotype in DRG sensory neurons, we first checked the levels of phosphorylated H2AX protein (p-H2AX). This is an early molecular hallmark of DNA damage that has been linked with the occurrence of cellular senescence and final downstream p21 up regulation (Jurk et al., 2012). By western blot, we observed an up-regulation of this protein in DRG of cisplatin-treated mice starting at 10 weeks of treatment (Figure 26a). Immunofluorescence analysis of DRG slices showed that the increase of p-H2AX protein occurs in neuronal nuclei (Figure 26c-d). Another feature of senescent cells is the development of a Senescence-Associated Secretory Phenotype (SASP) that consists of a concerted hyper-secretion of pro-inflammatory factors and extracellular matrix proteases (Basisty et al., 2020; Rodier et al., 2009). Thus, we checked the levels of Nfkb-p65 protein, an important inductor of the SASP phenotype (Chien et al., 2011). Results of western blot showed that cisplatin induces an up-regulation of the Nfkb-p65 protein at 16 weeks of the study (Figure 26b). This progressive significant expression of Nfkb-p65 protein was located in the nucleus of DRG neurons as shows the immunofluorescence analysis of cisplatin-treated mice (Figure 26c-d).

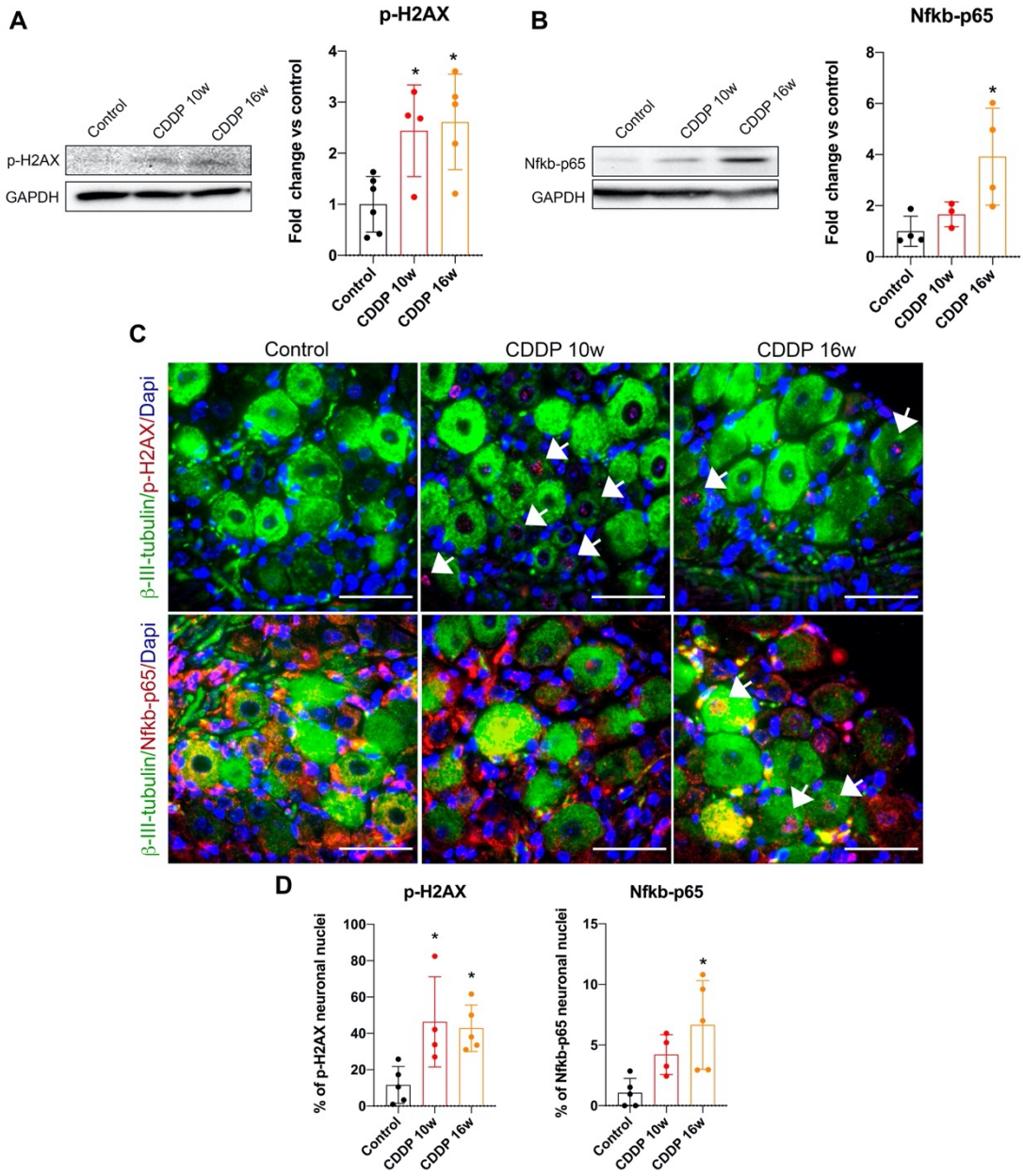

Figure 26. Cisplatin treatment induces molecular senescence hallmarks in mice DRG neurons. A-B: Quantification of p-H2AX (A) and Nfkp-p65 (B) protein levels by western blot analysis of DRG from control and cisplatin-treated (CDDP) mice at 10 and 16 weeks. Representative cropped blots of the corresponding protein are shown. n=3-6 mice per group. One Way ANOVA with Bonferroni post-hoc test for multiple comparisons. *p<0.05 vs Control. Data is expressed as fold change vs the average of control group (Mean± SD). **C:** Representative images of Nfkb-p65 and p-H2AX immunofluorescence (red) in the DRG of control and CDDP mice. Neurons were stained with the pan-neuronal marker β-III-tubulin (green) and nuclei were counterstained with Dapi (blue). White arrows show neuronal nuclei positive for p-H2AX or Nfkb-p65. Scale bar: 50µm. **D:** quantification of the percentage of neuronal nuclei positive for p-H2AX and Nfkb-p65 proteins. n=4-5 mice per group. One Way ANOVA with Bonferroni post-hoc test for multiple comparisons. *p<0.05 vs Control. Data is represented as Mean± SD.

To further corroborate the senescence-like phenotype in sensory neurons after cisplatin treatment, we performed the senescence-associated β-galactosidase (SA-βGAL) assay in DRG slices, a widely used molecular marker of cellular senescence (Dimri et al., 1995). Mice treated with cisplatin showed a significantly higher intensity of the SA-βGAL staining at 16 weeks compared to controls (Figure 27).

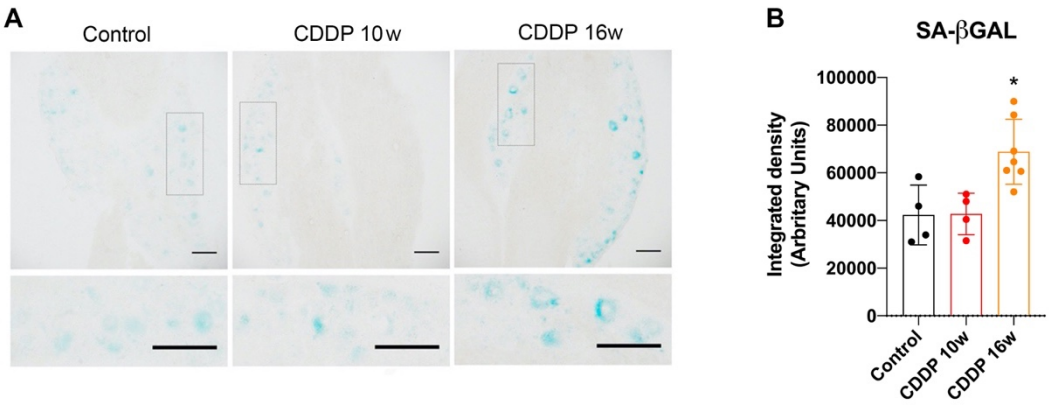

Figure 27. SA-βGAL staining of DRG. A: SA-βGAL positive neurons are seen in DRG of control and cisplatin-treated (CDDP) mice at 10 and 16 weeks of study. Images below correspond to a magnification of the box-delimited areas of the upper images. Scale bar: 100µm. **B:** quantification of the SA-βGAL staining intensity in control and CDDP mice n=3-7 mice per group. One Way ANOVA with Bonferroni post-hoc test for multiple comparisons. *$p<0.05$ vs Control. Data is represented as Group Mean± SD.

Finally, we evaluated the structural changes that DRG sensory neurons suffered after cisplatin treatment by Transmission Electron microscopy (TEM). In comparison to controls, neurons of cisplatin-treated animals presented larger mitochondria, with frequent fusion/fission like phenomena. Most of these neurons also presented an enlarged endoplasmic reticulum with autophagosome-like vesicles in the periplasmic membrane space. All these changes were qualitatively more pronounced at 16 than at 10 weeks (Figure 28). In addition, we observed accumulation of lipofuscin granules, another senescence hallmark (Georgakopoulou et al., 2013) in the neuronal cytoplasm of cisplatin-treated animals at 16 weeks (Figure 28g-h). These granules were not seen in controls nor in treated animals at 10 weeks.

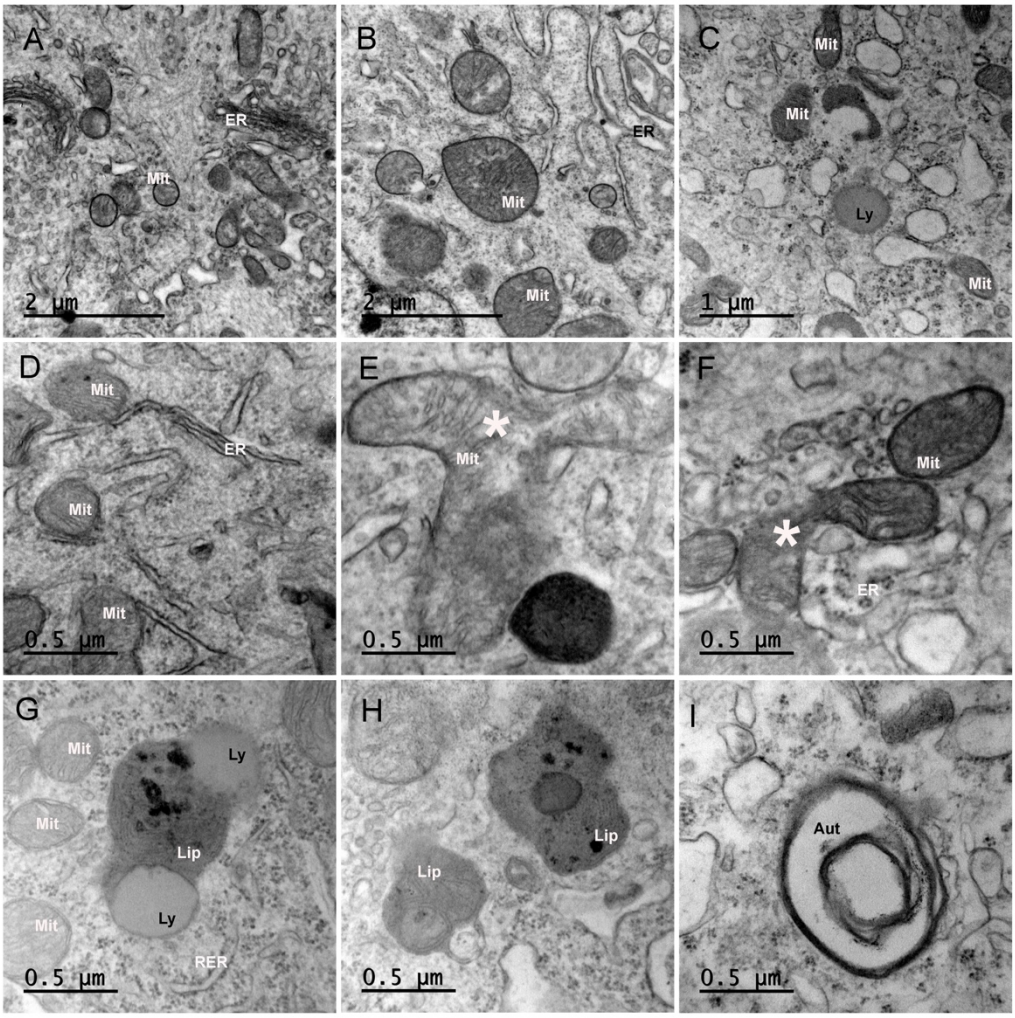

Figure 28. TEM images of DRG neurons from control and cisplatin-treated mice. A-C: General view of the neuronal cytoplasm of control (A) and cisplatin-treated mice at 10 weeks (B) and 16 weeks (C). Mitochondria (Mit) and endoplasmic reticulum (ER) appear dilated in cisplatin-treated animals at both 10 weeks and 16 weeks when compared with control. Moreover, at 16 weeks, neurons from the cisplatin condition present lysosome vesicles (Ly) and lipofuscin granules (Lip). **D-I:** magnified views of the neuronal cytoplasm of control (D) and cisplatin-treated mice (E-I). In the cisplatin conditions, it is frequent to see fission/fusion mitochondrial phenomena (indicated with an asterisk *, E-F), which are rare in the control condition. Lipofuscin granules (Lip), lysosomes vesicles (Ly) and Autophagosome-like vesicles (Aut) are seen in DRG sensory neurons from cisplatin-treated mice at 16 weeks.

3.2 Molecular mechanisms involved in the oxaliplatin-induced peripheral neuropathy

The gene expression study in the oxaliplatin animal model was performed at 8 weeks of study, so one week after treatment cessation.

3.2.1 Isolation and identification of DRG cell populations by scRNA-seq

From all the sorted cells, only the ones meeting the quality control parameters were used for the comparative analysis. It corresponded to a total of 113 cells coming from control mice and 136 cells coming from oxaliplatin-treated mice. After PCA analysis of expression magnitudes across all cells and genes sequenced, we found 8 distinct cellular clusters. These clusters are represented in t-SNE plot to simplify their visualization (Figure 29a). To identify potential cluster marker genes, we performed simple differential expressions tests between pairs of clusters. For each cluster, we performed t-test to identify DEGs to at least one other cluster. In Figure 29b-i, all pairwise tests for each cluster are combined into a single raking by taking the top genes from each pairwise comparison.

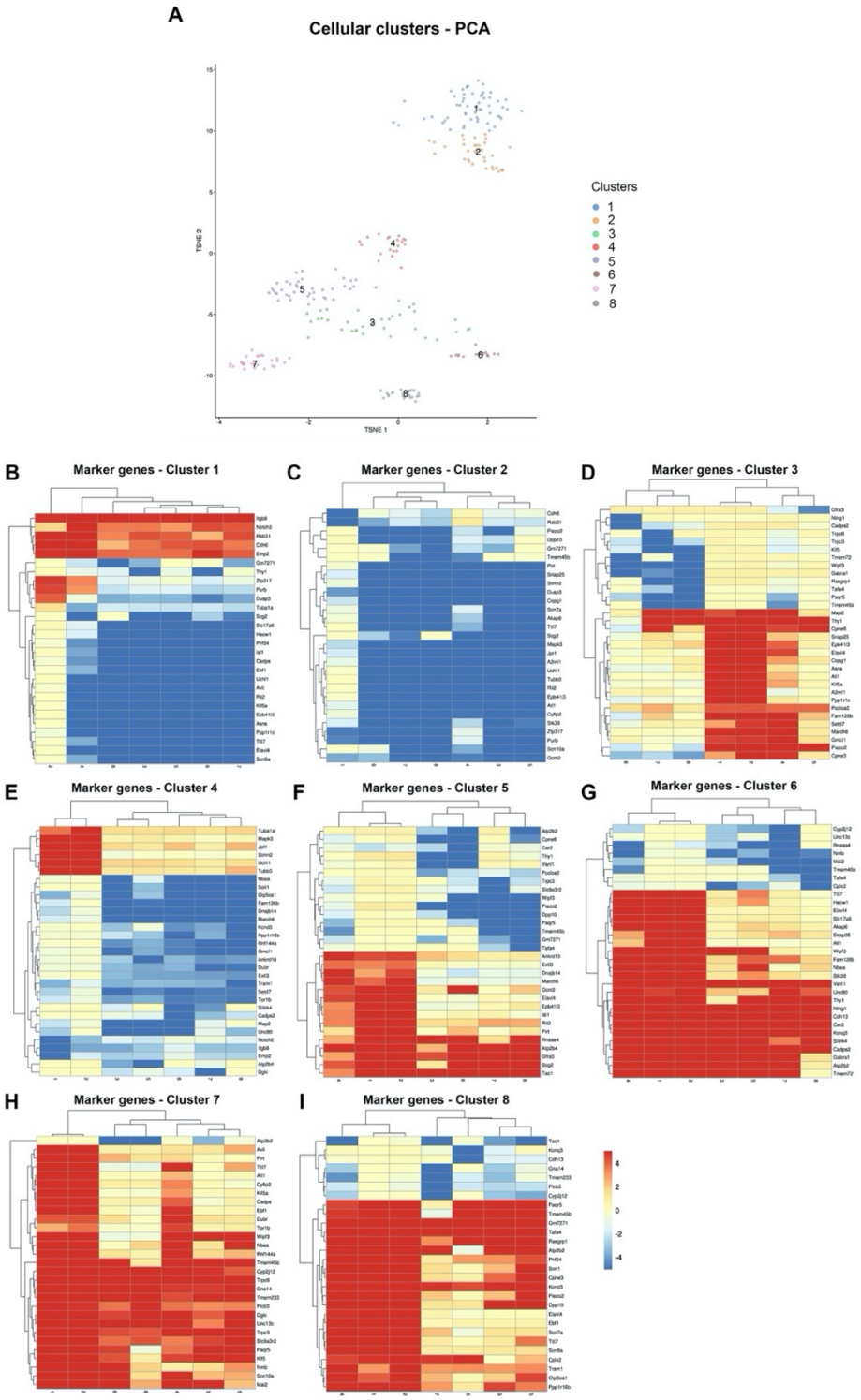

Figure 29. Cellular clusters obtained after scRNA-seq. A: t-SNA plot representing the data of the PCA analysis of mRNA transcriptome in the individual sorted DRG cells (each point refers to an individual cell). Cells were tagged for a specific cluster according to their different expression patterns. **B-I:** Heat map showing the top marker genes of each cellular cluster obtained from each pairwise comparison. Color key represents normalized gene expression in the cluster of interest with the highest expression (up-regulated) marked red and the lowest (down-regulated) marked blue.

The identification of specific cell populations was conducted by comparing the expression profile of each cell with the mouse nervous system scRNA-seq database published by Linnarsson Lab (Zeisel et al., 2018). We identified 7 distinct cell populations, which correspond to Peptidergic (PEP) neurons, Non-peptidergic neurons (NP, cluster 5), TH neurons, Neurofilament (NEF) neurons, SGCs, Schwann cells and vascular endothelial cells (VEC) (Figure 30). As seen in Figures 30a-b, cell populations and cellular clusters do not perfectly match. In fact, different cell populations were classified in the same cluster; and the same cell population had representation in different cellular clusters. After seeing this ubiquity between clusters and cell types, we decided to perform all the cell population-specific down-stream analysis based on the cell type classification rather than the cluster one. Figure 30c shows the t-SNA plot based on cell-type classification. All neuronal populations are characterized by the over-expression of *Tubb3* and *Eno2* neuronal markers (Figure 30d-e).

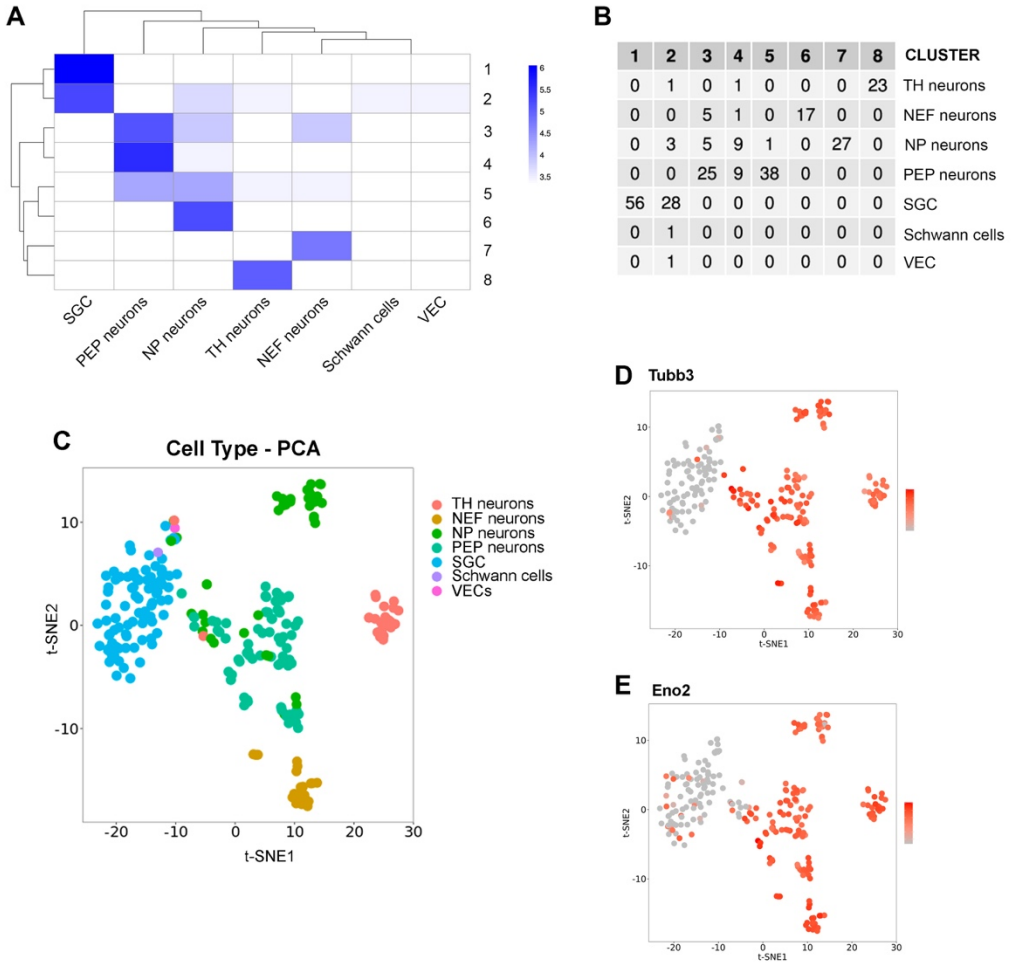

Figure 30. Specific DRG cell populations obtained by scRNA-seq. A: Heat map showing the enrichment of each cluster for a specific cell type. Color key represents normalized gene expression with the highest expression marked blue and the lowest marked white. **B:** Summary table specifying the number of cells obtained from each cluster and cell type. **C**: t-SNE plot showing the distribution of different cell populations obtained in the analysis. **D-E**: Neuronal populations overexpress the (continued on next page, legend follows)

specific neuronal markers *Tubb3* (D) and *Eno2*. (E). Color key represents normalized gene expression with the highest expression marked red and the lowest marked grey.

3.2.2 Transcriptomic changes in sensory neuron populations and SGCs after oxaliplatin treatment

On the first biggening, we tried to identify the DEGs between control and oxaliplatin-treated mice in the different neuronal subpopulations (TH, NEF, PEP and NP). However, due to the low number of cells per condition in each subpopulation, we did not obtain significant DEGs in terms of p-val-adj. Therefore, we decided to group all the neuronal populations as one unique cell population (tagged as Neurons). After grouping them, we found a total of 561 DEGs with p<0.05. From those genes, only 3 have a p-val-adj<0.05. The 3 DEGs of the neuronal population correspond to the protein coding genes Latexin (*Lxn*) and Kallikrein-5 (*Klk5*), and the unprocessed pseudogene *Gm5734*. All three DEGs were up-regulated in the OXA group (Figure 31a; Supplementary Table 4). Regarding SGCs, we found a total of 516 DEGs with p<0.05. After adjusting for multiple comparisons, 28 genes had a p-val-adj<0.05 (Figure 31b; Supplementary Table 5).

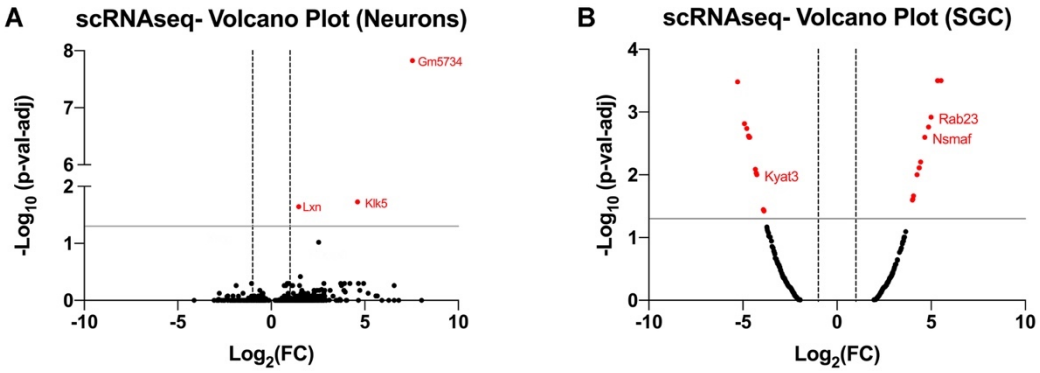

Figure 31. Transcriptomic changes in DRG sensory neurons and SGCs after oxaliplatin treatment. A-B: Volcano plots of DEGs with p<0.05 in sensory neurons (A) and SGCs (B) populations. The negative log of p-val-adj (base 10) is plotted on the Y-axis, and the log of the FC (base 2) is plotted on the X-axis. The red points on the graphs represent DEGs that are significantly differently expressed in oxaliplatin-treated mice compared to controls (p-val-adj<0.05). Vertical lines indicate Log_2(FC) of 1 or -1. Horizontal line indicates the point in which p-val-adj<0.05 ($-log_{10}$(p-val-adj)=1.3).

To corroborate the data seen in the scRNA-seq, we first checked the protein levels of *Lxn* and K*lk5* genes products (latexin and KLK5, respectively). As shown in Figure 32, no differences in the levels of these proteins were observed in western blot of DRGs between control and oxaliplatin-treated mice neither at 8 nor 10 weeks (Figure 32a-b). In contrast, the protein levels of KAT3, whose gene expression (*Kyat3*) appeared down-regulated in the SGCs population (Figure 31b), showed reduced levels in the DRG of oxaliplatin-treated mice by western blot analysis (Figure 32c).

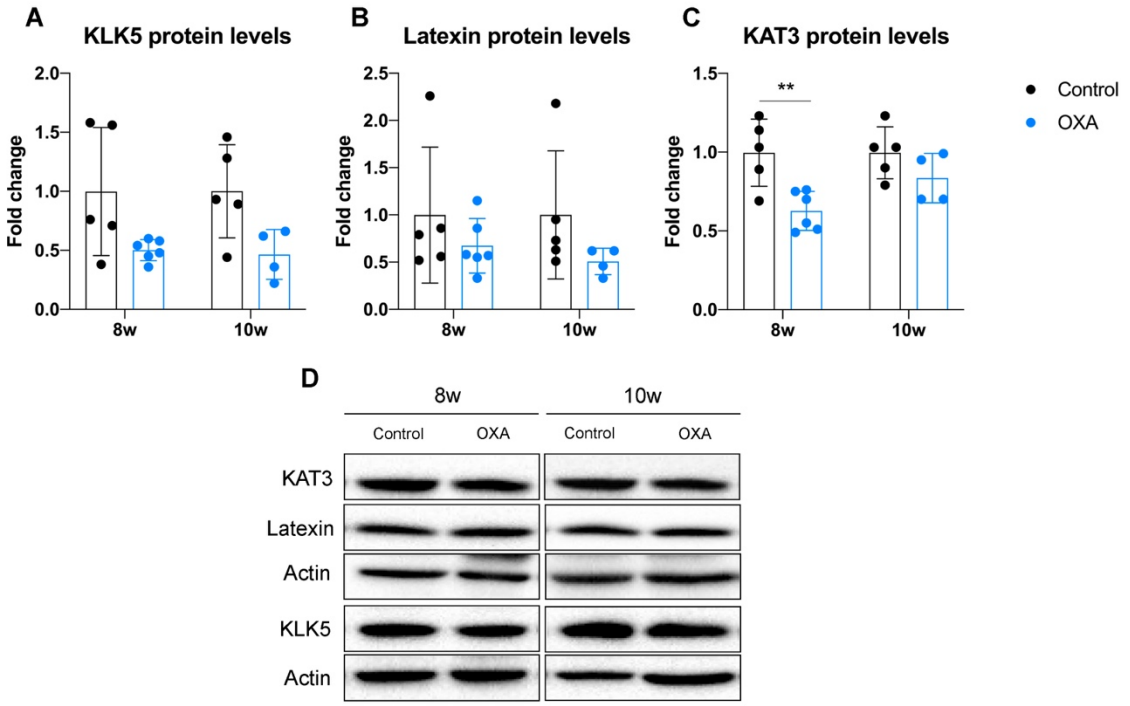

Figure 32. Protein levels of DEGs obtained by scRNA-seq of the DRG. **A-C**: quantification of the protein levels of KLK5 (A), latexin (B), and KAT3 (C) by western blot of DRGs of control oxaliplatin-treated (OXA) mice at 8 and 10 weeks. n=4-6 mice per group. Two Way ANOVA with Bonferroni post-hoc for multiple comparisons. **p<0.01 vs Control of the same time point. Data is expressed as fold change vs the average of control group for each time-point (Group Mean± SD). **D:** Representative blots of the corresponding proteins.

As western blot is a technique that analyze the whole DRG without discriminating cell populations, we hypothesize that the changes suffered by sensory neurons could be masked by the presence of SGCs, which are higher in proportion. Moreover, animals used for the scRNA-seq could not be analyzed by western blot due to lack of DRG samples. To bypass this problem, we performed immunofluorescence staining of DRGs from control and oxaliplatin-treated mice to identify changes in protein expression of KLK5 and latexin in the neuronal population. Although results showed no significant differences among experimental groups and timepoints, we saw that two of the three animals treated with oxaliplatin and used for the scRNA-seq analysis had higher number of neuronal nuclei with KLK5 protein expression at 8 weeks (Figure 33b-c).

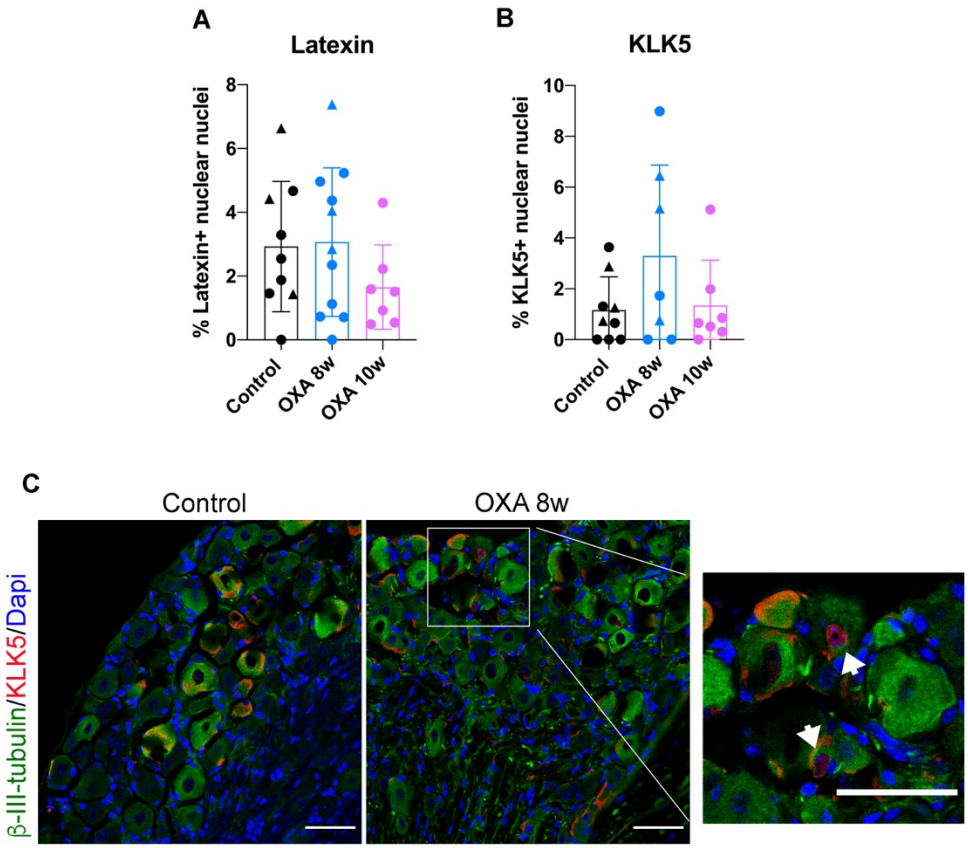

Figure 33 Immunolfuorescence analysis of KLK5 and latexin proteins in the DRG. A-B: Quantification of the percentage of DRG neuronal nuclei immunoreactive for latexin (A) or KLK5 (B) proteins in control and oxaliplatin-treated (OXA) mice. Triangles correspond to animals used for the scRNA-seq analysis. n=7-11 mice per group. One Way ANOVA with Bonferroni post-hoc test for multiple comparisons. Data is represented as Group Mean±SD. **C:** Representative images of KLK5 staining (red) in the DRG of control and OXA mice at 8 weeks. β-III-tubulin (green) was used to stain the neuronal population and nuclei were counterstained with Dapi (blue). White box is magnified for a better visualization of KLK5+ neuronal nuclei. White arrows indicate KLK+ neuronal nuclei. Scale bar: 100µm; Scale bar of magnified view: 50µm.

3.2.3 Inflammatory-Immunogenic response as a mechanism of oxaliplatin neurotoxicity

Both latexin and KLK5 have been involved in processes of inflammation, immune cell response and pain. Specifically, the kallikrein (KLK) family of proteins, which are serine proteases, can modulate and activate multiple players of the immune system (i.e. macrophages, dendritic cells, T and B lymphocytes) through different pathways, including the activation of Proteinase Activated Receptors (PARs) (Fiorucci and Distrutti, 2002; Emami and Diamandis, 2007; Mrozkova et al., 2016) and the modulation of nociceptors (Jimenez-Vargas et al., 2018). In contrast, latexin protein is the only reported carboxypeptidase A1 inhibitor and has been related with attenuation of pain and inflammatory responses (Jin et al., 2006; Kühlein et al., 2011; Li et al., 2020). Moreover, *Kyat3* encodes the KAT3 aminotransferase involved in the kynurenine pathway, which is tightly regulated

by cytokines. In fact, cytokines can affect the expression of various kynurenine enzymes, thus orchestrating metabolic changes that can influence immune cell responses and viceversa (Baumgartner et al., 2019). In addition, oxaliplatin is the only platinum drug described for activating the so-called Immunogenic Cell Death (ICD) in front of tumor cells (Rebé et al., 2019). ICD is a specific type of regulated cell death involving an inflammatory response that may culminate with the activation of cytotoxic T lymphocytes, driven adaptative immunity coupled with the establishment of immunological memory against tumor (Fumet et al., 2020). Considering all these data, we hypothesized that oxaliplatin treatment could be activating an inflammatory or immune response in mice DRG neurons as a response to KLK5 and latexin over-expression.

To corroborate this hypothesis, we checked the levels of some pro- and anti-inflammatory cytokines in DRGs and sciatic nerves of control and oxaliplatin-treated mice at 8 and 10 weeks of study. Animals treated with oxaliplatin had increased levels of some pro-inflammatory cytokines in both tissues. Significant changes were seen at 8 weeks, whereas the levels of cytokines were restored at 10 weeks (Figure 34). The most significant up-regulated cytokines in sciatic nerves of oxaliplatin-treated mice were MCP-1 (CCL2) and MIP-1α (CCL3). At the DRG level, GRO-α (CXCL1) was the only significant up-regulated cytokine. All of them are pro-inflammatory cytokines involved in the recruitment of immune cells like monocytes, neutrophiles and T-cells, as well as in the ICD establishment (Showalter et al., 2017). In accordance with that, animals treated with oxaliplatin had increased infiltrated cells in their sciatic nerves compared with control animals (Figure 19c-d)

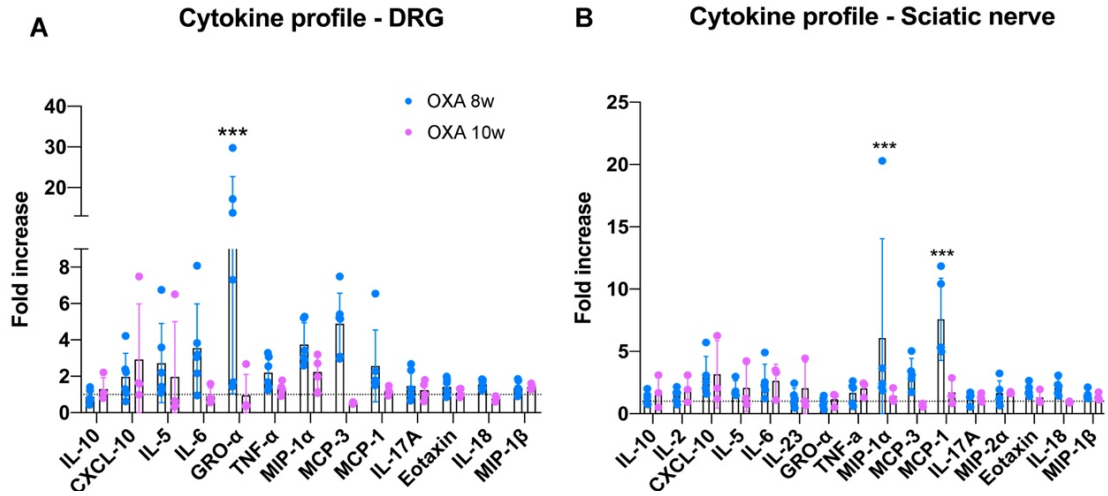

Figure 34. Cytokine profile in DRG and Sciatic nerves after oxaliplatin treatment. Bar graphs showing the quantification of cytokine protein levels in DRG (A) and Sciatic nerves (B) of oxaliplatin-treated (OXA) mice at 8 and 10 weeks. Horizontal lines indicate fold increase equal 1 corresponding to control animals. n=3-6 mice per group. Two-Way ANOVA with Bonferroni post-hoc test for multiple comparisons. ***p<0.001 vs Control. Data is expressed as fold increase vs average levels of control animals. (Group Mean± SD).

To determine the possible role of the ICD-like response in the establishment of oxaliplatin induced neuropathy, we checked the expression of calreticulin protein (Galluzzi et al., 2020). This is an endoplasmic reticulum (ER)-resident protein involved in many cellular processes. In healthy cells, calreticulin works as a chaperone and Ca^{2+} buffer to assist correct protein folding within the ER. It has been reported that cancer cells activating ICD expose calreticulin on their cell surface, promoting the uptake of the cell by professional phagocytes and ultimately supporting the initiation of anticancer immunity (Fucikova et al., 2020). By western blot of DRGs, we were not able to see differences in the calreticulin protein levels among experimental groups (Figure 35a). Similar, we did not see differences in the translocation of this protein to the cell surface of DRG sensory neurons in oxaliplatin-treated mice when comparing with control mice at any time point evaluated by immunofluorescence (Figure 35b-c).

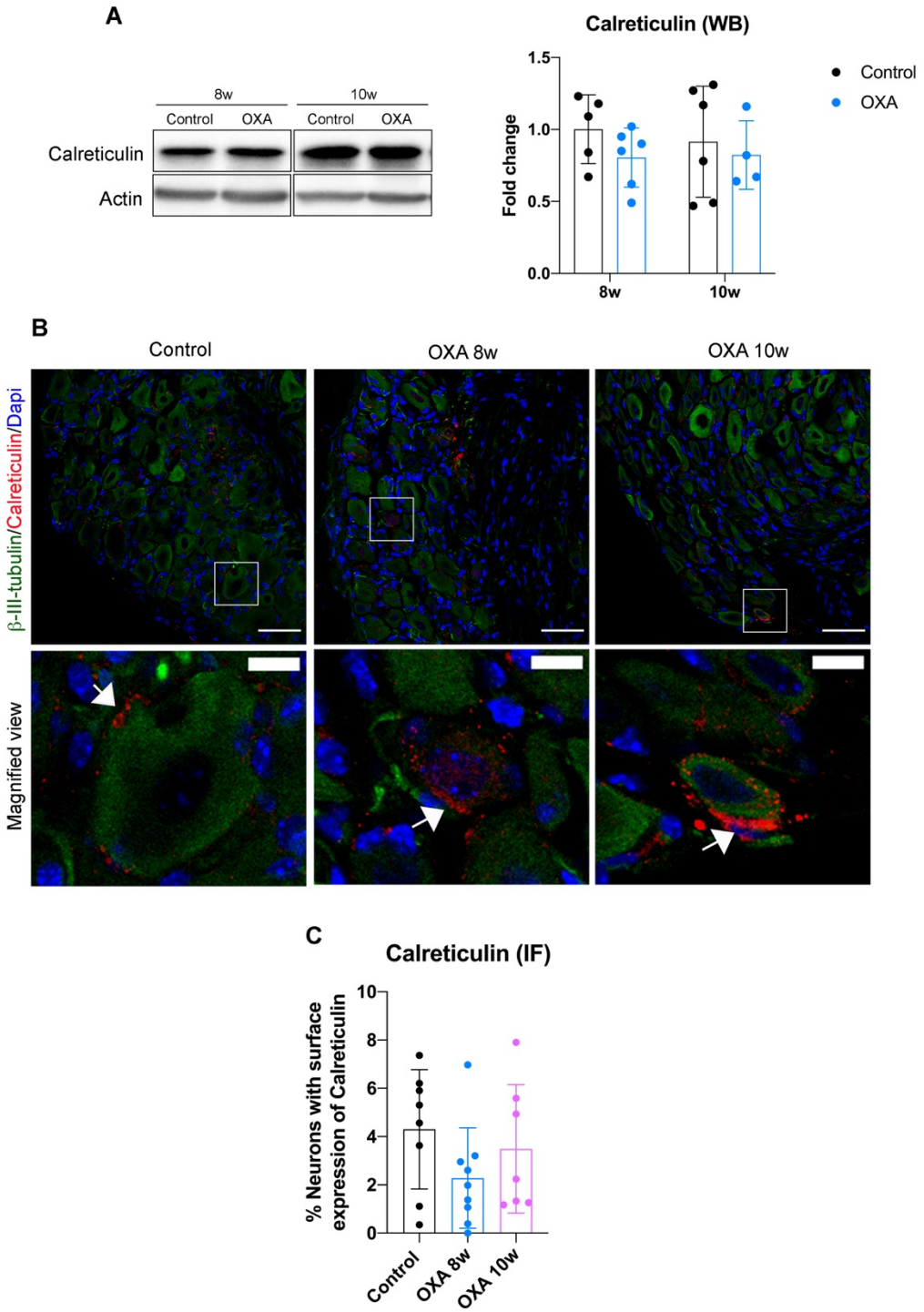

Figure 35. Protein levels of calreticulin in DRGs. A: Representative blots and quantification of calreticulin protein levels by western blot (WB) of DRGs from control and oxaliplatin-treated (OXA) mice at 8 and 10 weeks. n=4-6 mice per group. Data is expressed as fold change vs average of control animals in each time point (Group Mean± SD). Two Way ANOVA with Bonferroni post-hoc test for multiple comparisons. **B:** Representative images of calreticulin staining (red) in DRG of control and OXA mice. β-III-tubulin (green) was used to stain the neuronal population and nuclei were counterstained with Dapi (blue). White boxes are amplified in the images below (magnified view) for a better (continued on next page, legend follows)

visualization of calreticulin staining. White arrows indicate calreticulin staining in the cell surface. Scale bar: 100µm; Scale bar of magnified views: 20µm. **C:** Quantification of the percentage of neurons that present calreticulin expression in their cell surface. n=7-9 mice per group. One Way ANOVA with Bonferroni post-hoc test. Data is represented as Group Mean± SD.

Levels of other markers related with the activation and establishment of ICD, like Heat Shock Protein (Hsp) 70, the Hsp90 and the phosphorylated eIF2a protein at Ser51 (p-eIF2α) (Galluzzi et al., 2020), were not different among groups when performing western blot of DRG (Figure 36).

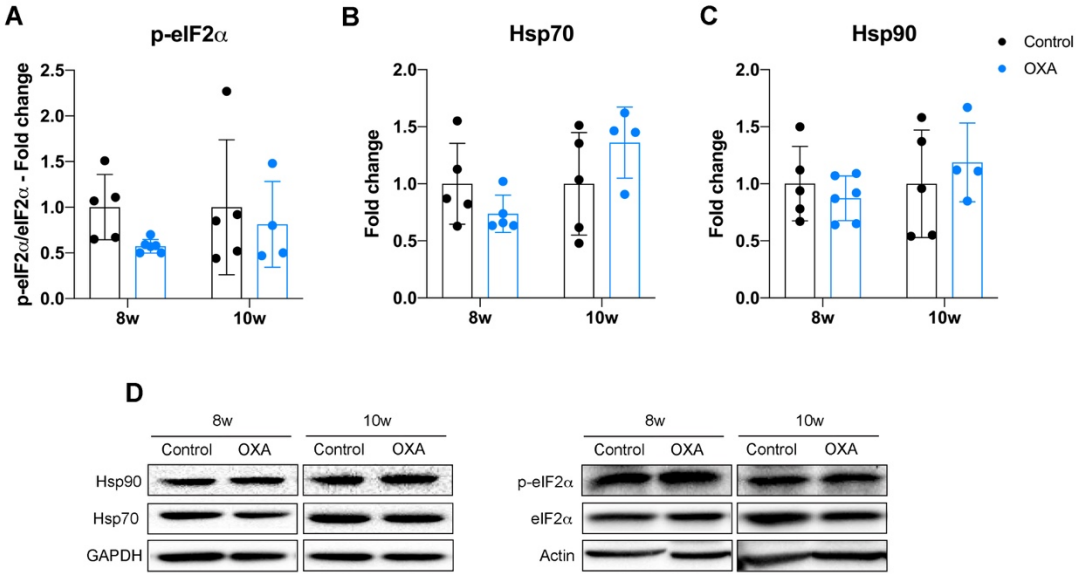

Figure 36. Protein levels of ICD-related proteins by western blot of DRG. A-C: bar graphs showing the quantification of the protein levels of Hsp90 (A), Hsp70 (B) and p-eIF2α (C) in the DRG of oxaliplatin-treated (OXA) and control mice at 8 and 10 weeks of study. n=4-6 animals per group and time point. Two Way ANOVA with Bonferroni post-hoc test. Data is expressed as fold change vs the average of control group for each time point (Group Mean± SD). **D**: Representative blots of the corresponding proteins.

All these results suggest that although a pro-inflammatory response was taking place in both DRG and sciatic nerve of oxaliplatin-treated mice, as indicated by the increased level of pro-inflammatory cytokines, this was not related with an ICD-like responses, at least at the time points evaluated.

3.2.4 Cellular senescence: a common pathway for platinum neurotoxicity?

Results of scRNA-seq of the oxaliplatin study did not show any significant (p-val-adj<0.05) DEG nor GO pathway related with DNA damage in the neuronal population (Supplementary Table 4, 6, 7). However, 3 genes related with the DDR appeared up-regulated (p<0.05) in our data set: *Mif*

(p=0.04), a proinflammatory cytokine that has been related with attenuation of ageing and senescence in different cell types and diseases (Palumbo et al., 2014; Xia et al., 2015; Xia and Hou, 2018; Hu et al., 2018); *Rbbp8* (p=0.005), encoding for the endonuclease CtIP required for homologous recombination-mediated DNA double-strand break repair (Quennet et al., 2011; Makharashvili et al., 2014; Hoa et al., 2015; Mijnes et al., 2018); and *Xrcc1*(p=0.011), which interacts with multiple repair enzymes that are involved mostly in the single-strand break repair pathway but also in other DNA repair pathways (London, 2015). Other genes related with DDR and senescence appeared down-regulated (p<0.05) in our data set. *Npm1* (p=0.035), which protein product travels from the nucleolus to the nucleoplasm in response to DNA damage, promotes p53 stabilization, and enhances DNA repair (Wu et al., 2002; Rubbi and Milner 2003; Kurki et al., 2004); and *Spred1* (p=0.016), an inhibitor of the RAS MAPK signaling pathways that acts as a tumor suppressor (Pasmant et al., 2015; Zhang et al., 2020) and has been linked to cellular senescence through its interaction with miRNA-126 (Yamakuchi, M., & Hashiguchi, 2018; Dominic et al., 2020) (Supplementary Table 4).

Thus, we checked the levels of p-H2AX protein in DRGs of control and oxaliplatin-treated mice by western blot. Results showed that the levels of this protein were increased in animals treated with oxaliplatin compared to controls at 8 weeks of study. In contrast, at 10 weeks of study, oxaliplatin-treated mice have similar levels of p-H2AX protein than control animals. These results suggests that oxaliplatin treatment induced DNA damage to DRG that was restored after oxaliplatin discontinuation (Figure 37).

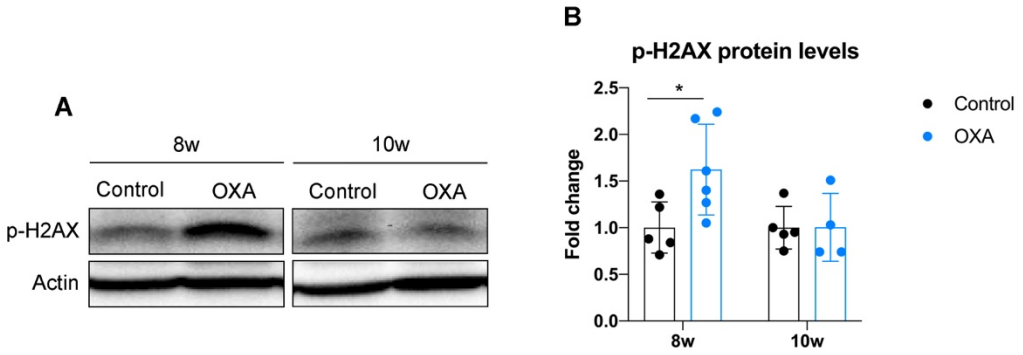

Figure 37. Protein levels of p-H2AX protein in DRG of control and oxaliplatin-treated (OXA) mice. A: representing blots of p-H2AX analysis by western blot at 8 and 10 weeks. **B**: quantification of the protein levels of p-H2AX at the same time points. n=4-6 animals per group and time point. Two Way ANOVA with Bonferroni post-hoc test for multiple comparisons. *p<0.05 vs Control of the same time point. Data is expressed as fold change vs the average of control group for each time point (Group Mean± SD).

We wondered whether the oxaliplatin-induced DNA damage could be activating senescence pathways in DRG as cisplatin did. Thus, we checked the levels of p21 and Nfkb-p65 proteins in the

DRG by western blot. Nfkb-p65 protein was increased in DRG of oxaliplatin-treated mice at 8 weeks. This increased levels of Nfkb-p65 were lost at 10 weeks. p21 protein levels showed a tendency to increase of this protein at 8 weeks that did not reach significance and that was normalized at 10 weeks (Figure 38).

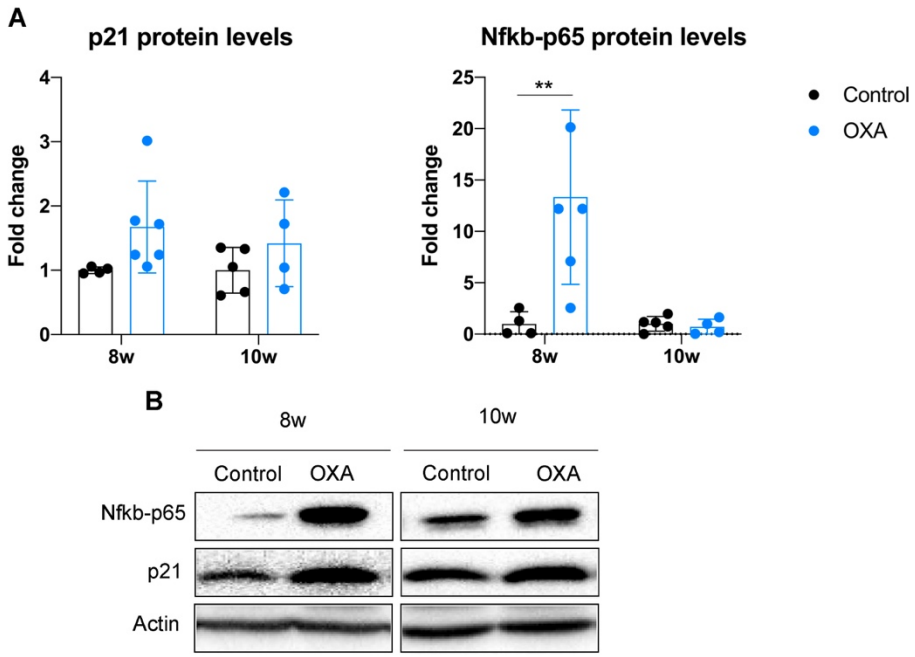

Figure 38. Transient induction of senescence hallmarks in DRG of oxaliplatin-treated (OXA) mice. A: Quantification of the p21 and Nfkb-p65 protein levels by western blot of DRGs of control and OXA mice at 8 and 10 weeks of study. n=4-5 mice per group. Two Way ANOVA with Bonferroni post-hoc test. **p<0.01 vs Control of the same time point. Data is expressed as fold change vs average of control group for each time point (Group Mean±SD). **B:** Representative blots of the corresponding proteins.

4. Characterization of an *in vitro* model of platinum neurotoxicity

This section will focus on the fourth objective of the thesis "To characterize an *in vitro* model of platinum neurotoxicity to test new therapeutical targets based on the *in vivo* data".

After demonstrating that senescence pathways are activated in the DRG after cisplatin treatment *in vivo*, it would be interesting to target senescence pathways as a potential neuroprotective treatment against PIPN. For this purpose, we first aimed to set up an *in vitro* model of platinum-induced neuronal senescence as a time- and cost-effective exploratory drug screening platform.

Some experiments reported in this section were performed in the Cellular Senescence and Age-related Pathologies Group from the European Research Institute for the Biology of Ageing (ERIBA), in the context of an international internship and under the supervision of Dr. Marco Demaria. Specifically, the RT-qPCR and the RNA-seq experiments were conducted during the stage.

4.1 Characterization of an *in vitro* model of cisplatin-induced neuronal senescence

After treating mouse DRG neuronal dissociated cultures with different doses of cisplatin (0.25, 1, and 4µg/ml for 24h in the medium) (Figure 39a), we found that 1µg/ml was the highest dose in which neuronal death was not induced in comparison with a Non-treated (NT) cultures (Figure 39b). Nevertheless, that dose was able to induce DNA damage to sensory neurons, as indicates the increased expression levels of p-H2AX protein by immunofluorescence (Figure 39c-d). p-H2AX was significant up-regulated at 1 day after starting the treatment. At 3 and 7 days post-treatment, p-H2AX levels persisted increased, although they were partially reduced suggesting that DNA damage was being partially repaired.

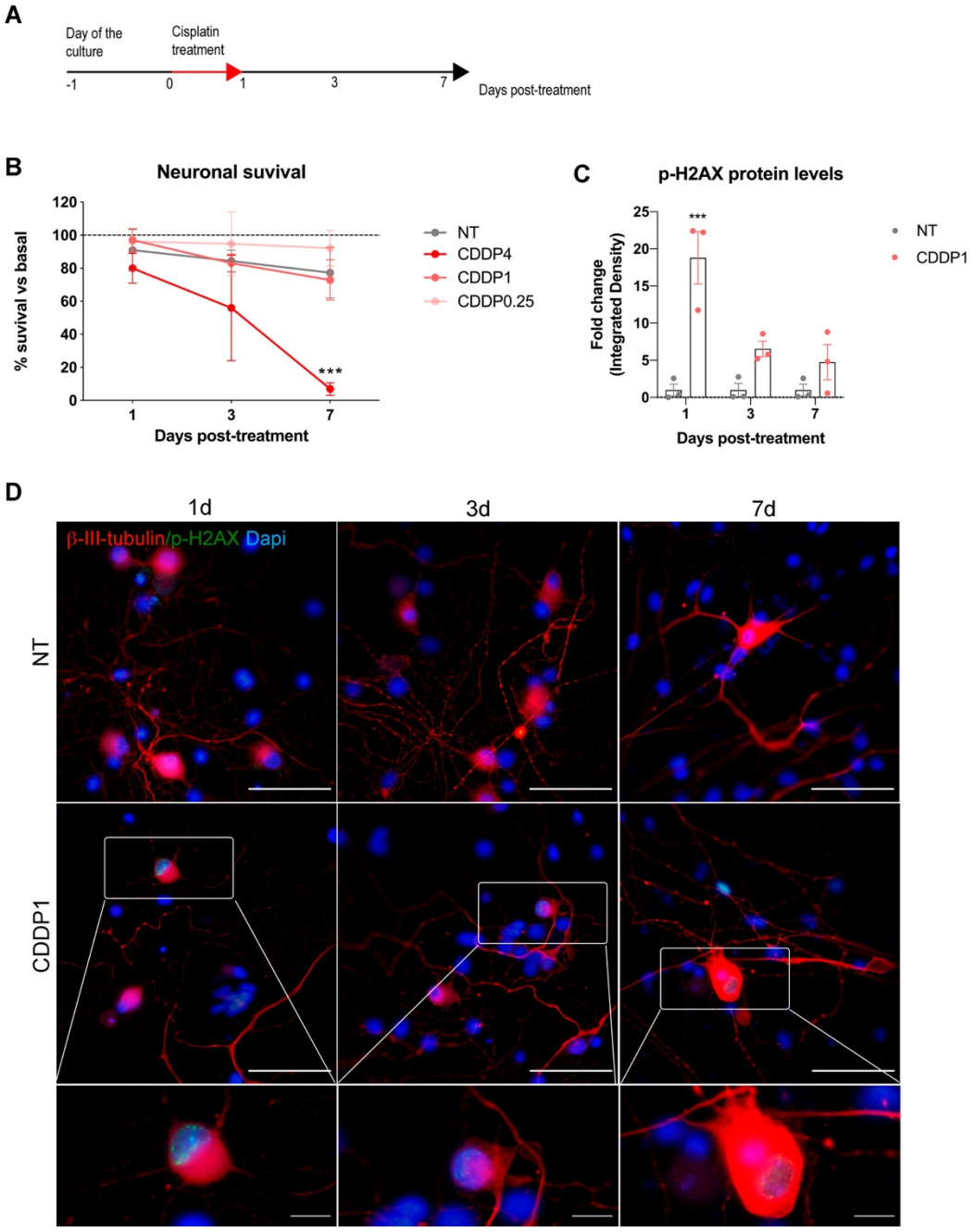

Figure 39 Neuronal survival and DNA damage after cisplatin treatment *in vitro*. A: Scheme of the cultures' follow-up after cisplatin treatment. **B:** Percentage of survival after cisplatin treatment is calculated vs basal values and represented for the different experimental conditions: NT, Non-Treated, CDDP4, cisplatin 4µg/ml; CDDP1, cisplatin 1µg/ml, CDDP0.25, cisplatin 0.25µg/ml. The horizontal line indicates the 100% survival. n=3-5 independent experiments per conditions. RM ANOVA with Bonferroni post-hoc test. *p<0.05 vs NT group. Data is represented as Group Mean±SD. **C:** Quantification of the p-H2AX fluorescence intensity in neuronal nuclei after treatment with 1µg/ml cisplatin (CDDP1). Data is expressed as fold change of integrated density vs NT condition for each time point. n= 3 independent experiments per condition. Two Way ANOVA with Bonferroni post-hoc test. ***p<0.001 vs NT group. Data is represented as Group Mean±SD. **D:** Representative images of p-H2AX (continued on next page, legend follows)

immunofluorescence staining at different time-points after treatment with 1µg/ml cisplatin (CDDP1). Images inside the white box are magnified below for a better visualization of the staining. Scale bar: 50µm. Scale bar of magnified views: 10µm.

To test whether 1µg/ml cisplatin was inducing a senescence phenotype to sensory neurons, we followed the algorithmic assessment for cellular senescence published by Kohli and colleagues (2021).

We first checked the expression levels of different senescence hallmarks by RT-qPCR at 3 days post-treatment. We saw a significant increase in the levels of p21 but not p16 mRNA (Figure 40a). Regarding SASP-related factors, IL-6, Cxcl1 and Mmp1α mRNA expression was significant up-regulated in treated cultures. In contrast, IL1α increase did not reach significance (Figure 40b). Gdnf levels were up-regulated in treated cultures (Figure 40c) and Lamin B1 (Lmnb1) appeared down-regulated (Figure 40d), which are also a typical feature of senescence phenotype.

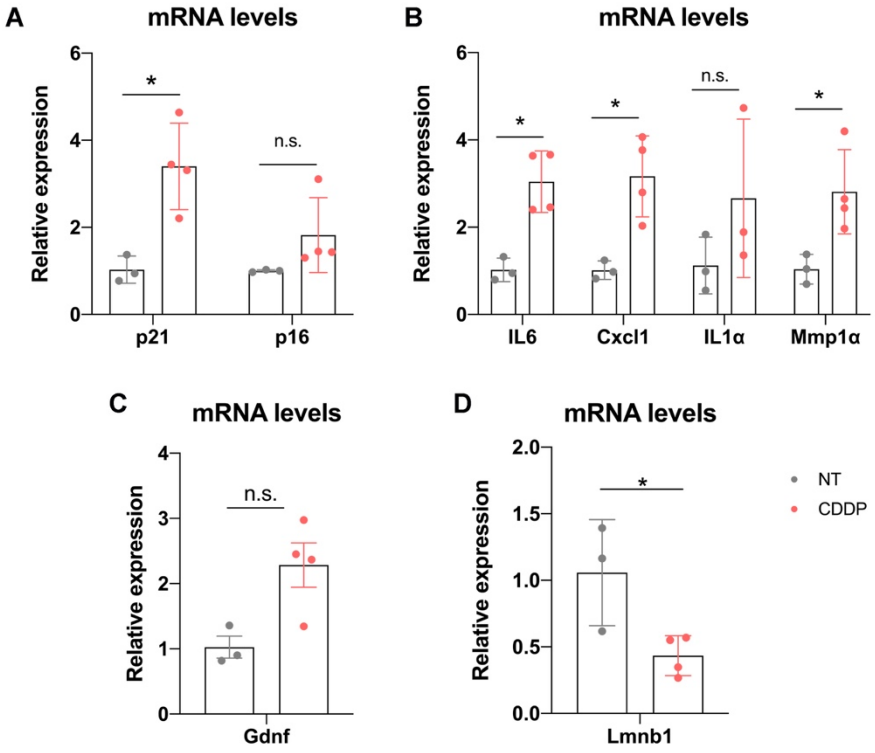

Figure 40. RT-qPCR of senescence hallmarks 3 days after 1µg/ml cisplatin treatment *in vitro*. A: expression levels of p21 and p16 senescence-inductors factors. **B:** expression levels of the SASP-related factors IL6, Cxcl1, IL1α and Mmp1α**. C:** Expression levels of Gdnf. **D:** expression levels of Lmnb1. n=3-4 independent experiments per condition. One Way ANOVA with Bonferroni post-hoc test. *p<0.05 vs NT; n.s., non-significant. Data is expressed as fold change vs NT condition and represented as Group Mean±SD.

Then, we evaluated the SA-βGAL activity in cultured neurons at 3 and 7 days post-treatment. Unexpectantly, we did not see differences among NT and cisplatin-treated cultures (Figure 41). In fact, we saw an increase in the percentage of SA-βGAL+ neurons along time in both experimental conditions, suggesting that SA-βGAL is not a good marker for senescence in DRG primary neuronal cultures.

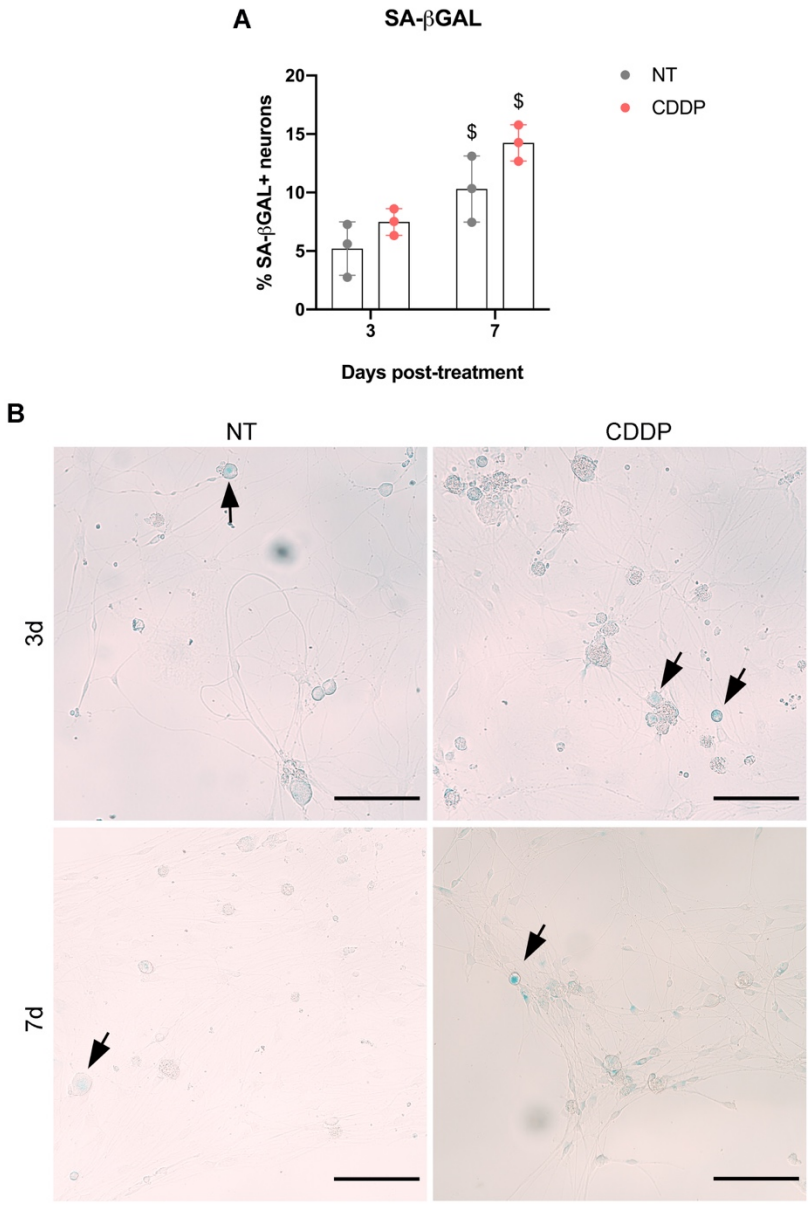

Figure 41. SA-βGAL staining of DRG primary neuron cultures at 3 and 7 days after treatment with 1µg/ml cisplatin. **A:** Quantification of the percentage of neurons positive for SA-βGAL in NT and cisplatin-treated (CDDP) cultures. 3 independent experiments were conducted at the different time points. Two-Way ANOVA with Bonferroni post-hoc test. $p<0.05 vs 3 days. Data is represented as Group Mean±SD**. B**: Representative images of the SA-βGAL staining in DRG primary sensory neuron cultures. Black arrows show neurons positive for SA-βGAL, seen as a blue precipitate. Scale bar: 100µm.

Some pro-inflammatory cytokines have been reported as typical SASP factors (Coppé et al., 2010). To know if cultured neurons treated with 1µg/ml cisplatin acquired a pro-inflammatory secretory phenotype, we checked the levels of some cytokines in the culture medium of NT and CDDP cultures at 1, 3 and 7 days post-treatment (Figure 42a). Eotaxin (CCL11) appeared as the only cytokine whose levels were significantly up-regulated in cisplatin-treated cultures at 3 and 7 days. Other cytokines analyzed appeared slightly increased at 1 day (IL-6, MIP-1α, Gro-α, RANTES) in cisplatin-treated cultures, although this increase was not significant. The levels of these cytokines progressive decreased at 3 and 7 days in treated cultures reaching even lower values than the ones of NT cultures supernatants at 7 days (Figure 42b).

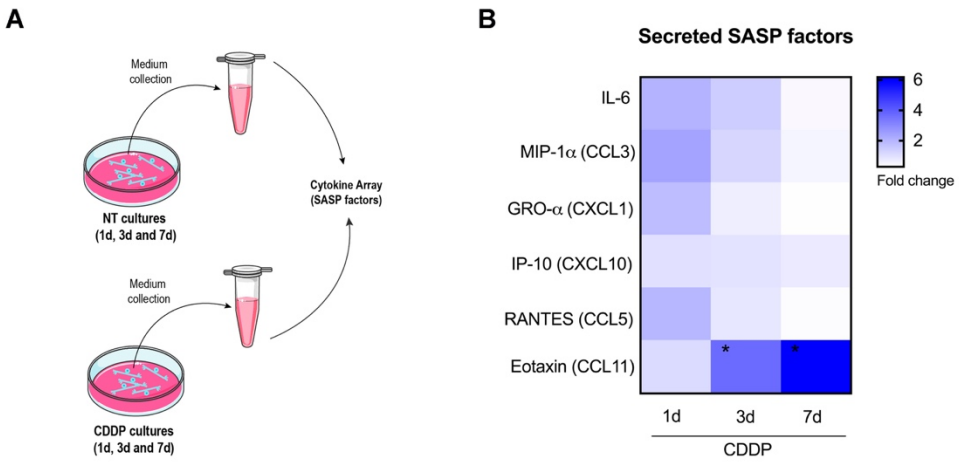

Figure 42. Levels of secreted SASP factors in culture supernatants. A: Schematic representation of the process followed to measure the SASP factors in culture supernatant of NT and cisplatin-treated (CDDP) cultures. At 1, 3 and 7 days after starting the treatment with 1µg/ml cisplatin, cell culture mediums were collected and analyzed by a multiplex cytokine assay. **B**: Heat map showing the fold change of each cytokine in CDDP cultures vs NT cultures of the same timepoint. The highest increase is marked blue. n=4 independent experiments for each condition and timepoint were included in the analysis. *$p<0.05$ vs NT of the same timepoint. Two-Way ANOVA with Bonferroni post-hoc test. Data is plotted as Group Mean.

4.2 Transcriptomic profile of senescent neurons *in vitro*

With the aim of obtaining a complete picture of the neuronal senescent phenotype, we performed RNA-seq of NT and cisplatin-treated (CDDP) cultures at 7 days post-treatment, when the senescence phenotype should be fully stablished (Figure 43).

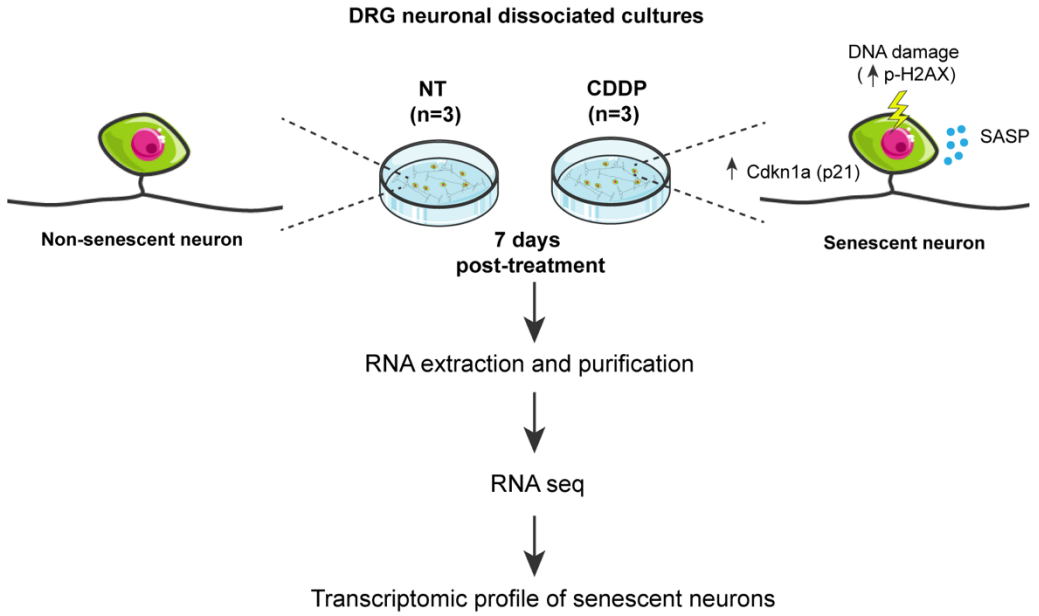

Figure 43. RNA-seq workflow. 7 days after treatment, RNA from NT and CDDP (1µg/ml) neuronal cultures was extracted, isolated, and processed for RNA-seq analysis. A total of n=3 independent biological replicates (culture #1, #2 and #3) were analyzed.

PCA of all 6 samples analyzed (n=3 NT and n=3 CDDP) showed gene expression differences by experimental condition (treatment) (Figure 44a). However, it also showed a separation of the samples from culture number #3 (Figure 44b). Indeed, hierarchical clustering of the samples showed that the samples from culture #3 cluster are closer than with the samples of their respective experimental group, indicating potential technical variability.

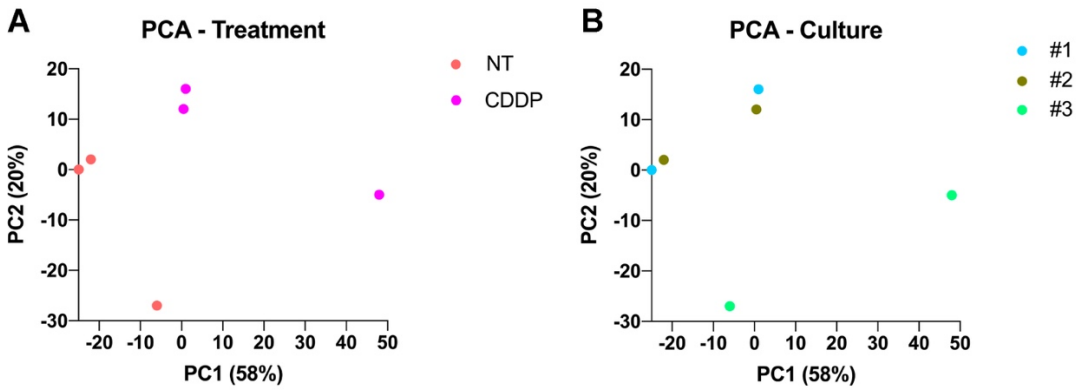

Figure 44. PCA of total 6 samples analyzed. **A:** Each dot represents a specific sample: 3 NT (red) and 3 CDDP (pink). **B**: each dot represents the same sample as A. However, in that case samples are labelled based on the biological replicate (culture #1, blue; #2, brown; or #3, green). PC1 and PC2 explained the 58% and 20% of the total variance, respectively.

The comparison between transcriptomic profiles of NT and CDDP samples showed a total of 122 DEGs up-regulated and 291 DEGs down-regulated in the CDDP condition (Figure 45a; Supplementary Table 8-9). The top 50 DEGs are plotted in a heat map for a better visualization (Figure 45b). *Cdkn1a* gene was significantly up-regulated in cisplatin-treated cultures altogether with other genes related with DDR pathways including *Btg2, Mdm2, Ccng1, Mgmt* or *Pidd1*. These data demonstrated that although the levels of p-H2AX protein were decreased at 7 days post-treatment (Figure 39c-d), DNA damage still present at that time point.

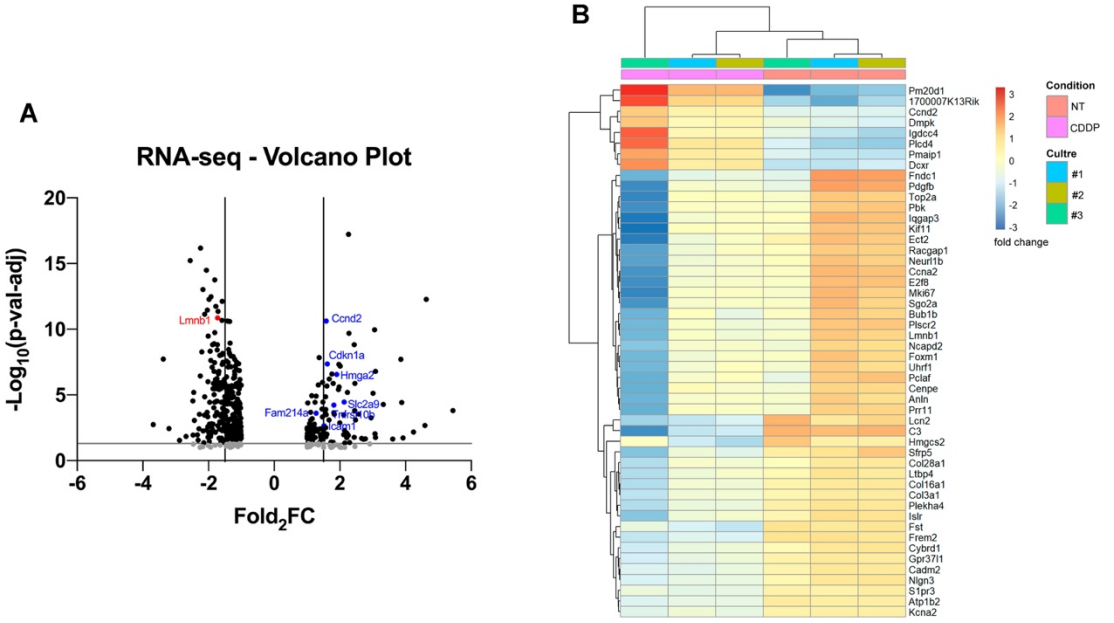

Figure 45. DEGs obtained in DRG neuronal cultures 7 days after 1µg/ml cisplatin treatment. A: Volcano plot of all the DEG (p-val-adj<0.1). The negative log of p-val-adj (base 10) is plotted on the Y-axis, and the log of the FC (base 2) is plotted on the X-axis. The black points on the graphs represent DEGs in the CDDP cultures (p-val-adj<0.05). Vertical lines indicate Log_2(FC) of 1.5 or -1.5. Horizontal line indicates the point in which p-val-adj<0.05 (-log_{10}(p-val-adj) =1.3). Relevant senescence genes are marked red (down-regulated) or blue (up-regulated). **B:** Heat map of top 50 DEGs (p-val-adj<0.05) between NT and CDDP cultures. Up-regulated genes are marker red and down-regulated genes, blue.

In addition to DNA-damage related genes, we found other up-regulated DEGs that have been previously linked to senescence (Hernandez-Segura et al., 2017)(Figure 45a; Supplementary Table 8): *Hmga2*, a non-histone chromosomal high mobility group protein that seems to specifically accumulate on senescent cell chromatin, where it acts as structural components of Senescence-associated heterocromatin focci (SAHFs) and contribute to the stable repression of proliferation-associated genes (Narita et al., 2006)*; Icam1,* a cell surface glycoprotein whose p53-dependent overexpression has been found in senescent cells (Gorgolius et al., 2005)*; Ccnd2,* a regulatory subunit of CD4 and CDK6 necessary for the G1/S transition (Meyyappan et al., 1998); *Tnfrsf10b,*

a member of the tumor necrosis factor receptor superfamily related with the p53-induced SASP (Vjetrovic et al., 2014); *Fam214a*, associated with SASP in different senescence data sets (Flanagan et al., 2017); and *Slc2a9,* a glucose transporter able to reduce ROS and protect against DNA damage due to its antioxidant action (Itahana et al., 2015). On the other hand, *Lmnb1* appeared significantly down-regulated in our data set (Figure 45a; Supplementary Table 9). However, the most significant changed DEG was the *Fndc1* gene, which appeared down-regulated in cisplatin-treated cultures (Supplementary Table 9). Interestingly, this gene has been linked to ageing processes of different tissues such as retina, brain and tumor (Shokhirev and Johnson, 2021; Brouwers, et al., 2017).

When looking for the main genes that comprises the senescence signature in mouse fibroblasts (Hernandez-Segura et al., 2017), we did not find any of them up-regulated in our data set (*Bcl2l2, Plxna3, Tspan13, EfnB3, Pdlm4, Gdnf, Dynlt3* and *Plk3*). Similar, the most common genes related with SASP where not identified and some even appeared down-regulated in our data set, including the *Cxcl5* (Supplementary Table 9). This data agrees with the results obtained in the Cytokine assay, in which there was a general decrease in most of the pro-inflammatory cytokines secreted in the medium of CDDP cultures compared to NT ones 7 days after treatment (Figure 42).

In terms of GO, the only significant term (p-val-adj<0.05) was related with "signal transduction by p53 class mediator". Others Go terms with p<0.05 were also related with "DNA damage", "metabolic process" and "inflammatory responses". Regarding the down-regulated GO terms, most were related with "cell cycle" and "cellular division" (Supplementary Table 10-11).

4.3 Effects of senescence in neuronal metabolism: a preliminarily study

It has been reported that senescent cells show increased aerobic glycolysis, similar than tumor cells (Sabbatinelli et al., 2019; James et al., 2015). In our RNA-seq data set, *Slc2a9* gene appeared up-regulated in the cisplatin-treated neuronal cultures (Figure 45a; Supplementary Table 8). This gene encodes for a facilitator of glucose transporter (GLUT9), and some components of this protein family have been linked with enhanced aerobic glycolysis in tumor cells (Han et al., 2020). Therefore, we explored the metabolic status of the senescent neurons in culture and evaluated a potential metabolic switch from oxidative to glycolytic. For that, we performed *in vitro* real time metabolic analysis by Seahorse technology (Agilent). At 3 and 7 days after cisplatin treatment, we measure the Oxygen Consumption Rate (OCR) and Extracellular Acidification Rate (ECAR) of DRG cultures at basal condition and after inducing a stress by Oligomycin and FCCP compounds. Preliminarily results pointed that at 3 days post-treatment, no differences in ECAR nor OCR metabolic potential were seen between experimental conditions. In contrast, cultures treated with cisplatin showed a higher ECAR metabolic potential at 7 days post-treatment compared to NT cultures (Figure 46).

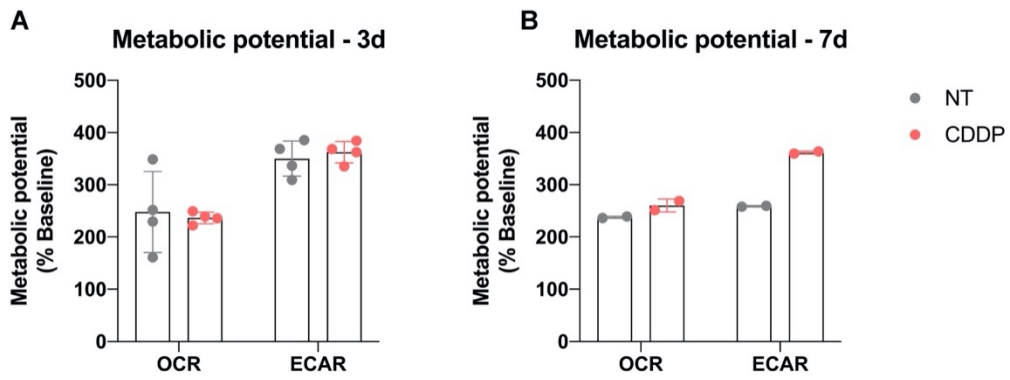

Figure 46. Metabolic potential of DRG neuronal cultures after cisplatin treatment. OCR (A) and ECAR (B) were registered at baseline and after adding stressors (Oligomycin and FCCP) in NT and cisplatin-treated (CDDP) cultures. Metabolic potential was calculated as (basal OCR or ECAR/stressed OCR or ECAR) x 100. Each dot corresponds to one well of 2 independent cultures (3 days) or one culture (7 days). Data is represented as Group Mean± SD.

ECAR is a robust indicator of glycolysis in most cell types. However, when highly aerobic cells are stressed, CO_2 production from the mitochondria can contribute to ECAR and over-report the contribution of glycolysis to metabolic potential (Divakaruni et al., 2014). To identify cells susceptible to this background CO_2 effect, the baseline OCR/ECAR ratio can be used. Cells with a baseline OCR/ECAR ratio<4 produce levels of CO_2 that negligible contribute to ECAR. In contrast, for cells with a baseline OCR/ECAR ratio>4, the stressed ECAR parameter could include both glycolysis and mitochondrial activity (Source: manufactured protocol, Agilent Seahorse XF Cell Energy Phenotype Test Kit). In our experiments, baseline OCR/ECAR ratio at 3 days post-treatment was 6,5±1,3 for NT cultures, and 7,66±1,43 for CDDP cultures. At 7 days pots-treatment, this ratio was 6,88±0,44 for NT cultures and 8,66±0,49 for cisplatin-treated cultures. As consequence, the increased levels of ECAR metabolic potential seen in CDDP cultures compared to the NT ones can be attributed to enhanced activity of both mitochondria respiration and glycolysis. However, OCR metabolic potential is not higher in cisplatin-treated cultures at any time-point, thus suggesting that mitochondrial respiration is not activated at higher levels than in NT cultures. All these data suggest that cisplatin treatment increased the glycolytic potential of sensory neurons in culture at 7 days. However, more experiments should be conducted to corroborate this data.

VII. DISCUSSION

Despite the efforts on developing new anti-cancer therapies to increase oncologic patient's survival and bypass adverse effects of cytostatic agents, platinum drugs still remain the first- or second-line treatment for many prevalent cancers. The development of PIPN, a severe non-resolved dose-limiting side effect of platinum drugs, impairs de quality of life of patients and can result on cancer treatment cessation before completion. Its disabling and long-lasting nature, altogether with the increased survival rate of cancer patients, makes PIPN a major clinical issue that represents a high economic burden for the society and health systems.

It is generally accepted that the main mechanism related with PIPN development is the binding of platinum drugs to both mt and nDNA of sensory neurons located in the DRGs, which results in increased levels of ROS, decrease in transcription and the final death of neurons by apoptosis. In addition, a dysfunction of ion channels, specially the Na_v ones, has emerge as a key component of the acute oxaliplatin-induced syndrome (Starobova and Vetter, 2017). Despite intensive research during the last decades, there has been a continuous failure in the translation of preclinical data into the clinics. Most of the strategies have been focused on modulating the main mechanisms described up until now, specifically the oxidative stress and the extracellular levels of Ca^{2+} and Mg^{2+} (Jordan et al., 2019). There are two major possible causes for the lack of translation of preclinical data. One is the lack of good experimental models that mimics the pathology observed in patients (Lehman et al., 2021; Calls et al., 2020). The second possibility is that studies performed up to now are mainly based on the known antineoplastic effects of platinum drugs on tumor cells.

With the goal to find the most relevant or even new molecular pathways related with PIPN and to identify relevant therapeutic targets, in this thesis we performed a high-throughput mechanistic study of DRG sensory neurons using two well characterized mouse models of PIPN (one by injecting either cisplatin or oxaliplatin) that mimic the disorder observed in patients. This discussion is structured based on the different sections of the Results section.

Animal models of PIPN

There are hundreds of published rodent models used for the study of PIPN (Calls et al., 2020). In almost all the cases, animal models have problems related with the interpretation of the results and the different susceptibility to drug action between strains. Despite the recommendations of some agencies about the extrapolation of equivalent doses between species, not all the research groups follow the same guidelines. Furthermore, few platinum models achieve the total cumulated human equivalent doses (HED) (Reagan-Shaw et al., 2008; Nair and Jacob, 2016). In our studies, treatment schedules of cisplatin and oxaliplatin were planned to ensure that the TCD that mice received at the end of the study was closer to HED in which patients start developing the neuropathy. TCD were 80mg/kg for oxaliplatin (HED: 240mg/m^2) and 42mg/kg for cisplatin (HED: 125mg/m^2) (Reagan-

Shawn et al., 2008; Nair and Jacob, 2016). Although we were far from the doses in which patients manifest the neuropathy, especially in the oxaliplatin model, the TCD was not well tolerated by most of the mice and were sufficient to cause a dramatically weight loss (>20%) in some of the treated animals. Thus, we were not able to increase the total dose administered.

However, we were able to induce a neuropathy in an important percentage of mice in both treatment groups. This neuropathy was measured by evaluating NCS, that is commonly performed in patients and can be also similarly performed in mice. In many animal models reported in the bibliography, NCS are often not performed or performed incompletely, assessing only conduction velocities and not the nerve amplitudes (Calls et al., 2020). The animal model of cisplatin-induced neuropathy developed in this thesis reproduce a similar pathology than the one seen in patients, with decreased sensory amplitudes recorded in the digital and caudal nerves and preservation of the motor ones (Roelofs et al., 1984; Krarup-Hansen et al., 2007). Moreover, the decrease in sensory amplitudes worsened along time after treatment discontinuation, indicative of a coasting-effect also typical of patients treated with platinum agents (Albany et al., 2019). In the case of the oxaliplatin model, we were able to induce a slight-mild neuropathy with a decrease in sensory amplitudes in the digital and caudal nerves at the end of the treatment that did not worsen in a coasting effect. Indeed, after treatment cessation, some animals start recovering their sensory amplitudes at the digital nerve.

It is important to highlight that in both animal models, a percentage of mice treated with platinum drugs did not develop a sensory neuropathy based on NCS. In humans, diagnose of PIPN is mainly based on anamnesis and clinical exploration by different scales (i.e. Total Neuropathy Score (TNS) or National Cancer Institute-Common Toxicity Criteria, NCI-CTC). The role of NCS in the diagnose and grade of PIPN is controversial between clinicians, with some reporting that it is complementary and others defending that the sensory action potential recorded in the sural nerve is necessary for PIPN diagnose. However, these technics do not always correlate with the severity of the neuropathy reported by patients (Velasco and Bruna, 2010). Nevertheless, when assessing PIPN in animal models, NCS appear as one of the most reliable outcomes to determine the appearance of neuropathy in mice and rats. In fact, the alternative methods to NCS are the behavioral tests (i.e. Cold plate, Von Frey, Rotarod, etc.) which present difficulties in the interpretation of the results and need to be carefully analyzed (Currie et al., 2019). However, in our experiments, even when sensory amplitudes were preserved, most of the animals did develop mechanical allodynia assessed by Von Frey test in both animal models. Thus, the diagnose of PIPN exclusively by NCS in animal models is not recommended.

A well-known feature of oxaliplatin is the development of an acute syndrome characterized by cold hyperalgesia, starting some hours after treatment infusion, and lasting up to three weeks (Lehky et al., 2004). In our animal model, there is a decrease in the withdrawal threshold to cold stimuli only

during the first 4 weeks of study. After that, mice treated with oxaliplatin present a tendency to increase the time of paw flick to cold stimuli, suggesting a phenomenon of hypoesthesia. It is consistent with previous results, in which at low oxaliplatin doses (TCD 30-80 mg/kg), both rats and mice become more sensitive to thermal and mechanical stimuli. However, at the highest cumulative doses (≥80 mg/kg), there is a switch in sensory responses (Calls et al., 2020). In contrast, allodynia to mechanical stimuli is maintained even after treatment discontinuation in our study.

In the two experimental models that we set up in this thesis, we could not observe signs of peripheral nerve degeneration, assessed by the number of myelinated axons in sciatic and tibial nerves and the IENFD on the hind paw pad of mice. These finding are consistent with data reported in some but not all animal models previously reported (Calls et al., 2020). In fact, there is a high controversy in regards with degeneration of peripheral nerves in both animal models and patients (Velasco et al., 2017; Kroigard et al., 2014; Koskinen et al., 2011; Burakgazi et al., 2011). Similar, some studies performing morphometry in mouse and rat DRGs report that cisplatin treatment causes a decrease in the soma, nucleus, and nucleoli size of DRG sensory neurons, altogether with nucleoli eccentricity and segregation (Tredici et al., 1998; Agthong et al., 2015; Lessans et al., 2019). In our work, we did not see differences in any of these parameters in sensory neurons between control and cisplatin-treated mice. Again, the heterogeneity among animal models is reflected in the outcomes analyzed. Although we did not quantify the total number of neurons in the DRG, we did not find any evidence of cell death. Overall, all these data suggest that the decrease in sensory amplitudes recorded by NCS is not caused by a loss of peripheral nerve fibers nor sensory neuronal death.

An interesting morphological finding in our cisplatin model is that the number of CGRP+ IENFs were reduced in comparison with control mice at 10 weeks of study, so one week after withdrawal of treatment. In contrast, the levels of CGRP+ IENF were restored at 16 weeks, so at the end of the coasting effect period. Early reduction of CGRP immunoreactivity in IENF is consistent with previous published work (Verdú et al., 1999), where it was linked to altered responses of sensory neurons in front of peripheral stimuli (Verdú et al., 1999). In contrast, oxaliplatin treated mice did not show changes in the number of CGRP+ IENF, which could be attributed to the light severe profile of the neuropathy when compared to the cisplatin-induced one.

Effects of tumor environment in the development of PIPN

Dysregulation of immune response and the chronic overexpression of inflammatory mediators is a major feature of tumor microenvironment (Tsai et al., 2014). It has been reported that several advanced cancer patients show an immunosuppressive state with decreased T-cell activity (Kusmartsev et al., 2004; Dunn et al., 2006; Kim et al., 2006; Kalathil and Thanavala, 2016). On the other hand, immune system has been linked to PIPN development (Makker et al., 2017; Xu et

al., 2018; Stojanovska et al., 2018, 2019) especially related with pain behaviors (Boyette-Davis and Dougherty, 2011; Di Cesare Mannelli et al., 2014). Based on these data, we wanted to know whether a cancer environment could interfere with the development of PIPN. Our results suggest that a controlled tumor environment does not affect the development neither the progression of PIPN, at list in terms of NCS, mechanical allodynia and peripheral nerve degeneration. This affirmation is endorsed by the fact that C-26 cell line has a potent pro-inflammatory and pro-cachexia effect on mice (Bonetto et al., 2016), meaning that it really generates a "noxious" systemic environment. However, we cannot dismiss the limitation of our testing model. In this study, tumor cells were injected 7 days before starting chemotherapy treatment, and this period might not be long enough to change the inflammatory response of mice. Indeed, we did not check immunologic parameters in mice inoculated with tumor.

Whereas cisplatin treatment was able to avoid the growth of tumor from the first dose, oxaliplatin failed in that action. It seems paradoxical as oxaliplatin is the treatment of preference for colon malignancies (Grothey and Goldberg, 2004), and the tumor cell line used in this thesis was the C-26, derived from mouse colon adenocarcinoma. The lack of anti-cancer effect of oxaliplatin cannot be attributed to technical problems in the administration, since the weight lost and pain development seen in oxaliplatin-treated mice point out that the cytostatic drug had a systemically action. In fact, when comparing the tumor growth rate between OXA+Tx mice and Tx mice (data not shown), we saw that animals that did not receive oxaliplatin had a faster tumor growth, meaning that oxaliplatin was acting somehow on the tumor.

Molecular mechanisms involved in PIPN

When studying the molecular mechanisms involved in PIPN development, all the reported studies up until now uses molecular downstream analysis (i.e. RT-qpCR, western blot or RNA-seq) that analyze the whole DRG without previous isolation of cell populations. In all the cases, the obtained data is extrapolated to the sensory neuronal population. However, it is well known that DRG not only harbor the cell bodies of sensory neurons but also other cell types like the endothelial, fibroblasts and SGCs, even at higher proportion than neurons (Gonçalves et al. 2018; Hanani and Spray, 2020). On the recent years, research has demonstrated that SGCs are not passive observers in PIPN development but can have an important role in its pathophysiology (Ledda et al., 2009; Huang et al., 2010; Warwik and Hanani, 2013; Di Cesare Mannelli et al., 2013, 2014). Similar, different neuronal populations respond distinctly to the same noxious stimuli (Jamieson et al., 2005; Hu et al., 2016), probably due to differences in their neurotrophic dependence and biochemical properties. Thus, it is important to ensure that each cellular population (neuronal subpopulations and SGCs) is studied independently of each other to avoid the masking of significant results. For

that reason, before preforming the transcriptomic study, we isolated DRG cells by single-cell sorting followed by scRNA-seq of each sorted cell. With this technique, we were able to distinguish different populations of the DRG as previously performed by others (Usoskin et al., 2015; Hu et al., 2016; Li et al., 2016). Moreover, we were able to reproduce the results in the two independent experiments (cisplatin and oxaliplatin), which were conducted by different facilities, thus demonstrating the robustness of this technique. However, the methodology we implemented in this thesis has some limitations. In both cisplatin and oxaliplatin studies, the isolation of cells by single cell sorting was not 100% efficient, meaning that not all the wells of the 96-well plates were filled with a cell. In fact, some were filled with cellular debris that do not have genetic material. Moreover, due to cost- and technical-limitations, we were able to sequence a small number of plates in each study. Altogether, the final number of cells sequenced was very low in comparison with other works (Usoskin et al., 2015; Hu et al., 2016; Li et al., 2016). Due to the limited number of cells, we were not able to compare the transcriptomic profile of different neuronal populations between control and platinum-treated mice. Moreover, the low number of sequenced cells can also explain the reduced DEGs obtained in the comparisons between control and platinum-treated mice.

Effects of cisplatin on DRG populations

The findings obtained in this study suggest that cisplatin administration induces a senescence-like phenotype in sensory neurons of the mouse DRG. This cellular process is already activated 10 weeks after the first cisplatin administration, as indicated by the increased levels of *Cdnk1a* gene expression, p-H2AX protein and a concomitant reduction of sensory nerve potential amplitudes. The senescence-like phenotype progresses and is well established by 16 weeks, when multiple molecular and morphological events are observed in the DRG neurons. At this point in time, even when cisplatin has been withdrawn for 6 weeks, a more marked reduction of the amplitude of nerve action potentials is observed in the coasting effect.

After DNA damage, cells activate the DDR, a complex and tightly regulated network of signaling pathways that constitute intended to safeguard genome integrity (Jackson and Bartek, 2009). When the DDR cannot deal with this damage, cells undergo apoptosis or activate senescence pathways to preserve their function or minimize tissue damage (Fielder et al., 2017). While apoptotic programs are well defined (D'Arcy, 2019), cell senescence is a collective phenotype of multiple effector programs, mostly described in replicative cells (Hernandez-Segura et al., 2018). In fact, the most accepted starting point definition of cell senescence state is provided by the stress-induced arrest and resistance to mitogenic stimuli (Campisi and d'Adda di Faganga, 2007; Sharpless and Sherr, 2015). However, this definition is difficult to fit in the postmitotic differentiated cells. Interestingly, molecular markers and effector pathways resembling the senescence phenotype processes have also been identified in non-replicative cells like Purkinje and cortical brain neurons (Jurk et al., 2012;

Geng et al., 2010). In fact, in the context of the neural tissue, with low or restricted regenerative capacity in response to cellular insults, predominance of the senescence response seems more adaptive than activation of pro-apoptotic programs. In this study, we demonstrate that cisplatin treatment induces a senescence-like phenotype in DRG sensory neurons in a well-established animal model of cisplatin peripheral neuropathy. Since senescence is a collective phenotype of multiple effector programs, the induced senescence-phenotype by cisplatin has been corroborated by using a variety of accepted markers implicated in this response.

scRNA-seq of sorted neurons from DRG of cisplatin-treated mice showed an up-regulation of GO terms involved in DNA damage responses and the increase of *Cdkn1a* levels. The progressive increased expression of *Cdkn1a* protein product p21 and the early phosphorylation of H2AX as a fast responder to DNA damage corroborated the initial findings obtained in the scRNA-seq analysis. Reinforcing our data, previous studies pointed to platinum-induced inter- and intra-strand DNA crosslink damage as the main cause of platinum neurotoxicity (McDonald et al., 2005; Ta et al., 2006). Moreover, there is neither cleaved caspase-3 nor nuclear apoptotic morphological changes observed in DRG neurons of cisplatin treated mice, indicating that the DDR does not lead to neuronal death by apoptosis. On the other hand, the preservation of myelinated nerve fibers in our model with significant reduction in the amplitude of the compound nerve action potentials are compatible with neuronal survival but with a dysfunctional phenotype.

Most studies regarding cisplatin neurotoxicity are focused on activation of the apoptotic pathway triggered by inefficient DNA repair mechanisms. Evidence from *in vitro* neuronal cultures demonstrated involvement of apoptosis (Gill and Windebank, 1998; McDonald and Windebank, 2002). However, the evidence in animal models is scarce or even absent (Calls et al., 2020). It has been well established that the cellular response to DNA insults varies depending on the degree and duration of damage. Mild or low prolonged DNA damage results in increased levels of SMAR1, activation of p21 and the direct transcriptional inhibition of BAX and PUMA (Sinha et al., 2010). In contrast, severe DNA damage induces the sequestration of SMAR1 and the activation of apoptotic programs (Jalota et al., 2020). Therefore, a reliable experimental model that closely mimics the clinical situation, with similar equivalent cumulated dose and clinical features, is crucial to identify the etiopathogenic mechanisms of this neuropathy, especially when adequate patients sample is not available.

A previous report on microarray analysis of whole DRG from cisplatin-treated rats supports our results, as it also found an increased expression of *Cdkn1a* and *Mmp9* (Alaedini et al., 2008). The authors related these changes with apoptosis, although the overexpression of these genes can also be involved in senescence. In addition, our hypothesis of cisplatin-induced senescence-like phenotype was further supported by the activation of other senescent markers, like increased

activity of SA-βGAL, a maker of lysosome activity (Lee et al., 2006) and overexpression of Nfkb-p65, a key factor in SASP induction (Chien et al., 2011). Nfkb-p65 regulates many cellular processes including proliferation, apoptosis and survival. When inactivated, Nfkb-p65 stays in the cytoplasm by binding to their inhibitor Ikb. After activation, Ikb is degraded through the proteasome pathway and Nfkb-p65 is phosphorylated for its translocation to the nucleus (Wan et al., 2010). Thus, the localization of p65 into the nucleus is a proxy for Nfkb activation (Maguire et al., 2011).

These molecular features are reinforced by the morphological changes that we have found in DRG sensory neurons of cisplatin-treated mice, also reported to be characteristic of cellular senescence, including mitochondrial disturbances, reticulum enlargements and accumulation of intracytoplasmic granules (Hernandez-Segura et al., 2018; Denoyelle et al., 2006).

Most of the senescence markers and the cellular changes observed in our model are more marked 16 weeks after the onset of treatment including 6 weeks withdrawal, while neuropathy continues progressing in what we call the coasting effect, which is widely described in patients (Brouwers et al., 2009). In contrast, p-H2AX increase was already significant at 10 weeks. Phosphorylation of H2AX in Ser139 is a fast response in front DNA damage (Sharma et al., 2012) that has been involved with the development of senescence (Jurk et al., 2012). Therefore, it is to be expected in a situation of active DNA damage, like the one caused by the presence of cisplatin in the cells.

The senescence-like phenotype that sensory neurons develop as a response to cisplatin-induced DNA damage demonstrated in this study helps to fit some of the previous findings reported in other models of cisplatin-induced neuropathy. In addition, it also proposes a new etiopathogenic mechanism of platinum-induced peripheral neuropathy that may lead to new approaches in the prevention or even treatment of this important clinical condition that has seen a lack of relevant advances during past decades. In fact, a recent work shows that the peripheral neuropathy induced by cisplatin ameliorates in the p16-3MR mouse model, that allows the specific depletion of senescent neurons expressing p16 protein (Acklin et al., 2021). However, our data from *in vivo* and *in vitro* sequencing do not show up-regulation of *Cdkn2b* (p16) expression at any of the time points evaluated.

Effects of oxaliplatin on DRG populations

The results obtained in this study suggest that oxaliplatin administration induces a transient inflammatory response in mouse DRG that is already activated at 8 weeks of study, as indicated by the increased levels of some pro-inflammatory cytokines and the Nfkb-p65 protein. Moreover, at that time point the levels of pro-inflammatory cytokines are also increased in sciatic nerves of oxaliplatin-treated mice, altogether with a higher number of infiltrated cells compared with control

animals. These phenomena are endorsed by the results of the scRNA-seq, in which *Lxn* and *Klk5* genes appeared up-regulated in sensory neurons of oxaliplatin-treated mice. This inflammatory response is reverted at 10 weeks of study, so three weeks after the last oxaliplatin administration. These results are consistent with the lack of coasting effect seen in mice treated with oxaliplatin. Indeed, the levels of p-H2AX protein in the DRG were highly increased at 8 weeks of study in oxaliplatin-treated mice but were similar to control levels at 10 weeks. This finding suggests that the DNA damage induced by oxaliplatin is repaired after treatment cessation, which could explain the lack of a coasting effect and a well-established molecular senescence phenotype. In accordance with that, results obtained from the scRNAseq show that, although no significant in terms of p-adj-val, some genes related with the DDR were modulated in favor of a repair of DNA damage and an inhibition of senescence pathways. The presence of a DACH group in the oxaliplatin compound results in the formation of Pt-DNA adducts that are structurally different from those induced by cisplatin (Saris et al., 1996; Woynarowski et al., 2000; Channey et al., 2005). Whether the lesions in the DNA template induced by oxaliplatin can be easier repaired by the endogenous mechanisms of the cells is not known. However, our results suggest that DNA damage caused by oxaliplatin is repaired faster in mouse DRG once the treatment is withdrawal in comparison with cisplatin. On the other, a recent work demonstrated that the main mechanism related with oxaliplatin toxicity is not caused the DNA damage but by inducing ribosome biogenesis stress to tumor cells (Bruno et al., 2017).

Results from the scRNA-seq (performed at 8 weeks of study) show a significant increase of two specific genes in DRG sensory neurons of oxaliplatin-treated mice: *Lxn* and *Klk5*. KLK5 is a member of the KLK protein family, which are serine proteases known to be involved in diverse range of physiological and pathophysiological processes (i.e. normal skin desquamation, tooth development, neuronal plasticity or Alzheimer diseases) (Clements et al., 2004). As proteases, KLKs activate PARs, which in the nervous system can be found in neurons and glial cells (Striggow et al., 2002; Suo et al., 2003; Wang et al., 2020; Wang et al., 2004). Once activated, PARs can regulate different signaling pathways and physiological functions. Among them is the pathway of mitogen-activated protein kinases (MAPKs) that links PARs with Nfkb pathways modulating proinflammatory responses (Oikonomopoulou et al., 2006; Rothmeier and Ruf, 2012). In fact, activation of PARs favors the migration of inflammatory cells, vascular permeability, leukocyte margination and extravasation. All these events may contribute to developing an acute inflammatory environment with increased levels of IL-1, TNF-α, IL-6, MCP-1, IL-8 and IL-10 (Mella et al., 2020). This data is consistent with the results obtained in this thesis, in which we have seen increased levels of Nfkb-p65 protein and pro-inflammatory cytokines in the DRG of oxaliplatin treated mice. Similar, these mice also present increased number of infiltrated cells and chemokines in their sciatic nerves. On the other hand, latexin is the only known mammalian

carboxypeptidase inhibitor (Aagaard et al., 2005), and has been linked to inflammation and pain. Whether this protein has a positive or negative role on those responses is controversy. Some studies show that latexin deficiency contribute to pain development (Kühlein et al., 2011) and inflammation (Li et al., 2020) thorough increased levels of carboxypeptidases. In that scenario, increased levels of latexin would have a protectant role for tissue homeostasis. However, other studies show that reduced levels of latexin decrease pain sensitivity (Jin et al., 2006). On the other hand, latexin has been reported to act as a tumor suppressor after genotoxic stress (Li et al., 2011; You et al., 2014).

scRNA-seq results also show a down-regulation of the *Kyat3* gene in SGCs of oxaliplatin-treated mice. This gene encodes for an aminotransferase (KAT3) participating in the kynurenine pathway, the major metabolic route of tryptophan metabolism. This pathway can be divided in two main branches: the neuroprotective and the neurotoxic. Kynurenic acid is the end-point stable metabolite of the neuroprotectant branch, in which KAT enzymes are essential (Muneer, 2020). On the other hand, the neurotoxic pathway is characterized by the production of excitotoxic products of tryptophan catabolism (i.e. Quinolinic Acid, 3-hydroxil-antrhallic acid or 3-hydroxy-kynurenine) (Muneer, 2020). Interestingly, it has been reported that cytokines can affect the expression of various kynurenine enzymes, thus orchestrating metabolic changes that can influence immune cell responses and *vice versa* (Baumgartner et al., 2019). In fact, triggered by inflammatory processes, the balance between neurotoxic and neuroprotective branches of the kynurenine pathway is disturbed (Muneer, 2020). Several studies have demonstrated that altered kynurenine metabolism plays an important role in the pathogenesis of several neurodegenerative diseases (Tan et al., 2012). In that sense, *Kyat3* down-regulation could favor the accumulation of excitotoxic metabolites and so contribute to PIPN.

Despite the increased inflammatory response seen in DRG and sciatic nerves of oxaliplatin-treated mice, which is consistent with the results obtained in the scRNA-seq, we were not able to corroborate the increased levels of KLK5 and latexin at the protein level neither by western blot nor by immunofluorescence. In contrast, the levels of KAT3 protein did appear down-regulated in DRGs of oxaliplatin-treated mice by western blot. It is important to take in mind that in those types of studies, changes in gene transcription not always correlate with changes at the protein level. In fact, in the cisplatin study, the increased levels of p21 protein were seen at 16 weeks and not at 10 weeks, when the scRNA-seq was performed. Thus, the changes in KLK5 and latexin protein levels could be taking place at different time points that the ones evaluated. The methods used to measure the protein levels can also be a limitation. On one hand, western blot analyzes the whole DRG, so that the changes taking place in sensory neurons can be masked by other cell types like SGCs. On the other hand, analysis of immunofluorescence staining can be difficult and controversial when a situation of “present or non-present” is not obtained. In that situation, the interpretation of the

staining pattern is very hard as fluorescence intensities are not always reliable due to background effects. Nevertheless, it was interesting to see that two of three animals used for the scRNA-seq had increased number of neurons with KLK5 protein translocation to the nucleus. KLKs are mainly known as secreted proteins with extracellular functions, and the contribution of their nuclear localization to the pathogenesis of human diseases has not been studied. Nevertheless, it has been reported that KLK4, another member of the kallikrein family, is predominantly a nuclear protein acting as transcriptomic factor in prostate cancer (Xi et al., 2004; Klokk et al., 2007). Considering that data, other KLKs could have nuclear roles in some pathological conditions. But it is important to consider that the nuclear localization of KLK5 was not seen in most of the animals treated with oxaliplatin. Again, the heterogeneity of PIPN is reflected in the outcome analyzed and highlights the importance of using a high sample size in the studies.

Interestingly, the levels of Nfkb-p65 and pro-inflammatory cytokines in the DRG are consistent with the levels of p-H2AX, which are restored at 10 weeks of study. Although we did not see a significant increase in p21 protein levels, data suggests that the DNA damage induced by oxaliplatin could be activating senescence pathways. In fact, latexin protein has been also involved in senescence due to its tumor suppressor activity (Liang and Van Zant, 2008; Ni et al., 2014; Zhang et al., 2020), and some of the cytokines up regulated in DRG and sciatic nerves of oxaliplatin-treated mice are known to be SASP factors (Coppé et al., 2010). However, the rapid DNA repair after treatment cessation could avoid the establishment of a full and durable senescence phenotype. In line with that, it has been reported that the permanent activation of DDR is necessary for both the initiation and the maintenance of senescent phenotypes (Rodier et al., 2009; Olivieri et al. 2015).

Overall, the results obtained from this study point out that oxaliplatin treatment induces a slight-mild neuropathy to mice, characterized by a marked proinflammatory response in DRG and sciatic nerves. Interestingly, this response is attenuated after treatment discontinuation and so could explain the oxaliplatin-induced acute syndrome, mainly characterized by the development of positive symptoms (i.e. cold hypersensitivity).

In vitro model of cisplatin-induced neuronal senescence

Most of the *in vitro* models published for the study of PIPN use neuronal survival as the main outcome measure. It is probably based on the idea that apoptosis of DRG sensory neurons is the main mechanisms reported for PIPN development. DNA damage leads to the activation of different cell fates including apoptosis, senescence, or autophagy. The decision between these cell fates will depend on the intensity of DNA damage, the status of key DDR proteins, the regulation of DNA repair genes and the persistence of the DNA lesion (Campisi & d'Adda di Fagagna 2007). Thus, as higher is the damage, higher is the probability to activate apoptotic pathways. In contrast, when

DNA damage is slight or mild, cells can activate alternative pathways that results in the establishment of a senescent phenotype (Shinha et al., 2010; Jalota et al., 2020). The results obtained in our *in vitro* studies clearly show this duality in cell fate. In our experiments, the treatment of DRG neuronal cultures with cisplatin doses similar to those used in published data (4μg/ml; Gill and Windebank, 1998; Ta et al., 2006; Jiang et al., 2008; Melli et al., 2008; Podratz et al., 2011) induced a rapid death of sensory neurons in culture. In contrast, the treatment of cultures with lower doses of cisplatin that those reported in the literature (1 or 0.25μg/ml) preserve neuronal viability at similar levels than NT cultures. Despite no cell death is taking place at low doses, cisplatin treatment induces a DNA damage in sensory neurons, as indicated by increased levels of p-H2AX protein.

We failed to observe increased SA-βGAL activity in our treated cultures compared to the NT ones. The SA-βGAL assay is one of the most commonly used markers for detecting senescent cells under various stimuli (i.e. irradiation, doxorubicin treatment, oxidative stress, proliferate senescence, etc.) (Kohli et al., 2021). However, it has been reported that SA-βGAL activity increases in other situations like in quiescent cells induced by serum starvation or confluence (Yang and Hu, 2005). Interestingly, in our experiments, we have found that both NT and cisplatin-treated neurons increase the activity of SA-βGAL along time in culture. Moreover, neuronal viability is slightly reduced along time even in the NT cultures, as published in other *in vitro* models (Ta et al., 2006; Podratz et al., 2011; Fadda et al., 2016), suggesting that these neurons are somehow stressed despite they show normal cellular brightness and neurite arborization. In line with that, different studies demonstrate that long term cultured cortical neurons (27 days *in vitro*) acquire a senescence-like phenotype with increased levels of different senescence hallmarks like p-H2AX or SA-βGAL without treating them with any genotoxic insult (Bigagli et al., 2016; Moreno-Blas et al., 2019). In our case, 8 days in culture (7 days-post treatment) are sufficient to induce the increased activity of SA-βGAL in NT condition. However, RT-qPCR results show that despite SA-βGAL is increased in both NT and cisplatin-treated cultures, the senescence hallmarks *Cdkn1a* (p21), *Gdnf*, *Il6* and *Mmp1* are up-regulated in the CDDP condition compared with the NT one. Similar, *Lmnb1* down-regulation, another senescence hallmark, also takes place in CDDP cultures. Thus, it is crucial to always have a control condition of the paradigm of interest in each time point of evaluation. In our case, the control condition (NT cultures) let us know that the senescent phenotype induced by cisplatin is not due culture limitations, despite SA-βGAL activity is increased independently of cisplatin treatment. In fact, it was demonstrated that fibroblasts lacking the GLB1 gene (which encodes for the β-galactosidase enzyme) can underwent replicative senescence, and thus SA-βGAL is not required for senescence establishment (Lee et al., 2006).

On the other hand, a persistent DDR activation in senescent cells is necessary to promote and maintain SASP (Rodier et al., 2009; Olivieri et al. 2015). Our results show that the secretion of pro-inflammatory factors by cisplatin-treated neurons is increased at one day post-treatment and then progressive decreased until 7 days post-treatment. This profile is consistent with the levels of p-H2AX protein and so DDR, which have an 18-fold increase at one day post-treatment and are progressive decreased to a 5-fold increase at 7 days. The only cytokine that increases its levels along time and does not follow the fluctuations seen in other secreted factors is the Eotaxin (CCL11). Interestingly, this chemokine has been associated with aging, neurodegenerative, neuroinflammation and neuropsychiatric disorders (Villeda et al., 2011; Ivanovska et al., 2020).

In the recent years, some studies have been conducted with the aim to find a common signature of cellular senescence, comparing the transcriptomic profile of different senescent cell types (Hernandez-Segura et al., 2017; Casella et al., 2019). None of these studies included neurons in the comparison, probably because senescence has been classically attributed to proliferative cells. However, interest around neuronal senescence and its role on neurodegenerative diseases has been growing on the last years (Geng et al., 2010; Jurk et al., 2012; Bigagli et al., 2016; Moreno-Blas et al., 2019). In our study, we found up regulation of some genes that also appear in the common signature of a senescence phenotype reported by previous works (Hernandez-Segura et al., 2017; Casella et al., 2019), indicating that this senescence phenotype is maintained independently of the cell type and the senescent stimuli. An interesting thing about our model is that senescence establishment and maintenance depends on *Cdkn1a* (p21) rather than *Cdkn2b* (p16), which also occurs in the *in vivo* model.

In contrast to apoptotic or quiescent cells, senescent cells remain high metabolically active, which is intimately linked to SASP acquisition (Wiley and Campisi, 2016). However, senescent cells have been shown to acquire a more glycolytic state even in presence of high oxygen levels, in a way similar to cancer cells (the so-called Warburg effect or aerobic glycolysis) (Sabbatinelli et al., 2019). In fact, several markers of increased glycolysis have been found in media from senescent fibroblast (James et al., 2015), suggesting that the metabolic shift from oxidative to glycolytic is an important attribute of senescent cells. In our *in vitro* model, preliminary results point that senescent neurons increase their glycolytic metabolism, seen by the increased ECAR after stressors at 7 days post-treatment. The metabolic shift of senescent neurons from oxidative to glycolytic, in which the final production of ATP molecules is reduced, could explain the typical decrease in nerve conductions observed in PIPN. However, further studies must be conducted to corroborate the increase in glycolysis of the sensory neurons and its possible role in nerve conduction failure and PIPN establishment.

Summary and future considerations

Overall, the results presented in this thesis provide new insights about significant molecular mechanisms involved in the development of PIPN.

Specifically, we found that the DNA-damage induced by cisplatin in mouse DRG sensory neurons results in the establishment of a senescence-like phenotype, characterized by up-regulation p21 protein, increased levels of Nfkb-p65 and increased lysosomal activity. Thus, we think that the modulation of senescence pathways emerges as a promising therapy for PIPN, as supported by Acklin and colleagues (2020). The establishment of a well characterized *in vitro* model of cisplatin-induced neuronal senescence will help to screening potential pathways and better elucidate the features of senescent neurons and the role of this cellular response in PIPN.

In addition and based on the results obtained from the oxaliplatin study, the modulation of inflammatory responses emerges as a potential neuroprotective therapy for oxaliplatin-induced neuropathy, specifically the acute syndrome.

VIII. CONCLUSIONS

1. Cisplatin treatment for 10 weeks until reaching a TCD of 42mg/kg causes a pure sensory and painful neuropathy in mice, with a marked coasting-effect after treatment cessation.
2. Oxaliplatin treatment for 8 weeks until reaching a TCD of 80mg/kg causes a slight pure sensory and painful neuropathy with no coasting effect after treatment discontinuation.
3. A controlled tumor environment does not affect the development of PIPN in adult mice.
4. Cisplatin treatment induces DNA damage and the up regulation of p21 protein in sensory neurons of mice DRG, which are not reverted after treatment discontinuation.
5. Increased p21 by cisplatin treatment does not lead to apoptosis activation in DRG, since levels of active caspase-3 and Bcl-2 are not induced by the drug, and no apoptotic nuclear changes are observed in sensory neurons of treated mice.
6. Cisplatin induces a senescence-like phenotype in DRG sensory neurons, which is characterized by increase of p-H2AX, p21 and Nfkb-p65 proteins levels, SA-βGAL activity and the presence of lipofuscin granules.
7. Oxaliplatin treatment induces a transient inflammatory response in DRGs and sciatic nerves of adult mice, characterized by increased levels of Nfkb-p65 protein, pro-inflammatory cytokines and infiltrated cells, which does not persist after treatment discontinuation.
8. Oxaliplatin treatment induces a transient DNA damage in mice DRG that is reverted after treatment discontinuation.
9. In culture, 1μg/ml cisplatin for 24 hours induces DNA damage to adult mouse DRG sensory neurons that is partially restored along time and does not induce neuronal death.
10. In culture, 1μg/ml cisplatin for 24 hours induces a senescence-like phenotype in DRG sensory neurons, with a maintained expression of *Cdkn1a* gene along time and a transient secretion of SASP factors.
11. SA-βGAL activity is increased in cultured DRG sensory neurons along time in both non-treated and cisplatin-treated conditions and so it is not a useful marker to detect senescent neurons in vitro.
12. Cisplatin-induced senescent neurons could increase their glycolytic metabolism in culture.

IX. REFERENCES

Aagaard, A., Listwan, P., Cowieson, N., … Martin, J. L. (2005). An inflammatory role for the mammalian carboxypeptidase inhibitor latexin: relationship to cystatins and the tumor suppressor TIG1. Structure, 13(2), 309–317.

Acharyya, S., Ladner, K. J., Nelsen, L. L., … Guttridge, D. C. (2004). Cancer cachexia is regulated by selective targeting of skeletal muscle gene products. J Clin Invest, 114(3), 370–378.

Acklin, S., Zhang, M., Du, W., …Xia, F. (2020). Depletion of senescent-like neuronal cells alleviates cisplatin-induced peripheral neuropathy in mice. Sci Rep 10, 14170.

Acklin, S., & Xia, F. (2021). The Role of Nucleotide Excision Repair in Cisplatin-Induced Peripheral Neuropathy: Mechanism, Prevention, and Treatment. Int J Mol Sci, 22(4), 1975.

Adelsberger, H., Quasthoff, S., Grosskreutz, J., … Lersch, C. (2000). The chemotherapeutic oxaliplatin alters voltage-gated Na(+) channel kinetics on rat sensory neurons. Eur J Pharmacol, 406(1), 25–32.

Agthong, S., Kaewsema, A., & Charoensub, T. (2015). Curcumin Ameliorates Functional and Structural Abnormalities in Cisplatin-induced Neuropathy. Exp Neurobiol, 24(2), 139–145.

Alaedini, A., Xiang, Z., Kim, H., … Latov, N. (2008). Up-regulation of apoptosis and regeneration genes in the dorsal root ganglia during cisplatin treatment. Exp Neurol, 210(2), 368–374.

Albany, C., Dockter, T., Wolfe, E., … Costello, B. A. (2021). Cisplatin-associated neuropathy characteristics compared with those associated with other neurotoxic chemotherapy agents (Alliance A151724). Support Care Cancer, 29(2), 833–840.

Allen, B. M., Hiam, K. J., Burnett, C. E., … Spitzer, M. H. (2020). Systemic dysfunction and plasticity of the immune macroenvironment in cancer models. Nat Med, 26(7), 1125–1134.

Allen, D. T., & Kiernan, J. A. (1994). Permeation of proteins from the blood into peripheral nerves and ganglia. Neuroscience, 59(3), 755–764.

Albers, J. W., Chaudhry, V., Cavaletti, G., & Donehower, R. C. (2014). Interventions for preventing neuropathy caused by cisplatin and related compounds. Cochrane Database Syst Rev, (3), CD005228.

Alshawaf, A. J., Viventi, S., Qiu, W., … Dottori, M. (2018). Phenotypic and Functional Characterization of Peripheral Sensory Neurons derived from Human Embryonic Stem Cells. Sci Rep, 8(1), 603.

Ang, W. H., Myint, M., & Lippard, S. J. (2010). Transcription inhibition by platinum-DNA cross-links in live mammalian cells. J Am Chem Soc, 132(21), 7429–7435.

Areti, A., Yerra, V. G., Naidu, V., & Kumar, A. (2014). Oxidative stress and nerve damage: role in chemotherapy induced peripheral neuropathy. Redox Biol, 2, 289–295.

Areti, A., Komirishetty, P., & Kumar, A. (2017). Carvedilol prevents functional deficits in peripheral nerve mitochondria of rats with oxaliplatin-evoked painful peripheral neuropathy. Toxicol Appl Pharmacol, 322, 97–103.

Argyriou, A. A., Bruna, J., Marmiroli, P., & Cavaletti, G. (2012). Chemotherapy-induced peripheral neurotoxicity (CIPN): an update. Crit Rev Oncol Hematol, 82(1), 51–77.

Argyriou, A. A., Kyritsis, A. P., Makatsoris, T., & Kalofonos, H. P. (2014). Chemotherapy-induced peripheral neuropathy in adults: a comprehensive update of the literature. Cancer management and research, 6, 135–147.

Argyriou, A. A., Bruna, J., Genazzani, A., & Cavaletti, G. (2017). Chemotherapy-induced peripheral neurotoxicity: management informed by pharmacogenetics. Nat Rev Neurol, 13, 492–504.

Armstrong, C. M., & Cota, G. (1999). Calcium block of Na+ channels and its effect on closing rate. Proc Natl Acad of Sci U S A, 96(7), 4154–4157.

Avraham, O., Deng, P. Y., Jones, S., … Cavalli, V. (2020). Satellite glial cells promote regenerative growth in sensory neurons. Nat Commun, 11(1), 4891.

Basisty, N., Kale, A., Jeon, O. H., … Schilling, B. (2020). A proteomic atlas of senescence-associated secretomes for aging biomarker development. PLoS Biol, 18(1), e3000599.

Baumgartner, R., Forteza, M. J., & Ketelhuth, D. (2019). The interplay between cytokines and the Kynurenine pathway in inflammation and atherosclerosis. Cytokine, 122, 154148.

Bengtson, M., Nittve, M., & Näsström, J. (2018). Persistent prevention of oxaliplatin-induced peripheral neuropathy using calmangafodipir (PledOx®): a placebo-controlled randomised phase II study (PLIANT). Acta Oncol, , 57(3), 393–402.

Bennett, D. L., Averill, S., Clary, D. O., … McMahon, S. B. (1996). Postnatal changes in the expression of the trkA high-affinity NGF receptor in primary sensory neurons. Eur J Neurosci, 8(10), 2204–2208.

Bennett, G. J., Doyle, T., & Salvemini, D. (2014). Mitotoxicity in distal symmetrical sensory peripheral neuropathies. Nat Rev Neurol, 10(6), 326–336.

Bernardi, P., Krauskopf, A., Basso, E., … Forte, M. A. (2006). The mitochondrial permeability transition from in vitro artifact to disease target. FENS J, 273(10), 2077–2099.

Bhagra, A., & Rao, R. D. (2007). Chemotherapy-induced neuropathy. Curr Oncol Rep, 9(4), 290–299.

Bigagli, E., Luceri, C., Scartabelli, T., … Giovannelli, L. (2016). Long-term Neuroglial Cocultures as a Brain Aging Model: Hallmarks of Senescence, MicroRNA Expression Profiles, and Comparison With In Vivo Models. J Gerontol A Biol Sci Med Sci, 71(1), 50–60.

Biswas, A.K., and Acharyya, S. (2020). Cancer-Associated Cachexia: A Systemic Consequence of Cancer Progression. Annu Rev Cancer Biol, 4(1)

Boekelheide, K., Arcila, M. E., & Eveleth, J. (1992). cis-diamminedichloroplatinum (II) (cisplatin) alters microtubule assembly dynamics. Toxicol App Pharmacol, 116(1), 146–151.

Bonetto, A., Rupert, J. E., Barreto, R., & Zimmers, T. A. (2016). The Colon-26 Carcinoma Tumor-bearing Mouse as a Model for the Study of Cancer Cachexia. J Vis Exp, (117), 54893

Boyette-Davis, J., & Dougherty, P. M. (2011). Protection against oxaliplatin-induced mechanical hyperalgesia and intraepidermal nerve fiber loss by minocycline. Exp Neurol, 229(2), 353–357.

Briani, C., Argyriou, A. A., Izquierdo, C., … Kalofonos, H. P. (2014). Long-term course of oxaliplatin-induced polyneuropathy: a prospective 2-year follow-up study. J Peripher Nerv Syst 19(4), 299–306.

Brouwers, E. E., Huitema, A. D., Boogerd, W., … Schellens, J. H. (2009). Persistent neuropathy after treatment with cisplatin and oxaliplatin. Acta Oncol, 48(6), 832–841.

Brouwers, B., Fumagalli, D., Brohee, S., … Wildiers, H. (2017). The footprint of the ageing stroma in older patients with breast cancer. Breast Cancer Res. 2017;19(1):78.

Bruna, J., Videla, S., Argyriou, A.A. … Plata-Salamán, C. (2018). Efficacy of a Novel Sigma-1 Receptor Antagonist for Oxaliplatin-Induced Neuropathy: A Randomized, Double-Blind, Placebo-Controlled Phase IIa Clinical Trial. Neurotherapeutics 15, 178–189.

Bruno, P. M., Liu, Y., Park, G. Y., Murai, J., …Hemann, M. T. (2017). A subset of platinum-containing chemotherapeutic agents kills cells by inducing ribosome biogenesis stress. Nat Med, 23(4), 461–471.

Burakgazi, A. Z., Messersmith, W., Vaidya, D., … Polydefkis, M. (2011). Longitudinal assessment of oxaliplatin-induced neuropathy. Neurology, 77(10), 980–986.

Callizot, N., Andriambeloson, E., Glass, J., … Dreano, M. (2008). Interleukin-6 protects against paclitaxel, cisplatin and vincristine-induced neuropathies without impairing chemotherapeutic activity. Cancer Chemother Pharmacol, 62(6), 995–1007.

Calls, A., Carozzi, V., Navarro, X., … Bruna, J. (2020). Pathogenesis of platinum-induced peripheral neurotoxicity: Insights from preclinical studies. Exp Neurol, 325, 113141.

Campisi, J., & d'Adda di Fagagna, F. (2007). Cellular senescence: when bad things happen to good cells. Nat Rev Mol Cell Biol, 8(9), 729–740.

Canta, A., Pozzi, E., & Carozzi, V. A. (2015). Mitochondrial Dysfunction in Chemotherapy-Induced Peripheral Neuropathy (CIPN). Toxics, 3(2), 198–223.

Carozzi, V. A., Canta, A., & Chiorazzi, A. (2015). Chemotherapy-induced peripheral neuropathy: What do we know about mechanisms?. Neurosc Lett, 596, 90–107.

Casella, G., Munk, R., Kim, K. M., … Gorospe, M. (2019). Transcriptome signature of cellular senescence. Nucleic Acids Res, 47(14), 7294–7305.

Chambers, S. M., Mica, Y., Studer, L., & Tomishima, M. J. (2011). Converting human pluripotent stem cells to neural tissue and neurons to model neurodegeneration. Methods Mol Biol, 793, 87–97.

Chaney, S. G., Campbell, S. L., Bassett, E., & Wu, Y. (2005). Recognition and processing of cisplatin- and oxaliplatin-DNA adducts. Crit Rev Oncol Hematol, 53(1), 3–11.

Chaudhry, V., Rowinsky, E. K., Sartorius, S. E., … Cornblath, D. R. (1994). Peripheral neuropathy from taxol and cisplatin combination chemotherapy: clinical and electrophysiological studies. Ann Neurol, 35(3), 304–311.

Chaudhry, V., Chaudhry, M., Crawford, T. O., … Griffin, J. W. (2003). Toxic neuropathy in patients with pre-existing neuropathy. Neurology, 60(2), 337–340.

Cheah, M., Fawcett, J. W., & Andrews, M. R. (2017). Assessment of Thermal Pain Sensation in Rats and Mice Using the Hargreaves Test. Bio-protocol, 7(16), e2506.

Chien, Y., Scuoppo, C., Wang, X., … Lowe, S. W. (2011). Control of the senescence-associated secretory phenotype by NF-κB promotes senescence and enhances chemosensitivity. Genes Dev, 25(20), 2125–2136.

Chu, E. & DeVita, Jr. V.T. (2021). Physicians' Cancer Chemotherapy Drug Manual. Jones and Barlett Publishers.

Clements, J. A., Willemsen, N. M., Myers, S. A., & Dong, Y. (2004). The tissue kallikrein family of serine proteases: functional roles in human disease and potential as clinical biomarkers. Cri Rev Clin Lab Sci, 41(3), 265–312.

Cook, A. D., Christensen, A. D., Tewari, D., … Hamilton, J. A. (2018). Immune Cytokines and Their Receptors in Inflammatory Pain. Trends Immunol, 39(3), 240–255.

Coppé, J. P., Desprez, P. Y., Krtolica, A., & Campisi, J. (2010). The senescence-associated secretory phenotype: the dark side of tumor suppression. Annual Rev Pathol, 5, 99–118.

Corsetti, G., Rodella, L., Rezzani, R., … Bianchi, R. (2000). Cytoplasmic changes in satellite cells of spinal ganglia induced by cisplatin treatment in rats. Ultrastruct Pathol, 24(4), 259–265.

Cullen, K. J., Yang, Z., Schumaker, L., & Guo, Z. (2007). Mitochondria as a critical target of the chemotheraputic agent cisplatin in head and neck cancer. J Bioenerg Biomembr, 39(1), 43–50.

Currie, G. L., Angel-Scott, H. N., Colvin, L., … Sena, E. S. (2019). Animal models of chemotherapy-induced peripheral neuropathy: A machine-assisted systematic review and meta-analysis. PLoS Biol, 17(5), e3000243.

D'Arcy M. S. (2019). Cell death: a review of the major forms of apoptosis, necrosis and autophagy. Cell Biol Int, 43(6), 582–592.

de Gramont, A., Figer, A., Seymour, M., … Bonetti, A. (2000). Leucovorin and fluorouracil with or without oxaliplatin as first-line treatment in advanced colorectal cancer. J Clin Oncol, 18(16), 2938–2947.

Denoyelle, C., Abou-Rjaily, G., Bezrookove, V., … Soengas, M. S. (2006). Anti-oncogenic role of the endoplasmic reticulum differentially activated by mutations in the MAPK pathway. Nat Cell Biol, 8(10), 1053–1063.

Descoeur, J., Pereira, V., Pizzoccaro, A., … Bourinet, E. (2011). Oxaliplatin-induced cold hypersensitivity is due to remodelling of ion channel expression in nociceptors. EMBO Mol Med, 3(5), 266–278.

Deuis, J. R., Zimmermann, K., Romanovsky, A. A., … & Vetter, I. (2013). An animal model of oxaliplatin-induced cold allodynia reveals a crucial role for Nav1.6 in peripheral pain pathways. Pain, 154(9), 1749–1757.

Deuis, J. R., Lim, Y. L., Rodrigues de Sousa, S., … Vetter, I. (2014). Analgesic effects of clinically used compounds in novel mouse models of polyneuropathy induced by oxaliplatin and cisplatin. Neuro Oncol, 16(10), 1324–1332.

Di Cesare Mannelli, L., Pacini, A., Bonaccini, L., … Ghelardini, C. (2013). Morphologic features and glial activation in rat oxaliplatin-dependent neuropathic pain. J Pain, 14(12), 1585–1600.

Di Cesare Mannelli, L., Pacini, A., Micheli, L., … Ghelardini, C. (2014). Glial role in oxaliplatin-induced neuropathic pain. Exp Neurol, 261, 22–33.

Dimri, G. P., Lee, X., Basile, G., … Pereira-Smith, O. (1995). A biomarker that identifies senescent human cells in culture and in aging skin in vivo. Proc Natl Acad Sci U S A, 92(20), 9363–9367.

Divakaruni, A. S., Paradyse, A., Ferrick, D. A., … Jastroch, M. (2014). Analysis and interpretation of microplate-based oxygen consumption and pH data. Methods Enzymol, 547, 309–354.

Dominic, A., Banerjee, P., Hamilton, D. J., … Abe, J. I. (2020). Time-dependent replicative senescence vs. disturbed flow-induced pre-mature aging in atherosclerosis. Redox Biol, 37, 101614.

Donzelli, E., Carfi, M., Miloso, M., … Tredici, G. (2004). Neurotoxicity of platinum compounds: comparison of the effects of cisplatin and oxaliplatin on the human neuroblastoma cell line SH-SY5Y. J neurooncol, 67(1-2), 65–73.

Dunn, G. P., Koebel, C. M., & Schreiber, R. D. (2006). Interferons, immunity and cancer immunoediting. Nat Rev Immunol, 6(11), 836–848.

Dyson, P. J., & Sava, G. Metal-based antitumour drugs in the post genomic era. Dalton Trans, (16), 1929–1933 (2006).

Dzagnidze, A., Katsarava, Z., Makhalova, J., … Thomale, J. (2007). Repair capacity for platinum-DNA adducts determines the severity of cisplatin-induced peripheral neuropathy. J Neurosci, 27(35), 9451–9457.

Ebert, A. M., Childs, S. J., Hehr, C. L., … McFarlane, S. (2014). Sema6a and Plxna2 mediate spatially regulated repulsion within the developing eye to promote eye vesicle cohesion. Development, 141(12), 2473–2482.

Egashira, N., Hirakawa, S., Kawashiri, T., … Oishi, R. (2010). Mexiletine reverses oxaliplatin-induced neuropathic pain in rats. J Pharmacol Sci 112(4), 473–476.

Ehrsson, H., Wallin, I., & Yachnin, J. (2002). Pharmacokinetics of oxaliplatin in humans. Med Oncol, 19(4), 261–265.

Emami, N., & Diamandis, E. P. (2007). Human tissue kallikreins: a road under construction. Clin Chim Acta, 381(1), 78–84.

Erol, K., Yiğitaslan, S., Ünel, Ç., … Yıldırım, E. (2016). Evaluation of Cisplatin Neurotoxicity in Cultured Rat Dorsal Root Ganglia via Cytosolic Calcium Accumulation. Balkan Med J, 33(2), 144–151.

Fadda, A., Bärtschi, M., Hemphill, A., … Oevermann, A. (2016). Primary Postnatal Dorsal Root Ganglion Culture from Conventionally Slaughtered Calves. PloS one, 11(12), e0168228.

Fielder, E., von Zglinicki, T., & Jurk, D. (2017). The DNA Damage Response in Neurons: Die by Apoptosis or Survive in a Senescence-Like State?. J Alzheimers Dis, 60(s1), S107–S131.

Filbin M. T. (1995). Myelin-associated glycoprotein: a role in myelination and in the inhibition of axonal regeneration? Curr Opin Neurobiol, 5(5), 588–595.

Finak, G., McDavid, A., Yajima, M., … Gottardo, R. (2015). MAST: a flexible statistical framework for assessing transcriptional changes and characterizing heterogeneity in single-cell RNA sequencing data. Genome Biol, 16, 278.

Fiorucci, S., & Distrutti, E. (2002). Role of PAR2 in pain and inflammation. Trends Pharmacol Sci, 23(4), 153–155.

Flanagan, K. C., Alspach, E., Pazolli, E., … Stewart, S. A. (2017). c-Myb and C/EBPβ regulate OPN and other senescence-associated secretory phenotype factors. Oncotarget, 9(1), 21–36.

Fucikova, J., Spisek, R., Kroemer, G., & Galluzzi, L. (2021). Calreticulin and cancer. Cell Res, 31, 5–16.

Fukuda, Y., Li, Y., & Segal, R. A. (2017). A Mechanistic Understanding of Axon Degeneration in Chemotherapy-Induced Peripheral Neuropathy. Front Neurosci, 11, 481.

Fumet, J. D., Limagne, E., Thibaudin, M., & Ghiringhelli, F. (2020). Immunogenic Cell Death and Elimination of Immunosuppressive Cells: A Double-Edged Sword of Chemotherapy. Cancers, 12(9), 2637.

Galluzzi, L., Vitale, I., Warren, S., …Marincola, F. M. (2020). Consensus guidelines for the definition, detection and interpretation of immunogenic cell death. J Immunother Cancer, 8(1), e000337.

Gauchan, P., Andoh, T., Kato, A., & Kuraishi, Y. (2009) Involvement of increased expression of transient receptor potential melastatin 8 in oxaliplatin-induced cold allodynia in mice. Neurosci Lett, 458(2), 93–95.

Geden, M. J., Romero, S. E., & Deshmukh, M. (2021). p53 is required for nuclear but not mitochondrial DNA damage-induced degeneration. Cell Death Dis, 12(1), 104.

Geng, Y. Q., Guan, J. T., Xu, X. H., & Fu, Y. C. (2010). Senescence-associated beta-galactosidase activity expression in aging hippocampal neurons. Biochem Biophys Res Commun, 396(4), 866–869.

Georgakopoulou, E. A., Tsimaratou, K., Evangelou, K., …Gorgoulis, V. G. (2013). Specific lipofuscin staining as a novel biomarker to detect replicative and stress-induced senescence. A method applicable in cryo-preserved and archival tissues. Aging, 5(1), 37–50.

George, D., Ahrens, P., & Lambert, S. (2018). Satellite glial cells represent a population of developmentally arrested Schwann cells. Glia, 66(7), 1496–1506.

Ghosh, S. (2019). Cisplatin: The first metal based anticancer drug. Bioorg Chem, 88, 102925.

Gietema, J. A., Meinardi, M. T., Messerschmidt, J., … Sleijfer, D. T. (2000). Circulating plasma platinum more than 10 years after cisplatin treatment for testicular cancer. Lancet, 355(9209), 1075–1076.

Gill, J. S., & Windebank, A. J. (1998). Cisplatin-induced apoptosis in rat dorsal root ganglion neurons is associated with attempted entry into the cell cycle. J Clin Invest, 101(12), 2842–2850.

Glimelius, B., Manojlovic, N., Pfeiffer, P., … Näsström, J. (2018). Persistent prevention of oxaliplatin-induced peripheral neuropathy using calmangafodipir (PledOx®): a placebo-controlled randomised phase II study (PLIANT). Acta Oncol, 57(3), 393–402.

Gonçalves, N. P., Vægter, C. B., & Pallesen, L. T. (2018). Peripheral Glial Cells in the Development of Diabetic Neuropathy. Front Neurol., 9, 268.

Gorgoulis, V. G., Pratsinis, H., Zacharatos, P., … Kletsas, D. (2005). p53-dependent ICAM-1 overexpression in senescent human cells identified in atherosclerotic lesions. Lab Invest, 85(4), 502–511.

Gregg, R. W., Molepo, J. M., Monpetit, V. J., … Stewart, D. J. (1992). Cisplatin neurotoxicity: the relationship between dosage, time, and platinum concentration in neurologic tissues, and morphologic evidence of toxicity. J Clin Oncol, 10(5), 795–803.

Groen, C. M., Podratz, J. L., Treb, K., & Windebank, A. J. (2018). Drosophila strain specific response to cisplatin neurotoxicity. Fly, 12(3-4), 174–182.

Grolleau, F., Gamelin, L., Boisdron-Celle, M., … Gamelin, E. (2001). A possible explanation for a neurotoxic effect of the anticancer agent oxaliplatin on neuronal voltage-gated sodium channels. J Neurophysiol, 85(5), 2293–2297.

Grothey, A., & Goldberg, R. M. (2004). A review of oxaliplatin and its clinical use in colorectal cancer. Expert Opin Pharmacother, 5(10), 2159–2170.

Han, W., Shi, J., Cao, J., … Guan, W. (2020). Emerging Roles and Therapeutic Interventions of Aerobic Glycolysis in Glioma. Onco Targets Ther, 13, 6937–6955.

Hanani, M., & Spray, D.C. (2020). Emerging importance of satellite glia in nervous system function and dysfunction. Nat Rev Neurosci. 21, 485–498.

Hernandez-Segura, A., de Jong, T. V., Melov, S., … Demaria, M (2017). Unmasking Transcriptional Heterogeneity in Senescent Cells. Curr Biol, 27(17), 2652–2660.e4.

Hernandez-Segura, A., Nehme, J., & Demaria, M. (2018). Hallmarks of Cellular Senescence. Trends Cell Biol, 28(6), 436–453.

Hershman, D. L., Lacchetti, C., Dworkin, R. H., … American Society of Clinical Oncology. (2014). Prevention and management of chemotherapy-induced peripheral neuropathy in survivors of adult cancers: American Society of Clinical Oncology clinical practice guideline. J Clin Oncol, 32(18), 1941–1967.

Hill, A., Bergin, P., Hanning, F., … McKeage, M. J. (2010). Detecting acute neurotoxicity during platinum chemotherapy by neurophysiological assessment of motor nerve hyperexcitability. BMC Cancer, 10, 451.

Hoa, N. N., Kobayashi, J., Omura, M., … Sasanuma, H. (2015). BRCA1 and CtIP Are Both Required to Recruit Dna2 at Double-Strand Breaks in Homologous Recombination. PloS one, 10(4), e0124495.

Hoelting, L., Klima, S., Karreman, C., … Leist, M. (2016). Stem Cell-Derived Immature Human Dorsal Root Ganglia Neurons to Identify Peripheral Neurotoxicants. Stem Cells Transl Med, 5(4), 476–487.

Hou, S., Huh, B., Kim, H. K., … Abdi, S. (2018). Treatment of Chemotherapy-Induced Peripheral Neuropathy: Systematic Review and Recommendations. Pain Physician, 21(6), 571–592.

Hu, G., Huang, K., Hu, Y., … Fan, G. (2016). Single-cell RNA-seq reveals distinct injury responses in different types of DRG sensory neurons. Sci Rep, 6, 31851.

Hu, L. Y., Mi, W. L., Wu, G. C., … Mao-Ying, Q. L. (2019). Prevention and Treatment for Chemotherapy-Induced Peripheral Neuropathy: Therapies Based on CIPN Mechanisms. Current Neuropharmacol, 17(2), 184–196.

Hu, Y., Xia, W., & Hou, M. (2018). Macrophage migration inhibitory factor serves a pivotal role in the regulation of radiation-induced cardiac senescencethrough rebalancing the microRNA-34a/sirtuin 1 signaling pathway. Int J Mol Med, 42(5), 2849–2858.

Huang, T. Y., Belzer, V., & Hanani, M. (2010). Gap junctions in dorsal root ganglia: possible contribution to visceral pain. Eur J Pain, 14(1).

Iftinca, M., Basso, L., Flynn, R., … Altier, C. (2020). Chronic morphine regulates TRPM8 channels via MOR-PKCβ signaling. Mol Brain, 13(1), 61.

Imai, S., Koyanagi, M., Azimi, Z., … Matsubara, K. (2017). Taxanes and platinum derivatives impair Schwann cells via distinct mechanisms. Sci Rep, 7(1), 5947.

Isensee, J., Schild, C., Schwede, F., & Hucho, T. (2017). Crosstalk from cAMP to ERK1/2 emerges during postnatal maturation of nociceptive neurons and is maintained during aging. J Cell Sci, 130(13), 2134–2146.

Itahana, Y., Han, R., Barbier, S., … Itahana, K. (2015). The uric acid transporter SLC2A9is a direct target gene of the tumor suppressor p53 contributing to antioxidant defense. Oncogene 34, 1799–1810.

Ivanovska, M., Abdi, Z., Murdjeva, M., … Maes, M. (2020) CCL-11 or Eotaxin-1: An Immune Marker for Ageing and Accelerated Ageing in Neuro-Psychiatric Disorders. Pharmaceuticals (Basel), 13(9), 230.

Jackson, S. P., & Bartek, J. (2009). The DNA-damage response in human biology and disease. Nature, 461(7267), 1071–1078.

Jalota, A., Singh, K., Pavithra, L., … Chattopadhyay, S. (2020). Withdrawal: Tumor suppressor SMAR1 activates and stabilizes p53 through its arginine-serine-rich motif. J Biol Chem, 295(10), 3390.

James, E. L., Michalek, R. D., Pitiyage, G. N., … Parkinson, E. K. (2015). Senescent human fibroblasts show increased glycolysis and redox homeostasis with extracellular metabolomes that overlap with those of irreparable DNA damage, aging, and disease. J Proteome Res, 14(4), 1854–1871.

Jamieson, S. M., Liu, J., Connor, B., & McKeage, M. J. (2005). Oxaliplatin causes selective atrophy of a subpopulation of dorsal root ganglion neurons without inducing cell loss. Cancer chemother Pharmacol, 56(4), 391–399.

Jiang, Y., Guo, C., Vasko, M. R., & Kelley, M. R. (2008). Implications of apurinic/apyrimidinic endonuclease in reactive oxygen signaling response after cisplatin treatment of dorsal root ganglion neurons. Cancer Res, 68(15), 6425–6434.

Jimenez-Vargas, N. N., Pattison, L. A., Zhao, P., … Bunnett, N. W. (2018). Protease-activated receptor-2 in endosomes signals persistent pain of irritable bowel syndrome. Procs of Natl Acad Sci U S A, 115(31), E7438–E7447.

Jin, M., Ishida, M., Katoh-Fukui, Y., … Arimatsu, Y. (2006). Reduced pain sensitivity in mice lacking latexin, an inhibitor of metallocarboxypeptidases. Brain Res, 1075(1), 117–121.

Jong, N. N., Nakanishi, T., Liu, J. J., … McKeage, M. J. (2011). Oxaliplatin transport mediated by organic cation/carnitine transporters OCTN1 and OCTN2 in overexpressing human embryonic kidney 293 cells and rat dorsal root ganglion neurons. J Pharmacol Exp Ther, 338(2), 537–547.

Jordan, B., Jahn, F., Sauer, S., & Jordan, K. (2019). Prevention and Management of Chemotherapy-Induced Polyneuropathy. Breast Care (Basel), 14(2), 79–84.

Jurk, D., Wang, C., Miwa, S., … von Zglinicki, T. (2012). Postmitotic neurons develop a p21-dependent senescence-like phenotype driven by a DNA damage response. Aging cell, 11(6), 996–1004.

Kagiava, A., Tsingotjidou, A., Emmanouilides, C., & Theophilidis, G. (2008). The effects of oxaliplatin, an anticancer drug, on potassium channels of the peripheral myelinated nerve fibres of the adult rat. Neurotoxicology, 29(6), 1100–1106.

Kalathil, S. G., & Thanavala, Y. (2016). High immunosuppressive burden in cancer patients: a major hurdle for cancer immunotherapy. Cancer Immunol Immunother, 65(7), 813–819.

Kannarkat, G., Lasher, E. E., & Schiff, D. (2007). Neurologic complications of chemotherapy agents. Curr Opin Neurol, 20(6), 719–725.

Kanzawa-Lee, G. A., Larson, J. L., Resnicow, K., & Smith, E. (2020). Exercise Effects on Chemotherapy-Induced Peripheral Neuropathy: A Comprehensive Integrative Review. Cancer Nurs, 43(3), E172–E185.

Karlsson, J. O., Ignarro, L. J., Lundström, I., … Almén, T. (2015). Calmangafodipir [Ca4Mn(DPDP)5], mangafodipir (MnDPDP) and MnPLED with special reference to their SOD mimetic and therapeutic properties. Drug Discov Today, 20(4), 411–421.

Kawashiri, T., Egashira, N., Kurobe, K., … Oishi, R. (2012). L type Ca^{2+} channel blockers prevent oxaliplatin-induced cold hyperalgesia and TRPM8 overexpression in rats. Mol Pain, 8, 7.

Kedar, A., Cohen, M. E., & Freeman, A. I. (1978). Peripheral neuropathy as a complication of cis-dichlorodiammineplatinum(II) treatment: a case report. Cancer Treat Rep, 62(5), 819–821.

Kelley, M. R., Wikel, J. H., Guo, C., … Vasko, M. R. (2016). Identification and Characterization of New Chemical Entities Targeting Apurinic/Apyrimidinic Endonuclease 1 for the Prevention of Chemotherapy-Induced Peripheral Neuropathy. J Pharmacol Exp Ther, 359(2), 300–309.

Khasabova, I. A., Khasabov, S. G., Olson, J. K., … Simone, D. A. (2019). Pioglitazone, a PPARγ agonist, reduces cisplatin-evoked neuropathic pain by protecting against oxidative stress. Pain, 160(3), 688–701.

Kim, H. S., Guo, C., Thompson, E. L., … Lee, S. H. (2015). APE1, the DNA base excision repair protein, regulates the removal of platinum adducts in sensory neuronal cultures by NER. Mutat Res, 779, 96–104.

Kim, R., Emi, M., & Tanabe, K. (2006). Cancer immunosuppression and autoimmune disease: beyond immunosuppressive networks for tumour immunity. Immunology, 119(2), 254–264.

Kleckner, I. R., Kamen, C., Gewandter, J. S., … Mustian, K. M. (2018). Effects of exercise during chemotherapy on chemotherapy-induced peripheral neuropathy: a multicenter, randomized controlled trial. Support Care Cancer, 26(4), 1019–1028.

Klokk, T. I., Kilander, A., Xi, Z., … Saatcioglu, F. (2007). Kallikrein 4 is a proliferative factor that is overexpressed in prostate cancer. Cancer Res, 67(11), 5221–5230.

Kohli, J., Wang, B., Brandenburg, S.M., & Demaria, M. (2021). Algorithmic assessment of cellular senescence in experimental and clinical specimens. Nat Protoc 16, 2471–2498.

Koskinen, M. J., Kautio, A. L., Haanpää, M. L., … Hietaharju, A. J. (2011). Intraepidermal nerve fiber density in cancer patients receiving adjuvant chemotherapy. Anticancer Res, 31(12), 4413–4416.

Krarup-Hansen, A., Helweg-Larsen, S., Schmalbruch, H., … Krarup, C. (2007). Neuronal involvement in cisplatin neuropathy: prospective clinical and neurophysiological studies. Brain, 130(Pt 4), 1076–1088.

Krishnan, A. V., Goldstein, D., Friedlander, M., & Kiernan, M. C. (2005). Oxaliplatin-induced neurotoxicity and the development of neuropathy. Muscle Nerve, 32(1), 51–60.

Krøigård, T., Schrøder, H. D., Qvortrup, C., … Sindrup, S. H. (2014). Characterization and diagnostic evaluation of chronic polyneuropathies induced by oxaliplatin and docetaxel comparing skin biopsy to quantitative sensory testing and nerve conduction studies. Eur J Neurol, 21(4), 623–629.

Kühlein, H. N., Tegeder, I., Möser, C., … Niederberger, E. (2011). Nerve injury evoked loss of latexin expression in spinal cord neurons contributes to the development of neuropathic pain. PloS One, 6(4), e19270.

Kunath, J., Delaroque, N., Szardenings, M., … Straub, R. H. (2017). Sympathetic nerve repulsion inhibited by designer molecules in vitro and role in experimental arthritis. Life Sci, 168, 47–53.

Kurki, S., Peltonen, K., Latonen, L., … Laiho, M. (2004). Nucleolar protein NPM interacts with HDM2 and protects tumor suppressor protein p53 from HDM2-mediated degradation. Cancer cell, 5(5), 465–475.

Kusmartsev, S., Nefedova, Y., Yoder, D., & Gabrilovich, D. I. (2004). Antigen-specific inhibition of CD8+ T cell response by immature myeloid cells in cancer is mediated by reactive oxygen species. J Immunol, 172(2), 989–999.

Ledda, M., Blum, E., De Palo, S., & Hanani, M. (2009). Augmentation in gap junction-mediated cell coupling in dorsal root ganglia following sciatic nerve neuritis in the mouse. Neuroscience, 164(4), 1538–1545.

Lee, B. Y., Han, J. A., Im, J. S., … Hwang, E. S. (2006). Senescence-associated beta-galactosidase is lysosomal beta-galactosidase. Aging cell, 5(2), 187–195.

Lee, J. H., & Kim, W. (2020). The Role of Satellite Glial Cells, Astrocytes, and Microglia in Oxaliplatin-Induced Neuropathic Pain. Biomedicines, 8(9), 324.

Lehmann, H. C., Staff, N. P., & Hoke, A. (2020). Modeling chemotherapy induced peripheral neuropathy (CIPN) in vitro: Prospects and limitations. Experimental neurology, 326, 113140.

Lehky, T. J., Leonard, G. D., Wilson, R. H., … Floeter, M. K. (2004). Oxaliplatin-induced neurotoxicity: acute hyperexcitability and chronic neuropathy. Muscle Nerve, 29(3), 387–392.

Leo, M., Schmitt, L. I., Jastrow, H., … Hagenacker, T. (2017). Cisplatin alters the function and expression of N-type voltage-gated calcium channels in the absence of morphological damage of sensory neurons. Mol Pain, 13, 1744806917746565.

Leo, M., Schmitt, L. I., Küsterarent, P., … Hagenacker, T. (2020). Platinum-Based Drugs Cause Mitochondrial Dysfunction in Cultured Dorsal Root Ganglion Neurons. Int J Mol Sci, 21(22), 8636.

Leo, M., Schmitt, L. I., Kutritz, A., … Hagenacker, T. (2021). Cisplatin-induced activation and functional modulation of satellite glial cells lead to cytokine-mediated modulation of sensory neuron excitability. Exp Neurol, 341, 113695.

Lessans, S., Lassiter, C. B., Carozzi, V., … Dorsey, S. G. (2019). Global Transcriptomic Profile of Dorsal Root Ganglion and Physiological Correlates of Cisplatin-Induced Peripheral Neuropathy. Nurs Res, 68(2), 145–155.

Li, C. L., Li, K. C., Wu, D., … Zhang, X. (2016). Somatosensory neuron types identified by high-coverage single-cell RNA-sequencing and functional heterogeneity. Cell Res, 26(1), 83–102.

Li, Y., Huang, B., Yang, H., … Chen, M. (2020). Latexin deficiency in mice up-regulates inflammation and aggravates colitis through HECTD1/Rps3/NF-κB pathway. Sci Rep, 10(1), 9868.

Li, Y., Basang, Z., Ding, H., … Ke, Y. (2011). Latexin expression is downregulated in human gastric carcinomas and exhibits tumor suppressor potential. BMC Cancer, 11, 121.

Liang, Y., & Van Zant, G. (2008). Aging stem cells, latexin, and longevity. Exp Cell Res, 314(9), 1962–1972.

Lin, H., Heo, B. H., & Yoon, M. H. (2015). A New Rat Model of Cisplatin-induced Neuropathic Pain. Korean J Pain, 28(4), 236–243.

Liu, J. J., Kim, Y., Yan, F., … McKeage, M. J. (2013). Contributions of rat Ctr1 to the uptake and toxicity of copper and platinum anticancer drugs in dorsal root ganglion neurons. Biochem Pharmacol, 85(2), 207–215.

Lokich, J., & Anderson, N. (1998). Carboplatin versus cisplatin in solid tumors: an analysis of the literature. Ann Oncol, 9(1), 13–21.

London R. E. (2015). The structural basis of XRCC1-mediated DNA repair. DNA Repair, 30, 90–103.

López-González, M. J., Soula, A., Landry, M., & Favereaux, A. (2018). Oxaliplatin treatment impairs extension of sensory neuron neurites in vitro through miR-204 overexpression. Neurotoxicology, 68, 91–100.

Loprinzi, C. L., Maddocks-Christianson, K., Wolf, S. L., … Dyck, P. J. (2007). The Paclitaxel acute pain syndrome: sensitization of nociceptors as the putative mechanism. Cancer J, 13(6), 399–403.

Loprinzi, C. L., Reeves, B. N., Dakhil, S. R., … Lachance, D. H. (2011). Natural history of paclitaxel-associated acute pain syndrome: prospective cohort study NCCTG N08C1. J Clin Oncol, 29(11), 1472–1478.

Maggioni, D., Nicolini, G., Chiorazzi, A., … Tredici, G. (2010). Different effects of erythropoietin in cisplatin- and docetaxel-induced neurotoxicity: an in vitro study. J Neurosci Res, 88(14), 3171–3179.

Maguire, O., Collins, C., O'Loughlin, K., … Minderman, H (2011). Quantifying nuclear p65 as a parameter for NF-κB activation: Correlation between ImageStream cytometry, microscopy, and Western blot. Cytometry A, 79(6), 461–469.

Makharashvili, N., Tubbs, A. T., Yang, S. H., … Paull, T. T. (2014). Catalytic and noncatalytic roles of the CtIP endonuclease in double-strand break end resection. Mol Cell, 54(6), 1022–1033.

Makker, P. G., Duffy, S. S., Lees, J. G., … Moalem-Taylor, G. (2017). Characterisation of Immune and Neuroinflammatory Changes Associated with Chemotherapy-Induced Peripheral Neuropathy. PloS one, 12(1), e0170814.

Malcangio, M. (2019). Role of the immune system in neuropathic pain. Scand J Pain, 20(1), 33–37.

Manu, K. A., Cao, P., Chai, T. F., … Wang, M. (2019). p21cip1/waf1 Coordinate Autophagy, Proliferation and Apoptosis in Response to Metabolic Stress. Cancers, 11(8), 1112.

Marmiroli, P., Cavaletti, G., Carozzi, V., … Genazzani, A. A. (2015). Calcium-related neurotoxicity of oxaliplatin: understanding the mechanisms to drive therapy. Curr Med Chem, 22(32), 3682–3694.

Marmiroli, P., Riva, B., Pozzi, E., … Carozzi, V. A. (2017). Susceptibility of different mouse strains to oxaliplatin peripheral neurotoxicity: Phenotypic and genotypic insights. PloS one, 12(10), e0186250.

Massicot, F., Hache, G., David, L., … Coudoré, F. (2013). P2X7 Cell Death Receptor Activation and Mitochondrial Impairment in Oxaliplatin-Induced Apoptosis and Neuronal Injury: Cellular Mechanisms and In Vivo Approach. PloS one, 8(6), e66830.

McDonald, E. S., & Windebank, A. J. (2002). Cisplatin-induced apoptosis of DRG neurons involves bax redistribution and cytochrome c release but not fas receptor signaling. Neurobiol Dis, 9(2), 220–233.

McDonald, E. S., Randon, K. R., Knight, A., & Windebank, A. J. (2005). Cisplatin preferentially binds to DNA in dorsal root ganglion neurons in vitro and in vivo: a potential mechanism for neurotoxicity. Neurobiol Dis, 18(2), 305–313.

McLean, W.G. (1984). Neurotoxicity and axonal transport. Trends Pharmacol. Sci. 4, 243–246.

McLean W. G. (1997). The role of axonal cytoskeleton in diabetic neuropathy. Neurochem Res, 22(8), 951–956.

Mcllwain, D. R., Berger, T., & Mak, T. W. (2013). Caspase functions in cell death and disease. Cold Spring Harb Perspect Biol,7(4), a026716.

Mella, C., Figueroa, C. D., Otth, C., & Ehrenfeld, P. (2020). Involvement of Kallikrein-Related Peptidases in Nervous System Disorders. Front Cellular Neurosci, 14, 166.

Melli, G., Taiana, M., Camozzi, F., … Lauria, G. (2008). Alpha-lipoic acid prevents mitochondrial damage and neurotoxicity in experimental chemotherapy neuropathy. Exp Neurol, 214(2), 276–284.

Meyyappan, M., Wong, H., Hull, C., & Riabowol, K. T. (1998). Increased expression of cyclin D2 during multiple states of growth arrest in primary and established cells. Mol Cell Biol, 18(6), 3163–3172.

Mijnes, J., Veeck, J., Gaisa, N. T., … Rose, M. (2018). Promoter methylation of DNA damage repair (DDR) genes in human tumor entities: RBBP8/CtIP is almost exclusively methylated in bladder cancer. Clinical epigenetics, 10, 15.

Mizoguchi, S., Andoh, T., Yakura, T., & Kuraishi, Y. (2016). Involvement of c-Myc-mediated transient receptor potential melastatin 8 expression in oxaliplatin-induced cold allodynia in mice. Pharmacol Rep, 68(3), 645–648.

Molliver, D. C., & Snider, W. D. (1997). Nerve growth factor receptor TrkA is down-regulated during postnatal development by a subset of dorsal root ganglion neurons. J Comp Neurol, 381(4), 428–438.

Moreno-Blas, D., Gorostieta-Salas, E., Pommer-Alba, A., … Castro-Obregón, S. (2019). Cortical neurons develop a senescence-like phenotype promoted by dysfunctional autophagy. Aging, 11(16), 6175–6198.

Mrozkova, P., Palecek, J., & Spicarova, D. (2016). The role of protease-activated receptor type 2 in nociceptive signaling and pain. Physiological research, 65(3), 357–367.

Mukhopadhyay, G., Doherty, P., Walsh, F. S., … Filbin, M. T. (1994). A novel role for myelin-associated glycoprotein as an inhibitor of axonal regeneration. Neuron, 13(3), 757–767.

Muneer, A. (2020). Kynurenine Pathway of Tryptophan Metabolism in Neuropsychiatric Disorders: Pathophysiologic and Therapeutic Considerations. *Clin Psychopharmacol Neurosci*, *18*(4), 507–526.

Nair, A. B., & Jacob, S. (2016). A simple practice guide for dose conversion between animals and human. J Basic Clin Pharm, 7(2), 27–31.

Narita, M., Narita, M., Krizhanovsky, V., … Lowe, S. W. (2006). A novel role for high-mobility group a proteins in cellular senescence and heterochromatin formation. Cell, 126(3), 503–514.

Nassini, R., Gees, M., Harrison, S., … Geppetti, P. (2011). Oxaliplatin elicits mechanical and cold allodynia in rodents via TRPA1 receptor stimulation. Pain, 152(7), 1621–1631.

Ni, Q. F., Tian, Y., Kong, L. L., … Kong, L. B. (2014). Latexin exhibits tumor suppressor potential in hepatocellular carcinoma. Oncol Rep, 31(3), 1364–1372.

Nieto, F. R., Cendán, C. M., Sánchez-Fernández, C., … Baeyens, J. M. (2012). Role of sigma-1 receptors in paclitaxel-induced neuropathic pain in mice. J Pain, 13(11), 1107–1121.

Nieto, F. R., Cendán, C. M., Cañizares, F. J., … Baeyens, J. M. (2014). Genetic inactivation and pharmacological blockade of sigma-1 receptors prevent paclitaxel-induced sensory-nerve mitochondrial abnormalities and neuropathic pain in mice. Mol Pain, 10, 11.

Nouspikel, T., & Hanawalt, P. C. (2002). DNA repair in terminally differentiated cells. DNA repair, 1(1), 59–75.

Oguri, S., Sakakibara, T., Mase, H., … Smyth, R. D. (1998). Clinical pharmacokinetics of carboplatin. J Clin Pharmacol, 28(3), 208–215.

Oikonomopoulou, K., Hansen, K. K., Saifeddine, M., … Hollenberg, M. D. (2006). Kallikrein-mediated cell signalling: targeting proteinase-activated receptors (PARs). Biol Chem, 387, 817–824.

Okine, B. N., Gaspar, J. C., & Finn, D. P. (2019). PPARs and pain. Br J Pharmacol, 176(10), 1421–1442.

Olivieri, F., Albertini, M. C., Orciani, M., …Bonafè, M. (2015). DNA damage response (DDR) and senescence: shuttled inflamma-miRNAs on the stage of inflamm-aging. Oncotarget, 6(34), 35509–35521.

Palumbo, S., Tsai, T. L., & Li, W. J. (2014). Macrophage migration inhibitory factor regulates AKT signaling in hypoxic culture to modulate senescence of human mesenchymal stem cells. Stem Cell Dev, 23(8), 852–865.

Park, S. B., Lin, C. S., Krishnan, A. V., … Kiernan, M. C. (2009). Oxaliplatin-induced neurotoxicity: changes in axonal excitability precede development of neuropathy. Brain, 132(Pt 10), 2712–2723.

Park, S. B., Lin, C. S., Krishnan, A. V., … Kiernan, M. C. (2011). Dose effects of oxaliplatin on persistent and transient Na+ conductances and the development of neurotoxicity. PloS one, 6(4), e18469.

Park, S. B., Goldstein, D., Krishnan, A. V., … Kiernan, M. C. (2013). Chemotherapy-induced peripheral neurotoxicity: a critical analysis. CA Cancer J Clin. 63(6), 419–437 (2013).

Pasmant, E., Gilbert-Dussardier, B., Petit, A., … Ballerini, P. (2015). SPRED1, a RAS MAPK pathway inhibitor that causes Legius syndrome, is a tumour suppressor downregulated in paediatric acute myeloblastic leukaemia. Oncogene, 34(5), 631–638.

Pathak, D., Berthet, A., & Nakamura, K. (2013). Energy failure: does it contribute to neurodegeneration? Ann Neurol, 74(4), 506–516.

Picelli, S., Faridani, O. R., Björklund, A. K., … Sandberg, R. (2014). Full-length RNA-seq from single cells using Smart-seq2. Nat Protoc, 9(1), 171–181.

Pike, C. T., Birnbaum, H. G., Muehlenbein, C. E., … Natale, R. B. (2012). Healthcare costs and workloss burden of patients with chemotherapy-associated peripheral neuropathy in breast, ovarian, head and neck, and nonsmall cell lung cancer. Chemother Res Pract, 913848.

Podratz, J. L., Knight, A. M., Ta, L. E., … Windebank, A. J. (2011). Cisplatin induced mitochondrial DNA damage in dorsal root ganglion neurons. Neurobiol Dis, 41(3), 661–668.

Podratz, J. L., Kulkarni, A., Pleticha, J., … Windebank, A. J. (2016). Neurotoxicity to DRG neurons varies between rodent strains treated with cisplatin and bortezomib. J Neurol Sci, 362, 131–135.

Podratz, J. L., Lee, H., Knorr, P., … Windebank, A. (2017). Cisplatin induces mitochondrial deficits in Drosophila larval segmental nerve. Neurobiol Dis, 97(Pt A), 60–69.

Priestley, J. V., Michael, G. J., Averill, S., … Willmott, N. (2002). Regulation of nociceptive neurons by nerve growth factor and glial cell line derived neurotrophic factor. Can J of Physiol Pharmacol, 80(5), 495–505.

Quennet, V., Beucher, A., Barton, O., … Löbrich, M. (2011). CtIP and MRN promote non-homologous end-joining of etoposide-induced DNA double-strand breaks in G1. Nucleic Acids Res, 39(6), 2144–2152.

Quintão, N., Santin, J. R., Stoeberl, L. C., … Costa, R. (2019). Pharmacological Treatment of Chemotherapy-Induced Neuropathic Pain: PPARγ Agonists as a Promising Tool. Front Neurosci, 13, 907.

Reagan-Shaw, S., Nihal, M., & Ahmad, N. (2008). Dose translation from animal to human studies revisited. FASEB J, 22(3), 659–661.

Rébé, C., Demontoux, L., Pilot, T., & Ghiringhelli, F. (2019). Platinum Derivatives Effects on Anticancer Immune Response. Biomolecules, 10(1), 13.

Reinhold A.K., Rittner H.L. (2020). Characteristics of the nerve barrier and the blood dorsal root ganglion barrier in health and disease. Exp Neurol 327, 113244.

Ritchie, M. E., Phipson, B., Wu, D., … Smyth, G. K. (2015). limma powers differential expression analyses for RNA-sequencing and microarray studies. Nucleic Acids Res, 43(7), e47.

Rodier, F., Coppé, J. P., Patil, C. K., … Campisi, J. (2009). Persistent DNA damage signalling triggers senescence-associated inflammatory cytokine secretion. Nat Cell Biol, 11(8), 973–979.

Roelofs, R. I., Hrushesky, W., Rogin, J., & Rosenberg, L. (1984). Peripheral sensory neuropathy and cisplatin chemotherapy. Neurology, 34(7), 934–938.

Romero, L., Zamanillo, D., Nadal, X., … Vela, J. M. (2012). Pharmacological properties of S1RA, a new sigma-1 receptor antagonist that inhibits neuropathic pain and activity-induced spinal sensitization. B J Farmacol, 166(8), 2289–2306.

Rothmeier, A. S., & Ruf, W. (2012). Protease-activated receptor 2 signaling in inflammation. Semi Immunopathol, 34, 133–149.

Rubbi, C. P., & Milner, J. (2003). Disruption of the nucleolus mediates stabilization of p53 in response to DNA damage and other stresses. *EMBO J*, *22*(22), 6068–6077.

Sabbatinelli, J., Prattichizzo, F., Olivieri, F., … Giuliani, A. (2019). Where Metabolism Meets Senescence: Focus on Endothelial Cells. Front Physiol, 10, 1523.

Sakurai, M., Egashira, N., Kawashiri, T., … Oishi, R. (2009). Oxaliplatin-induced neuropathy in the rat: involvement of oxalate in cold hyperalgesia but not mechanical allodynia. Pain, 147(1-3), 165–174.

Saris, C. P., van de Vaart, P. J., Rietbroek, R. C., & Blommaert, F. A. (1996). In vitro formation of DNA adducts by cisplatin, lobaplatin and oxaliplatin in calf thymus DNA in solution and in cultured human cells. Carcinogenesis, 17(12), 2763–2769.

Schmitt, L. I., Leo, M., Kleinschnitz, C., & Hagenacker, T. (2018). Oxaliplatin Modulates the Characteristics of Voltage-Gated Calcium Channels and Action Potentials in Small Dorsal Root Ganglion Neurons of Rats. Mol Neurobiol, 55(12), 8842–8855.

Schwaid, A.G., Krasowka-Zoladek, A., Chi, A., & Cornella-Taracido, I. (2018). Comparison of the Rat and Human Dorsal Root Ganglion Proteome. Sci Rep, 8, 13469.

Seto, Y., Okazaki, F., Horikawa, K., … To, H. (2016). Influence of dosing times on cisplatin-induced peripheral neuropathy in rats. BMC Cancer, 16(1), 756.

Shah, A., Hoffman, E. M., Mauermann, M. L., … Staff, N. P. (2018). Incidence and disease burden of chemotherapy-induced peripheral neuropathy in a population-based cohort. J Neurol Neurosurg Psychiatry, 89(6), 636–641.

Sharma, A., Singh, K., & Almasan, A. (2012). Histone H2AX phosphorylation: a marker for DNA damage. Methods Mol Biol, 920, 613–626.

Sharpless, N. E., & Sherr, C. J. (2015). Forging a signature of in vivo senescence. Nat Rev Cancer, 15(7), 397–408.

Shidahara, Y., Ogawa, S., Nakamura, M., … Takamatsu, H. (2016). Pharmacological comparison of a nonhuman primate and a rat model of oxaliplatin-induced neuropathic cold hypersensitivity. Pharmacol Res Perspect, 4(1), e00216.

Shokhirev, M. N., & Johnson, A. A. (2021). Modeling the human aging transcriptome across tissues, health status, and sex. Aging cell, 20(1), e13280.

Showalter, A., Limaye, A., Oyer, J. L., … Khaled, A. R. (2017). Cytokines in immunogenic cell death: Applications for cancer immunotherapy. Cytokine, 97, 123–132.

Siau, C., & Bennett, G. J. (2006). Dysregulation of cellular calcium homeostasis in chemotherapy-evoked painful peripheral neuropathy. Anesth Analg, 102(5), 1485–1490.

Siddik, Z. H., Newell, D. R., Boxall, F. E., & Harrap, K. R. (1987). The comparative pharmacokinetics of carboplatin and cisplatin in mice and rats. Biochem Pharmacol, 36(12), 1925–1932.

Sinha, S., Malonia, S. K., Mittal, S. P., … Chattopadhyay, S. (2010). Coordinated regulation of p53 apoptotic targets BAX and PUMA by SMAR1 through an identical MAR element. EMBO J, 29(4), 830–842.

Sittl, R., Lampert, A., Huth, T., … Carr, R.W. (2012). Anticancer drug oxaliplatin induces acute cooling-aggravated neuropathy via sodium channel subtype Na(V)1.6-resurgent and persistent current. Proc Natl Acad Sci U S A, 109, 6704–6709.

Smith, E. M., Pang, H., Cirrincione, C., … Alliance for Clinical Trials in Oncology. (2013). Effect of duloxetine on pain, function, and quality of life among patients with chemotherapy-induced painful peripheral neuropathy: a randomized clinical trial. JAMA, 309(13), 1359–1367.

Sprowl, J. A., Ness, R. A., & Sparreboom, A. (2013). Polymorphic transporters and platinum pharmacodynamics. Drug Metab Pharmacokinet, 28(1), 19–27.

Sprowl, J., Ong, S., Gibson, A., … Pabla, N. (2016). A phosphotyrosine switch regulates organic cation transporters. Nat Commun 7, 10880.

Staff, N. P., Cavaletti, G., Islam, B., … Tamburin, S. (2019). Platinum-induced peripheral neurotoxicity: From pathogenesis to treatment. J Peripher Nerv Syst : JPNS, 24 Suppl 2(Suppl 2), S26–S39.

Starobova, H., & Vetter, I. (2017). Pathophysiology of Chemotherapy-Induced Peripheral Neuropathy. Front Mol Neurosci, 10, 174.

Stojanovska, V., McQuade, R. M., Fraser, S., … Nurgali, K. (2018). Oxaliplatin-induced changes in microbiota, TLR4+ cells and enhanced HMGB1 expression in the murine colon. PloS one, 13(6), e0198359.

Stojanovska, V., Prakash, M., McQuade, R., … Nurgali, K. (2019). Oxaliplatin Treatment Alters Systemic Immune Responses. Biomed Res Int, 2019, 4650695.

Striggow, F., Riek-Burchardt, M., Kiesel, A., … Reiser, G. (2002). Four different types of protease-activated receptors are widely expressed in the brain and are up-regulated in hippocampus by severe ischemia. Eur J Neurosci, 14, 595–608.

Styr, B., Gonen, N., Zarhin, D., … Slutsky, I. (2019). Mitochondrial Regulation of the Hippocampal Firing Rate Set Point and Seizure Susceptibility. Neuron, 102(5), 1009–1024.e8.

Suo, Z., Wu, M., Citron, B. A., … Festoff, B. W. (2003). Persistent protease-activated receptor 4 signaling mediates thrombin-induced microglial activation. J Biol Chem, 278, 31177–31183.

Szilvássy, J., Sziklai, I., Sári, R., … Szilvássy, Z. (2006). Neurogenic insulin resistance in guinea-pigs with cisplatin-induced neuropathy. Eur J Pharmacol, 531(1-3), 217–225.

Ta, L. E., Espeset, L., Podratz, J., & Windebank, A. J. (2006). Neurotoxicity of oxaliplatin and cisplatin for dorsal root ganglion neurons correlates with platinum-DNA binding. Neurotoxicology, 27(6), 992–1002.

Ta, L. E., Bieber, A. J., Carlton, S. M., … Windebank, A. J. (2010). Transient Receptor Potential Vanilloid 1 is essential for cisplatin-induced heat hyperalgesia in mice. Mol Pain, 6, 15.

Tan, L., Yu, J. T., & Tan, L. (2012). The kynurenine pathway in neurodegenerative diseases: mechanistic and therapeutic considerations. J Neurol Sci, 323(1-2), 1–8.

Tanay, M., Armes, J., Moss-Morris, R., … Robert, G. (2021). A systematic review of behavioural and exercise interventions for the prevention and management of chemotherapy-induced peripheral neuropathy symptoms. J Cancer Surviv.

Thibault, K., Calvino, B., Dubacq, S., … Pezet, S. (2012). Cortical effect of oxaliplatin associated with sustained neuropathic pain: exacerbation of cortical activity and down-regulation of potassium channel expression in somatosensory cortex. Pain, 153(8), 1636–1647.

Thompson, S. W., Davis, L. E., Kornfeld, M., … Standefer, J. C. (1984). Cisplatin neuropathy. Clinical, electrophysiologic, morphologic, and toxicologic studies. Cancer, 54(7), 1269–1275.

Todd, R. C., & Lippard, S. J. (2010). Consequences of cisplatin binding on nucleosome structure and dynamics. Chem Biol, 17(12), 1334–1343.

Tomaszewski, A., & Büsselberg, D. (2007). Cisplatin modulates voltage gated channel currents of dorsal root ganglion neurons of rats. Neurotoxicology, 28(1), 49–58.

Tredici, G., Tredici, S., Fabbrica, D., … Cavaletti, G. (1998). Experimental cisplatin neuronopathy in rats and the effect of retinoic acid administration. J Neurooncol, 36, 31–40.

Tsai, M. J., Chang, W. A., Huang, M. S., & Kuo, P. L. (2014). Tumor microenvironment: a new treatment target for cancer. ISRN Biochem, 2014, 351959.

Tulub, A. A., & Stefanov, V. E. (2001). Cisplatin stops tubulin assembly into microtubules. A new insight into the mechanism of antitumor activity of platinum complexes. Int J Biol Macromol, 28(3), 191–198.

Ulisse, V., Dey, S., Rothbard, D. E., … Yaron, A. (2020). Regulation of axonal morphogenesis by the mitochondrial protein Efhd1. Life Sci Alliance, 3(7), e202000753.

Usoskin, D., Furlan, A., Islam, S., … Ernfors, P. (2015). Unbiased classification of sensory neuron types by large-scale single-cell RNA sequencing. Nat Neurosci 18, 145–153.

Velasco, R. & Bruna, J. (2010). Neuropatía inducida por quimioterapia: un problema no resuelto [Chemotherapy-induced peripheral neuropathy: an unresolved issue]. Neurología. 25(2), 116-131.

Velasco, R., & Bruna, J. (2014). Oxaliplatin neurotoxicity. Curr Colorectal Cancer Rep, 10(3), 303-312.

Velasco, R., Videla, S., Villoria, J. & Bruna, J. (2015). Reliability and accuracy of quantitative sensory testing for oxaliplatin-induced neurotoxicity. Acta Neurol Scand, 131(5), 282–289.

Velasco, R., Navarro, X., Gil-Gil, M., … Bruna, J. (2017). Neuropathic Pain and Nerve Growth Factor in Chemotherapy-Induced Peripheral Neuropathy: Prospective Clinical-Pathological Study. J Pain Symptom Manage, 54(6), 815–825.

Verdú, E., Vilches, J. J., Rodríguez, F. J., … Navarro, X. (1999). Physiological and immunohistochemical characterization of cisplatin-induced neuropathy in mice. *Muscle Nerve*, *22*(3), 329–340.

Verstappen, C. C., Heimans, J. J., Hoekman, K., & Postma, T. J. (2003). Neurotoxic complications of chemotherapy in patients with cancer: clinical signs and optimal management. Drugs, 63(15), 1549–1563.

Viens, P., Petit, T., Yovine, A., … Cvitkovic, E. (2006). A phase II study of a paclitaxel and oxaliplatin combination in platinum-sensitive recurrent advanced ovarian cancer patients. Ann Oncol, 17(3), 429–436.

Vjetrovic, J., Shankaranarayanan, P., Mendoza-Parra, M. A., & Gronemeyer, H. (2014). Senescence-secreted factors activate Myc and sensitize pretransformed cells to TRAIL-induced apoptosis. Aging cell, 13(3), 487–496.

Villeda, S. A., Luo, J., Mosher, K. I., … Wyss-Coray, T. (2011). The ageing systemic milieu negatively regulates neurogenesis and cognitive function. Nature, 477(7362), 90–94.

Wainger, B. J., Buttermore, E. D., Oliveira, J. T., … Woolf, C. J. (2015). Modeling pain in vitro using nociceptor neurons reprogrammed from fibroblasts. Nat Neurosci, 18(1), 17–24.

Wan, F., & Lenardo, M. J. (2010). The nuclear signaling of NF-kappaB: current knowledge, new insights, and future perspectives. Cell Res, 20(1), 24–33.

Wang, H., Ubl, J. J., & Reiser, G. (2020). Four subtypes of protease-activated receptors, co-expressed in rat astrocytes, evoke different physiological signaling. Glia 37, 53–63.

Wang, J., Jiang, C., Ba, X., … Hao, Y. (2021). Selective activation of metabotropic glutamate receptor 7 blocks paclitaxel-induced acute neuropathic pain and suppresses spinal glial reactivity in rats. Psychopharmacology, 238(1), 107–119.

Wang, X. M., Lehky, T. J., Brell, J. M., & Dorsey, S. G. (2012). Discovering cytokines as targets for chemotherapy-induced painful peripheral neuropathy. Cytokine, 59(1), 3–9.

Wang, Y., Richter-Landsberg, C., & Reiser, G. (2004). Expression of protease-activated receptors (PARs) in OLN-93 oligodendroglial cells and mechanism of PAR-1-induced calcium signaling. Neuroscience, 126, 69–82.

Warwick, R. A., & Hanani, M. (2013). The contribution of satellite glial cells to chemotherapy-induced neuropathic pain. Eur J Pain, 17(4), 571–580.

Waseem, M., & Parvez, S. (2016). Neuroprotective activities of curcumin and quercetin with potential relevance to mitochondrial dysfunction induced by oxaliplatin. Protoplasma, 253(2), 417–430.

Watson, C. (2012). The Mouse Nervous System; Chapter 21 - The Somatosensory System. Academic Press. 563-570.

Webster, R. G., Brain, K. L., Wilson, R. H., … Vincent, A. (2005). Oxaliplatin induces hyperexcitability at motor and autonomic neuromuscular junctions through effects on voltage-gated sodium channels. Br J Pharmacol, 146(7), 1027–1039.

Wheeler, H. E., Wing, C., Delaney, S. M., … Dolan, M. E. (2015). Modeling chemotherapeutic neurotoxicity with human induced pluripotent stem cell-derived neuronal cells. PloS one, 10(2), e0118020.

Wiley, C. D., & Campisi, J. (2016). From Ancient Pathways to Aging Cells-Connecting Metabolism and Cellular Senescence. Cell Metab, 23(6), 1013–1021.

Wilson, R. H., Lehky, T., Thomas, R. R., … Grem, J. L. (2002). Acute oxaliplatin-induced peripheral nerve hyperexcitability. J Clin Oncol, 20(7), 1767–1774.

Wing, C., Komatsu, M., Delaney, S. M., … Dolan, M. E. (2017). Application of stem cell derived neuronal cells to evaluate neurotoxic chemotherapy. Stem Cell Res, 22, 79–88.

Wolf, S., Barton, D., Kottschade, L., … Loprinzi, C. (2008). Chemotherapy-induced peripheral neuropathy: prevention and treatment strategies. Eur J Cancer, 44(11), 1507–1515.

Working, P. K., Newman, M. S., Sullivan, T., … Turner, N. (1998). Comparative intravenous toxicity of cisplatin solution and cisplatin encapsulated in long-circulating, pegylated liposomes in cynomolgus monkeys. Toxicol Sci, 46(1), 155–165.

Woynarowski, J. M., Faivre, S., Herzig, M. C., … Juniewicz, P. E. (2000). Oxaliplatin-induced damage of cellular DNA. Mol Pharmacol, 58(5), 920–927.

Wu, M. H., Chang, J. H., & Yung, B. Y. (2002). Resistance to UV-induced cell-killing in nucleophosmin/B23 over-expressed NIH 3T3 fibroblasts: enhancement of DNA repair and up-regulation of PCNA in association with nucleophosmin/B23 over-expression. Carcinogenesis, 23(1), 93–100.

Xi, Z., Klokk, T. I., Korkmaz, K., … Saatcioglu, F. (2004). Kallikrein 4 is a predominantly nuclear protein and is overexpressed in prostate cancer. Cancer Res, 64(7), 2365–2370.

Xia, W., Zhang, F., Xie, C., … Hou, M. (2015). Macrophage migration inhibitory factor confers resistance to senescence through CD74-dependent AMPK-FOXO3a signaling in mesenchymal stem cells. Stem Cell Res Ther, 6(1), 82.

Xia, W., & Hou, M. (2018). Macrophage migration inhibitory factor rescues mesenchymal stem cells from doxorubicin-induced senescence though the PI3K-Akt signaling pathway. Int J Mol Med, 41(2), 1127–1137.

Xiao, W. H., Zheng, H., & Bennett, G. J. (2012). Characterization of oxaliplatin-induced chronic painful peripheral neuropathy in the rat and comparison with the neuropathy induced by paclitaxel. Neuroscience, 203, 194–206.

Xu, B., Zeng, M., Zeng, J., … Yu, L. (2018). Meta-analysis of clinical trials comparing the efficacy and safety of liposomal cisplatin versus conventional nonliposomal cisplatin in nonsmall cell lung cancer (NSCLC) and squamous cell carcinoma of the head and neck (SCCHN). Medicine, 97(46), e13169.

Xu, D., Zhao, H., Gao, H., … Li, J. (2018). Participation of pro-inflammatory cytokines in neuropathic pain evoked by chemotherapeutic oxaliplatin via central GABAergic pathway. Mol Pain, 14, 1744806918783535.

Yamakuchi, M., & Hashiguchi, T. (2018). Endothelial Cell Aging: How miRNAs Contribute?. J Clin Med, 7(7).

Yamamoto, K., Chiba, N., Chiba, T., … Taguchi, K. (2015). Transient receptor potential ankyrin 1 that is induced in dorsal root ganglion neurons contributes to acute cold hypersensitivity after oxaliplatin administration. Mol Pain, 11, 69.

Yan, F., Liu, J. J., Ip, V., … McKeage, M. J. (2015). Role of platinum DNA damage-induced transcriptional inhibition in chemotherapy-induced neuronal atrophy and peripheral neurotoxicity. J Neurochem, 135(6), 1099–1112.

Yang, N. C., & Hu, M. L. (2005). The limitations and validities of senescence associated-beta-galactosidase activity as an aging marker for human foreskin fibroblast Hs68 cells. Exp Gerontol, 40(10), 813–819.

You, Y., Wen, R., Pathak, R., … Liang, Y. (2014). Latexin sensitizes leukemogenic cells to gamma-irradiation-induced cell-cycle arrest and cell death through Rps3 pathway. Cell Death Dis, 5(10), e1493.

Zeisel, A., Hochgerner, H., Lönnerberg, P., … Linnarsson, S. (2018). Molecular Architecture of the Mouse Nervous System. Cell, 174(4), 999–1014.e22.

Zhang, C., Fondufe-Mittendorf, Y. N., Wang, C., … Liang, Y. (2020). Latexin regulation by HMGB2 is required for hematopoietic stem cell maintenance. Haematologica, 105(3), 573–584.

Zhang, H., Yoon, S. Y., Zhang, H., & Dougherty, P. M. (2012). Evidence that spinal astrocytes but not microglia contribute to the pathogenesis of Paclitaxel-induced painful neuropathy. J Pain, 13(3), 293–303.

Zhang, H., Li, Y., de Carvalho-Barbosa, M., … Dougherty, P. M. (2016). Dorsal Root Ganglion Infiltration by Macrophages Contributes to Paclitaxel Chemotherapy-Induced Peripheral Neuropathy. J Pain, 17(7), 775–786.

Zhang, R., Zhang, Y., Lu, X., … Li, Y. (2020). SPRED1 Is Downregulated and a Prognostic Biomarker in Adult Acute Myeloid Leukemia. Front Oncol, 10, 204.

Zhuo, M., Gorgun, M. F., & Englander, E. W. (2018). Translesion Synthesis DNA Polymerase Kappa Is Indispensable for DNA Repair Synthesis in Cisplatin Exposed Dorsal Root Ganglion Neurons. Mol Neurol, 55(3), 2506–2515.

X. SUPPLEMENTARY DATA

Supplementary Table 1. DEGs in the DRG neuronal population of cisplatin-treated (CDDP) mice (p<0.05). Avg_log$_2$FC: average of log$_2$ fold expression differences value. A negative avg_log$_2$FC means that a gene is down-regulated in the CDDP group. A positive avg_log$_2$FC means that a gene is up-regulated in the CDDP group. p: p value (non-adjusted). p-val-adj: p value adjusted for multiple comparisons. DEGs are ordered by significance.

Gene	avg_log$_2$FC	p	p-val-adj
Cdkn1a	0,9981	9,4E-6	0,0018
Rbm3	0,4594	0,0002	0,0322
Rcor3	0,271	0,0005	0,0446
Igsf3	0,2884	0,0005	0,0446
Brix1	0,2986	0,0006	0,0446
Gabbr2	0,2813	0,0009	0,0575
Ifrd1	0,3713	0,0011	0,0575
Emc10	-0,359	0,0014	0,0593
Timm8a1	0,2935	0,0015	0,0593
G3bp2	0,2777	0,0016	0,0593
Vps8	0,339	0,002	0,0693
Denr	0,3114	0,0029	0,0833
Stx12	0,4361	0,0035	0,0833
Spcs2	0,3266	0,0035	0,0833
Prmt3	0,2846	0,0036	0,0833
Nap1l1	0,2735	0,0037	0,0833
Tipin	0,2661	0,0039	0,0833
Lrrtm3	0,2647	0,0042	0,0833
Exosc2	0,2501	0,0046	0,0833
Ptov1	-0,4401	0,0049	0,0833
Lin37	-0,2808	0,0049	0,0833
Alkbh1	0,3035	0,005	0,0833
Psmd3	0,3387	0,0051	0,0833
Mllt11	0,3049	0,0061	0,09
Gnas	-0,3564	0,0061	0,09
Commd1	-0,2689	0,0065	0,09
Gstt1	-0,3725	0,0067	0,09
Ccdc127	0,2691	0,007	0,09
Aen	0,3179	0,0072	0,09
Atp8a2	0,2608	0,0073	0,09
Hsp90b1	-0,2561	0,0076	0,09
Fbxl4	0,2994	0,0077	0,09
Pdcd6	-0,4222	0,0082	0,0904

Gene	avg_log$_2$FC	p	p-val-adj
Litaf	-0,521	0,0084	0,0904
Fam89a	-0,2929	0,0088	0,0904
Ttc9	0,355	0,0093	0,0904
Lamtor5	-0,3058	0,0095	0,0904
Nqo2	-0,2542	0,0095	0,0904
Coro1c	-0,2834	0,0098	0,0904
Lancl1	0,3547	0,0102	0,0904
Cptp	0,3438	0,0106	0,0904
Tceal1	-0,281	0,0106	0,0904
Dalrd3	-0,2548	0,0106	0,0904
Ube2a	-0,2807	0,011	0,0904
Sytl3	-0,3795	0,0115	0,0904
Ccnl1	0,3117	0,0116	0,0904
Acd	-0,4275	0,0117	0,0904
Pcnp	0,3121	0,0118	0,0904
Rad23a	-0,2615	0,0118	0,0904
Cept1	-0,3838	0,0126	0,0943
9530077C05Rik	-0,4761	0,0128	0,0944
Isyna1	-0,5211	0,0131	0,0947
Ubxn2a	-0,3045	0,0143	0,0948
Madd	-0,2992	0,0146	0,0948
Mob4	0,2824	0,0146	0,0948
Parp2	-0,2545	0,0146	0,0948
Plxdc2	-0,4632	0,0147	0,0948
Tmem151a	0,3275	0,0148	0,0948
Arfgef1	0,292	0,0151	0,0948
5430403G16Rik	-0,2736	0,0152	0,0948
Robo2	0,3354	0,0157	0,0964
Uspl1	-0,2579	0,0161	0,0974
Sv2c	0,3495	0,0164	0,0974
Plpbp	0,3052	0,0178	0,1001
2010111I01Rik	0,3254	0,0179	0,1001
Pdha1	0,2769	0,0179	0,1001

Gene	avg_log$_2$FC	p	p-val-adj
Ccm2	-0,2918	0,0179	0,1001
Prr14l	-0,2701	0,0183	0,1001
Zkscan3	-0,2739	0,0187	0,1001
Wdr83	-0,2845	0,0188	0,1001
Zmynd8	-0,2604	0,019	0,1001
Pan2	-0,2504	0,0196	0,1019
Atf3	1,14	0,0198	0,1019
Ttc1	0,2926	0,021	0,1059
Ache	-0,4641	0,0212	0,1059
Sfxn4	-0,3174	0,0216	0,1067
Pabpn1	-0,3194	0,0229	0,1104
Xist	-0,412	0,0232	0,1104
Edf1	-0,2773	0,0233	0,1104
Fhl1	0,3054	0,0237	0,1113
Crot	-0,3816	0,0243	0,1113
Gtpbp1	-0,2991	0,0243	0,1113
Ntsr2	0,3137	0,0252	0,1138
Sacm1l	-0,2676	0,026	0,114
Hax1	0,3164	0,0264	0,114
Hmgcs1	-0,3426	0,0264	0,114
Rbm6	0,2662	0,0266	0,114
Gbe1	0,2546	0,027	0,114
Scn11a	-0,3237	0,027	0,114
Atp8a1	-0,2774	0,0276	0,115
Rraga	0,2599	0,0282	0,116
Clcn3	0,3427	0,0293	0,1194
Rgs4	1,02	0,0309	0,1227
Tmem100	0,5186	0,031	0,1227

Gene	avg_log$_2$FC	p	p-val-adj
Rpp21	0,2638	0,0311	0,1227
Myc	0,4155	0,0327	0,1276
Cplx1	0,4425	0,036	0,1346
Cacnb3	0,2772	0,036	0,1346
Nop53	0,2915	0,036	0,1346
Dtna	0,2557	0,0363	0,1346
Tmc5	0,4723	0,0364	0,1346
Tbc1d14	0,2613	0,0366	0,1346
Slc17a5	0,2748	0,037	0,1347
Bdnf	0,3096	0,0388	0,1387
Rhoc	0,2594	0,0391	0,1387
Isl2	0,4395	0,0392	0,1387
Hspb1	0,5243	0,0415	0,1434
Fkbp9	-0,2632	0,0418	0,1434
Abl1	-0,3848	0,0418	0,1434
Gsap	-0,3408	0,0421	0,1434
Eif2ak1	-0,2759	0,0431	0,1444
Sec1	-0,3221	0,0431	0,1444
Rgs2	0,3214	0,0443	0,1459
Kcnip4	0,6843	0,0449	0,1459
Mff	0,2544	0,0455	0,1459
Ndrg4	0,2504	0,0455	0,1459
Tmem130	-0,3133	0,0455	0,1459
Pds5b	-0,2553	0,046	0,1461
Dgka	-0,3652	0,0488	0,1507
Xrcc1	-0,2505	0,0489	0,1507
Arcn1	0,2795	0,049	0,1507
Chordc1	-0,271	0,049	0,1507

Supplementary Table 2. DEGs in the SGC population of cisplatin-treated (CDDP) mice (p<0.05). Avg_log$_2$FC: average of log$_2$ fold expression differences value. A negative avg_log$_2$FC means that a gene is down-regulated in the CDDP group. A positive avg_log$_2$FC means that a gene is up-regulated in the CDDP group. p: p value (non-adjusted). p-val-adj: p value adjusted for multiple comparisons. DEGs are ordered by significance.

Gene	avg_log$_2$FC	p	p-val-adj
Cdkn1a	1,1606	9,4E-6	0,0107
Socs3	1,3703	0,0001	0,0409
Ephx1	0,9478	0,0003	0,0744
Fos	1,2274	0,0003	0,0744
Cdca4	-0,5015	0,0004	0,0744
Lbhd2	-0,3586	0,0004	0,0744
Ier3	0,7049	0,0005	0,0747
Tab1	0,4878	0,0006	0,0809
Serpina3n	0,8945	0,0006	0,0809
Ppp1r16a	-0,2955	0,0008	0,0823
Adam15	-0,2701	0,0008	0,0823
Gstm7	0,7059	0,0009	0,0823
Mrpl17	0,4274	0,0010	0,0906
Gpr180	0,3166	0,0014	0,1142
Wdr24	-0,3067	0,0017	0,1188
Mettl16	-0,3515	0,0017	0,1188
Rxylt1	0,3278	0,0018	0,1188
Cirbp	0,6050	0,0020	0,1256
H3f3b	0,4441	0,0025	0,1489
Ccnd1	-0,5099	0,0035	0,1669
Itih5	0,2641	0,0036	0,1669
Phgdh	0,4119	0,0037	0,1669
Pot1a	-0,4200	0,0037	0,1669
Fastkd2	-0,3249	0,0037	0,1669
Anapc16	-0,5752	0,0038	0,1669
Rtca	0,2894	0,0041	0,1669
mt-Atp6	-0,3322	0,0041	0,1669
Gm42047	0,2578	0,0043	0,1669
Usp39	0,4141	0,0044	0,1669
Olfm2	0,4385	0,0044	0,1669
sept-08	-0,7211	0,0054	0,1825
Efemp1	-0,7695	0,0055	0,1825
Junb	0,9639	0,0057	0,1825

Gene	avg_log$_2$FC	p	p-val-adj
Sbspon	0,5530	0,0058	0,1825
Gm7901	0,2891	0,0062	0,1825
Tmem30a	0,6753	0,0066	0,1825
Mgst1	-0,3326	0,0069	0,1825
Slc43a3	-0,3950	0,0069	0,1825
mt-Nd1	-0,3234	0,0069	0,1825
Gde1	0,4877	0,0072	0,1825
Rps27l	0,3381	0,0073	0,1825
Txnip	1,0061	0,0074	0,1825
Gas2l3	0,7458	0,0076	0,1825
Ndc1	-0,3226	0,0079	0,1825
Def8	-0,3293	0,0079	0,1825
Uxs1	0,3151	0,0080	0,1825
Tmem39a	-0,5678	0,0083	0,1825
Tbxa2r	0,2608	0,0083	0,1825
Slc9a6	0,2914	0,0083	0,1825
Map6	0,3264	0,0083	0,1825
Gm10033	0,3044	0,0083	0,1825
Rras2	0,2548	0,0083	0,1825
Brd8	0,4909	0,0087	0,1867
Tnfaip1	-0,6286	0,0089	0,1884
Mob2	-0,5193	0,0095	0,1949
Mtfr1l	0,4564	0,0096	0,1949
Atp8a1	-0,4954	0,0098	0,1962
Mta2	-0,4614	0,0112	0,2203
Abcd3	0,6830	0,0116	0,2234
Hexa	-0,6100	0,0122	0,2280
Nt5m	-0,3977	0,0122	0,2280
Itm2b	-0,3110	0,0126	0,2319
Wdr77	-0,5806	0,0137	0,2486
Wbp1	0,2644	0,0145	0,2532
Rdx	0,4492	0,0148	0,2532
Cipc	-0,7017	0,0149	0,2532

Gene	avg_log$_2$FC	p	p-val-adj
Rabep1	-0,5182	0,0156	0,2532
Fam126a	-0,5409	0,0157	0,2532
Ptn	-0,3460	0,0158	0,2532
Mt2	0,3356	0,0161	0,2532
Ddx1	-0,7883	0,0161	0,2532
Lhpp	-0,3732	0,0163	0,2532
Armcx3	-0,4937	0,0166	0,2532
Hmgn2	0,2670	0,0169	0,2532
Ralb	0,6069	0,0169	0,2532
Mt1	0,2890	0,0171	0,2532
Ubc	0,5571	0,0173	0,2532
Nop58	0,2846	0,0173	0,2532
Atp6v1e1	-0,3973	0,0176	0,2533
Ier2	0,7789	0,0180	0,2533
Mark3	-0,4676	0,0181	0,2533
Nek4	-0,3757	0,0182	0,2533
Gtf2h2	-0,3749	0,0186	0,2542
Hmgcl	0,3749	0,0187	0,2542
Dennd1a	0,3462	0,0198	0,2639
Ednrb	-0,5675	0,0200	0,2639
Notch1	-0,3970	0,0203	0,2639
Prss23	0,5278	0,0204	0,2639
Armcx1	-0,6144	0,0208	0,2641
Selenom	0,3204	0,0209	0,2641
Dync2h1	-0,3591	0,0212	0,2641
Ccnc	-0,4639	0,0215	0,2641
Smc4	0,2785	0,0215	0,2641
Stk38	-0,3444	0,0218	0,2646
Herpud1	-0,4928	0,0226	0,2694
mt-Nd2	-0,3720	0,0227	0,2694
Efcab14	-0,3019	0,0230	0,2699
Ube2g1	0,5731	0,0240	0,2787
Glrx3	0,4713	0,0244	0,2808
Eif4g2	-0,4077	0,0248	0,2824
Ak3	0,5741	0,0261	0,2827
Zfp983	0,5954	0,0262	0,2827
Slc25a39	0,3705	0,0263	0,2827
Gtf2a2	0,5785	0,0270	0,2827

Gene	avg_log$_2$FC	p	p-val-adj
Huwe1	0,6056	0,0270	0,2827
Ric8a	-0,2885	0,0271	0,2827
Atp6v1d	-0,4636	0,0272	0,2827
Scamp3	-0,4775	0,0275	0,2827
Cdh11	0,3476	0,0282	0,2827
Tmem185a	0,3731	0,0285	0,2827
Arhgdia	0,4915	0,0288	0,2827
Stard4	0,6819	0,0289	0,2827
Tmem9b	-0,3128	0,0289	0,2827
Pak1ip1	0,4472	0,0290	0,2827
Golph3	0,6819	0,0292	0,2827
Mical3	-0,3107	0,0293	0,2827
Dmd	0,4693	0,0294	0,2827
Zfp36	0,7335	0,0297	0,2827
Chmp2a	0,2559	0,0297	0,2827
Bex4	-0,2669	0,0298	0,2827
Rfxank	-0,3984	0,0303	0,2851
Tmem29	-0,4152	0,0308	0,2851
Ltbp2	-0,4507	0,0311	0,2851
Gfm1	-0,3347	0,0311	0,2851
Fkbp4	-0,4233	0,0313	0,2851
Igbp1	0,4169	0,0324	0,2929
Erbb3	-0,3202	0,0329	0,2946
Anxa5	-0,2526	0,0331	0,2946
Snx14	-0,4462	0,0336	0,2947
Gtpbp6	-0,3378	0,0336	0,2947
Actr1b	-0,4484	0,0343	0,2950
Abca8a	-0,3891	0,0345	0,2950
Fsd1l	-0,3039	0,0345	0,2950
Them4	-0,3665	0,0349	0,2950
Rplp0	0,2527	0,0350	0,2950
Kidins220	-0,3744	0,0353	0,2950
Rnf7	0,2676	0,0354	0,2950
Akr1a1	0,3373	0,0359	0,2964
Btg2	0,8935	0,0364	0,2966
Nop56	0,5941	0,0367	0,2966
Vps53	0,4956	0,0372	0,2966
Acd	0,4518	0,0373	0,2966

Gene	avg_log$_2$FC	p	p-val-adj
Arid4b	-0,4230	0,0375	0,2966
Peg3	-0,4339	0,0376	0,2966
Purb	0,3510	0,0381	0,2966
Eif4e2	0,3291	0,0381	0,2966
Bax	0,2928	0,0389	0,2966
Rab12	-0,2991	0,0391	0,2966
Nudt16l1	0,4356	0,0394	0,2966
Ptk2	-0,4462	0,0394	0,2966
Rpl18	0,2741	0,0394	0,2966
Nr1d1	0,4276	0,0402	0,2966
Scfd1	0,5851	0,0403	0,2966
Ephb6	-0,4208	0,0408	0,2966
Cmc4	0,2806	0,0409	0,2966
Fh1	0,4791	0,0410	0,2966
Ddx3x	0,6116	0,0411	0,2966
Rps25	0,2692	0,0411	0,2966
Cdkl3	0,2802	0,0416	0,2969

Gene	avg_log$_2$FC	p	p-val-adj
Tgoln1	-0,6208	0,0417	0,2969
Nipsnap3b	-0,2776	0,0422	0,2970
Slc44a2	-0,4443	0,0422	0,2970
Fosb	0,4900	0,0425	0,2976
Pebp1	0,2695	0,0429	0,2985
Prmt2	-0,5480	0,0436	0,2998
Ssr3	-0,3931	0,0436	0,2998
Ost4	-0,2720	0,0439	0,2999
Sgk1	0,6380	0,0448	0,3042
Dnajc19	0,2975	0,0453	0,3054
Ufc1	0,3203	0,0456	0,3055
Unc80	-0,3173	0,0458	0,3056
Uap1l1	0,3730	0,0464	0,3076
Arl1	-0,3360	0,0478	0,3151
Sfrp1	-0,3654	0,0486	0,3169
Sf3a3	0,4063	0,0486	0,3169
Tmem14a	-0,2943	0,0496	0,3183

Supplementary Table 3. GO terms up-regulated (p<0.01) in the neuronal population of cisplatin-treated (CDDP) mice. Only up-regulated DEGs with p<0.01 were used for the GO analysis. All Terms correspond to the Ontology "Biological Process". N: number of genes that have been described for the corresponding term in the genome of reference (*Mus Musculus*). UP: number of genes related with the specific term that are up-regulated in our study. p: p value (non-adjusted) of the corresponding term in our study. Go Terms are ordered by significance.

Term ID	Term Name	N	UP	p
GO:0042771	intrinsic apoptotic signaling pathway in response to DNA damage by p53 class mediator	31	2	6,92E-04
GO:0097193	intrinsic apoptotic signaling pathway	155	3	8,35E-04
GO:0009314	response to radiation	414	4	1,38E-03
GO:0072332	intrinsic apoptotic signaling pathway by p53 class mediator	51	2	1,78E-03
GO:0042246	tissue regeneration	52	2	1,85E-03
GO:0071840	cellular component organization or biogenesis	5345	14	1,85E-03
GO:0044773	mitotic DNA damage checkpoint	58	2	2,28E-03
GO:1990983	tRNA demethylation	1	1	2,36E-03
GO:0044774	mitotic DNA integrity checkpoint	61	2	2,51E-03
GO:0002101	tRNA wobble cytosine modification	2	1	3,54E-03
GO:0071049	nuclear retention of pre-mRNA with aberrant 3'-ends at the site of transcription	2	1	3,54E-03
GO:0071031	nuclear mRNA surveillance of mRNA 3'-end processing	2	1	3,54E-03
GO:1905179	negative regulation of cardiac muscle tissue regeneration	2	1	3,54E-03
GO:1905178	regulation of cardiac muscle tissue regeneration	2	1	3,54E-03
GO:0062029	positive regulation of stress granule assembly	2	1	3,54E-03
GO:0042245	RNA repair	2	1	3,54E-03
GO:0072331	signal transduction by p53 class mediator	74	2	3,62E-03
GO:0016043	cellular component organization	5151	13	3,81E-03
GO:0008630	intrinsic apoptotic signaling pathway in response to DNA damage	78	2	4,01E-03
GO:0097190	apoptotic signaling pathway	273	3	4,09E-03
GO:0006906	vesicle fusion	80	2	4,20E-03
GO:0009628	response to abiotic stimulus	938	5	4,43E-03
GO:0035552	oxidative single-stranded DNA demethylation	3	1	4,72E-03
GO:0043111	replication fork arrest	3	1	4,72E-03
GO:0090174	organelle membrane fusion	86	2	4,82E-03
GO:0000077	DNA damage checkpoint	91	2	5,37E-03
GO:0072594	establishment of protein localization to organelle	310	3	5,81E-03
GO:0009416	response to light stimulus	311	3	5,86E-03
GO:0003011	involuntary skeletal muscle contraction	4	1	5,89E-03
GO:0002188	translation reinitiation	4	1	5,89E-03
GO:0071043	CUT metabolic process	4	1	5,89E-03
GO:0071034	CUT catabolic process	4	1	5,89E-03
GO:0016189	synaptic vesicle to endosome fusion	4	1	5,89E-03

Term ID	Term Name	N	UP	p
GO:0019919	peptidyl-arginine methylation, to asymmetrical-dimethyl arginine	4	1	5,89E-03
GO:0031570	DNA integrity checkpoint	97	2	6,06E-03
GO:0031099	regeneration	101	2	6,55E-03
GO:0048284	organelle fusion	105	2	7,05E-03
GO:0071033	nuclear retention of pre-mRNA at the site of transcription	5	1	7,07E-03
GO:0035513	oxidative RNA demethylation	5	1	7,07E-03
GO:0062028	regulation of stress granule assembly	5	1	7,07E-03
GO:0035247	peptidyl-arginine omega-N-methylation	5	1	7,07E-03
GO:0150099	neuron-glial cell signaling	5	1	7,07E-03
GO:0061092	positive regulation of phospholipid translocation	5	1	7,07E-03
GO:0006974	cellular response to DNA damage stimulus	670	4	7,62E-03
GO:0007093	mitotic cell cycle checkpoint	110	2	7,70E-03
GO:0006307	DNA dealkylation involved in DNA repair	6	1	8,24E-03
GO:0106354	tRNA surveillance	6	1	8,24E-03
GO:0071046	nuclear polyadenylation-dependent ncRNA catabolic process	6	1	8,24E-03
GO:0071038	nuclear polyadenylation-dependent tRNA catabolic process	6	1	8,24E-03
GO:0071035	nuclear polyadenylation-dependent rRNA catabolic process	6	1	8,24E-03
GO:0071029	nuclear ncRNA surveillance	6	1	8,24E-03
GO:0035246	peptidyl-arginine N-methylation	6	1	8,24E-03
GO:0061091	regulation of phospholipid translocation	6	1	8,24E-03
GO:0006996	organelle organization	3178	9	8,38E-03
GO:0040008	regulation of growth	699	4	8,81E-03
GO:0048583	regulation of response to stimulus	3899	0	9,26E-03
GO:0032808	lacrimal gland development	7	1	9,41E-03
GO:0032790	ribosome disassembly	7	1	9,41E-03
GO:0071051	polyadenylation-dependent snoRNA 3'-end processing	7	1	9,41E-03
GO:0043634	polyadenylation-dependent ncRNA catabolic process	7	1	9,41E-03
GO:0035511	oxidative DNA demethylation	7	1	9,41E-03
GO:0010212	response to ionizing radiation	126	2	9,95E-03

Supplementary Table 4. DEGs (p<0.01) in the neuronal population of oxaliplatin-treated (OXA) mice. log_2FC: log_2 fold expression differences value, reported as maximum likelihood estimate. A negative log_2FC means that a gene is down-regulated in the OXA group. A positive log_2FC means that a gene is up-regulated in the OXA group. p: p value (non-adjusted). p-val-adj: p value adjusted for multiple comparisons. DEGs are ordered by significance.

Gene	log_2FC	p	p-val-adj
Gm5734	7,6	8,0E-13	1,5E-08
Klk5	4,6	2,0E-06	0,0188
Lxn	1,5	3,7E-06	0,0227
Nnat	2,5	2,1E-05	0,0955
Smyd3	1,6	0,0001	0,3806
Eml1	0,9	0,0002	0,5048
9130204L05Rik	4,7	0,0002	0,5048
Fli1	3,9	0,0002	0,5048
Ifi47	4,2	0,0003	0,5048
Gm7967	3,7	0,0003	0,5048
Agtr1a	4,9	0,0003	0,5048
Slitrk1	2,8	0,0004	0,5048
Ccl7	4,9	0,0004	0,5048
Scg2	-1,1	0,0004	0,5048
Aldoc	0,9	0,0004	0,5048
Golga7b	1,1	0,0005	0,5490
Avil	0,8	0,0005	0,5490
Eno1	0,7	0,0006	0,5490
Slc16a12	6,6	0,0006	0,5490
Arpc1b	1,1	0,0007	0,5490
Otoa	3,8	0,0007	0,5490
Ctxn3	1,5	0,0007	0,5490
Plxnc1	1,1	0,0007	0,5490
Gm29968	-1,9	0,0007	0,5490
Gm32633	2,7	0,0009	0,6423
Gm45052	2,6	0,0009	0,6674
Plau	2,9	0,0011	0,6675
Tmem233	1,6	0,0011	0,6675
Srgn	2,6	0,0012	0,6675
Gm15486	3,9	0,0012	0,6675
Pls3	-0,6	0,0012	0,6675
Gm47817	2,3	0,0012	0,6675

Gene	log_2FC	p	p-val-adj
Rtl4	3,1	0,0012	0,6675
Smim5	2,4	0,0012	0,6675
Mab21l1	4,7	0,0013	0,6675
Rfx4	4	0,0014	0,7121
Acta2	2,3	0,0015	0,7455
Pcsk2	0,9	0,0016	0,7455
D630045J12Rik	-1,5	0,0016	0,7455
Mrgprb5	5,2	0,0016	0,7455
Adgrf5	2,8	0,0017	0,7455
Telo2	1,6	0,0017	0,7455
Mfsd9	1,6	0,0017	0,7455
Adra2b	1,8	0,0018	0,7455
Pcdhb7	-2,8	0,0019	0,7455
Kcnj11	2	0,0019	0,7455
Kcnip2	1,2	0,0019	0,7455
Slc9a3r2	1,7	0,0019	0,7455
Rgs16	-0,4	0,0020	0,7461
Cops2	-0,5	0,0022	0,8016
Iqce	1,7	0,0023	0,8189
Ranbp3	1,4	0,0024	0,8342
Hsph1	-0,7	0,0025	0,8342
Gm44744	2,8	0,0025	0,8342
Ptrh1	1,8	0,0025	0,8342
Gpc3	2,6	0,0026	0,8342
Lyz2	5,6	0,0027	0,8342
mt-Tp	-0,9	0,0027	0,8342
C920021L13Rik	1,7	0,0027	0,8342
Nupr1	5,7	0,0027	0,8342
Nt5e	2,2	0,0028	0,8359
Ptges3	-0,5	0,0028	0,8359
Gm26532	2,2	0,0029	0,8359
Gm27042	-2	0,0030	0,8359

Gene	log_2FC	p	p-val-adj
C130073E24Rik	1,9	0,0030	0,8359
Gm48585	2	0,0030	0,8359
Phf7	-2,3	0,0031	0,8359
Marcks	-0,9	0,0032	0,8359
Ncs1	0,7	0,0032	0,8359
Serpinb5	1,9	0,0032	0,8359
Mrgprc1-ps	0,9	0,0032	0,8359
St6gal2	2,3	0,0033	0,8396
Cope	0,7	0,0034	0,8396
Ncln	1,3	0,0034	0,8396
Pcdh19	2,7	0,0034	0,8396
Slc14a1	1,9	0,0035	0,8396
Crip2	0,9	0,0036	0,8396
Gpr179	2,5	0,0036	0,8396
Hmgn5	-1,8	0,0036	0,8396
Cd82	1,5	0,0037	0,8396
Pogk	-1,1	0,0037	0,8396
Nlrx1	1,8	0,0037	0,8396
Mov10l1	1,6	0,0038	0,8396
Cited1	3,3	0,0038	0,8396
Eif4a2	-0,4	0,0038	0,8396
Gm6994	1,6	0,0039	0,8422
Uchl1	0,7	0,0040	0,8422
Nxpe5	2,9	0,0040	0,8422
Gm45222	2,2	0,0041	0,8493
Gm6257	1,8	0,0041	0,8493
Isg20	2,4	0,0042	0,8560
Gm49883	-2,4	0,0042	0,8560
Fyb2	2	0,0043	0,8635
Plpp7	2,2	0,0045	0,8816
Gm14236	1,5	0,0046	0,8972
Cd55	1,3	0,0047	0,9012
Cfl1	0,6	0,0048	0,9096
Zfp52	-1,2	0,0049	0,9096
Aif1	2,8	0,0049	0,9096
Carhsp1	1,2	0,0049	0,9096
Acbd4	1,1	0,0050	0,9096
Shcbp1l	2,1	0,0050	0,9096

Gene	log_2FC	p	p-val-adj
Rbbp8	1,4	0,0051	0,9219
Ifi27l2a	1,9	0,0052	0,9283
Ofd1	1,6	0,0053	0,9283
Gm45941	1,8	0,0053	0,9283
Npy5r	-0,3	0,0054	0,9283
Haghl	1,6	0,0054	0,9325
Pcdhb11	2	0,0055	0,9336
Dnajb4	-0,8	0,0056	0,9336
Aprt	0,9	0,0056	0,9336
Hnrnph2	-0,5	0,0057	0,9382
Akt1s1	1,7	0,0057	0,9382
Xlr3b	3,7	0,0059	0,9523
Gnao1	0,6	0,0059	0,9562
Pgr	-2,8	0,0060	0,9562
Fam114a1	1,5	0,0061	0,9562
Gpx4	0,7	0,0061	0,9562
Ppp1r3b	0,4	0,0063	0,9784
Pln	1,8	0,0063	0,9784
Cxcl1	2,6	0,0064	0,9856
Klhl5	1,3	0,0065	0,9856
Gm21284	3,1	0,0065	0,9856
Tubb3	0,7	0,0067	0,9960
Cd24a	0,6	0,0067	0,9991
Hip1	-0,8	0,0068	1,0000
Fam83h	1,8	0,0072	1,0000
Ipcef1	-2,3	0,0072	1,0000
Dok4	0,8	0,0073	1,0000
Frzb	2	0,0073	1,0000
Rabep1	-0,6	0,0073	1,0000
3222401L13Rik	1,7	0,0076	1,0000
Smpx	0,2	0,0076	1,0000
6530409C15Rik	1,8	0,0076	1,0000
Ldlrad4	2,2	0,0077	1,0000
Aldoa	0,4	0,0078	1,0000
Rcn1	-1,6	0,0079	1,0000
AA414768	-2	0,0079	1,0000
Gm40557	0,5	0,0079	1,0000
Hsp90aa1	-0,4	0,0080	1,0000

Gene	log_2FC	p	p-val-adj
Tmed1	1,4	0,0082	1,0000
Ctdsp1	1,5	0,0084	1,0000
Hs6st2	1,4	0,0084	1,0000
Ccdc192	2,1	0,0084	1,0000
Gm13293	-1,9	0,0088	1,0000
Gm29946	0,4	0,0088	1,0000
Ccdc82	-0,7	0,0088	1,0000
Gm38042	2,2	0,0089	1,0000
Mdh2	0,7	0,0089	1,0000
Smim11	-0,7	0,0089	1,0000
Cbln1	0,4	0,0091	1,0000
Slc25a4	0,5	0,0093	1,0000

Gene	log_2FC	p	p-val-adj
Gm18349	6,8	0,0093	1,0000
2610307P16Rik	1,6	0,0093	1,0000
Cav1	5,9	0,0094	1,0000
Trpv1	-1,4	0,0095	1,0000
Gm26594	-2	0,0095	1,0000
Cystm1	0,7	0,0096	1,0000
Syt5	1,6	0,0099	1,0000
Xrcc1	1,5	0,0111	1,0000
Spred1	-0,8	0,0161	1,0000
Npm1	-0,4	0,0352	1,0000
Mif	0,7	0,0422	1,0000

Supplementary Table 5. DEGs (p<0.01) in the SGC population of the oxaliplatin-treated (OXA) mice. log_2FC: log_2 fold expression differences value, reported as maximum likelihood estimate. A negative log_2FC means that a gene is down-regulated in the OXA group. A positive log_2FC means that a gene is up-regulated in the OXA group. p: p value (non-adjusted). p-val-adj: p value adjusted for multiple comparisons. DEGs are ordered by significance.

Gene	log_2FC	p	p-val-adj
Mttp	6,7	3,3E-08	0,0003
Etohd2	5,8	8,2E-08	0,0003
Golm1	6,1	9,3E-08	0,0003
Gm44220	-6,4	1,3E-07	0,0003
Rab23	6,3	5,9E-07	0,0012
Kiz	-5,9	9,0E-07	0,0015
Pkp4	5,5	1,2E-06	0,0017
Tesk2	-5,5	1,6E-06	0,0018
Aasdh	-5,7	1,6E-06	0,0018
Gart	-5,2	2,6E-06	0,0024
Neo1	-6,6	2,6E-06	0,0024
Tmeff1	-5,5	3,0E-06	0,0025
Nsmaf	7,1	3,2E-06	0,0025
Syce2	-4,8	3,5E-06	0,0025
B2m	1,1	9,2E-06	0,0063
Ptprb	5,7	1,2E-05	0,0078
Lcmt2	6	1,3E-05	0,0078
Zfp772	-5,3	1,4E-05	0,0081
Dynll2	-5,4	1,8E-05	0,0094
Trmu	-4,9	2,0E-05	0,0100
Kyat3	-5,7	2,1E-05	0,0100
Sema3g	6,4	2,2E-05	0,0100
Rassf3	5,4	4,9E-05	0,0216
Tgtp2	6,2	5,8E-05	0,0244
Slc25a32	6	6,2E-05	0,0252
Nova1	-3,9	9,2E-05	0,0359
Setx	-6,5	9,6E-05	0,0364
Pcdh1	-4,4	0,0001	0,0375
4933412E12Rik	-5,5	0,0002	0,0677
Abca7	-3,7	0,0002	0,0677
Zfp467	-5,4	0,0002	0,0709
Gm14399	-5,6	0,0002	0,0755

Gene	log_2FC	p	p-val-adj
A730049H05Rik	7,2	0,0003	0,0805
Cyp4v3	-5,5	0,0003	0,0805
Ttl	-5,2	0,0003	0,0847
Tmem248	5,7	0,0003	0,0941
Gm38162	-5,5	0,0004	0,0978
Gm42047	4,7	0,0004	0,0978
Dgka	-5,5	0,0004	0,0978
Tango6	-4,4	0,0004	0,0978
Pgrmc2	7,2	0,0004	0,0978
Pold1	4,7	0,0004	0,1028
Ttc30b	-5,7	0,0005	0,1133
Dock2	6	0,0005	0,1133
Ccdc138	6,1	0,0005	0,1178
Zfp773	-5,5	0,0006	0,1253
Iigp1	8,4	0,0006	0,1391
Gm10509	-4,8	0,0007	0,1467
Tgfa	5,8	0,0007	0,1467
Zfp236	-5,3	0,0008	0,1568
Prrc1	-3,2	0,0008	0,1641
Rnf11	-6,2	0,0008	0,1644
1600020E01Rik	6,6	0,0009	0,1720
Syt4	-4,3	0,0009	0,1720
Nqo2	-7	0,0009	0,1756
Otulin	-5	0,0010	0,1845
Nat9	-5,5	0,0012	0,2129
Rnf114	-5,2	0,0013	0,2172
Hmbox1	-5,1	0,0013	0,2172
Zrsr2	5,5	0,0013	0,2245
Caprin2	6,2	0,0013	0,2245
Chmp4c	-5,4	0,0014	0,2298
Carf	-6,7	0,0015	0,2411
Mettl15	-5,2	0,0015	0,2425

Gene	log_2FC	p	p-val-adj
Rnpc3	-5,7	0,0016	0,2434
Yipf6	-8	0,0017	0,2587
9930017N22Rik	-5,1	0,0017	0,2587
Prpf19	5	0,0017	0,2608
Gm9968	-6	0,0018	0,2638
Mdm2	6	0,0018	0,2645
Gm47702	6,7	0,0019	0,2682
Lurap1	6,3	0,0019	0,2682
Ppp1r1c	-5,6	0,0019	0,2682
Lcor	6,3	0,0020	0,2682
Lacc1	6,5	0,0020	0,2682
Rbm33	-5,8	0,0020	0,2748
Itih3	-5,8	0,0021	0,2753
Pvr	-6,5	0,0022	0,2837
Orc2	5,9	0,0023	0,2942
Alas1	-5,2	0,0023	0,2960
Slc20a2	5,4	0,0024	0,2960
Prickle2	6,1	0,0025	0,3051
Pald1	6,9	0,0026	0,3176
Zfp90	-4,7	0,0027	0,3238
Dhx35	-5,3	0,0027	0,3283
Gpnmb	-6,1	0,0028	0,3283
Adam15	-3,9	0,0029	0,3345
Nsmf	5,3	0,0029	0,3397
Cutc	6	0,0031	0,3508
Mir22hg	5,8	0,0033	0,3688
Zfp729a	-5,5	0,0033	0,3688
Tbl2	-5,1	0,0033	0,3688
Gm47917	5,9	0,0034	0,3688
Fmn2	-5,6	0,0034	0,3688
Erlin1	5,7	0,0035	0,3737
Cdk11b	2	0,0037	0,3917
Chd7	-5,7	0,0038	0,4020
Pdp2	2,2	0,0039	0,4020
Gm15764	-4,9	0,0039	0,4020
Dcaf12	-6,4	0,0039	0,4020
Efhd2	6,2	0,0041	0,4145
Tgfbr1	6,1	0,0042	0,4188

Gene	log_2FC	p	p-val-adj
Sptlc1	7,2	0,0043	0,4198
Itpr2	-4,9	0,0043	0,4198
U2af2	4,4	0,0043	0,4219
Hunk	-5,4	0,0044	0,4231
1810014B01Rik	-5,6	0,0044	0,4231
Trappc6b	-5,9	0,0046	0,4365
Hapln1	-6	0,0047	0,4367
Rnase4	5,9	0,0048	0,4367
Tmem106a	5,6	0,0048	0,4367
Asah2	-4,9	0,0049	0,4367
Oxsr1	-6,5	0,0049	0,4367
Vps52	-5,2	0,0049	0,4367
Slc35f5	6,7	0,0049	0,4367
Cd274	6,5	0,0051	0,4430
Tomm40l	-4,4	0,0051	0,4430
Tep1	-5,1	0,0052	0,4430
C130051F05Rik	5,9	0,0052	0,4430
Sec23a	-6,5	0,0053	0,4430
Setd3	6,9	0,0053	0,4430
Gxylt1	-6,3	0,0053	0,4430
Hint3	-6,1	0,0054	0,4469
Gbp5	5,5	0,0054	0,4469
Nudt19	-5,9	0,0055	0,4491
2610044O15Rik8	-6	0,0058	0,4676
Rraga	4,7	0,0058	0,4676
Ltbr	5,4	0,0059	0,4726
Zmat1	-7,2	0,0061	0,4805
Ascc2	-5,7	0,0062	0,4845
Phlpp2	5,8	0,0062	0,4845
Pdik1l	-6	0,0064	0,4912
Auh	-5,8	0,0065	0,4952
Pik3c3	-6	0,0065	0,4957
Gnl1	-4,1	0,0066	0,4977
Hspb1	6,2	0,0068	0,5070
Sema6d	5,9	0,0068	0,5070
E130311K13Rik	-5,1	0,0071	0,5203
D330050G23Rik	-5,4	0,0071	0,5203
Cyld	5,7	0,0072	0,5203

Gene	log_2FC	p	p-val-adj
Dnm3	5,2	0,0072	0,5203
Arfgef2	-5,6	0,0072	0,5203
Srpk3	5,1	0,0073	0,5210
Elp3	5,7	0,0075	0,5272
Mkks	-5,7	0,0075	0,5272
Ndn	-5,2	0,0076	0,5274
Pex11b	5,7	0,0077	0,5274
Gm10226	-3,9	0,0078	0,5274
Tyk2	5,1	0,0078	0,5274
B230219D22Rik	7,2	0,0078	0,5274
Acad8	-7,9	0,0078	0,5274
Men1	5,2	0,0079	0,5281
Lrrc9	5,6	0,0080	0,5331
Ints7	6	0,0081	0,5345
Ino80	-5,9	0,0083	0,5447
Gm37219	-5,7	0,0084	0,5468

Gene	log_2FC	p	p-val-adj
Usp10	5,3	0,0085	0,5546
Fmo5	5,9	0,0089	0,5711
Mvk	6,3	0,0089	0,5711
Tasp1	6,3	0,0090	0,5711
Cd36	6,4	0,0090	0,5711
Fastkd2	6,6	0,0091	0,5711
Slc4a2	-5,6	0,0092	0,5711
Bach2	-5,5	0,0092	0,5711
Ttc4	7,3	0,0092	0,5711
Tnfsf12	-3,6	0,0095	0,5799
Mul1	6,5	0,0095	0,5799
Klhdc3	-4	0,0096	0,5799
Abi3bp	-4,8	0,0096	0,5799
Gm6712	-5,1	0,0098	0,5857
Acot9	-5,4	0,0099	0,5857
BC067074	-5,9	0,0099	0,5857

Supplementary Table 6. GO terms up-regulated (p<0.01) in the neuronal population of oxaliplatin-treated (OXA) mice. Only up-regulated DEGs with p<0.01 were used for the GO analysis. All Terms correspond to the Ontology "Biological Process". N: number of genes that have been described for the corresponding term in the genome of reference (*Mus Musculus*). UP: number of genes related with the specific term that are up-regulated in our study. p: p-value (non-adjusted) of the corresponding term in our study. GO Terms are ordered by significance.

Term ID	Term Name	N	UP	p
GO:0030042	actin filament depolymerization	21	3	1,86E-04
GO:0006096	glycolytic process	30	3	4,85E-04
GO:0046031	ADP metabolic process	31	3	5,30E-04
GO:0006757	ATP generation from ADP	31	3	5,30E-04
GO:0009135	purine nucleoside diphosphate metabolic process	31	3	5,30E-04
GO:0009179	purine ribonucleoside diphosphate metabolic process	31	3	5,30E-04
GO:0009185	ribonucleoside diphosphate metabolic process	31	3	5,30E-04
GO:0046939	nucleotide phosphorylation	35	3	7,38E-04
GO:0006165	nucleoside diphosphate phosphorylation	35	3	7,38E-04
GO:0008154	actin polymerization or depolymerization	85	4	8,03E-04
GO:0009132	nucleoside diphosphate metabolic process	41	3	1,13E-03
GO:0051261	protein depolymerization	42	3	1,21E-03
GO:0043254	regulation of protein-containing complex assembly	96	4	1,24E-03
GO:0001933	negative regulation of protein phosphorylation	50	3	1,95E-03
GO:0007015	actin filament organization	186	5	2,02E-03
GO:0043624	cellular protein complex disassembly	51	3	2,05E-03
GO:0016052	carbohydrate catabolic process	51	3	2,05E-03
GO:0042326	negative regulation of phosphorylation	52	3	2,17E-03
GO:0048870	cell motility	301	6	3,18E-03
GO:0051674	localization of cell	301	6	3,18E-03
GO:0031400	negative regulation of protein modification process	62	3	3,49E-03
GO:0045936	negative regulation of phosphate metabolic process	62	3	3,49E-03
GO:0010563	negative regulation of phosphorus metabolic process	62	3	3,49E-03
GO:0006091	generation of precursor metabolites and energy	129	4	3,51E-03
GO:0005975	carbohydrate metabolic process	142	4	4,88E-03
GO:0032984	protein-containing complex disassembly	72	3	5,21E-03
GO:0030833	regulation of actin filament polymerization	73	3	5,41E-03
GO:0023051	regulation of signaling	828	10	5,75E-03
GO:0010646	regulation of cell communication	828	10	5,75E-03
GO:0008064	regulation of actin polymerization or depolymerization	75	3	5,81E-03
GO:0030832	regulation of actin filament length	75	3	5,81E-03

Term ID	Term Name	N	UP	p
GO:0046034	ATP metabolic process	76	3	6,02E-03
GO:0009150	purine ribonucleotide metabolic process	154	4	6,44E-03
GO:0030041	actin filament polymerization	79	3	6,68E-03
GO:0032271	regulation of protein polymerization	80	3	6,90E-03
GO:0009259	ribonucleotide metabolic process	160	4	7,33E-03
GO:0044087	regulation of cellular component biogenesis	161	4	7,48E-03
GO:0110053	regulation of actin filament organization	83	3	7,61E-03
GO:0016477	cell migration	261	5	8,20E-03
GO:0072657	protein localization to membrane	167	4	8,46E-03
GO:0019693	ribose phosphate metabolic process	169	4	8,81E-03
GO:0030036	actin cytoskeleton organization	268	5	9,11E-03
GO:0006163	purine nucleotide metabolic process	173	4	9,52E-03
GO:0030837	negative regulation of actin filament polymerization	30	2	9,75E-03
GO:0007010	cytoskeleton organization	628	8	9,81E-03

Supplementary Table 7. GO terms down-regulated (p<0.01) in the neuronal population of oxaliplatin-treated (OXA) mice. Only down-regulated DEGs with p<0.01 were used for the GO analysis. All Terms correspond to the Ontology "Biological Process". N: number of genes that have been described for the corresponding term in the genome of reference (*Mus Musculus*). DOWN: number of genes related with the specific term that are down-regulated in our study. p: p-value (non-adjusted) of the corresponding term in our study. GO Terms are ordered by significance.

Term ID	Term Name	N	DOWN	p
GO:0051085	chaperone cofactor-dependent protein refolding	33	3	1.02E-05
GO:0035966	response to topologically incorrect protein	128	2	1.03E-02
GO:2000586	regulation of platelet-derived growth factor receptor-beta signaling pathway	8	1	1.06E-02
GO:0050955	thermoception	8	1	1.06E-02
GO:0032229	negative regulation of synaptic transmission, GABAergic	8	1	1.06E-02
GO:1901299	negative regulation of hydrogen peroxide-mediated programmed cell death	8	1	1.06E-02
GO:0032049	cardiolipin biosynthetic process	8	1	1.06E-02
GO:0006655	phosphatidylglycerol biosynthetic process	9	1	1.18E-02
GO:0014050	negative regulation of glutamate secretion	9	1	1.18E-02
GO:0050847	progesterone receptor signaling pathway	9	1	1.18E-02
GO:0031649	heat generation	9	1	1.18E-02
GO:0051133	regulation of NK T cell activation	9	1	1.18E-02
GO:1903748	negative regulation of establishment of protein localization to mitochondrion	9	1	1.18E-02
GO:0032103	positive regulation of response to external stimulus	403	3	1.18E-02
GO:0030518	intracellular steroid hormone receptor signaling pathway	42	2	1.23E-03
GO:0022602	ovulation cycle process	42	2	1.23E-03
GO:0014047	glutamate secretion	10	1	1.29E-02
GO:0050821	protein stabilization	181	3	1.30E-03
GO:0006458	'de novo' protein folding	38	3	1.51E-05
GO:0051084	'de novo' posttranslational protein folding	38	3	1.51E-05
GO:0045429	positive regulation of nitric oxide biosynthetic process	47	2	1.52E-03
GO:0043401	steroid hormone mediated signaling pathway	47	2	1.52E-03
GO:0051972	regulation of telomerase activity	48	2	1.59E-03
GO:1904407	positive regulation of nitric oxide metabolic process	48	2	1.59E-03
GO:0007004	telomere maintenance via telomerase	14	2	1.59E-04
GO:0006278	RNA-dependent DNA biosynthetic process	14	2	1.59E-04
GO:0034605	cellular response to heat	50	2	1.72E-03
GO:1904036	negative regulation of epithelial cell apoptotic process	54	2	1.99E-03
GO:0019219	regulation of nucleobase-containing compound metabolic process	3704	11	2.00E-03
GO:1905323	telomerase holoenzyme complex assembly	4	2	2.01E-05
GO:0042698	ovulation cycle	55	2	2.06E-03

Term ID	Term Name	N	DOWN	p
GO:0042981	regulation of apoptotic process	1468	8	2.10E-04
GO:0051131	chaperone-mediated protein complex assembly	17	2	2.27E-04
GO:1901594	response to capsazepine	1	1	2.36E-03
GO:1904709	negative regulation of granulosa cell apoptotic process	1	1	2.36E-03
GO:1900260	negative regulation of RNA-directed 5'-3' RNA polymerase activity	1	1	2.36E-03
GO:1900259	regulation of RNA-directed 5'-3' RNA polymerase activity	1	1	2.36E-03
GO:0071897	DNA biosynthetic process	60	2	2.43E-03
GO:0051017	actin filament bundle assembly	60	2	2.43E-03
GO:0043067	regulation of programmed cell death	1504	8	2.48E-04
GO:0048286	lung alveolus development	62	2	2.59E-03
GO:1903428	positive regulation of reactive oxygen species biosynthetic process	62	2	2.59E-03
GO:0061572	actin filament bundle organization	63	2	2.67E-03
GO:0045428	regulation of nitric oxide biosynthetic process	68	2	3.08E-03
GO:0080164	regulation of nitric oxide metabolic process	70	2	3.26E-03
GO:0010833	telomere maintenance via telomere lengthening	21	2	3.34E-04
GO:0006457	protein folding	154	4	3.38E-05
GO:0000723	telomere maintenance	73	2	3.53E-03
GO:0007015	actin filament organization	259	3	3.54E-03
GO:0090212	negative regulation of establishment of blood-brain barrier	2	1	3.54E-03
GO:2000573	positive regulation of DNA biosynthetic process	74	2	3.62E-03
GO:0032200	telomere organization	74	2	3.62E-03
GO:0043279	response to alkaloid	79	2	4.10E-03
GO:0061077	chaperone-mediated protein folding	55	3	4.32E-05
GO:0060454	positive regulation of gastric acid secretion	3	1	4.72E-03
GO:0045585	positive regulation of cytotoxic T cell differentiation	3	1	4.72E-03
GO:0045583	regulation of cytotoxic T cell differentiation	3	1	4.72E-03
GO:0060112	generation of ovulation cycle rhythm	3	1	4.72E-03
GO:2000588	positive regulation of platelet-derived growth factor receptor-beta signaling pathway	3	1	4.72E-03
GO:0050968	detection of chemical stimulus involved in sensory perception of pain	3	1	4.72E-03
GO:1904708	regulation of granulosa cell apoptotic process	3	1	4.72E-03
GO:0060748	tertiary branching involved in mammary gland duct morphogenesis	3	1	4.72E-03
GO:0031647	regulation of protein stability	292	3	4.93E-03
GO:0030522	intracellular receptor signaling pathway	88	2	5.04E-03
GO:0009408	response to heat	91	2	5.37E-03
GO:0071383	cellular response to steroid hormone stimulus	93	2	5.60E-03
GO:0009755	hormone-mediated signaling pathway	93	2	5.60E-03
GO:0060083	smooth muscle contraction involved in micturition	4	1	5.89E-03
GO:0045040	protein insertion into mitochondrial outer membrane	4	1	5.89E-03

Term ID	Term Name	N	DOWN	p
GO:0090210	regulation of establishment of blood-brain barrier	4	1	5.89E-03
GO:0050960	detection of temperature stimulus involved in thermoception	4	1	5.89E-03
GO:0042921	glucocorticoid receptor signaling pathway	4	1	5.89E-03
GO:0042637	catagen	4	1	5.89E-03
GO:1903751	negative regulation of intrinsic apoptotic signaling pathway in response to hydrogen peroxide	4	1	5.89E-03
GO:1903750	regulation of intrinsic apoptotic signaling pathway in response to hydrogen peroxide	4	1	5.89E-03
GO:1904035	regulation of epithelial cell apoptotic process	96	2	5.95E-03
GO:0010556	regulation of macromolecule biosynthetic process	3668	10	6.66E-03
GO:0006986	response to unfolded protein	104	2	6.92E-03
GO:0019233	sensory perception of pain	105	2	7.05E-03
GO:0007008	outer mitochondrial membrane organization	5	1	7.07E-03
GO:0001660	fever generation	5	1	7.07E-03
GO:0031958	corticosteroid receptor signaling pathway	5	1	7.07E-03
GO:0010641	positive regulation of platelet-derived growth factor receptor signaling pathway	5	1	7.07E-03
GO:0060548	negative regulation of cell death	1061	5	7.42E-03
GO:1903426	regulation of reactive oxygen species biosynthetic process	108	2	7.44E-03
GO:2000379	positive regulation of reactive oxygen species metabolic process	110	2	7.70E-03
GO:0051973	positive regulation of telomerase activity	33	2	7.79E-04
GO:0010941	regulation of cell death	1667	9	7.98E-05
GO:0045345	positive regulation of MHC class I biosynthetic process	6	1	8.24E-03
GO:0002865	negative regulation of acute inflammatory response to antigenic stimulus	6	1	8.24E-03
GO:1902949	positive regulation of tau-protein kinase activity	6	1	8.24E-03
GO:2000278	regulation of DNA biosynthetic process	118	2	8.79E-03
GO:0043085	positive regulation of catalytic activity	1106	5	8.80E-03
GO:0031326	regulation of cellular biosynthetic process	3833	10	9.11E-03
GO:0045343	regulation of MHC class I biosynthetic process	7	1	9.41E-03
GO:0038001	paracrine signaling	7	1	9.41E-03
GO:0051135	positive regulation of NK T cell activation	7	1	9.41E-03
GO:1903753	negative regulation of p38MAPK cascade	7	1	9.41E-03
GO:0060745	mammary gland branching involved in pregnancy	7	1	9.41E-03
GO:0071407	cellular response to organic cyclic compound	377	3	9.88E-03

Supplementary Table 8. Up-regulated DEGs in cisplatin-treated (CDDP) neuronal cultures at 7 days post-treatment (p-val-adj<0.05). DEGs are ordered by significance.

Gene	Log_2FC	p	p-val-adj
Pmaip1	2,2603	4,4E-22	6,0E-18
Pm20d1	4,6324	3,5E-16	5,3E-13
Ccnd2	1,5856	3,0E-14	2,4E-11
Plcd4	3,0581	1,6E-13	1,1E-10
Igdcc4	2,2773	3,3E-13	2,0E-10
Dcxr	2,4391	3,1E-12	1,5E-09
Dmpk	1,3676	4,3E-11	1,5E-08
1700007K13Rik	3,8592	6,0E-11	1,9E-08
Cdkn1a	1,6175	1,6E-10	4,4E-08
Notch3	1,9713	1,8E-10	4,7E-08
Atp10b	2,0073	2,5E-10	6,3E-08
Tyrp1	3,0819	7,6E-10	1,6E-07
Ano3	1,7552	1,2E-09	2,5E-07
Hmga2	1,9021	1,4E-09	2,8E-07
Gm5424	1,6761	3,4E-09	6,3E-07
Ftl1	1,4669	6,4E-09	1,1E-06
Rprm	2,4562	8,5E-09	1,3E-06
Svop	1,7940	8,9E-09	1,3E-06
Exoc4	1,3445	1,3E-08	1,8E-06
Btg2	1,6020	1,6E-08	2,1E-06
Abcg1	1,9552	3,5E-08	3,9E-06
Ckmt1	2,2281	5,8E-08	6,4E-06
Tshr	3,0112	7,1E-08	7,5E-06
Ccnd1	1,1439	1,1E-07	1,2E-05
Kcnc3	1,5602	1,4E-07	1,4E-05
Slc2a9	2,1291	3,9E-07	3,5E-05
A330023F24Rik	1,4824	3,9E-07	3,5E-05
Ecm1	1,2458	4,1E-07	3,6E-05
Alox5	3,8838	4,3E-07	3,7E-05
Apod	1,0201	4,7E-07	4,0E-05
Klhdc7a	3,3261	6,8E-07	0,0001
Tnfrsf10b	1,8135	7,5E-07	0,0001
Dusp15	1,4574	1,7E-06	0,0001
Mdk	1,5728	1,8E-06	0,0001
1700003M07Rik	5,4431	2,2E-06	0,0002

Gene	Log_2FC	p	p-val-adj
Podn	2,4530	2,2E-06	0,0002
Aen	1,1130	3,1E-06	0,0002
9530053A07Rik	1,8180	3,5E-06	0,0002
Gpx3	1,5555	3,7E-06	0,0002
Fam214a	1,2793	3,9E-06	0,0002
Ces2g	2,5741	4,5E-06	0,0003
Perp	1,8295	4,7E-06	0,0003
Gzmb	1,5831	5,2E-06	0,0003
Btbd19	2,1141	5,5E-06	0,0003
Adamtsl4	1,4697	8,3E-06	0,0005
Celf5	2,9467	9,8E-06	0,0006
Pqlc3	1,1584	1,1E-05	0,0006
Mmrn2	2,4738	1,5E-05	0,0008
Frrs1	1,6708	1,5E-05	0,0008
Ercc5	1,1129	1,6E-05	0,0008
Insyn2a	1,9970	2,7E-05	0,0013
Dusp4	1,0773	3,2E-05	0,0015
Pvt1	1,2207	3,6E-05	0,0017
Hs3st4	4,5926	4,7E-05	0,0021
Icam1	1,5141	4,9E-05	0,0022
Lacc1	1,1248	0,0001	0,0030
Sesn2	1,2004	0,0001	0,0031
Thyn1	1,5451	0,0001	0,0031
Smco3	1,5706	0,0001	0,0031
Ccn2	1,0428	0,0001	0,0032
Cgref1	1,0047	0,0001	0,0032
Gm2225	1,4183	0,0001	0,0038
Mapkapk3	1,2766	0,0001	0,0040
Ass1	1,3617	0,0001	0,0040
Rps17	1,0032	0,0001	0,0041
Tmem255a	1,3095	0,0001	0,0044
Rpl31-ps9	1,2850	0,0001	0,0047
Aldh4a1	1,1590	0,0001	0,0048
Espn	2,1407	0,0001	0,0051
Gm12191	1,0289	0,0002	0,0055

Gene	Log_2FC	p	p-val-adj
Dkk3	1,3179	0,0002	0,0059
Gm5453	1,2284	0,0002	0,0059
Cpz	4,2422	0,0002	0,0067
Gm6030	1,5088	0,0002	0,0069
Gm7226	2,2133	0,0003	0,0082
Ptp4a3	1,0068	0,0003	0,0088
Gm4342	1,1154	0,0003	0,0090
Ltbp2	1,4899	0,0003	0,0090
Acta2	1,0659	0,0003	0,0090
Nipal4	3,0674	0,0003	0,0091
9230114K14Rik	1,4561	0,0003	0,0093
Mgat5b	1,6002	0,0003	0,0098
Pid1	1,1720	0,0003	0,0103
Hmcn2	2,1192	0,0003	0,0106
Zfp612	1,0166	0,0004	0,0113
Gm4963	1,5549	0,0004	0,0113
Rps27l	1,0591	0,0004	0,0113
Dennd2c	1,4078	0,0004	0,0113
Rps9	1,1202	0,0004	0,0114
Npnt	2,2586	0,0004	0,0120
Rpl35a	1,0029	0,0005	0,0138
Cartpt	1,5791	0,0005	0,0148
Cd80	1,4708	0,0005	0,0148
Slc17a8	1,4789	0,0006	0,0158

Gene	Log_2FC	p	p-val-adj
Polr1e	1,4145	0,0006	0,0163
Sh3rf3	1,4530	0,0006	0,0164
Mgmt	2,4368	0,0006	0,0167
Myh11	1,2533	0,0007	0,0175
Gm12002	3,0805	0,0007	0,0176
Aqp4	2,2103	0,0007	0,0183
Wdr72	3,9201	0,0007	0,0189
Rps19-ps3	1,0026	0,0008	0,0197
Cox6b2	2,6604	0,0008	0,0202
Dglucy	1,0578	0,0008	0,0202
Uba52-ps	1,1524	0,0009	0,0218
Pltp	2,7789	0,0009	0,0222
Rplp2	1,0957	0,0009	0,0223
Gm15987	3,6107	0,0010	0,0232
Kcnj4	2,7183	0,0010	0,0236
Pcdhgc5	1,4293	0,0010	0,0244
Rps28	1,4827	0,0011	0,0266
Ptges	1,1717	0,0012	0,0282
Art4	1,7283	0,0019	0,0394
Gm16170	1,7988	0,0019	0,0403
Trp53cor1	1,3833	0,0020	0,0415
Prom2	2,2954	0,0020	0,0416
Ndufb6	1,0366	0,0022	0,0448
Ly6a	2,1472	0,0022	0,0453

Supplementary Table 9. Down-regulated DEGs in cisplatin-treated (CDDP) neuronal cultures at 7 days post-treatment (p-val-adj<0.05). DEGs are ordered by significance.

Gene	Log_2FC	p	p-val-adj
Fndc1	-2,2446	9,9E-21	6,8E-17
Lcn2	-2,5563	1,3E-19	5,9E-16
Ccna2	-2,0659	9,6E-19	3,3E-15
Fst	-1,8126	6,3E-18	1,7E-14
Pdgfb	-2,1704	4,1E-17	9,4E-14
Mki67	-1,9228	1,7E-16	3,4E-13
Frem2	-1,9819	3,1E-16	5,3E-13
Plekha4	-1,5820	5,5E-16	7,5E-13
Plscr2	-1,7787	1,4E-15	1,8E-12
Sfrp5	-2,0335	3,1E-15	3,5E-12
Foxm1	-1,7105	4,2E-15	4,5E-12
Iqgap3	-2,1164	7,4E-15	7,2E-12
Lmnb1	-1,7205	1,5E-14	1,4E-11
Anln	-1,5915	2,5E-14	2,1E-11
Cadm2	-1,4225	3,2E-14	2,4E-11
Gpr37l1	-1,3545	3,6E-14	2,6E-11
Racgap1	-1,8115	2,8E-13	1,8E-10
E2f8	-2,0078	5,7E-13	3,4E-10
Atp1b2	-1,3434	2,0E-12	1,2E-09
Bub1b	-1,8298	2,4E-12	1,3E-09
Hmgcs2	-1,7283	3,0E-12	1,5E-09
Sgo2a	-1,8751	3,0E-12	1,5E-09
Ncapd2	-1,3867	7,4E-12	3,5E-09
Top2a	-1,7359	8,1E-12	3,7E-09
Neurl1b	-1,9521	1,1E-11	4,8E-09
Ect2	-2,2065	1,3E-11	5,4E-09
Cybrd1	-1,3643	1,6E-11	6,4E-09
Uhrf1	-1,5672	1,7E-11	6,9E-09
Col16a1	-1,3567	1,9E-11	7,4E-09
Prr11	-1,5916	2,3E-11	8,6E-09
Islr	-1,6589	2,6E-11	9,7E-09
Ltbp4	-1,3164	3,1E-11	1,1E-08
Col3a1	-1,2513	3,5E-11	1,2E-08
C3	-3,3739	5,7E-11	1,9E-08
Col28a1	-1,2024	6,2E-11	2,0E-08

Gene	Log_2FC	p	p-val-adj
Kif11	-1,9330	7,6E-11	2,4E-08
Cenpe	-1,4494	8,9E-11	2,7E-08
S1pr3	-1,1454	1,1E-10	3,2E-08
Pclaf	-1,5567	1,1E-10	3,2E-08
Nlgn3	-1,4012	1,2E-10	3,3E-08
Pbk	-1,8135	1,2E-10	3,5E-08
Kcna2	-1,0847	1,5E-10	4,2E-08
Cxcl5	-1,5864	1,8E-10	4,7E-08
Pcdh10	-1,1836	2,6E-10	6,3E-08
Rrm2	-1,3143	2,9E-10	7,1E-08
H19	-1,4061	3,2E-10	7,6E-08
E2f7	-1,8885	3,3E-10	7,8E-08
Hspg2	-1,1561	4,8E-10	1,1E-07
Olfml2a	-1,0662	6,0E-10	1,4E-07
Ncapg2	-1,2004	7,2E-10	1,6E-07
Kif20a	-1,6853	7,6E-10	1,6E-07
Tk1	-1,8315	7,5E-10	1,6E-07
Col20a1	-1,6945	1,2E-09	2,5E-07
Plce1	-1,2057	1,4E-09	2,8E-07
Agtr2	-2,2513	1,8E-09	3,6E-07
Hmgb2	-1,4498	2,2E-09	4,3E-07
Atp1a2	-1,2036	2,4E-09	4,6E-07
Egflam	-1,2347	2,8E-09	5,4E-07
Kif4	-1,7445	3,1E-09	5,7E-07
C4b	-1,0429	3,7E-09	6,7E-07
Prc1	-1,5142	3,8E-09	6,7E-07
Aurkb	-1,7898	4,0E-09	6,9E-07
Kif14	-2,0154	5,7E-09	9,9E-07
Tpx2	-1,6130	6,9E-09	1,1E-06
Adam12	-1,6693	7,2E-09	1,2E-06
Birc5	-1,5749	7,2E-09	1,2E-06
Ephb2	-1,0712	7,4E-09	1,2E-06
Nusap1	-1,6669	7,4E-09	1,2E-06
Vcam1	-1,0995	7,6E-09	1,2E-06
Trim59	-1,5063	8,9E-09	1,3E-06

Gene	Log_2FC	p	p-val-adj
Knl1	-1,8503	8,9E-09	1,3E-06
Mis18bp1	-1,7289	9,1E-09	1,3E-06
Srcin1	-1,1599	9,8E-09	1,4E-06
Esco2	-1,7010	1,0E-08	1,5E-06
Col4a1	-1,1020	1,1E-08	1,5E-06
Kif15	-1,5024	1,1E-08	1,6E-06
Spag5	-1,8162	1,2E-08	1,6E-06
Col1a2	-1,0050	1,3E-08	1,8E-06
Phf19	-1,6951	1,4E-08	1,9E-06
Col1a1	-1,2932	1,4E-08	2,0E-06
Incenp	-1,2842	1,6E-08	2,1E-06
Slc43a3	-1,1994	1,6E-08	2,1E-06
Adgra2	-1,0421	1,7E-08	2,2E-06
Cdk1	-1,7407	1,8E-08	2,2E-06
Espl1	-1,5440	1,8E-08	2,2E-06
Kif20b	-1,3886	1,8E-08	2,2E-06
Reck	-1,2407	1,9E-08	2,4E-06
Ppic	-1,1314	2,0E-08	2,4E-06
Crym	-1,3004	2,2E-08	2,6E-06
Kif22	-1,4771	2,3E-08	2,8E-06
Egfl8	-1,3345	2,5E-08	3,0E-06
Kcnh2	-1,6193	2,7E-08	3,2E-06
Cdca3	-1,8656	2,8E-08	3,3E-06
Cdca2	-1,7609	2,8E-08	3,3E-06
Gpam	-1,0616	3,0E-08	3,5E-06
Kif2c	-1,8309	3,1E-08	3,5E-06
Ube2c	-1,6775	3,5E-08	3,9E-06
Cip2a	-1,3875	3,8E-08	4,2E-06
Mrgprf	-1,2667	5,7E-08	6,3E-06
Mxd3	-2,4477	6,0E-08	6,5E-06
Erbb2	-1,3262	6,5E-08	7,1E-06
Robo2	-1,4238	6,6E-08	7,1E-06
Atad2	-1,0870	7,1E-08	7,5E-06
Melk	-1,8307	9,1E-08	9,6E-06
Aldh1l2	-1,2347	1,3E-07	1,3E-05
Vmn1r181	-1,5049	1,3E-07	1,3E-05
Ankle1	-2,1181	1,4E-07	1,4E-05
Slfn9	-1,2313	1,5E-07	1,4E-05

Gene	Log_2FC	p	p-val-adj
C1ra	-1,3781	1,7E-07	1,6E-05
Kif18b	-1,3205	1,7E-07	1,6E-05
Zfp469	-1,2960	1,8E-07	1,7E-05
C4a	-1,1178	2,2E-07	2,1E-05
Ncapg	-1,4820	2,4E-07	2,2E-05
Sapcd2	-2,4765	3,1E-07	2,9E-05
Nuf2	-1,7380	3,2E-07	3,0E-05
Brip1	-1,7625	3,4E-07	3,1E-05
Clspn	-1,4038	3,4E-07	3,1E-05
Lmf2	-1,0725	3,8E-07	3,5E-05
Asf1b	-1,5891	4,0E-07	3,5E-05
Tgm1	-1,9662	4,2E-07	3,7E-05
Cep55	-1,8079	4,2E-07	3,7E-05
Cdc20	-1,6109	4,2E-07	3,7E-05
Mad2l1	-1,1613	4,5E-07	3,8E-05
Ercc6l	-1,5280	5,3E-07	4,4E-05
Prrg1	-1,3365	5,7E-07	4,7E-05
Slc25a10	-1,2980	5,9E-07	4,8E-05
Gm8203	-1,0413	6,0E-07	4,8E-05
Knstrn	-1,4275	6,2E-07	5,0E-05
Metrn	-1,0483	7,1E-07	0,0001
Cdkn2c	-1,2371	8,9E-07	0,0001
Lama5	-1,0607	1,1E-06	0,0001
Fbln5	-1,1263	1,1E-06	0,0001
Kntc1	-1,1506	1,2E-06	0,0001
Tril	-1,2028	1,2E-06	0,0001
Ccnb2	-1,8340	1,3E-06	0,0001
Marveld1	-1,0263	1,3E-06	0,0001
Brca1	-1,1451	1,3E-06	0,0001
Nek2	-1,5720	1,4E-06	0,0001
Fbln7	-1,4689	2,3E-06	0,0002
Lmnb2	-1,1493	2,4E-06	0,0002
Dlgap5	-1,4391	2,6E-06	0,0002
Col11a1	-1,1268	3,0E-06	0,0002
Haspin	-1,7496	3,2E-06	0,0002
E2f2	-2,0406	3,2E-06	0,0002
Tnfrsf1b	-1,0625	3,4E-06	0,0002
Sdk2	-1,5610	3,7E-06	0,0002

Gene	Log_2FC	p	p-val-adj
Adamts20	-1,2155	4,4E-06	0,0003
Cdca8	-1,6865	4,7E-06	0,0003
Pdgfrl	-2,2758	4,8E-06	0,0003
Fam83d	-1,7423	4,9E-06	0,0003
Slc1a5	-1,0544	5,3E-06	0,0003
Neil3	-1,2580	5,4E-06	0,0003
Acod1	-2,1207	5,8E-06	0,0003
Troap	-1,7956	6,5E-06	0,0004
Bub1	-1,2414	6,9E-06	0,0004
Ndc80	-1,4845	7,0E-06	0,0004
Wnt6	-1,6233	7,1E-06	0,0004
Clca3a1	-2,0256	7,8E-06	0,0005
Smtn	-1,1818	9,3E-06	0,0005
Csmd1	-1,0142	1,1E-05	0,0006
Stil	-1,5448	1,2E-05	0,0007
H2afx	-1,3224	1,2E-05	0,0007
Pxylp1	-1,1599	1,3E-05	0,0007
Psmb8	-1,4207	1,4E-05	0,0007
Sdk1	-1,2383	1,6E-05	0,0008
Rtn4rl2	-2,4319	1,7E-05	0,0009
Cdh20	-1,3854	1,7E-05	0,0009
Plk4	-1,1131	1,8E-05	0,0009
C1rb	-1,6537	2,1E-05	0,0011
Chadl	-1,0289	2,4E-05	0,0012
Pcdh11x	-1,5959	2,6E-05	0,0013
Dnaic2	-1,0306	2,6E-05	0,0013
Lig1	-1,0285	2,6E-05	0,0013
Fanca	-1,6132	2,7E-05	0,0013
Dhrs3	-1,0882	3,0E-05	0,0014
Wdr90	-1,2200	3,0E-05	0,0014
Galnt6	-1,0465	3,0E-05	0,0014
Rarb	-1,1045	3,0E-05	0,0014
Tacc3	-1,1937	3,3E-05	0,0016
Spc24	-1,9089	3,3E-05	0,0016
Adamts12	-1,1148	3,5E-05	0,0016
Ska1	-1,8616	3,5E-05	0,0016
Afmid	-1,5219	3,5E-05	0,0016
Fbn2	-1,9679	3,7E-05	0,0017

Gene	Log_2FC	p	p-val-adj
Gm21451	-1,4083	3,7E-05	0,0017
Palld	-1,0470	3,9E-05	0,0018
Sncaip	-3,6817	4,0E-05	0,0018
Prr5l	-1,4927	4,0E-05	0,0018
Ccnb1-ps	-1,7137	4,9E-05	0,0022
Spdl1	-1,4532	0,0001	0,0024
Adamts2	-1,2064	0,0001	0,0024
Mns1	-1,3023	0,0001	0,0024
Atp10a	-1,1084	0,0001	0,0025
Tst	-1,2510	0,0001	0,0025
C1qtnf1	-1,1180	0,0001	0,0025
Tns2	-1,0069	0,0001	0,0025
Dab1	-1,4762	0,0001	0,0026
Cdkn3	-2,0263	0,0001	0,0027
Sgo1	-1,2030	0,0001	0,0030
Ttk	-1,5348	0,0001	0,0031
Cdc25b	-1,4821	0,0001	0,0032
Diaph3	-1,3244	0,0001	0,0033
Fbxo5	-1,2850	0,0001	0,0035
Pik3ap1	-3,2001	0,0001	0,0036
Nxph4	-2,2901	0,0001	0,0037
Atp1a4	-1,8907	0,0001	0,0037
Notch4	-1,1959	0,0001	0,0038
Paqr6	-1,1364	0,0001	0,0039
Foxp2	-1,6680	0,0001	0,0040
Uba7	-1,0215	0,0001	0,0044
Wdr62	-1,2292	0,0001	0,0046
Aldh1a3	-2,0594	0,0001	0,0047
Gbp5	-1,2433	0,0001	0,0048
Igf2	-1,8775	0,0001	0,0048
Cmklr1	-1,4800	0,0001	0,0048
Grid2	-1,3624	0,0001	0,0049
Ticrr	-1,3478	0,0001	0,0051
Gpx7	-1,0155	0,0001	0,0053
Cdca5	-1,5763	0,0002	0,0054
Pif1	-2,1603	0,0002	0,0055
Igfbp4	-1,0910	0,0002	0,0057
Depdc1a	-1,4634	0,0002	0,0067

Gene	Log_2FC	p	p-val-adj
Col4a4	-1,9892	0,0002	0,0068
Lyz2	-1,3441	0,0002	0,0070
Sytl5	-1,7897	0,0002	0,0070
Cenpl	-1,3598	0,0002	0,0072
Dbf4	-1,0445	0,0002	0,0075
Loxl2	-1,0158	0,0002	0,0077
Slc2a13	-1,1258	0,0003	0,0082
Cenpm	-1,9856	0,0003	0,0083
H1f10	-1,3938	0,0003	0,0100
Siglecf	-1,9302	0,0003	0,0103
Kctd12b	-1,2533	0,0003	0,0105
Angpt1	-2,3400	0,0004	0,0110
Fanci	-1,1839	0,0004	0,0113
Gfap	-2,4730	0,0004	0,0113
Eva1b	-1,4360	0,0004	0,0116
Marco	-2,4721	0,0004	0,0116
Cit	-1,0046	0,0004	0,0119
Col6a2	-1,1951	0,0004	0,0123
Hspb6	-1,2962	0,0004	0,0125
Rxrg	-1,0793	0,0005	0,0141
Aspm	-1,9360	0,0005	0,0144
C1ql1	-2,6833	0,0005	0,0144
Parpbp	-1,3623	0,0005	0,0148
Exo1	-1,2747	0,0005	0,0148
Dtl	-1,0612	0,0005	0,0149
Tedc1	-1,0767	0,0006	0,0155
Mamstr	-1,3643	0,0006	0,0165
Pkmyt1	-1,3180	0,0006	0,0167
Hmmr	-2,0187	0,0006	0,0168
Kif18a	-1,4030	0,0007	0,0173
Aurka	-1,1422	0,0007	0,0173
Fancd2	-1,2548	0,0007	0,0175
Zbp1	-1,0787	0,0007	0,0184
Gen1	-1,1308	0,0007	0,0187
Olfm2	-1,1969	0,0007	0,0187

Gene	Log_2FC	p	p-val-adj
Lrp2	-1,6780	0,0008	0,0192
Ppp1r1b	-1,6025	0,0008	0,0193
Arhgef39	-1,6541	0,0008	0,0198
Fgl2	-1,0258	0,0008	0,0199
Inava	-1,1838	0,0008	0,0199
Adgrb2	-1,0025	0,0008	0,0199
Tlr2	-1,3522	0,0008	0,0207
Wwc1	-1,1354	0,0009	0,0208
Ska3	-1,1861	0,0010	0,0232
Fabp7	-1,0421	0,0010	0,0242
Galk1	-1,0369	0,0010	0,0245
Mfap2	-1,1561	0,0012	0,0267
Htra3	-1,2808	0,0012	0,0269
Spata18	-1,1962	0,0012	0,0269
Chtf18	-1,5270	0,0012	0,0273
Cenpf	-2,3173	0,0012	0,0278
4930558J18Rik	-2,8856	0,0013	0,0285
Cenpi	-1,0905	0,0013	0,0287
Fen1	-1,0468	0,0013	0,0289
Haus4	-1,1387	0,0013	0,0297
B130024G19Rik	-1,1741	0,0016	0,0346
Mcm10	-1,1000	0,0016	0,0350
Slc1a2	-1,6258	0,0016	0,0351
Erfe	-1,9784	0,0016	0,0354
Skida1	-1,0998	0,0017	0,0356
Traip	-1,4421	0,0017	0,0369
Sh2d3c	-1,0988	0,0018	0,0377
Kcnmb4	-1,3798	0,0019	0,0393
Oip5	-1,5883	0,0019	0,0398
Slco2a1	-1,5291	0,0019	0,0400
Entpd2	-2,1450	0,0021	0,0433
Epyc	-1,4249	0,0023	0,0462
St8sia2	-1,3394	0,0024	0,0480
Il3ra	-1,0544	0,0024	0,0484

Supplementary Table 10. GO terms up-regulated in cisplatin-treated (CDDP) neuronal cultures at 7 days post-treatment (p<0.01). Only up-regulated DEGs with p-val-adj<0.05 were used for the GO analysis. All Terms correspond to the Ontology "Biological Process". N: number of genes that have been described for the corresponding term in the genome of reference (*Mus Musculus*). UP: number of genes related with the specific term that are up-regulated in our study. p: p-value (non-adjusted) of the corresponding term in our study. FDR: adjusted p-value by FDR method of the corresponding term in our study. Data is ordered by significance.

Term ID	Term Name	N	UP	p	FDR
GO:0072331	signal transduction by p53 class mediator	74	6	1,51E-06	2,37E-02
GO:0072332	intrinsic apoptotic signaling pathway by p53 class mediator	51	5	4,95E-06	3,90E-02
GO:0042771	intrinsic apoptotic signaling pathway in response to DNA damage by p53 class mediator	31	4	1,72E-05	9,01E-02
GO:0031571	mitotic G1 DNA damage checkpoint	18	3	1,06E-04	4,18E-01
GO:0044783	G1 DNA damage checkpoint	19	3	1,23E-04	3,86E-01
GO:0044819	mitotic G1/S transition checkpoint	20	3	1,41E-04	3,69E-01
GO:0042127	regulation of cell population proliferation	1691	19	1,63E-04	3,68E-01
GO:1904996	positive regulation of leukocyte adhesion to vascular endothelial cell	23	3	2,05E-04	4,03E-01
GO:1904994	regulation of leukocyte adhesion to vascular endothelial cell	29	3	3,83E-04	6,70E-01
GO:0030330	DNA damage response, signal transduction by p53 class mediator	31	3	4,59E-04	7,22E-01
GO:0008630	intrinsic apoptotic signaling pathway in response to DNA damage	78	4	4,89E-04	7,00E-01
GO:0106014	regulation of inflammatory response to wounding	6	2	5,36E-04	7,04E-01
GO:0015914	phospholipid transport	81	4	5,60E-04	6,79E-01
GO:0043604	amide biosynthetic process	423	8	6,71E-04	7,54E-01
GO:0002232	leukocyte chemotaxis involved in inflammatory response	7	2	6,87E-04	7,22E-01
GO:0097193	intrinsic apoptotic signaling pathway	155	5	7,40E-04	7,28E-01
GO:0043603	cellular amide metabolic process	665	10	8,30E-04	7,69E-01
GO:0006518	peptide metabolic process	446	8	9,39E-04	8,21E-01
GO:0043269	regulation of ion transport	1370	15	1,13E-03	9,35E-01
GO:0097190	apoptotic signaling pathway	273	6	1,54E-03	1,00E+00
GO:0008284	positive regulation of cell population proliferation	995	12	1,66E-03	1,00E+00
GO:2000379	positive regulation of reactive oxygen species metabolic process	110	4	1,67E-03	1,00E+00
GO:0015748	organophosphate ester transport	110	4	1,67E-03	1,00E+00
GO:0006978	DNA damage response, signal transduction by p53 class mediator resulting in transcription of p21 class mediator	12	2	1,71E-03	1,00E+00
GO:0034375	high-density lipoprotein particle remodeling	12	2	1,71E-03	1,00E+00
GO:2000045	regulation of G1/S transition of mitotic cell cycle	114	4	1,90E-03	1,00E+00
GO:0042772	DNA damage response, signal transduction resulting in transcription	13	2	1,97E-03	1,00E+00
GO:0048523	negative regulation of cellular process	4817	35	2,00E-03	1,00E+00
GO:0042593	glucose homeostasis	198	5	2,12E-03	1,00E+00
GO:0033500	carbohydrate homeostasis	199	5	2,17E-03	1,00E+00

Term ID	Term Name	N	UP	p	FDR
GO:0009064	glutamine family amino acid metabolic process	56	3	2,30E-03	1,00E+00
GO:2000377	regulation of reactive oxygen species metabolic process	206	5	2,51E-03	1,00E+00
GO:0044773	mitotic DNA damage checkpoint	58	3	2,53E-03	1,00E+00
GO:0042770	signal transduction in response to DNA damage	58	3	2,53E-03	1,00E+00
GO:0006412	translation	304	6	2,60E-03	1,00E+00
GO:2000134	negative regulation of G1/S transition of mitotic cell cycle	59	3	2,65E-03	1,00E+00
GO:0010212	response to ionizing radiation	126	4	2,70E-03	1,00E+00
GO:0050679	positive regulation of epithelial cell proliferation	211	5	2,78E-03	1,00E+00
GO:0044774	mitotic DNA integrity checkpoint	61	3	2,90E-03	1,00E+00
GO:0070372	regulation of ERK1 and ERK2 cascade	313	6	3,00E-03	1,00E+00
GO:0006869	lipid transport	316	6	3,14E-03	1,00E+00
GO:1902807	negative regulation of cell cycle G1/S phase transition	63	3	3,17E-03	1,00E+00
GO:0006974	cellular response to DNA damage stimulus	670	9	3,22E-03	1,00E+00
GO:0070374	positive regulation of ERK1 and ERK2 cascade	219	5	3,25E-03	1,00E+00
GO:1902806	regulation of cell cycle G1/S phase transition	133	4	3,26E-03	1,00E+00
GO:0006915	apoptotic process	811	10	3,50E-03	1,00E+00
GO:0021542	dentate gyrus development	18	2	3,51E-03	1,00E+00
GO:0043043	peptide biosynthetic process	325	6	3,59E-03	1,00E+00
GO:0032879	regulation of localization	2837	23	3,78E-03	1,00E+00
GO:2000116	regulation of cysteine-type endopeptidase activity	231	5	4,05E-03	1,00E+00
GO:0006520	cellular amino acid metabolic process	232	5	4,12E-03	1,00E+00
GO:0044321	response to leptin	20	2	4,25E-03	1,00E+00
GO:0000028	ribosomal small subunit assembly	20	2	4,25E-03	1,00E+00
GO:0097186	amelogenesis	20	2	4,25E-03	1,00E+00
GO:2001056	positive regulation of cysteine-type endopeptidase activity	144	4	4,30E-03	1,00E+00
GO:0009411	response to UV	146	4	4,51E-03	1,00E+00
GO:0042274	ribosomal small subunit biogenesis	72	3	4,54E-03	1,00E+00
GO:0000079	regulation of cyclin-dependent protein serine/threonine kinase activity	74	3	4,89E-03	1,00E+00
GO:0012501	programmed cell death	852	10	4,92E-03	1,00E+00
GO:0010875	positive regulation of cholesterol efflux	22	2	5,05E-03	1,00E+00
GO:0002693	positive regulation of cellular extravasation	22	2	5,05E-03	1,00E+00
GO:0010876	lipid localization	352	6	5,25E-03	1,00E+00
GO:0001678	cellular glucose homeostasis	76	3	5,25E-03	1,00E+00
GO:0000082	G1/S transition of mitotic cell cycle	76	3	5,25E-03	1,00E+00
GO:0034369	plasma lipoprotein particle remodeling	23	2	5,47E-03	1,00E+00
GO:0034368	protein-lipid complex remodeling	23	2	5,47E-03	1,00E+00
GO:0050790	regulation of catalytic activity	1887	17	5,56E-03	1,00E+00
GO:0044843	cell cycle G1/S phase transition	78	3	5,63E-03	1,00E+00
GO:1904029	regulation of cyclin-dependent protein kinase activity	78	3	5,63E-03	1,00E+00
GO:0010165	response to X-ray	24	2	5,91E-03	1,00E+00

Term ID	Term Name	N	UP	p	FDR
GO:0002523	leukocyte migration involved in inflammatory response	24	2	5,91E-03	1,00E+00
GO:0006536	glutamate metabolic process	24	2	5,91E-03	1,00E+00
GO:0043648	dicarboxylic acid metabolic process	81	3	6,23E-03	1,00E+00
GO:1901605	alpha-amino acid metabolic process	161	4	6,30E-03	1,00E+00
GO:0034367	protein-containing complex remodeling	25	2	6,36E-03	1,00E+00
GO:0007606	sensory perception of chemical stimulus	1223	0	6,62E-03	1,00E+00
GO:0008219	cell death	891	10	6,67E-03	1,00E+00
GO:0007605	sensory perception of sound	164	4	6,70E-03	1,00E+00
GO:0045737	positive regulation of cyclin-dependent protein serine/threonine kinase activity	26	2	6,83E-03	1,00E+00
GO:1904659	glucose transmembrane transport	26	2	6,83E-03	1,00E+00
GO:0030325	adrenal gland development	26	2	6,83E-03	1,00E+00
GO:0010950	positive regulation of endopeptidase activity	165	4	6,84E-03	1,00E+00
GO:0050678	regulation of epithelial cell proliferation	375	6	7,05E-03	1,00E+00
GO:0044070	regulation of anion transport	902	10	7,24E-03	1,00E+00
GO:0046330	positive regulation of JNK cascade	86	3	7,30E-03	1,00E+00
GO:0008645	hexose transmembrane transport	27	2	7,32E-03	1,00E+00
GO:0030198	extracellular matrix organization	268	5	7,43E-03	1,00E+00
GO:0045229	external encapsulating structure organization	269	5	7,54E-03	1,00E+00
GO:0043062	extracellular structure organization	269	5	7,54E-03	1,00E+00
GO:0010155	regulation of proton transport	28	2	7,82E-03	1,00E+00
GO:0033627	cell adhesion mediated by integrin	28	2	7,82E-03	1,00E+00
GO:0010952	positive regulation of peptidase activity	174	4	8,19E-03	1,00E+00
GO:0045685	regulation of glial cell differentiation	90	3	8,24E-03	1,00E+00
GO:0015749	monosaccharide transmembrane transport	29	2	8,33E-03	1,00E+00
GO:1904031	positive regulation of cyclin-dependent protein kinase activity	29	2	8,33E-03	1,00E+00
GO:0007050	cell cycle arrest	91	3	8,48E-03	1,00E+00
GO:0000077	DNA damage checkpoint	91	3	8,48E-03	1,00E+00
GO:0048519	negative regulation of biological process	5264	35	8,81E-03	1,00E+00
GO:0010189	vitamin E biosynthetic process	1	1	8,85E-03	1,00E+00
GO:0038194	thyroid-stimulating hormone signaling pathway	1	1	8,85E-03	1,00E+00

Supplementary Table 11. GO terms down-regulated in cisplatin-treated (CDDP) neuronal cultures at 7 days post-treatment (p-val-adj(FDR)<0.05). Only down-regulated DEGs with p-val-adj<0.05 were used for the GO analysis. All Terms correspond to the Ontology "Biological Process". N: number of genes that have been described for the corresponding term in the genome of reference (*Mus Musculus*). DOWN: number of genes related with the specific term that are down-regulated in our study. FDR: p-val-adj by FDR method of the corresponding term in our study. Data is ordered by significance.

Term ID	Term name	N	DOWN	FDR
GO:0007049	cell cycle	1219	97	1.53E-43
GO:0000278	mitotic cell cycle	539	66	3.19E-38
GO:0022402	cell cycle process	814	75	1.85E-36
GO:1903047	mitotic cell cycle process	468	60	1.28E-35
GO:0051301	cell division	487	59	8.38E-34
GO:0007059	chromosome segregation	271	46	2.14E-31
GO:0000280	nuclear division	295	45	6.46E-29
GO:0098813	nuclear chromosome segregation	212	39	1.91E-27
GO:0048285	organelle fission	328	45	3.01E-27
GO:0000819	sister chromatid segregation	129	33	6.13E-27
GO:0140014	mitotic nuclear division	155	33	9.49E-25
GO:0000070	mitotic sister chromatid segregation	106	29	3.49E-24
GO:0010564	regulation of cell cycle process	601	51	1.96E-22
GO:0051726	regulation of cell cycle	969	62	8.78E-22
GO:0007051	spindle organization	149	24	4.55E-15
GO:0090068	positive regulation of cell cycle process	258	29	8.80E-15
GO:0000226	microtubule cytoskeleton organization	513	38	2.57E-14
GO:0045787	positive regulation of cell cycle	361	32	8.40E-14
GO:0016043	cellular component organization	5151	131	2.18E-13
GO:0051276	chromosome organization	943	49	3.02E-13
GO:0007346	regulation of mitotic cell cycle	447	34	5.36E-13
GO:0051983	regulation of chromosome segregation	84	18	6.49E-13
GO:1902850	microtubule cytoskeleton organization involved in mitosis	118	20	8.15E-13
GO:0007017	microtubule-based process	767	43	1.66E-12
GO:0071840	cellular component organization or biogenesis	5345	131	2.73E-12
GO:1901990	regulation of mitotic cell cycle phase transition	265	26	5.64E-12
GO:1901987	regulation of cell cycle phase transition	299	27	1.05E-11
GO:0010965	regulation of mitotic sister chromatid separation	60	15	1.89E-11
GO:0051321	meiotic cell cycle	295	26	5.14E-11
GO:1905818	regulation of chromosome separation	67	15	6.90E-11
GO:0033045	regulation of sister chromatid segregation	67	15	7.13E-11
GO:1903046	meiotic cell cycle process	181	21	9.67E-11
GO:0007052	mitotic spindle organization	88	16	1.65E-10
GO:0140013	meiotic nuclear division	165	20	1.65E-10
GO:0051225	spindle assembly	90	16	2.11E-10
GO:0007088	regulation of mitotic nuclear division	108	17	2.20E-10
GO:0051783	regulation of nuclear division	141	18	1.07E-09
GO:0051128	regulation of cellular component organization	2455	75	1.10E-09
GO:0030071	regulation of mitotic metaphase/anaphase transition	56	13	1.61E-09
GO:0051310	metaphase plate congression	57	13	1.91E-09
GO:0051985	negative regulation of chromosome segregation	32	11	1.98E-09
GO:0033047	regulation of mitotic sister chromatid segregation	44	12	2.02E-09
GO:1902099	regulation of metaphase/anaphase transition of cell cycle	59	13	2.59E-09

Term ID	Term name	N	DOWN	FDR
GO:0009987	cellular process	15087	247	2.65E-09
GO:0051303	establishment of chromosome localization	75	14	2.72E-09
GO:0050000	chromosome localization	77	14	3.64E-09
GO:0048518	positive regulation of biological process	6165	135	4.03E-09
GO:0032465	regulation of cytokinesis	80	14	5.50E-09
GO:0051302	regulation of cell division	163	18	7.35E-09
GO:0007010	cytoskeleton organization	1109	45	8.18E-09
GO:0045841	negative regulation of mitotic metaphase/anaphase transition	28	10	1.09E-08
GO:0071174	mitotic spindle checkpoint	28	10	1.11E-08
GO:0031577	spindle checkpoint	29	10	1.34E-08
GO:0033046	negative regulation of sister chromatid segregation	29	10	1.36E-08
GO:0033048	negative regulation of mitotic sister chromatid segregation	29	10	1.39E-08
GO:2000816	negative regulation of mitotic sister chromatid separation	29	10	1.42E-08
GO:1901988	negative regulation of cell cycle phase transition	150	17	1.58E-08
GO:1902100	negative regulation of metaphase/anaphase transition of cell cycle	30	10	1.71E-08
GO:0007093	mitotic cell cycle checkpoint	110	15	2.01E-08
GO:1905819	negative regulation of chromosome separation	31	10	2.16E-08
GO:0033044	regulation of chromosome organization	285	22	2.29E-08
GO:1901991	negative regulation of mitotic cell cycle phase transition	133	16	2.42E-08
GO:0048522	positive regulation of cellular process	5672	125	2.42E-08
GO:0010948	negative regulation of cell cycle process	215	19	5.30E-08
GO:0000075	cell cycle checkpoint	146	16	8.11E-08
GO:0006996	organelle organization	3178	83	8.24E-08
GO:0045839	negative regulation of mitotic nuclear division	38	10	1.01E-07
GO:0071173	spindle assembly checkpoint	26	9	1.02E-07
GO:0007094	mitotic spindle assembly checkpoint	26	9	1.04E-07
GO:0045930	negative regulation of mitotic cell cycle	210	18	2.30E-07
GO:2001251	negative regulation of chromosome organization	75	12	2.66E-07
GO:0045786	negative regulation of cell cycle	402	24	3.57E-07
GO:0007080	mitotic metaphase plate congression	45	10	3.95E-07
GO:0006974	cellular response to DNA damage stimulus	670	31	4.97E-07
GO:0051784	negative regulation of nuclear division	47	10	5.54E-07
GO:0051988	regulation of attachment of spindle microtubules to kinetochore	13	7	7.44E-07
GO:0032502	developmental process	5554	118	8.89E-07
GO:0033043	regulation of organelle organization	1182	42	1.20E-06
GO:0048856	anatomical structure development	5166	112	1.23E-06
GO:0030198	extracellular matrix organization	268	19	1.28E-06
GO:0043062	extracellular structure organization	269	19	1.33E-06
GO:0045229	external encapsulating structure organization	269	19	1.34E-06
GO:0022414	reproductive process	1470	48	1.40E-06
GO:0000003	reproduction	1471	48	1.40E-06
GO:0030261	chromosome condensation	40	9	2.03E-06
GO:0050789	regulation of biological process	11977	203	2.74E-06
GO:0000910	cytokinesis	97	12	2.99E-06
GO:0007275	multicellular organism development	4788	104	4.00E-06
GO:0000212	meiotic spindle organization	19	7	5.05E-06
GO:0090306	spindle assembly involved in meiosis	10	6	5.35E-06
GO:0007098	centrosome cycle	82	11	5.36E-06
GO:0048731	system development	4176	94	5.96E-06
GO:0050793	regulation of developmental process	2521	66	6.68E-06

Term ID	Term name	N	DOWN	FDR
GO:0000281	mitotic cytokinesis	65	10	6.93E-06
GO:0007144	female meiosis I	11	6	7.75E-06
GO:0071459	protein localization to chromosome, centromeric region	21	7	8.24E-06
GO:0044770	cell cycle phase transition	160	14	9.76E-06
GO:0061640	cytoskeleton-dependent cytokinesis	90	11	1.18E-05
GO:0007057	spindle assembly involved in female meiosis I	5	5	1.28E-05
GO:0065007	biological regulation	12582	208	1.47E-05
GO:0031023	microtubule organizing center organization	93	11	1.56E-05
GO:0048523	negative regulation of cellular process	4817	102	1.96E-05
GO:0007143	female meiotic nuclear division	39	8	2.07E-05
GO:0048519	negative regulation of biological process	5264	109	2.08E-05
GO:0007606	sensory perception of chemical stimulus	1223	0	2.10E-05
GO:0006259	DNA metabolic process	637	27	2.16E-05
GO:0007056	spindle assembly involved in female meiosis	6	5	2.17E-05
GO:0007127	meiosis I	121	12	2.24E-05
GO:0048513	animal organ development	3146	75	2.38E-05
GO:0006281	DNA repair	442	22	2.41E-05
GO:1901989	positive regulation of cell cycle phase transition	99	11	2.53E-05
GO:0061982	meiosis I cell cycle process	123	12	2.55E-05
GO:0050794	regulation of cellular process	11462	193	2.57E-05
GO:0034501	protein localization to kinetochore	15	6	2.71E-05
GO:0044772	mitotic cell cycle phase transition	150	13	2.72E-05
GO:2000026	regulation of multicellular organismal development	1446	44	3.30E-05
GO:0007062	sister chromatid cohesion	43	8	3.56E-05
GO:0051640	organelle localization	495	23	3.75E-05
GO:0051656	establishment of organelle localization	346	19	3.88E-05
GO:0010389	regulation of G2/M transition of mitotic cell cycle	85	10	5.24E-05
GO:1901992	positive regulation of mitotic cell cycle phase transition	85	10	5.28E-05
GO:0051239	regulation of multicellular organismal process	2787	68	5.29E-05
GO:0090307	mitotic spindle assembly	48	8	7.14E-05
GO:0051255	spindle midzone assembly	9	5	7.79E-05
GO:0044839	cell cycle G2/M phase transition	49	8	8.08E-05
GO:0032467	positive regulation of cytokinesis	33	7	8.67E-05
GO:0007608	sensory perception of smell	1123	0	9.51E-05
GO:0051129	negative regulation of cellular component organization	744	28	1.05E-04
GO:0008608	attachment of spindle microtubules to kinetochore	21	6	1.22E-04
GO:0045931	positive regulation of mitotic cell cycle	120	11	1.27E-04
GO:0022607	cellular component assembly	2029	53	1.97E-04
GO:1902749	regulation of cell cycle G2/M phase transition	101	10	2.04E-04
GO:0051781	positive regulation of cell division	79	9	2.33E-04
GO:0007417	central nervous system development	875	30	2.55E-04
GO:0051338	regulation of transferase activity	880	30	2.82E-04
GO:0016572	histone phosphorylation	26	6	3.37E-04
GO:0006275	regulation of DNA replication	110	10	4.01E-04
GO:0007399	nervous system development	2098	53	4.56E-04
GO:0051347	positive regulation of transferase activity	587	23	5.12E-04
GO:0000022	mitotic spindle elongation	6	4	5.87E-04
GO:0051256	mitotic spindle midzone assembly	6	4	5.92E-04
GO:0006260	DNA replication	174	12	6.07E-04
GO:0034502	protein localization to chromosome	69	8	7.21E-04
GO:0007420	brain development	648	24	7.62E-04
GO:0021537	telencephalon development	245	14	7.75E-04

Term ID	Term name	N	DOWN	FDR
GO:0006468	protein phosphorylation	652	24	8.29E-04
GO:0051231	spindle elongation	7	4	8.76E-04
GO:0006323	DNA packaging	152	11	9.31E-04
GO:0060322	head development	703	25	9.31E-04
GO:0007155	cell adhesion	846	28	9.55E-04
GO:0022610	biological adhesion	856	28	1.17E-03
GO:0045132	meiotic chromosome segregation	100	9	1.20E-03
GO:0071103	DNA conformation change	192	12	1.44E-03
GO:0070925	organelle assembly	681	24	1.57E-03
GO:0006950	response to stress	3227	70	1.61E-03
GO:0051653	spindle localization	56	7	1.61E-03
GO:0030900	forebrain development	383	17	1.83E-03
GO:0033554	cellular response to stress	1454	39	2.25E-03
GO:0072698	protein localization to microtubule cytoskeleton	41	6	2.91E-03
GO:0051094	positive regulation of developmental process	1419	38	3.04E-03
GO:0044085	cellular component biogenesis	2256	53	3.17E-03
GO:0051315	attachment of mitotic spindle microtubules to kinetochore	11	4	3.18E-03
GO:0009653	anatomical structure morphogenesis	2260	53	3.20E-03
GO:0009966	regulation of signal transduction	2805	62	3.47E-03
GO:0015740	C4-dicarboxylate transport	25	5	3.52E-03
GO:0000086	G2/M transition of mitotic cell cycle	45	6	4.44E-03
GO:0044380	protein localization to cytoskeleton	45	6	4.47E-03
GO:0010971	positive regulation of G2/M transition of mitotic cell cycle	27	5	4.79E-03
GO:0008283	cell population proliferation	550	20	4.91E-03
GO:0007076	mitotic chromosome condensation	13	4	5.14E-03
GO:0090329	regulation of DNA-dependent DNA replication	47	6	5.38E-03
GO:0010639	negative regulation of organelle organization	339	15	5.41E-03
GO:0032501	multicellular organismal process	7324	128	6.07E-03
GO:0051130	positive regulation of cellular component organization	1203	33	6.29E-03
GO:0032875	regulation of DNA endoreduplication	4	3	6.35E-03
GO:1902751	positive regulation of cell cycle G2/M phase transition	30	5	7.14E-03
GO:0048609	multicellular organismal reproductive process	852	26	7.20E-03
GO:0045860	positive regulation of protein kinase activity	435	17	7.41E-03
GO:0001655	urogenital system development	351	15	7.51E-03
GO:0030199	collagen fibril organization	51	6	7.75E-03
GO:0072001	renal system development	312	14	7.77E-03
GO:0051293	establishment of spindle localization	51	6	7.79E-03
GO:0045859	regulation of protein kinase activity	670	22	8.22E-03
GO:0010646	regulation of cell communication	3214	67	8.40E-03
GO:0006396	RNA processing	769	0	8.61E-03
GO:0023051	regulation of signaling	3226	67	8.64E-03
GO:0032504	multicellular organism reproduction	869	26	8.84E-03
GO:0051960	regulation of nervous system development	534	19	8.94E-03
GO:0098739	import across plasma membrane	136	9	9.22E-03
GO:0070192	chromosome organization involved in meiotic cell cycle	80	7	1.08E-02
GO:0090231	regulation of spindle checkpoint	17	4	1.11E-02
GO:0016310	phosphorylation	914	27	1.17E-02
GO:0031572	G2 DNA damage checkpoint	35	5	1.24E-02
GO:0072359	circulatory system development	923	27	1.24E-02
GO:0051298	centrosome duplication	35	5	1.25E-02
GO:0033674	positive regulation of kinase activity	506	18	1.30E-02

Term ID	Term name	N	DOWN	FDR
GO:0031536	positive regulation of exit from mitosis	6	3	1.30E-02
GO:0051383	kinetochore organization	18	4	1.30E-02
GO:0070777	D-aspartate transport	6	3	1.31E-02
GO:0070779	D-aspartate import across plasma membrane	6	3	1.31E-02
GO:0007276	gamete generation	727	23	1.32E-02
GO:0002040	sprouting angiogenesis	58	6	1.33E-02
GO:0040001	establishment of mitotic spindle localization	36	5	1.34E-02
GO:0032506	cytokinetic process	36	5	1.34E-02
GO:0007292	female gamete generation	145	9	1.34E-02
GO:0016070	RNA metabolic process	1205	3	1.41E-02
GO:0006835	dicarboxylic acid transport	59	6	1.42E-02
GO:0007064	mitotic sister chromatid cohesion	19	4	1.47E-02
GO:0009790	embryo development	1196	32	1.47E-02
GO:0001822	kidney development	297	13	1.51E-02
GO:0035295	tube development	956	27	1.57E-02
GO:0061351	neural precursor cell proliferation	87	7	1.58E-02
GO:0031401	positive regulation of protein modification process	1042	29	1.59E-02
GO:0051294	establishment of spindle orientation	38	5	1.60E-02
GO:0051299	centrosome separation	7	3	1.70E-02
GO:0090232	positive regulation of spindle checkpoint	7	3	1.71E-02
GO:0098657	import into cell	186	10	1.71E-02
GO:0090267	positive regulation of mitotic cell cycle spindle assembly checkpoint	7	3	1.71E-02
GO:0031399	regulation of protein modification process	1556	38	2.02E-02
GO:0006928	movement of cell or subcellular component	1454	36	2.03E-02
GO:0051240	positive regulation of multicellular organismal process	1565	38	2.08E-02
GO:0070839	metal ion export	41	5	2.13E-02
GO:0045595	regulation of cell differentiation	1581	38	2.24E-02
GO:0070601	centromeric sister chromatid cohesion	8	3	2.25E-02
GO:0051246	regulation of protein metabolic process	2483	53	2.35E-02
GO:0009887	animal organ morphogenesis	1029	28	2.40E-02
GO:0048585	negative regulation of response to stimulus	1597	38	2.45E-02
GO:0007600	sensory perception	1645	7	2.65E-02
GO:0042940	D-amino acid transport	9	3	2.87E-02
GO:0044784	metaphase/anaphase transition of cell cycle	9	3	2.88E-02
GO:0006883	cellular sodium ion homeostasis	24	4	2.89E-02
GO:0007091	metaphase/anaphase transition of mitotic cell cycle	9	3	2.90E-02
GO:0048608	reproductive structure development	455	16	2.90E-02
GO:0061458	reproductive system development	459	16	3.11E-02
GO:0009314	response to radiation	414	15	3.15E-02
GO:0045740	positive regulation of DNA replication	46	5	3.26E-02
GO:0034508	centromere complex assembly	25	4	3.26E-02
GO:0006310	DNA recombination	207	10	3.46E-02
GO:0048869	cellular developmental process	3611	70	3.51E-02
GO:0044703	multi-organism reproductive process	1011	27	3.56E-02
GO:1901978	positive regulation of cell cycle checkpoint	10	3	3.57E-02
GO:0043408	regulation of MAPK cascade	704	21	3.58E-02
GO:0140354	lipid import into cell	26	4	3.63E-02
GO:0018209	peptidyl-serine modification	210	10	3.76E-02
GO:0048583	regulation of response to stimulus	3899	74	3.86E-02
GO:0042306	regulation of protein import into nucleus	75	6	3.94E-02
GO:0051704	multi-organism process	1028	27	4.09E-02
GO:0001944	vasculature development	571	18	4.15E-02
GO:0045937	positive regulation of phosphate metabolic process	963	26	4.28E-02

Term ID	Term name	N	DOWN	FDR
GO:0010562	positive regulation of phosphorus metabolic process	963	26	4.30E-02
GO:0001934	positive regulation of protein phosphorylation	805	23	4.32E-02
GO:0140115	export across plasma membrane	50	5	4.33E-02
GO:0018107	peptidyl-threonine phosphorylation	77	6	4.37E-02
GO:0051641	cellular localization	2192	47	4.38E-02
GO:0051247	positive regulation of protein metabolic process	1476	35	4.83E-02
GO:0019953	sexual reproduction	884	24	4.85E-02

XI. SCIENTIFIC CONTRIBUTIONS

Published scientific papers:

Calls A, Torres-Espin A, Navarro X, Yuste VJ, Udina E, Bruna J. Cisplatin-induced peripheral neuropathy is associated with neuronal senescence-like response. Neuro Oncol. 2021; 23(1):88-99. Doi: 10.1093/neuonc/noaa151.

Published Reviews:

Calls A, Carozzi V, Navarro X, Monza L, Bruna J. Pathogenesis of platinum-induced peripheral neurotoxicity: Insights from preclinical studies. Exp Neurol. 2020; 325:113141. Doi: 10.1016/j.expneurol.2019.113141.

Other collaborations

In addition to the first-author publications, during all the time I have been done the PhD I have participated in other projects and works that have been published:

Bruna J, Alberti P, **Calls-Cobos A**, Caillaud M, Damaj MI, Navarro X. Methods for in vivo studies in rodents of chemotherapy induced peripheral neuropathy. Exp Neurol. 2020; 325:113154. Doi: 10.1016/j.expneurol.2019.113154.

Sanchez-Brualla I, **Calls-Cobos A**, Udina E. Minocycline Does Not Reduce the Regenerative Capacity of Peripheral Motor and Sensory Neurons after a Conditioning Injury in Mice. Anat Rec (Hoboken). 2018; 301(10):1638-1645. Doi: 10.1002/ar.23845.

Velasco R, Navarro X, Gil-Gil M, Herrando-Grabulosa M, **Calls A**, Bruna J. Neuropathic Pain and Nerve Growth Factor in Chemotherapy-Induced Peripheral Neuropathy: Prospective Clinical-Pathological Study. J Pain Symptom Manage. 2017; 54(6):815-825. Doi: 10.1016/j.jpainsymman.2017.04.021.

Alé A, Bruna J, **Calls A**, Karamita M, Haralambous S, Probert L, Navarro X, Udina E. Inhibition of the neuronal NFκB pathway attenuates bortezomib-induced neuropathy in a mouse model. Neurotoxicology. 2016; 55:58-64. Doi: 10.1016/j.neuro.2016.05.004.

XII. ACKNOWLEDGMENTS

M’agradaria acabar aquesta tesi donant les gràcies a totes les persones que, directa o indirectament, m’han ajudat a realitzar-la. A en Xavi, per deixar-me formar part d’aquest meravellós grup que tan m’ha aportat. A l’Esther, per confiar en mi quan no era més que una recent graduada i donar-me l’oportunitat de créixer i aprendre al seu costat. Ets una inspiració. A en Jordi, per acceptar-me en aquesta bombarda de projecte que tan ens ha costat tirar endavant. Al final ha donat els seus fruits, i la veritat és que han resultat ser molt dolços. A la Jessica, la Mònica, i l’Israel, per ser sempre a la rereguarda posant ordre al nostre caos. A la Mireia, per ajudar-me tants i tants cops amb temes de molecular. A en Quino, per fer-nos els dies una mica més feliços, i a la Maite, per cuidar de nosaltres com si de fills es tractés. A tots i cadascun dels doctorands amb qui he compartir la M4-119, als del principi i als del final, infinites gràcies. A l’Alba, per tot el que m’ha arribat ensenyar al llarg d’aquests anys. Et trobo molt a faltar. A en Jesús, el dinamitzador del grup. Enyoro els moments en què ens creiem dives de l’escenari i en teníem prou amb la Lady Gaga sonant a la UAB radio per muntar un *show*. A la Maria, per ajudar-me sempre que ho he necessitat, ets pura bondat. A la Neus, l’alegria del laboratori. Gràcies per encomanar-me amb el teu bon rotllo. A la Sara M, per la confiança que sempre ha dipositat en mi, des dels primers principis en aquella *poiata* transformada en despatx. I a la Núria, per ser-hi sempre. Per tirar de mi quan no tenia força ni ganes de continuar. Has sigut un pilar fonamental durant tots aquests anys. Gràcies a la Judith i a la Sara B, que m’han descobert un món d’unicorns, cors i *wonderful lifes*. Sou les persones més *kukis* que he conegut mai i espero emportar-me una mica de vosaltres allà on vagi. Som l’Equip Udina, o com a mi m’agrada dir-li “Los Angeles de Esther”. A en Bruno *el Asturiano*, per ajudar-me sempre en temes d’informàtica i sobretot, per les receptes tan espectaculars que ens has descobert. Gràcies a la Vera, l’Andrea, la Carla, la Georgina, la Joana, la Raquel, en Diego i en Néstor. Sou el relleu dels doctorands NFIS, i no tinc cap dubte que sabreu mantenir el nivell de la “Phd life” (o inclús superar-lo!).

Thanks to Marco and all the member of his incredible group, especially to Jamil, Abel and Marta. My stage at Groningen wouldn’t have been the same without all you (and the Oliebollen full of nutella!). Marta, gracias por enseñarme tanto. Ojalá volvamos a vernos.

Gràcies a l’Abel i a en Marc, per la seva incommensurable ajuda amb l’anàlisi bioinformàtica. Sense vosaltres dos aquesta tesi no existiria, literalment. I a la Laura, per les hores passades al confocal.

Als de Santa Agnès, les d’Arbúcies, la Sandra i les Biomeds, que hi eren molt abans d’embarcar-me en la tesi i han seguit al meu costat.

Gràcies Francesc, per ensenyar-me que tot a la vida és relatiu, i que entre el blanc i el negre hi ha un immens arc iris de colors. Joana i Ot, gràcies pel gran orgull que profaneu cap a mi i que no em mereixo. Gràcies papa i mama. Avui dia no seria aquí sense l’ enorme esforç que heu hagut de fer durant tots aquests anys. Tan de bo us pugui recompensar algun dia.